1986

Spectroscopic Studies of Bacterial Iron-Sulfur Proteins (Electron Paramagnetic Resonance, Magnetic Circular Dichroism).

Deborah Ellen Bennett
Louisiana State University and Agricultural & Mechanical College

Bennett, Deborah Ellen

SPECTROSCOPIC STUDIES OF BACTERIAL IRON-SULFUR PROTEINS

The Louisiana State University and Agricultural and Mechanical Col. PH.D. 1986

PLEASE NOTE:

In all cases this material has been filmed in the best possible way from the available copy. Problems encountered with this document have been identified here with a check mark __√__.

1. Glossy photographs or pages _____
2. Colored illustrations, paper or print _____
3. Photographs with dark background _____
4. Illustrations are poor copy _____
5. Pages with black marks, not original copy _____
6. Print shows through as there is text on both sides of page _____
7. Indistinct, broken or small print on several pages __√__
8. Print exceeds margin requirements _____
9. Tightly bound copy with print lost in spine _____
10. Computer printout pages with indistinct print _____
11. Page(s) _____ lacking when material received, and not available from school or author.
12. Page(s) _____ seem to be missing in numbering only as text follows.
13. Two pages numbered _____. Text follows.
14. Curling and wrinkled pages _____
15. Dissertation contains pages with print at a slant, filmed as received _____
16. Other _____

_____

_____

University
Microfilms
International

SPECTROSCOPIC STUDIES OF BACTERIAL IRON-SULFUR PROTEINS

A Dissertation

Submitted to the Graduate Faculty of the
Louisiana State University and
Agricultural and Mechanical College
in partial fulfillment of the
requirements for the degree of
Doctor of Philosophy

in

Chemistry

by
Deborah E. Bennett
B.S., Duke University, 1980
August 1986

ACKNOWLEDGEMENTS

I wish to express my sincere gratitude to Dr. Michael Johnson for his patient instruction and invaluable guidance.

To Dr. Brian Hales for many helpful discussions, and for the generous use of his equipment.

To Joyce Morningstar, Isabel Zambrano, Barbara Dixon, Yvonne Onate, Andrzej Kowal, and Melinda Oliver for making the work enjoyable.

To Robert Zinn for his assistance with the computer applications.

To the staff of the office, electronics, machine, and glass shops without whom research would not be possible.

To Dr. James Fee, Dr. William Sweeney, and Dr. Michael Adams and Dr. Leonard Mortenson for kindly supplying the *Tt* Fd, *Av* Fd I, and the *E. coli* nitrate reductase, respectively.

To my parents for believing in me.

And to Gene and Jennifer for standing by me.

This work was supported by the National Institute of Health, the Louisiana State University Center for Energy Studies, and the Petroleum Research Fund.

Table of Contents

Abstract

Iron-sulfur proteins play a vital role in metabolism; mediating such life-sustaining processes as aerobic and anaerobic respiration, nitrogen fixation, and photosynthesis. This work employs low temperature magnetic circular dichroism (MCD), electron paramagnetic resonance (EPR), and UV-visible spectroscopy to characterize the iron-sulfur clusters of the following bacterial proteins: Azotobacter vinelandii ferredoxinI, Thermus thermophilus ferredoxin, Escherichia coli nitrate reductase and the rubredoxin and ferredoxin from Clostridium pasteurianum.

Novel [3Fe-xS] clusters were identified in A. vinelandii FdI, T. thermophilus Fd, ferricyanide treated C. pasteurianum Fd, and E. coli nitrate reductase. The uniformity of the magnetic and electronic properties of these clusters in both the oxidized and the reduced states indicates a common iron-sulfur core structure for this type of cluster. E. coli nitrate reductase is the first example of an active enzyme which contains a [3Fe-xS] cluster. This argues against the currently prevailing hypothesis that all such clusters are isolation artifacts.

This work has also developed the potential of low

temperature MCD for the detection and characterization of iron-sulfur clusters in multicluster enzymes. Studies on the well-characterized Clostridial proteins demonstrated that MCD magnetization curves provide a selective method of obtaining ground state g-values, spin states, and estimations of the polarizations of the electronic transitions for randomly oriented samples. Moreover, zero field splitting parameters were obtained by a detailed study of the temperature dependence of individual MCD transitions. This has led to a more detailed understanding of the complex Kramer's and non-Kramer's ground states exhibitied by reduced [3Fe-xS] clusters (S=2) and oxidized and reduced rubredoxin (S=5/2 and S=2 respectively).

Chapter 1

Introduction

1.1 General Introduction

Iron-Sulfur Proteins

Iron-sulfur proteins are believed to account for roughly 1% of the total iron content in mammals. In light of this, it is surprising that they were not discovered until the mid-1950's. We now know that iron-sulfur proteins are pervasive throughout nature, occuring in plants, animals, and bacteria. Many of these proteins are vital to important biological processes such as photosynthesis, aerobic and anaerobic respiration, and nitrogen and carbon fixation. The primary role of the iron-sulfur centers is one of electron transfer, and as such they are constituents of numerous redox enzymes. Structural, regulatory, and storage roles have also been proposed in some instances. They are the subject of several good reviews (1, 2). A partial list of some of the more important iron-sulfur proteins, along with their

enzymatic function when known is given in table I.1.

Presently, the term iron-sulfur protein refers to non-heme proteins, in which high spin iron is directly liganded to inorganic (acid labile) or cysteinyl sulfur. In all cases the coordination is nearly tetrahedral around the individual iron atoms. When more than one iron atom is present in the "cluster" strong antiferromagnetic coupling exists, so that the resultant spin of the ground state is not the sum of the spins of the individual iron atoms (see below).

The Nomenclature Committee of the International Union of Biochemistry has classified iron proteins into three major categories: hemoprotein, iron-sulfur proteins, and other iron containing proteins (3). Iron-sulfur proteins are further classified as either simple iron-sulfur proteins, those proteins which contain iron-sulfur clusters as their only prosthetic group, or complex iron-sulfur proteins which contain additional prosthetic groups such as other metal centers, hemes, flavins, etc.

Iron-sulfur proteins which have defined enzymatic functions are named for those functions, e.g. nitrogenase and hydrogenase. Those proteins without classical enzymatic functions are generally termed rubredoxins (Rd) or ferredoxins (Fd) (fig.I.1). Rubredoxins contain one or two 1Fe centers. Ferredoxins can contain [2Fe-2S], [3Fe-xS], or [4Fe-4S] clusters.

Iron-sulfur clusters

The centers which will be discussed are the monomeric 1Fe centers, and the [2Fe-2S], [3Fe-xS], and the [4Fe-4S] clusters. The latter three are often designated as 2Fe, 3Fe, and 4Fe clusters. Oxidation states are often indicated by superscripts indicating the net charge of the cluster, assuming that the cysteine residues are formally present as mercaptide and the labile sulfur as sulfide. The number of clusters present per protein molecule is indicated by an integer prefix. Other iron-sulfur clusters, such as the P and M clusters of nitrogenase, are known, but their structure and properties are less well characterized and beyond the scope of this work.

The 1Fe centers are unique among iron-sulfur clusters in that they contain no inorganic sulfur. Instead, a single iron atom is tetrahedrally coordinated to four cysteinyl sulfurs as shown in figure I.2a (4). The iron atom undergoes a one electron redox cycle, with a midpoint potential, E_m, between 0 and -100 mV versus the normal hydrogen electrode (NHE), at pH 7 (all potentials cited herein will be versus NHE, pH 7 unless otherwise stated). An oxidized 1Fe center has a ground state of S=5/2, while the reduced center has a ground state of S=2 (5). The oxidized center is thereby EPR active, while the reduced cluster is inactive due to the

presence of zero field splitting which prevents resonance from occurring even at very small magnetic fields.

X-ray diffraction of the [2Fe-2S] cluster of Spirulina platensis Fd confirmed the binuclear structure given in figure I.2b (6), although the structure was deduced by other methods prior to the diffraction results (7). Like the 1Fe centers, the [2Fe-2S] clusters can cycle between two oxidation states, with a midpoint potential ranging from +300 mV for the Rieske protein to -420 mV for spinach Fd. In the oxidized state, the cluster formally contains two ferric ions, which couple to produce a diamagnetic, S=0, ground state (8). The reduced [2Fe-2S] cluster has a so-called "trapped-valence" state, consisting of one Fe(II) and one Fe(III) (9). The unpaired electrons couple to produce an S=1/2 net ground state.

Based on EPR spectra and redox potentials, at least three slightly different types of 2Fe clusters have been identified. These are: (a) the plant-type Fd, typified by spincach Fd, E_m~ -420 mV, rhombic EPR spectra with g_{av}=1.96, (b) the hydroxylase-type clusters, typified by adrenodoxin, E_m~ -240 mV, axial EPR with g_{av}=1.96, and (c) the Rieske center, E_m~ +300 mV, rhombic EPR with g_{av}= 1.91. In contrast to reduced [4Fe-4S] clusters, reduced [2Fe-2S] clusters have relatively slow relaxation such that EPR signals can be observed at 77 K.

The existence of [3Fe-xS] clusters, where x is

either 3 or 4 was not known prior to Mossbauer analysis of Azotobacter Vinelandii (10). This was subsequently confirmed by the subsequent x-ray diffraction analysis of this protein (11). The oxidized [3Fe-xS] clusters consists of three ferric ions, coupled to produce a ground state of S=1/2 (12). In this state [3Fe-xS] clusters give rise to a near-isotropic EPR signal with g=2.01 (13). At potentials between 0 and -200 mV depending on the protein, these cluster undergo a reversible one electron reduction. This additional electron appears to be delocalized on two of the iron atoms. The reduced state, therefore is formally comprised of two ferric and one ferrous ion, but is more accurately described as one ferric ion and two ions which are intermediate between ferric and ferrous (11). Mossbauer studies also indicate a paramagnetic ground state for the reduced cluster despite the absence of an EPR signal. This ground state is thought to be even spin with S>1, and a negative zero field splitting parameter (11). Prior to 1980, many [3Fe-xS] clusters were erroneously characterized as High Potential [4Fe-4S] clusters (see below), based solely on the presence of a g-value greater than 2 when oxidized, and the absence of an EPR signal when reduced.

Many questions concerning these clusters remain unanswered. One important question concerns the structure of the [3Fe-xS] cluster. In the most recent

x-ray structure, Ghosh et al proposed the nearly planar [3Fe-3S] cluster depicted in figure II.2c (14) However, Resonance Raman (RR) of A.vinelandii Fd I, Thermus thermophilus Fd, D. gigas Fd II, and ferricyanide treated Clostridium pasteurianum Fd, indicate a cubane [3Fe-4S] cluster (fig.I.2d) (15), as does the Extended X-ray Absorption Fine Structure (EXAFS) of D. gigas Fd II (16) and of inactive aconitase (17). Very recently, the results of X-ray diffraction analysis of inactive aconitase (18) and the EXAFS studies of A. vinelandii Fd I (19) have been published. Both of these studies are consistent with a [3Fe-4S] cluster. The most recent review proposes the existence of two distinct types of [3Fe-xS] clusters (20).

Another question, still unresolved, involves the physiological significance of the [3Fe-xS] clusters. Many of the earliest characterized 3Fe clusters are believed to be isolation artifacts, that is they are not thought to exist in vivo, but are formed by oxidative degradation of [4Fe-4S] clusters during isolation. Among these are the 3Fe clusters in aconitase (21) and C. pasteurianum Fd (22). The question as to whether all [3Fe-xS] clusters in biological systems are artifacts of aerobic isolation remains to be answered.

Figure I.2e depicts the [4Fe-4S] cluster (23). These clusters are unusual in that they have three accessible oxidation states. The "conventional" or "Fd-type" 4Fe

clusters cycle between the 2+ and the 1+ oxidation states, E_m ~ -400mV, where the charge refers to the formal charge on the cluster without cysteine residues. The oxidized cluster formally contains two ferric and two ferrous ions, coupled to yield a diamagnetic, S=0, ground state (24). When reduced the cluster contains three ferrous and one ferric ion, coupled to produce and S=1/2 ground state. The electrons are delocalized over all four iron atoms in both oxidation states (25).

Those proteins containing [4Fe-4S] clusters which cycle between the 3+ and 2+ oxidation states, E_m ~ 350mV, are termed High Potential Iron-Sulfur Proteins, or HiPIP's. Oxidized HiPIP's contain three high spin ferric and one high spin ferrous ion. The ground state is S=1/2. The reduced HiPIP is analogous to the oxidized conventional [4Fe-4S] cluster.

Carter et al. were the first to propose a common structure for the conventional and HiPIP [4Fe-4S] clusters (26). Termed "the three-state hypothesis", because of the three oxidation states involved, this theory proposes that the oxidation potentials are modulated by subtle influences of the polypeptide backbone. Addition of 80% DMSO to HiPIP clusters will allow for their reduction to the $[4Fe\text{-}4S]^{+1}$ state of the reduced Fd, further substantiating the structural equivalence of the clusters (27).

Table I.2 contains a summary of the ground states of the iron-sulfur clusters and of their electronic and magnetic properties.

1.2 Research Objectives

In this work, iron-sulfur proteins of varying complexity were investigated by the complementary spectroscopic techniques of UV-visible absorption, low temperature Magnetic Circular Dichroism (MCD), and low temperature Electron Paramagnetic Resonance (EPR). Specifically, the proteins investigated are the Rd and eight-iron Fd from C. pasteurianum, the seven-iron Fds, T. thermophilus Fd and A. vinelandii Fd I, and nitrate reductase from Escherichia coli (E. coli). Although these proteins have been investigated by UV-visible and EPR spectroscopy, prior to the inception of this study, very little low temperature MCD had been published. Indeed, a major driving force for this research was to develop the potential of low temperature MCD spectroscopy for investigation of paramagnetic iron-sulfur clusters in metalloproteins. Hence, the proteins were chosen to encompass simple well characterized proteins, such as the Clostridial proteins, as well as complex multicomponent

metalloenzymes of ill-defined cluster composition, e.g. E. coli nitrate reductase.

The limited low temperature MCD data already in the literature has demonstrated the enormous utility of this technique as a method of identifying iron-sulfur cluster types in proteins (28). As paramagnetic chromophores can experience up to a seventy-fold enhancement upon cooling from room temperature to 4.2K, low temperature MCD becomes specifically an optical probe for chromophoric, paramagnetic centers (see chapter II.1). Therefore, MCD can selectively investigate the electronic and magnetic properties of a few iron atoms in a large protein matrix, as is found in iron-sulfur proteins.

In addition to the form of the MCD spectrum (i.e. the sign, frequency, an intensity of the bands), information concerning the ground state physics can be obtained by detailed investigation of the magnetic field and temperature dependence of discrete MCD transitions, called magnetization curves (chapter II.1). While such information is obtainable from EPR, Mossbauer, and magnetic susceptibility studies, MCD offers many advantages over these other techniques. It is applicable to paramagnets which are EPR silent, e.g. non-Kramer's systems with large zero-field splittings. Secondly, it is not restricted to iron, as is Mossbauer. Finally, unlike magnetic susceptibility studies, MCD can selectively monitor a single chromophore in a

multicomponent system. Magnetization curves still remain underexploited.

This research was therefore initiated to enhance the potential of MCD spectroscopy for the study of iron-sulfur proteins, and to better characterize iron-sulfur clusters. Specifically, the following objectives were persued: (1) to establish the structural, electronic, and magnetic diversity of both oxidized and reduced [3Fe-xS] clusters from a variety of bacterial sources, and thereby address the question of the existence of two distinct types of 3Fe clusters, (2) to ascertain the physiological significance of 3Fe clusters, and to study their production from 4Fe clusters, (3) to develop and exploit the use of low temperature MCD spectroscopy in identifying iron-sulfur cluster type in multicluster proteins, and (4) to develop the utility of MCD magnetization curves as a means of selectively probing the detailed electronic ground state properties of iron-sulfur centers, particularly those paramagnets which are unaccessable *via* EPR spectroscopy.

References

1. "Iron-Sulfur Proteins" (Lovenberg,W., ed.) vol. I and II, 1973 and vol. III 1977, Academic Press, New York

2. "Iron-Sulfur Proteins" (Spiro, T.G., ed.) 1982, Wiley and Sons, New York

3. Nomenclature Committee of the International Union of Biochemistry (1979) Eur. J. Biochem. 93, 427-430

4. Watenpaugh, K.D., Sieker, L.C., and Jensen, L.H., (1979) J. Mol. Bio. 131, 509-522 and 615-633

5. Phillips, W.D., Poe, M., Weiher, J.F., and McDonald, C.C., (1970) Nature 227, 574-577

6. Fukuyama, K., Hase, T., Matsumoto, S., Tsukihara, T., Katsube, Y., Tanaka, N., Kakudo, M., Wada, K., and Matsubara, H., (1980) Nature 286, 522-524

7. Britzinger, H., Palmer, G., and Sands, R.H., (1966) Proc. Nat. Acad. Sci. USA 55, 397-404

8. Bearden, A.J., and Moss, T.H. (1967) in "Magnetic Resonance in Biological Systems (Ehrenberg, A., Malmstrom, B.G., and Vanngard, T., eds) Pergamon Press, Oxford

9. Palmer, G., Dunham, W.R., Fee, J.A., Sands, R.H., Hzuka, T., and Yonetani, T. (1971) Biochim. Biophys. Acta 245, 201-207

10. Emptage, M.H., Kent, T.A., Huynh, B.H., Rawlings, J., Orme-Johnson, W.H., and Munck, E., (1980) J. Biol. Chem. 255, 1793-1796

11. Stout, C.D., Ghosh, D., Pattabhi, V., and Robbins, A.H., (1980) J. Biol. Chem. 255, 1797-1800

12. Kent, T.A., Huynh, B.H., and Munck, E., (1980) Proc. Nat. Acad. Sci. USA 77, 6574-6576

13. Gayda, J.P., Bertrand, P., and Theodule, F.X., (1982) J. Chem. Phys. 77, 3387-3391

14. Ghosh, D., O'Donnell, S., Furey, W. , Robbins, A.H., and Stout, C.D., (1982) J. Mol. Biol. 158, 73-109

15. Johnson, M.K., Czernuszewicz, R.S., Spiro, T.G., Fee, J.A., and Sweeney, W.V., (1983) J. Am. Chem. Soc. 105, 6671-6678

16. Antonio, M.R., Averill, B.A., Moura, I., Moura, J.J.G., Orme-Johnson, W.H., Teo, B.K., Xavier, A.V., (1982) J. Biol. Chem. 257, 6646-6649

17. Bienert, H., Emptage, M.H., Dreyer, J., Scott, R.A., Hahn, J.E., Hodgson, K.O., and Thompson, A.J., (1983) Proc. Nat. Acad. Sci. USA 80, 393-396

18. Robbins, A.H., and Stout, C.D., (1985) J. Biol. Chem. 260, 2328-2333

19. Stephens, P.J., Morgan, T.V., Devlin, F., Penner-Hahn, J.E., Hodgson, K.O., Scott, R.A., Stout, C.D., and Burgess, B.K., (1985) Proc. Nat. Acad. Sci. USA 82, 5661-5665

20. Beinert, H., and Thomson, A.J., (1983) Arch. Biochem. Biophys. 222, 333-361

21. Kent, T.A., Emptage, M.H., Merkle, H., Kennedy, M.C., Beinert, H., and Munck, E., (1985) J. Biol. Chem. 260, 6871-6881

22. Thompson, A.J., Robinson, A.E., Johnson, M.K., Cammack, R., Rao, K.K., and Hall, D.O. (1981) Biochim. Biophys. Acta 637, 423-432

23. Carter, C.W., Kraut, J., Freer, S.T., Alden, R.A., Sieker, L.C., Adman, E.T., and Jensen, L.H., (1972) Proc. Nat. Acad. Sci. USA 69, 3526-3529

24. Middleton, P., Dickson, D.P.E., Johnson, C.E., Rush, J.D., (1978) Eur. J. Biochem. 88, 135-141

25. Cammack, R., Dickson, D.P.E., Johnson, C.E., and Rush, J.D., (1977) in "Iron-Sulfur Proteins" (Lovenberg, W. ed.), pp. 283-330 Academic Press, New York

26. Carter, C.W., Freer, S. T., Xuong, N.H., Alden, R.A., and Kraut, J. (1971) Cold Spring Harbor Symp. Quant. Biol. 6, 381-385

27. Cammack, R. (1973) Biochem. Biophys. Res. Commun. 54, 548-554

28. Johnson, M.K., Robinson, A.E., and Thompson, A.J., in "Iron-Sulfur Proteins", (Spiro, T. ed.)

Table I.1 Some Iron-Sulfur containing metalloproteins

ENZYME	Process Catalysed	Centers employed
Hydrogenase	$2H^+ + 2e^- \rightarrow H_2$	Fe-S[a], (Ni)
Nitrogenase	$N_2 + 6H^+ + 6e^- \rightarrow 2NH_3$	Fe-S, Fe-Mo-S[b]
Sulfite Reductase	$SO_3^{2-} + 6e^- + 6H^+ \rightarrow S^{2-} + 3H_2O$	Fe-S, Siroheme, flavin
Nitrite Reductase	$NO_2^- + 8H^+ + 6e^- \rightarrow NH_4^+ + 2H_2O$	Fe-S, Siroheme, flavin
Nitrate Reductase	$NO_3^- + 2H^+ + 2e^- \rightarrow NO_2^- + H_2O$	Fe-S, Mo, (heme)
Xanthine oxidase	Xanthine + $H_2O \rightarrow$ Uric acid + $2H^+ + 2e^-$	Fe-S, Mo, flavin
Aconitase	Citrate → Isocitrate	Fe-S
NADH dehydrogenase	$NADH + H^+ \rightarrow NAD^+ + 2H^+ + 2e^-$	Fe-S, flavin
Succinate dehydrogenase	succinate → fumarate + $2H^+ + 2e^-$	Fe-S, flavin
Rubredoxin	electron transfer	Fe-S
Ferredoxin	electron transfer	Fe-S

[a]Fe-S = Iron-Sulfur cluster

[b]Fe-Mo-S = Iron-Molybdenum-Sulfur cluster

Table I.2. A summary of the electronic and magnetic properties of iron-sulfur clusters.

Cluster	oxidation state	Total spin	EPR	MCD temperature dependent?
1 Fe	oxidized	5/2	g=9, 4.3	yes
	reduced	2	none	yes
2 Fe	oxidized	0	none	no
	reduced	1/2	g=1.96	yes
3 Fe	oxidized	1/2	g=2.01	yes
	reduced	integer>1	none	yes
4Fe				
HiPIP	oxidized	1/2	g>2	yes
	reduced	0	none	no
Fd-type	oxidized	0	none	no
	reduced	1/2	g=1.96	yes

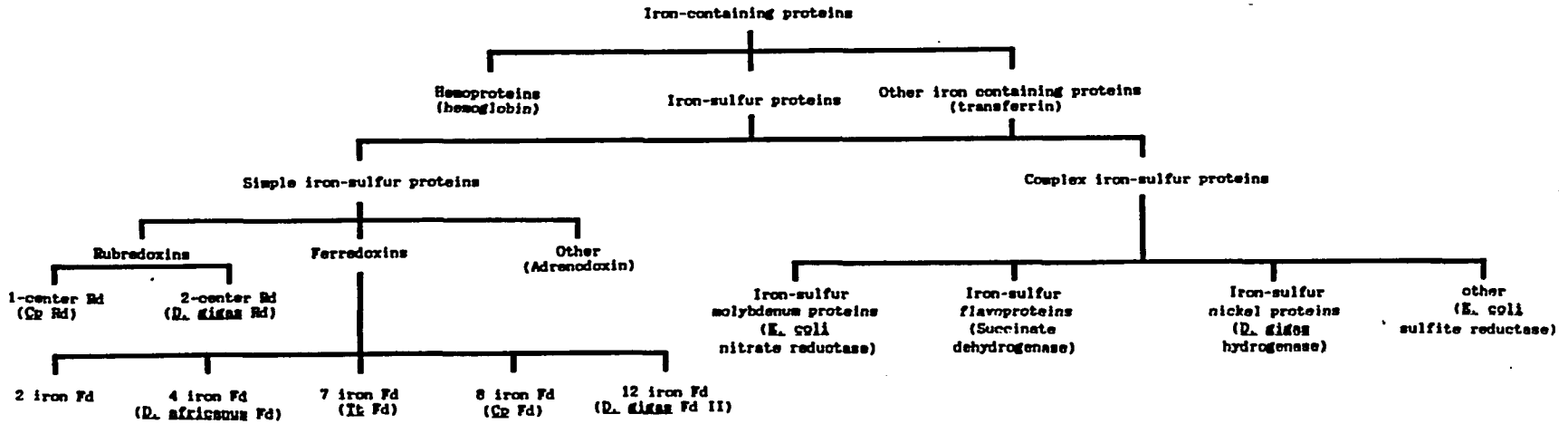

Figure I.1. Nomenclature of Iron-Sulfur Proteins as set forth by the Nomenclature Committee of the International Union of Biochemistry. An example of each type of protein is given in parenthesis under the appropriate designation.

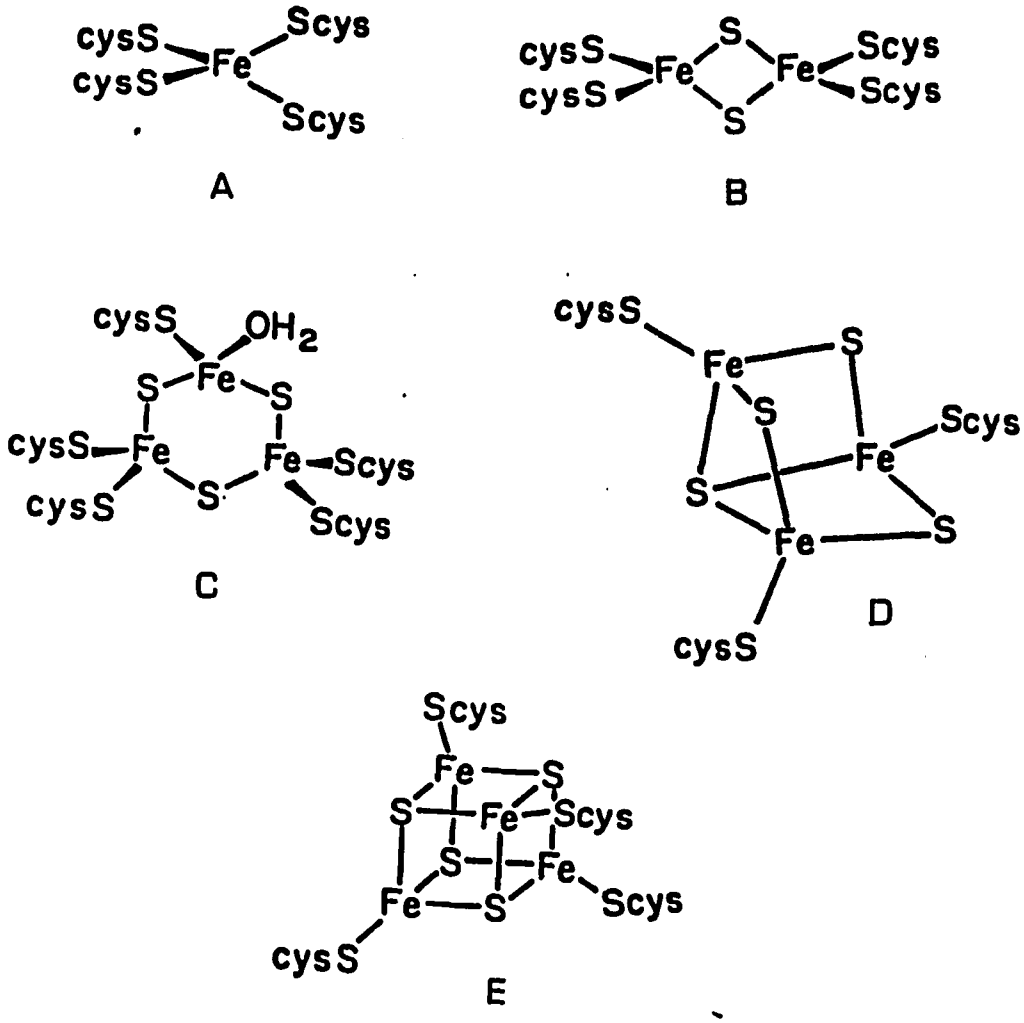

Figure I.2: Schematic of well characterized iron-sulfur clusters. (a) monomeric 1 Fe center (b) [2Fe-2S] cluster (c) [3Fe-3S] cluster (d) [3Fe-4S] cluster (e) [4Fe-4S] cluster

Chapter 2

THEORY

2.1 MCD

Plane polarized light can be considered as being the resultant of right and left circularly polarized light of equal amplitude and travelling along the same axis (designated by convention as the positive z-axis) in phase. Passage of plane polarized light through an optically active substance will result in a rotation in the plane of polarization due to differential refractive indices between left and right circularly polarized light. This rotation is termed Optical Rotary Dispersion (ORD). If the radiation is at a frequency such that it is absorbed, ellipticity will accompany the rotation due to a differential absorption of right and left circularly polarized light. Optical activity can arise from an

asymmetric center, or can be induced in all substances by a longitudinal magnetic field, according to the Faraday effect (1). The former is associated with natural Circular Dichroism (CD), whereas the later is Magnetic Circular Dichroism (MCD).

MCD bands can be both negative and positive. MCD spectra, therefore, contain much more fine structure and resolution than the corresponding absorption spectra. Thus, MCD has greater "fingerprinting" capability. Furthermore, the enhanced resolution allows for the assignment of individual transitions, particularly in well defined systems, possessing high symmetry. Two of the best treatments of the theory of MCD can be found in the treatises by Schatz and McCaffery, and by Stephens (2, 3) Several other reviews are also available (4-6). What follows is a brief summary of their results, with particular emphasis on the theory of low temperature MCD spectroscopy as it pertains to the study of bioinorganic molecules. Unless otherwise stated, the formalism of P.J. Stephens will be used throughout. The reader is refered to the above-cited references for further details.

For the transition from ground state A to excited state J, the MCD absorption, $\Delta A(=A_L-A_R)$, is defined as

$$\Delta A(A \rightarrow J) = +\delta\left\{a_1\left(\frac{-\partial f}{\partial \epsilon}\right)+\left(B_o+\frac{C_o}{kT}\right) f\right\}(\beta B)cz \qquad \text{eq. II.1}$$

$$\text{where} \quad \delta=\frac{N\pi^2\alpha^2\log_{10}e}{2500\hbar cn}\,;\ \int_o^{\infty}\frac{f(E_{JA},E)}{E}\,dE=1$$

N is Avogadro's number, δ is the absorption coefficient and related to the transition probability, c is the speed of light, h is Planck's constant, n is the refractive index, β is the Bohr magnetron, B is the magnetic flux, c is the concentration in moles per liter, z is the pathlength, E_{JA} is the energy difference between states A and J, f is a normalized lineshape function which defines the band shape, and A_1, B_o, and C_o are the three categories of MCD phenomena commonly refered to as MCD A-, B-, and C-terms.

A-terms arise from transitions in which either the ground state and/or the excited state exhibits degeneracy. For simplicity, an atomic transition ($^1S \rightarrow {}^1P$), in which only the excited state is degenerate will be considered (fig. II.1). In the presence of a magnetic field the energy levels of the excited state will undergo Zeeman splitting, resulting in three equally spaced energy levels with M_J = +1, 0, -1, separated by $g\beta B$, where g is the gyromagnetic ratio. A transition in which ΔM_J = +1 corresponds to absorption of left circularly polarized light, and ΔM_J = -1 corresponds to absorption of right circularly polarized light (see

selection rules, below). These transitions will be of equal intensity, but will differ in frequency by 2g$$B. The resultant MCD band, which corresponds to the differential absorption, will be a symmetrical biphasic signal, crossing the x-axis at ν_o. The intensity of an A-term is independent of temperature. For light propagating parallel to the z-direction an A-term is mathematically defined as:

$$C_1 = +\frac{1}{d_A}\sum_{\alpha,\lambda}\left[\,|\langle A_\alpha|m_-|J_\lambda\rangle^\circ|^2 - |\,A_\alpha|m_+|J_\lambda\rangle^\circ|^2\right] \qquad \text{eq. II.2}$$

$$\times\left[\langle J_\lambda\,|L_z + 2S_z|J_\lambda\rangle^\circ - \langle A_\alpha|L_z + 2S_z|A_\alpha\rangle^\circ\right]$$

where d_A is the degeneracy of the state A, α and β are the vibrational components of states A and J, respectively $m_\pm$ are the electric dipole moment operator for circularly polarized light, such that $m_\pm=(1/\sqrt{2})(m_x \pm i m_y)$, and L_z and S_z are the z-components of the orbital and spin angular momentum operators, respectively.

Unlike A-terms, there is no simple depiction of B-terms. They arise from magnetically induced mixing of states which were not necessarily degenerate. Like A-terms, their intensity is independent of temperature. However, unlike A-terms, B-terms exhibit absorption-shaped dispersion. Equation II.3 gives the mathematical expression of B-terms:

$$B_o = -\frac{2}{d\alpha} \sum_{\alpha,\lambda} \mathrm{Re}\left\{ \sum_{k_k \neq J} \left[\langle A_\alpha | m_- | J_\lambda \rangle^\circ \langle K_k | m_+ | A_\alpha \rangle^\circ \right.\right.$$

$$\left. - \langle A_\alpha | m_+ | J_\lambda \rangle^\circ \langle k_k | m_- | A_\alpha \rangle^\circ \right] \times \frac{\langle J_\lambda | L_z + 2S_z | K_k \rangle^\circ}{\omega_k^\circ - \omega_J} \qquad \text{eq. II.3}$$

$$+ \sum_{K_k \neq A} \left[\langle A_\alpha | m_- | J_\lambda \rangle^\circ \langle J_\lambda | m_+ | k_k \rangle^\circ - \langle A_\alpha | m_+ | J_\lambda \rangle^\circ \langle J_\lambda | m_- | K_k \rangle^\circ \right]$$

$$\left. \times \frac{\langle K_k | L_z + 2S_z | A_\alpha \rangle^\circ}{\omega_K^\circ - \omega_A^\circ} \right\}$$

where K_k is any other state which can be mixed with either A_α or J_λ when H = 0, $W_K - W_X$ is the energy difference between the two states when X = A or J, and Re is an operator which takes the real part of everything to the right.

C-terms arise from transitions which originate from a degenerate ground state. The example of a ^1P to a ^1S is given in figure II.2. Application of a magnetic field will separate the ground state into three Zeeman components. As in the case of the A-term, the maxima for the absorption of left and right circularly polarized light will be separated in frequency by $2g\beta B$. Due to the Boltzmann population over the Zeeman sublevels of the ground state, left and right circularly polarized light will not be absorbed equally. C-terms, therefore exhibit absorption-shaped dispersion. Furthermore, as the magnetic field increases, or the temperature decreases, the Boltzmann distribution will further enhance the

differential absorption, resulting in an increase in signal intensity. C-terms can be evaluated according to the following equation:

$$C_o = -\frac{1}{d\sigma} \sum_{\alpha,\lambda} \left[|\langle A_\alpha | m_- | J_\lambda \rangle^o|^2 - |\langle A_\alpha | m_+ | J_\lambda \rangle^o|^2 \right] \qquad \text{II.4}$$

$$\times \langle A_\alpha | L_z + 2S_z | A_\alpha \rangle^o$$

The relative contributions of A, B, and C terms to the total signal intensity is

$$A : B : C \approx \Gamma^{-1} : \Delta\omega^{-1} : (kT)^{-1} \qquad \text{eq. II.5}$$

where Γ is the linewidth, $\Delta\omega$ is the energy difference between the unmixed levels, k is the Boltzmann constant and T is the absolute temperature. For a room temperature transition, with a linewidth of 10^3 cm^{-1}, and an energy difference of 10^4 cm^{-1}, A:B:C~10:1:50. Upon cooling to liquid helium temperature the relative contributions become 10:1:3400. Clearly, low temperature MCD is dominated by C-terms. The degeneracy necessary for C-terms can arise either from orbital angular momentum degeneracy, or from spin angular momentum degeneracy. Transition metal centers in biology are almost invariably in low symmetry sites, and thus orbital angular momentum is almost completely quenched. Therefore, only spin angular momentum need be considered. Any small contributions from A and B-terms can be eliminated by

differencing a high temperature spectrum from a low temperature spectrum. As A and B-terms are independent of temperature, they are subtracted off, and only the enhancement of the C-terms, due to the increased population in the lowest sublevel, will remain. Variable temperature Magnetic Circular Dichroism is therefore specifically an optical probe for paramagnetic chromophores. As such it provides a valuable link between EPR and absorption spectroscopy.

SELECTION RULES

The angular momentum of a system is specified by the quantum numbers J and M_J, where J represents the total angular momentum, and M_J represents the z-component of the total angular momentum. In the absence of an external magnetic field an energy state with angular momentum J will have (2J+1)-fold degeneracy. In the presence of a magnetic field, the degeneracy is lifted, resulting in Zeeman components of energy of $g\beta BM_J$.

A circularly polarized photon has a well-defined z-component of angular momentum. For left circularly polarized light, $M_J = +1$, and for right circularly polarized light, $M_J = -1$. Absorption of circularly polarized light must be accompanied by a change in angular momentum of the chromophore. It therefore follows that the selection rules of left and right

circularly polarized light are $\Delta M_J = +1$ and $\Delta M_J = -1$ respectively.

Saturation and MCD Magnetization Curves

The above expression for a C-term applies only under conditions when the Curie law is obeyed, i.e. $\beta B << kT$. At very high magnetic fields, or very low temperatures the majority of spins occupy the lowest Zeeman sublevel. An increase in magnetic field strength, or a decrease in temperature will not lead to an increase in population in the lowest energy level, and therefore, no enhancement of the MCD signal is observed. The signal is then said to be magnetically saturated.

Detailed plots of MCD intensity, $\Delta\epsilon$, as a function of magnetic field and inverse temperature in both the Curie law region i.e. $\beta B << kT$ and at saturation i.e. $\beta B >> kT$ are termed MCD magnetization or saturation curves. To a first approximation, magnetization curves are dependent solely on the ground state. Furthermore, A- and B-terms need not be considered as they do not exhibit temperature dependence. All transitions originating from the same ground state will exhibit similar magnetization behavior, except when transitions originating from a highly anisotropic ground state exhibit markedly different polarizations. Magnetization curves can therefore be used to assign the ground states

from which electronic transitions originate. They often provide a method for deconvoluting the optical transitions in a multicomponent system. Moreover, detailed analysis of MCD magnetization curves can lead to the ground state spin and g-factors, as well as zero-field splitting parameters and/or magnetic coupling constants. Although EPR yields more accurate g-values, many systems such as most non-Kramer's systems, are not amenable to study by EPR.

Schatz, Mowery, and Krausz has written an excellent treatise on saturation theory (7). A brief summary of the relevant equations is given here.

The form of the MCD magnetization curve depends on both the effective ground state g-values and the polarization of the electronic transition. The algebraic equation used in evaluating theoretical MCD magnetization data for a randomly oriented paramagnetic chromophore exhibiting axial symmetry is:

$$\frac{\Delta\epsilon}{K} = m_+^2 \left\{ \int_0^{\pi/2} \frac{\cos^2\theta \sin\theta}{\Gamma} g_{\parallel} \tanh\left(\frac{\Gamma\beta B}{2kT}\right) \cdot d\theta \right. \qquad \text{eq. II.6}$$

$$\left. - \sqrt{2}\, \frac{m_z}{m_+} \int_0^{\pi/2} \frac{\sin^3\theta}{\Gamma} \cdot g_{\perp} \tanh\left(\frac{\Gamma\beta B}{2kT}\right) \cdot d\theta \right\}$$

where $\Delta\epsilon$ is the temperature dependent MCD intensity, K is a constant, θ is the angle between the molecular z-axis and the applied magnetic field, m_z is the transition dipole moment operator for the molecular

z-polarized transition, and $\Gamma = (g_{\parallel}^2 \cos^2\theta + g_{\perp}^2 \sin^2\theta)^{1/2}$. This expression is applicable to a transition from an isolated S = 1/2 ground state to an S = 1/2 excited state. Equation II.6 is the sum of two terms, the first of which is the contribution from the x,y-polarized component, and the second is the contribution from the z-polarized component. Since the sample consists of an assembly of molecules in a frozen glass, it is necessary to average over all angles by integration. Most iron-sulfur clusters are axial to a first approximation as the anisotropy in $g_{\perp}$ is generally small, and $g_{\perp}$ is defined as $[(g_x^2+g_y^2)/2]^{1/2}$.

By inspection of equation II.6, it is apparent that magnetization data for an axial chromophore can vary as a function of the wavelength of measurement as a result of varying amounts of z- and x,y- polarized transitions. There are, however, three special cases where the form of the magnetization data will be independent of the wavelength of measurement. The first case is where the electronic spectrum is dominated by transitions of a particular polarization, e.g. x,y-polarized transitions from porphyrin in hemes. In this instance, the second term of equation II.6 can be neglected.

The second case is an isotropic ground state, such that $g_{\parallel} = g_{\perp} = g$. In this instance equation II.6

simplifies to:

$$\frac{\Delta\epsilon}{K} = \frac{1}{3} m_+^2 \left(1 - 2\sqrt{2}\,\frac{m_z}{m_+}\right) \tanh\left(\frac{g\beta B}{2kT}\right) \qquad \text{eq. II.7}$$

The polarization ratio, m_z/m_+, attenuates the MCD intensity, but does not alter the form of the magnetization curve. Equation II.7 is applicable for analyzing magnetization data from S=1/2 ground states, which exhibit small g-value anisotropy.

The final special case that needs to be considered is an axial ground state doublet in which $g_{\parallel} \neq 0$, and $g_{\perp} = 0$. This type of doublet can arise as a result of axial zero field splitting of non-Kramers' ground state with S>0. Under these conditions, equation II.6 reduces to:

$$\frac{\Delta\epsilon}{K} = m_+^2 \int_0^{\pi/2} \cos\theta \sin\theta \cdot \tanh\left(g_{\parallel}\frac{\cos\theta\,\beta B}{2kT}\right) \cdot d\theta \qquad \text{eq. II.8}$$

As expected, when $g_{\perp} = 0$, all temperature-dependent MCD transitions from the ground state become x,y-polarized and the magnetization data becomes independent of wavelength.

The above equations are only rigorously valid for analyzing magnetization curves arising from transitions between isolated S=1/2 states. When a paramagnet contains more than one unpaired electron, the interaction

between the unpaired electrons and the ligand field results in the removal of the spin degeneracy even in the absence of a magnetic field. This splitting is termed zero field splitting (8,9).

Zero field splitting can be accommodated into the electronic spin Hamiltonian, H_e, by means of additional terms and parameters:

eq. II.9

$$H_e = g_o \beta \vec{B} \cdot \vec{S} + D\left(S_z^2 - S(S+1)/3\right) + E\left(S_x^2 - S_y^2\right)$$

where D and E are the axial and rhombic zero field splitting parameters, respectively. For completely rhombic symmetry E/D = 1/3. The sign of D depends on the type of axial distortion, i.e. elongation or compression. Changing the sign of D results in a reversal of the splitting pattern.

According to Kramers' rule, in the absence of a magnetic field, a paramagnet with an odd number of unpaired electrons will always exhibit at least two-fold degeneracy, regardless of symmetry. Therefore, this type of paramagnetic will always have at least a doublet as its lowest energy level. These doublets are called Kramers' doublets. For example, an S = 5/2 ground state will be split into three Kramers' doublets, M_S $\pm 1/2$, $\pm 3/2$, and $\pm 5/2$, by an axial ligand field with the separation between the doublets being 2D and 4D

respectively. A pictorial representation of the effect of increasing the zero field splitting in a S = 5/2 system is given in figure II.3. For a paramagnet with an even number of unpaired electrons, i.e. integer spin, a low symmetry ligand field can completely remove the degeneracy, even in the absence of a magnetic field. This can result in a singlet lying lowest in energy. Such systems are often refered to as "non-Kramers'" systems. The energy diagram for an S = 2 ground state exhibiting axial, E = 0, and near rhombic symmetry, E = 0.3 cm^{-1} and D = -2 cm^{-1}, is given in figure II.4.

Complete analysis of magnetization data for any S > 1/2 system presents a complex theoretical problem which requires inclusion of many additional parameters, e.g. D and E, effective g-values for each doublet, and the fractional population of each of the sublevels. Preliminary analysis of the data can be made by fitting the magnetization data only at the lowest temperature (in this work approximately 1.5 K), so that only the lowest doublet is significantly populated. The appropriate equation can then be used to determine the g-values and transition polarizations for the lowest lying doublet only. It should be noted that any field induced mixing of the zero-field components is neglected in this analysis. Furthermore, axial or higher symmetry is

assumed. By assessing the magnitude of the zero-field splitting parameter, via the temperature dependence of a discrete MCD transition (see below), the validity of all but the final assumption can be evaluated.

Ground state g-values can be obtained from experimental data either by fitting the data by non-linear regression to the appropriate equation, or by simulating the data using theoretical parameters. The latter approach was adopted in this work. Software for the simulation of magnetization curves and the plotting of experimental data was written by M. K. Johnson and D. E. Bennett for use on the BMC model 30 microcomputor, and given in Appendix I. As equations II.7 and II.8 cannot be solved analytically, they are approximated by the method of quadratures for numerical integration.

Determination of Zero-Field Splitting Parameters via Low Temperature MCD

It is often possible to determine the separation between energy states from the temperature dependence of an MCD transition (10-12). In practice, low temperature MCD can only be used to evaluate the energies of low lying excited states, higher states are not thermally accessable over the range of temperatures employed, e.g. 1.5-100 K. If the excited state lies outside this region, only the lower limit of the energy separation can be

obtained.

The following discussion is adapted from the treatise of Browett *et al*. Browett, however, deals solely with an S = 5/2 system. The MCD intensity defined in equation II.1 can be written as:

$$\Delta\epsilon = \sum_{i=1}^{n} \left(a_i + b_i + \frac{c_i}{kT}\right)\alpha_i \qquad \text{eq. II.10}$$

where a_i, b_i, and c_i are the contributions from the ith doublet to the total terms $A_1(\partial f/\partial \nu)$, $B_0 f$, and $C_0 f$, respectively, and α_i is the fractional population of state i. As previously stated, A and B-terms are independent of temperature and therefore can be omitted provided diamagnetic contributions are insignificant compared to the paramagnetic C-terms. Equation II.10 then becomes

$$\Delta\epsilon = \sum_{i=1}^{n} \left(\frac{c_i}{kT}\right) a_i \qquad \text{eq. II.11}$$

The fractional population will be dependent upon the absolute temperature and the energy separation according to the Boltzmann distribution, given in equation II.12

$$a_i = \frac{e^{-E_i/kT}}{\sum_{i}^{n} e^{-E_i/kT}} \qquad \text{eq. II.12}$$

where E_i is the energy difference between the ground and

the ith state. Hence the energy separation can be evaluated using nonlinear regression to fit the experimentally observed MCD intensity as a function of temperature to equation II.11. This regression can be constrained by consideration of two extreme conditions. The first condition exists when the energy separation is very much greater than kT, i.e. when only the lowest doublet is populated. In this case equation 11 reduces to

$$\Delta\epsilon = \frac{C_i}{kT} \qquad \text{eq. II.13}$$

In the second case the energy separation is much smaller than kT and all doublets are virtually, equally populated. In which case

$$\Delta\epsilon = \frac{C_1 + C_2 + \cdots C_n}{nkT} \qquad \text{eq. II.14}$$

The zero field splitting parameter is readily obtained since E_i values will be some multiple of D. The fractional populations, (Boltzmann coefficients), will be explicitly defined for two ground states, which are investigated in this work. Other states are easily derived from a knowledge of the ground state physics.

The fractional populations for any system with three distinct energy levels are given by:

$$\alpha_1 = 1/(1 + e^{-XD/kT} + e^{-YD/kT}) \qquad \text{eq. II.15}$$

$$\alpha_2 = e^{-XD/kT}/(1 + e^{-XD/kT} + e^{-YD/kT})$$

$$\alpha_3 = e^{-YD/kT}/(1 + e^{-XD/kT} + e^{-YD/kT})$$

For a rhombic system in which S = 5/2 and D > 0, X = 3.5 and Y = 7.0 (13) (fig.IV.5). An axial system, in which S = 2, and D < 0 has X = 3, and Y = 4 (10) (fig.II.4).

In light of the previous discussion on magnetization curves, it is apparent that the MCD intensity will be dependent on the polarization. In order to minimize the number of c_i terms in equation II.11, it is necessary to utilize only those transitions which are uniquely polarized in this analysis. Furthermore, it is also crucial that this analysis be conducted at low magnetic field strengths, since the above treatment is only applicable in the Curie law limit. The use of small magnetic fields will also minimize the amount of field induced mixing of the energy states, and will also lead to an estimation of the axial splitting parameter, which is nearly equal to the value at zero field.

The zero field splitting parameters were evaluated by varying the c_i terms and D of equation II.11 to yield the optimal fit to the experimental data. Any solutions

which did not meet the constraints of equations II. 12 and 13 were discarded. The regression software used was IMSL ZXSSQ as adapted by Robert Zinn for an IBM 3033 mainframe.

2.2 Electron Paramagnetic Resonance

Electron Paramagnetic Resonance (EPR) is the absorption of microwave radiation by paramagnets in an applied magnetic field. It is a highly sensitive and selective technique. As all known iron-sulfur clusters exhibit paramagnetism in at least one oxidation state, EPR is a very powerful tool for the investigation of such paramagnetic clusters. EPR studies of iron-sulfur proteins can yield the following information: 1) identification of the type and valence state of the cluster, 2) characterization of the spin state, S, for the electronic ground states, 3) assessment of the zero field splitting parameters for systems with S > 1/2, 4)

assessment of the anisotropy of the g-tensor, and hence the symmetry of the electron moment, and 5) quantitation of the number of unpaired electrons contributing to a given signal. Thus, EPR spectroscopy is both a useful method for identifying and characterizing iron-sulfur clusters, and a means of investigating the detailed physics of the electronic ground state of the paramagnetic clusters. General reviews on EPR theory can be found in references 10 and 14. References 15-17 emphasize the application of EPR to the study of iron-sulfur proteins. A brief summary of EPR theory follows here.

Basic theory

An unpaired electron will align either with or against an applied magnetic field. The energies of the two states are:

$$\omega = g\beta B \cdot m_s \qquad \text{eq. II.16}$$

where W is the energy, g is the gyromagnetic ratio or g-value, β is the Bohr magneton, B is the magnetic field strength, and M_S is the quantum number for a spin quantized about the magnetic field axis, e.g. $M_S = \pm 1/2$ for an unpaired electron, S = 1/2. The energy difference, ΔW, between the two levels for an S = 1/2 ground state

is then given by:

$$\Delta\omega = g\beta B \qquad \text{eq. II.17}$$

In order for resonance to occur, the energy difference must be equal to the applied energy, which for electrons is generally in the microwave region,

$$\Delta\omega = g\beta B = h\nu \qquad \text{eq. II.18}$$

where h is Plank's constant, and is the frequency (fig. II.5). If is expressed in GHz and B is in gauss, then the numerical expression for the observed g-value is given by:

$$g = \frac{714.5\nu}{B} \qquad \text{eq. II.19}$$

The selection rule for absorption of microwave radiation is $\Delta M_S = \pm 1$.

g-value anisotropy for S = 1/2 systems

For systems with negligible effective orbital angular momentum, g is equal to the free electron value of 2.0023 (14). Although the ground state orbital angular momentum of most first row transition metals is quenched, as a result of low symmetry, significant deviations from the free electron value are still commonly observed.

This is due to the mixing of a low-lying excited state by spin-orbit coupling. The spin-orbit Hamiltonian is given by:

$$\hat{H}_{S.O.} = \lambda(\hat{S}.\hat{L}) \qquad \text{eq. II.20}$$

where $\hat{S}$ and $\hat{L}$ are the spin and orbital angular momentum operators, respectively and λ is the spin-orbit coupling constant. The magnitude of the spin-orbit coupling will be determined by the symmetry and the energy separation of the ground and the excited states. Since, this coupling often has a spatial dependence, the value of g in a given direction depends on the orientation relative to the applied magnetic field, and therefore, the g-value is a third rank tensor. By prudent selection of an orthogonal coordinate system, the off-diagonal elements can be made to vanish, and the system can be defined by the diagonal or principal g-values, g_{xx}, g_{yy}, g_{zz}. These principal g-values are often abbreviated as g_x, g_y, and g_z.

In an anisotropic system, the resonant field is related to the orientation of the molecular axes with respect to the applied magnetic field. Three basic types of symmetry, isotropic, axial, and rhombic, as defined in chapter II.1, will be considered here. In isotropic symmetry, the principal g-values are all equivalent,

i.e. $g_x = g_y = g_z$, and only a single resonant line is observed, regardless of sample orientation. Two resonant fields are observed for axial systems in which $g_x = g_y \neq g_z$. These are designated as $g_\perp = g_z$ and $g_\parallel = g_x$ and g_y. Finally a rhombic system will give rise to three resonances, corresponding to g_x, g_y, and g_z.

The g-values can be obtained directly from EPR studies of single crystals or oriented solids, by monitoring the signal as a function of the angle of the crystal axis relative to the applied field. Most biological samples are, however, generally in the form of a glass or powder, i.e. the molecules are randomly oriented. Nevertheless, it is still possible to obtain the principal g-values for such a sample. Isotropic systems are independent of orientation, by definition, and therefore, an isotropic glass is no different than a single crystal. The EPR absorption spectrum of an isotropic paramagnet is given in figure II.6a. In order to enhance the perception of small features in the spectra, EPR spectra are most often depicted as the first derivative of the absorption spectra. All EPR spectra in this work are presented in this manner unless otherwise stated. The first derivative of figure II.6a is given in figure II.6b.

An axial system can be described by $g_\perp$ and $g_\parallel$. In

a randomly oriented glass there are more possible orientations that have the plane corresponding to $g_\perp$ parallel to the applied magnetic field, than those which have an axis defined by $g_\parallel$ aligned parallel to the applied magnetic field. If $g_\parallel > g_\perp$, the absorption will occur at all fields between $B_{min} = (h\nu)/(g_\parallel \beta)$ and $B_{max} = (h\nu)/(g_\perp \beta)$. Since all orientations are equally probable, the largest absorption will occur at B_{max}. The absorption spectrum for this system, and the corresponding first derivative spectrum, is given in figure II.6c and d. The analogous spectra, with $g_\perp < g_\parallel$ are depicted in figures II.6e and f. Similar arguements apply to rhombic systems, resulting in the spectra given in figures II.6g and h.

Factors which broaden and split the EPR spectra of S = 1/2 systems

Figure II.6 represents idealized spectra. In reality, several phenomena lead to EPR spectra which differ markedly from those depicted. The most important of these phenomena, in regards to this work, are nuclear hyperfine interaction, relaxation broadening, and spin-spin interaction.

Nuclear hyperfine interaction refers to the interaction of the electron spin magnetic dipole with nearby nuclei, which possess nuclear spin angular

momentum, i.e. $I \neq 0$. The local magnetic field arising from the magnetic moment associated with the nuclear spin angular momentum will either oppose or augment the applied magnetic field, thereby splitting the electronic Zeeman levels by a factor of 2I+1. This hyperfine interaction may be anisotropic, leading to very complex spectra. Splittings due to hyperfine interactions are not, however, observed for iron-sulfur clusters (except in the event of isotopic enrichment). ^{56}Fe, natural abundance, 97.8%, has a nuclear spin of 0. ^{57}Fe, I=1/2, will slightly broaden the iron-sulfur cluster spectra, although this effect will be small due to a low magnetogyric (g_n) ratio, 0.08644×10^{-4} rad G^{-1} (14). Nuclear hyperfine interactions were observed for the Cu-EDTA standard, as both ^{63}Cu and ^{65}Cu have nuclear spins of 3/2, natural abundances of 69% and 31% respectively, and g_n values of approximately 0.7×10^{-4} rad G^{-1} (14). Hyperfine splitting was also observed for the molybdenum signal from E. coli nitrate reductase (chapter VI) arising from both the molybdenum (^{95}Mo, 15.72% natural abundance, I = 5/2, g_n=0.17428×10^{-4} rad G^{-1}, ^{97}Mo, 9.46% natural abundance, I = 5/2, g_n=-0.17796×10^{-4} rad G^{-1}) and from a nearby proton (^{1}H, 99.9% natural abundance, I = 1/2, g_n=2.67510×10^{-4} rad G^{-1}) (14).

Relaxation broadening arises from two processes: 1) temperature broadening, and 2) power saturation. The former is as a consequence of the Heisenberg Uncertainty Principle, which requires that the linewidth of the signal be inversely proportional to the relaxation time. Since transition metal complexes generally have short relaxation times, due to the presence of low lying excited states, they often exhibit very broad EPR spectra. Relaxation can be slowed by decreasing the temperature and thereby reducing the thermal motion. Hence, iron-sulfur clusters are generally studied at cryogenic temperatures i.e. 1.5 to 100 K, as they give rise to signals which are too broad to be observed at room temperature. Lowering the temperature has the additional benefit of increasing the differential population of the Zeeman levels, resulting in an increase in signal intensity.

Microwave power saturation occurs when the incident radiation becomes sufficiently intense, such that the rate of promotion of the spins to the upper state exceeds the rate at which spins can relax to the lower state. This will result in nearly equal populations of spins in the ground and excited states, precluding any net absorption. In contrast to temperature broadening, power saturation occurs at low temperatures which are conducive

to longer relaxation times.

Spin-spin interactions are only pertinent to those metalloproteins which contain more than one paramagnet. Due to the large protein matrix, metalloproteins are necessarily magnetically dilute, therefore, interactions generally occur only between centers of the same protein molecule. Spin-spin interactions can have two effects on an EPR spectrum. First, spin-spin interaction leads to enhanced relaxation, and hence different power saturation characteristics. Second, dipolar coupling between the spins can lead to a splitting or broadening of the EPR spectrum, in much the same manner as the hyperfine interaction, discussed above. Spin coupled spectra may be very complex (see C. pasteurianum Fd, chapter IV.2), depending on the distance of the two paramagnets, the orientation, and the anisotropy of the two spin systems.

S ≥ 1/2 systems

For systems with more than one unpaired electron, interpretation of the EPR spectrum requires the addition of two more parameters, D, the axial distortion, and E, the rhombic distortion, which describe the zero field splitting (see section 1 of this chapter). For systems of intergral spin, i.e. non-Kramers' systems, the presence of zero field splitting will frequently lead to a separation between the energy states which is larger

than the incident radiation. Thus, EPR spectra are not generally observed for these systems. A Kramers' system, on the other hand, must always have a degenerate ground state, in the absence of a magnetic field, regardless of symmetry considerations. The spin Hamiltonian which describes the zero field splitting for systems with $S > 1/2$, is given by equation II.9. Since the microwave energy (9-10 GHz for X-band) is generally smaller than the zero field splitting, in iron-sulfur proteins, EPR transitions will only occur within each doublet and not between them (17). In order to simplify analysis of these systems, each doublet can be considered as an effective $S = 1/2$ system. The spin Hamiltonian for each doublet is:

$$H' = \beta B \cdot g' \cdot S' \qquad \text{eq. II.21}$$

where g' is the effective g-value for the doublet, and $S' = 1/2$. At high frequencies or large applied magnetic fields, mixing of the energy levels may occur, inducing field and frequency dependence in the effective g-value. Figure II.9 depicts the energy level diagram for an $S = 5/2$ system, for an axial (a) and a rhombic system (b). The effective g-values for each doublet, obtained from application of the spin Hamiltonian, for $E/D = 0$, and $E/D = 1/3$, respectively are given in the figure. The

intensity of the signal arising from each doublet is dependent on the fractional population. Therefore, spectra arising from systems with S > 1/2 are temperature dependent as a result of the relaxation broadening, discussed above, and the Boltzmann distribution (see C. pasteurianum Rd, chapter IV.1).

Quantitation of EPR spectra for S = 1/2 systems

The intensity of the EPR absorption signal is proportional to the number of unpaired electrons in the the sample, provided the sample is not power saturated. While it is not possible to correlate the absolute intensity to the spin concentration, very accurate quantitations can be obtained by comparison to a standard, run under identical conditions, of temperature, modulation amplitude, and microwave power. EPR spectra, which are obtained as the first derivative of the absorption, must be double integrated. The method used for double integration of EPR spectra was derived by Wyard (18) and the area is corrected for g-value dependence according to Aasa and Vanngard (19). The spin concentration of a sample is equal to:

eq. II.22

$$C_S = \left(\frac{A_s}{A_r}\right)\left(\frac{G_r}{G_s}\right)\left(\frac{g_r}{g_s}\right)\left(C_r\right)$$

where A is the area under the curve, obtained by double

integration and equal to :

eq. II.23

$$A = \frac{1}{2} h^2 \sum_{\ell=1}^{n} (n-2\ell+1) Y_\ell$$

c is the spin concentration, G is the spectrometer gain, g is equal to

eq. II.24

$$g = \frac{2}{3}\left\{(g_x^2 + g_y^2 + g_z^2)/3\right\}^{1/2} + \frac{1}{3}(g_x + g_y + g_z)/3$$

the subscripts r and s refer to reference and sample, respectively, h is the magnetic field interval, and y_1 is the magnitude of the EPR signal for the 1th integral.

Aasa and Vanngard have also formulated a method for obtaining the total intensity of an EPR spectrum from a single, isolated absorption-shaped component of an anisotropic resonance, provided the line width is smaller than the g-value anisotropy (18). This method is of great utility for integrating spectra which have broad high field resonances, or for which the entire spectrum is not available, due to interference from overlapping signals. Equation II.22 is still valid, but in this case the absorbance A, of the species which was integrated using only part of the total EPR spectrum is equal to:

eq. II.25

$$A = h \sum_{\ell=1}^{n} y_\ell$$

and g is given by:

$$g = \frac{(g_x^2 + g_y^2)}{g_z \times B_{max} \times [(1-\rho_x)(1-\rho_y)]^{1/2}}; \quad \rho_i = \frac{g_i^2}{g_z^2} \qquad \text{eq. II.26}$$

For temperatures between 100 and 20 K, a 1 mM solution of copper EDTA was used as the reference, and equations II.22-24 were used. Due to power saturation of the copper EDTA at temperatures below 20 K, it was necessary to employ a second standard, metmyoglobin cyanide. The g_x and g_y absorbances of metmyoglobin cyanide are very broad, and therefore the intensity of these absorbances are difficult to measure accurately. The intensity of the metmyoglobin cyanide was evaluated using equations II.22, 25-26.

The intensities were measured manually. The number of spins were then computed using an OKI IF model 30 microcomputer, with software written by M.K. Johnson and D.E. Bennett and given in appendix I. Prior to the quantitation of any unknown protein samples, the instrumentation and the method were calibrated by quantitating known solutions of metmyoglobin cyanide and cytochrome c against a known solution of copper EDTA. In all instances the precision was within 1%, and the accuracy within 5%. The accuracy of the less concentrated protein samples was estimated to be well within 10%,

unless otherwise stated. Care was taken to ensure than neither the sample, nor the reference was saturated.

References

1. Faraday, M., (1933) in "Faraday Diary" Vol. IV, G. Bell and Sons, London

2. Schatz, P.N. and McCaffery, A.J., (1969) Quart. Rev. 23, 552-584

3. Stephens, P.J., (1976) Adv. in Chem. Phys. 35, 197-264

4. Stephens, P.J., (1974) Ann. Rev. Phys. Chem. 25, 201-232

5. Buckingham, A.D., and Stephens, P.J., (1966) Ann. Rev. Phys. Chem. 17, 399-432

6. Stephens, P.J., (1976) J. Chem. Phys. 52, 3489-3516

7. Schatz, P.N., Mowery, R.I., and Krausz, E.R., (1978) Mole. Phys. 35, 1537-1557

8. Palmer, G., (1985) Biochem. Soc. Trans. 13, 548-560

9. Drago, R.S., (1977) in "Physical Methods in Chemistry", Chapters 9, 10, and 13, W.B. Saunders Co, Philidelphia

10. Thompson, A.J., Cammack, R., Hall, D.O., Rao, K.K., Briat, B., Rivoal, J.C., and Badoz, J. (1977), Biochim. Biophys. Acta 493, 132-141

11. Rivoal, J.C., Briat, B., Cammack, R., Hall, D.O., Rao, K.K., Douglas, I.N., and Thompson, A.J., (1977) Biochim. Biophys. Acta 493, 122-131

12. Browett, W.R., Fucaloro, A.F., Morgan, T.V., Stephens, P.J., (1983) J. Am. Chem. Soc. 105

13. Blumberg, W.E., and Peisach, J. (1979) Annal. N.Y. Acad. Sci., 222, 539-560

14. Wertz, J.E., and Bolton, J.R. (1972) in "Electron Spin Resonance" McGraw Hill, New York

15. Fee, J.A. (1978) Methods Enzymology 49, 512-522

16. Orme-Johnson, W.H., and Sands, R.H., (1973) in "Iron-Sulfur Proteins" Vol. II (Lovenberg, W., ed.) chapter 5, Academic Press, New York

17. Wyard, S.J., (1965) J. Sci. Instrum. 42, 769-770

18. Aasa, R., and Vanngard, T., (1975) J. Mag. Res. 19, 208-215

19. Smith, T.D., and Pilbrow, J.R. (1980) in "Biological Magnetic Resonance" (Berliner, L.J, and Reuben, J. eds.) pp. 85-153, Plenum Press, New York

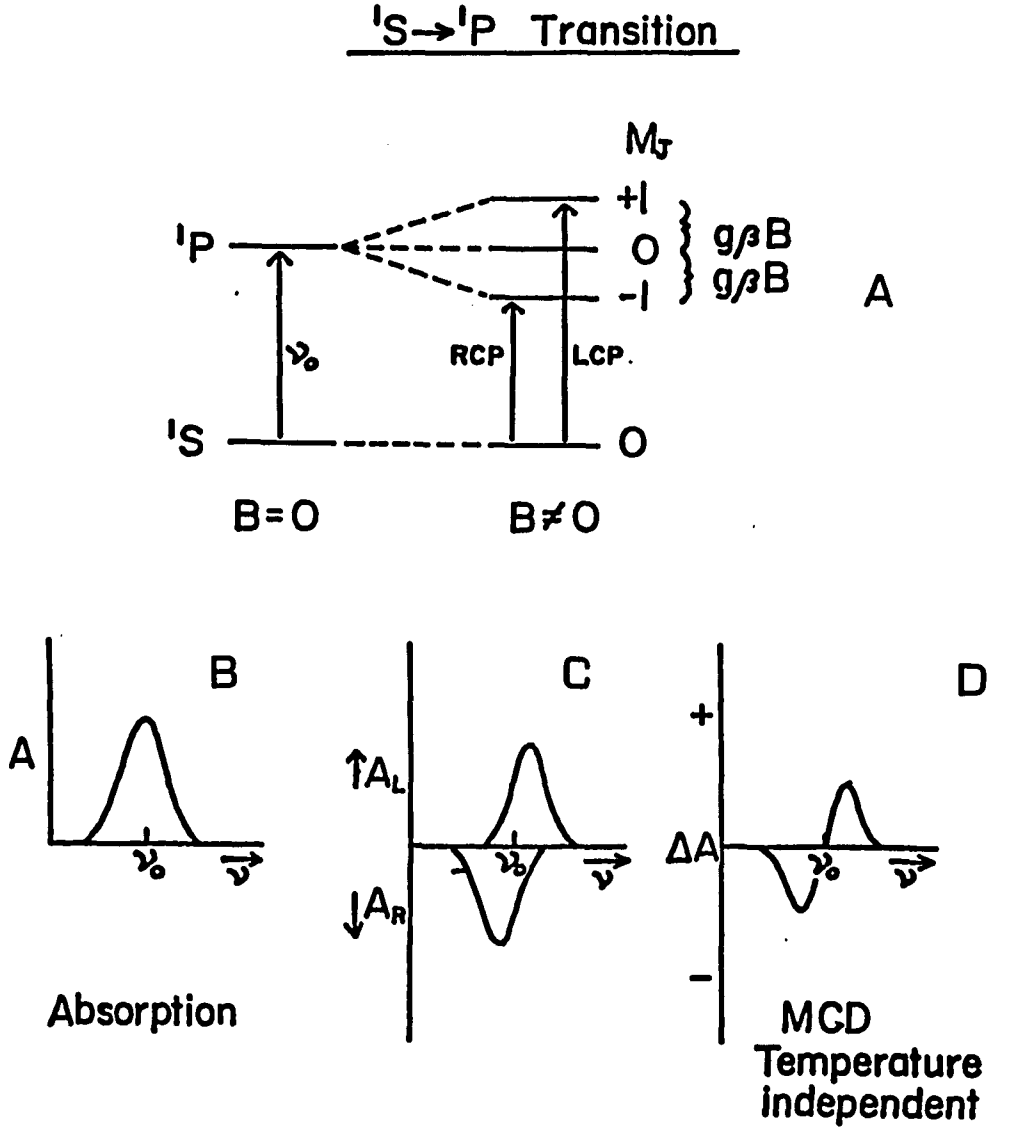

Figure II.1 Depiction of a MCD A-term for an atomic ^1S to ^1P transition. (a) energy level diagram (b) absorption spectrum (c) absorption spectra corresponding to the absorption of left and right circularly polarized light (d) MCD spectrum

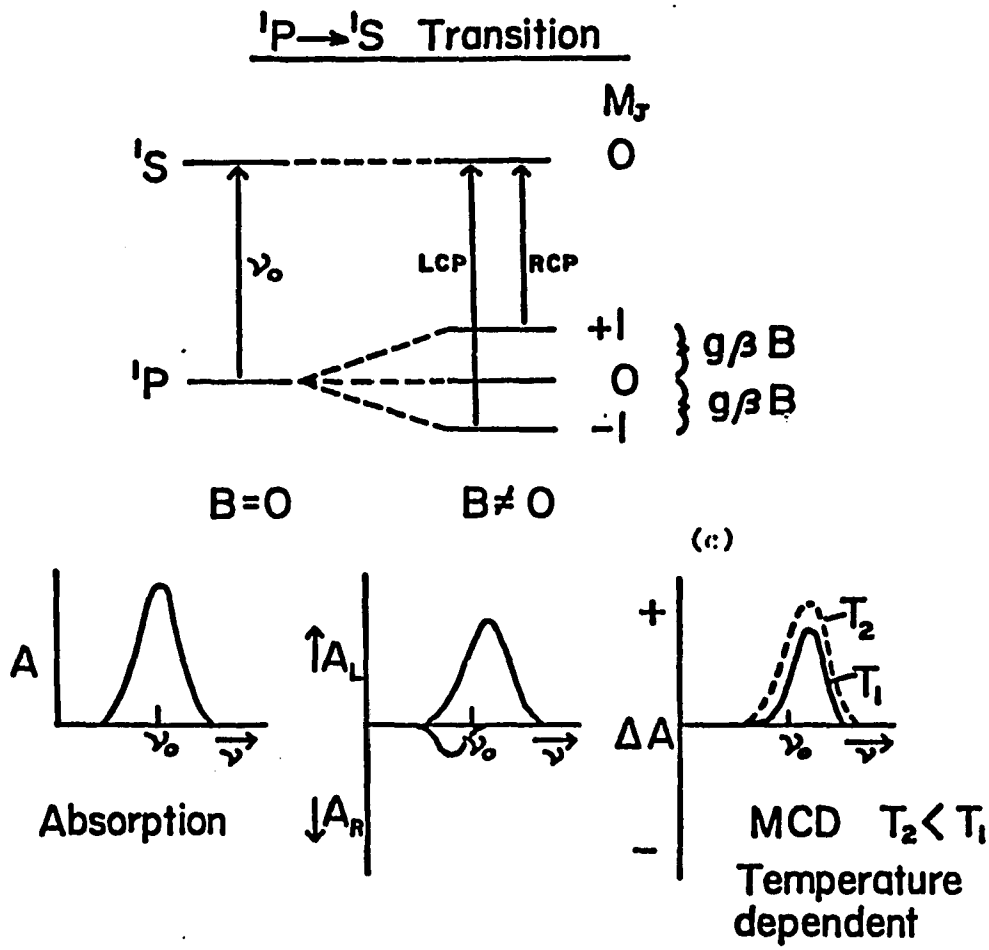

Figure II.2 Depiction of a MCD C-term for an atomic ^1P to ^1S transition. (a) energy level diagram (b) absorption spectrum (c) absorption spectra corresponding to the absorption of left and right circularly polarized light (d) MCD spectrum

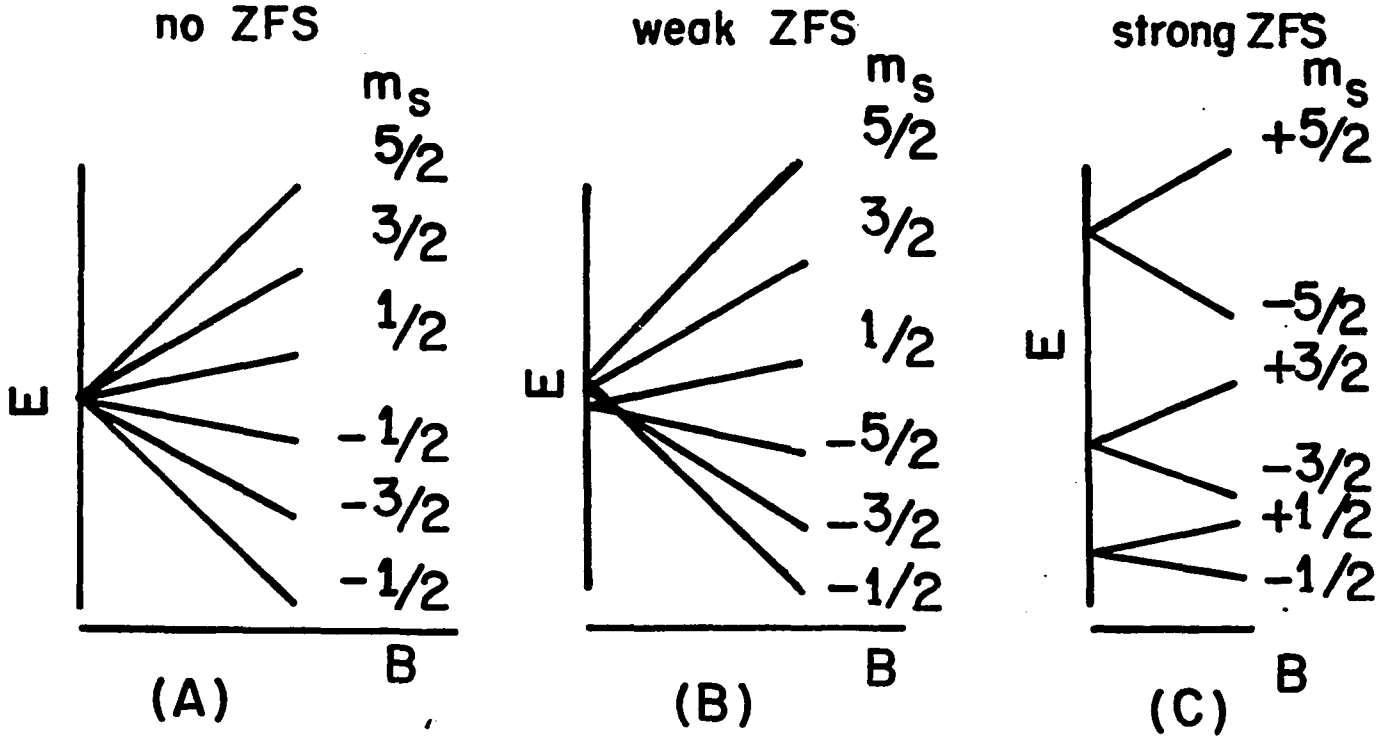

Figure II.3 The effect of increasing the zero field splitting on a S=5/2 system. (a) no zero field splitting (ZFS) (b) weak axial zero field splitting (c) strong axial zero field splitting

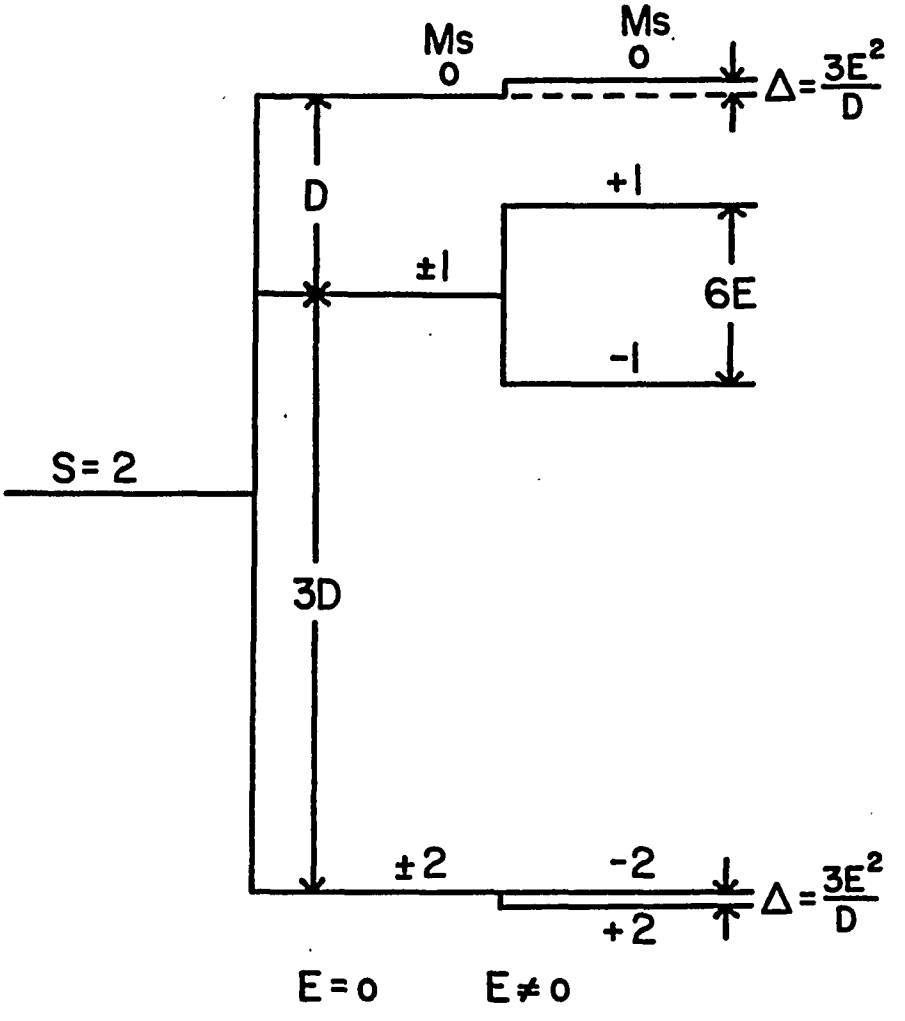

Figure II.4 Energy level diagram for an S=2 ground state. Axial (E=0), and rhombic (E≠0), zero field splitting for D < 0 are depicted. The energy levels for the rhombic case are drawn to scale for E = 0.3 cm^{-1} and D = -2.0 cm^{-1}.

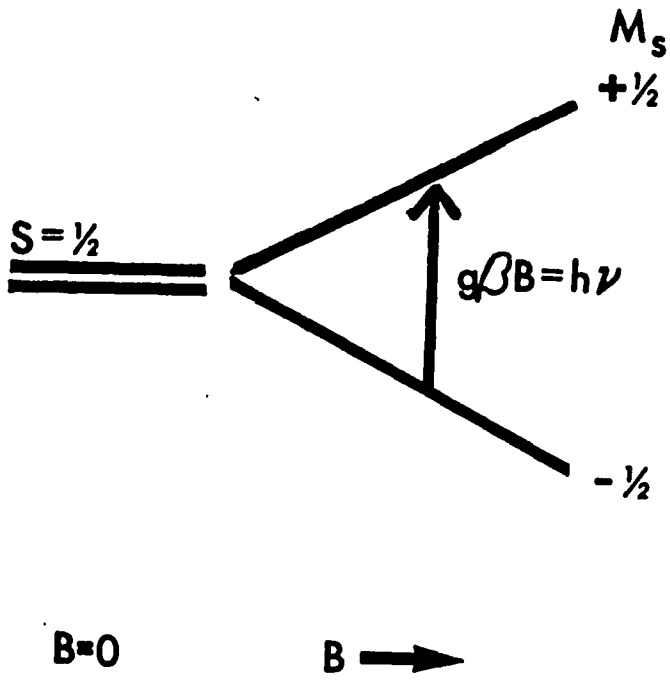

Figure II.5 Energy level diagram for an S=1/2 ground state in the presence and absence of an applied magnetic field. The arrow indicates absorption of microwave radiation corresponding to the EPR transition.

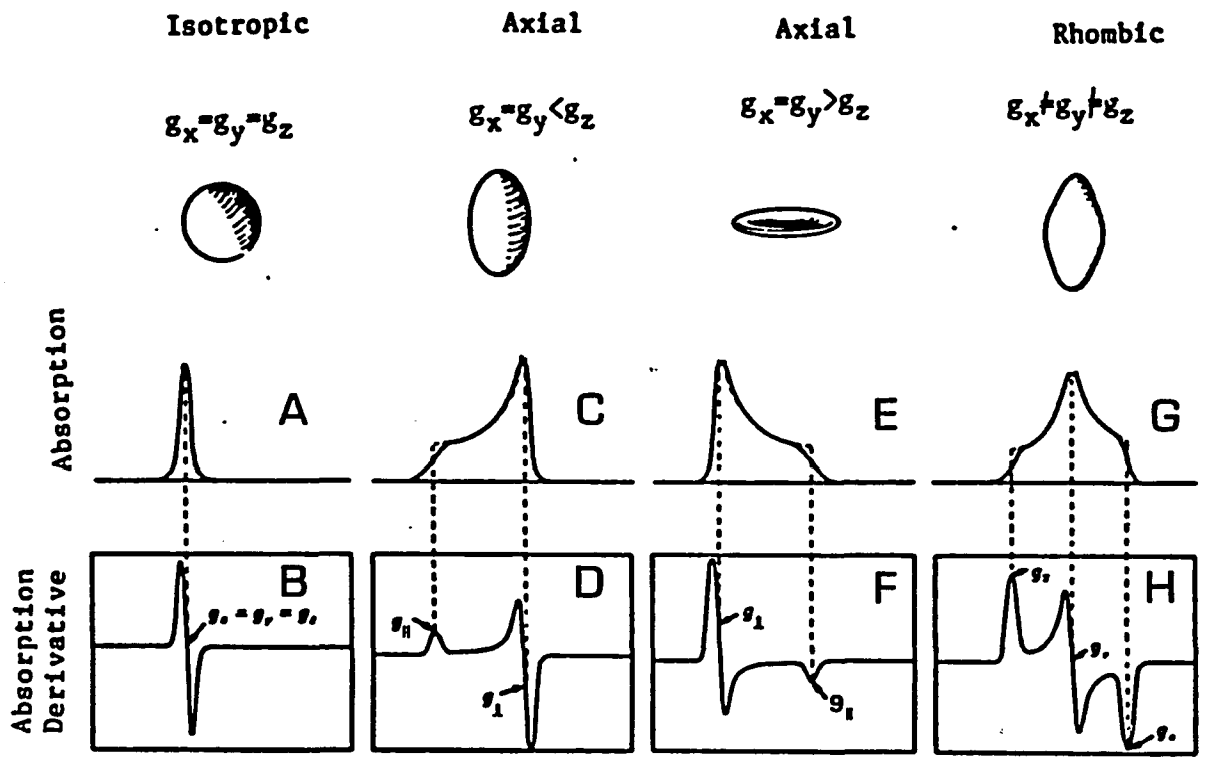

Figure II.6 **Idealized powder EPR spectra for an isotropic, axial, and rhombic, S = 1/2 system** (a) EPR absorption spectrum for an isotropic system (b) first derivative of the isotropic EPR absorption spectrum (c) EPR absorption spectrum for an axial system with $g_{\parallel} > g_{\perp}$ (d) First derivative of the axial EPR absorption spectrum "c" (e) EPR absorption spectrum for an axial system with $g_{\perp} > g_{\parallel}$ (f) first derviative of the axial EPR absorption spectrum shown in (e) (g) EPR absorption spectrum of a rhombic system (f) First derivative of the rhombic EPR absorption spectrum.

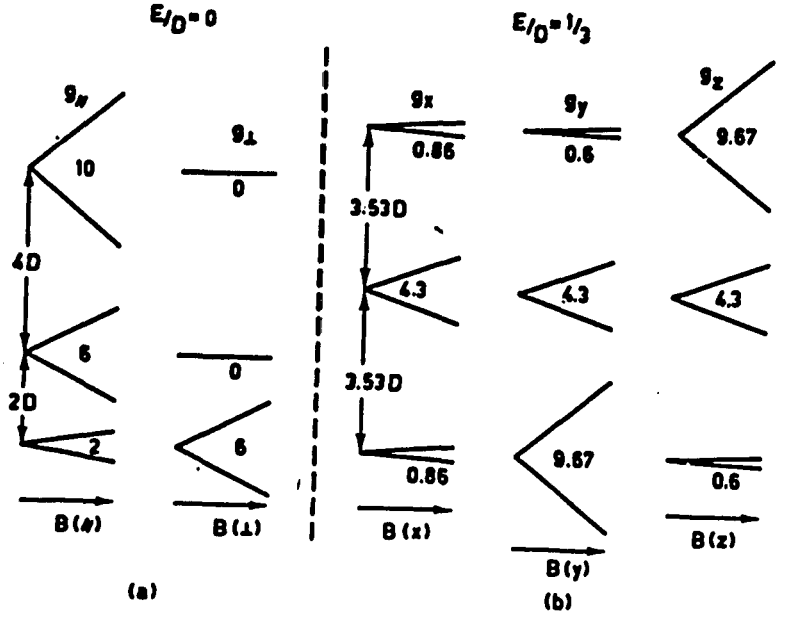

Figure II.7 The energy level diagram for an S=5/2 system with axial and rhombic symmetry. The effective g-values for each of the doublets are given in the figure. The figure is taken from reference 19.

Chapter 3

Materials and Methods

3.1 Instrumentation

3.1.1 MCD

Spectropolarimeter

The MCD spectropolarimeter used is comprised of a Jasco J500C spectropolarimeter mated to a superconducting magnet (fig. III.1). The Jasco J500C employs a xenon arc lamp as the source. The radiation is then passed through a conventional double monochrometer and a linear polarizer. Subsequently, a photoelastic modulator alternately generates left and right circularly polarized light from plane polarized light at a frequency of 50 kHz. The circularly polarized light is transmitted directly through the magnet and the sample contained therein, and finally to the photomultiplier tube (PMT). The PMT is locked into this frequency to obtain the differential absorption of left and right circularly

polarized light. Use of a phase-sensitive detector also increases the signal-to-noise ratio. The polarimeter, magnet, and the PMT were aligned using an optical rail, with the direction of light propagation being parallel to the magnetic field. Both the PEM and the PMT were separated from the magnet in space by at least one meter in order to minimize any magnetic effects on the electronics. An optical tube provided a path for the propagation of the applied radiation. The optical tube was rigidly fixed in position, to ensure maximal light intensity impinging on the PMT. The divergence of the light beam upon passage down the length of the tube was negligible, therefore a refocusing lens was not required. Placement of the magnet in the optical path did not have any significant effect on the signal intensity of the standard sample. This system is capable of recording spectra in the range of 200-1000 nm, at fields between 0 and 5 tesla, and at temperatures between 1.5 and 200 K.

Magnet and Probe

The magnet used was an Oxford SM3 split coil superconducting magnet, capable of obtaining magnetic fields up to 5 tesla. A schematic of the magnet is given in figure III.2. The magnet is comprised of dual coils of

Nb-Ti filament, immersed in a 5 liter helium bath. The helium is insulated by a 4.7 liter nitrogen jacket, and a vaccuum compartment. A needle valve connects the sample chamber to the main helium can. The magnet was equipped with an Oxford Instruments MK3 power supply. Magnetic fields were ramped in using an Oxford Instruments SG3 sweep generator. The magnetic fields at the sample were measured using a calibrated transverse Hall probe (Lake Shore Cryogenics) mounted in place of the sample on the sample probe. The magnet current field was digitally measured as a voltage across a two milliohm resistor, using a Dynasan Corporation 2830 Digital multimeter connected directly to the magnet power supply. The magnetic current versus field plot was found to be linear over the entire range 0-5 tesla, with 1 mV equal to 0.0546 tesla. Magnetic fields cited are accurate to within 0.03 tesla and are given in the figure legends. The sample probe, with the sample positioned at the bottom, is placed directly down the center of the magnet (fig III.3). Directly above the sample is a copper block which contains a calibrated carbon glass resistor and a Rh/Fe resistor. A second carbon glass resistor is placed directly below the sample. The carbon glass resistors, which were used to obtain temperature measurements, were accurate to within 0.5%. The temperature was read as a

function of voltage at a given constant current. Coefficients for a tenth order polynomial describing the resistance of the carbon-glass thermistors as a function of temperature were either provided by Lake Shore Cryogenics or computed using an IBM computer and the IMSL ZXSSQ routine as adapted by Robert Zinn. These coefficients were then incorporated into software written by Michael Johnson for the Oki IF 30 microcomputer. The Rh/Fe resistor was used to control the temperature (see below).

Temperatures between 1.4-2.2 K were obtained by reducing the pressure with a two-stage rotary pump. Spectra were not collected between liquid helium temperature and the lamba point due to the light scattering caused by the excessive bubbling. Temperatures above 4.2 K were obtained by passage of a flow of cold helium gas, controlled by a Rh/Fe resistor and a heater connected to an Oxford Instruments DTC2 temperature controller.

Sample cells

Sample cells were constructed from 1.5 cm^2 square plates of optical quality quartz, separated by a rubber spacer. Aerobic cells were sealed on three sides by epoxy resin. Anaerobic cells were sealed on all four

sides, expect for two small corners for sample injection. All anaerobic cells were repeatedly pumped and flushed with oxygen-scrubbed argon gas immediately prior to sample injection. The pathlength of each cell was determined by subtracting the thickness of the individual quartz plates from the total cell thickness. The cells were filled with sterile gas tight syringes. The samples were rapidly frozen by plunging the probe directly into liquid helium.

Data Collection

Spectra were recorded digitally using an OKI IF 800, Model 30, microcomputer, interfaced via a Jasco IF 500 interface. Software for data collection and manipulation was provided by Jasco Corp. and modified to suit the particular requirements of MCD spectroscopy. The data were sampled every 0.4 nm at a scan rate of 50 nm/min. The time constant was 2 seconds. Unless otherwise stated, each spectrum was scanned once. Between 800-510 nm, the slit openings were fixed at 100 micrometers. At higher energies, the slits were programmed to allow for a constant resolution of 2 nm.

Spectra were measured with the magnetic field both parallel (positive field) and antiparallel (negative field) to the direction of light propagation, as well as

in the absence of an applied magnetic field (zero field). Data was considered to be of good quality if the positive and negative field traces formed mirror images through the zero field trace, which corresponds to the natural CD spectrum. Measurement of one-half the difference between the positive and the negative field spectra yields the MCD spectrum corrected for both the natural CD and for any magnetic effects. Furthermore, recording of the signal in this manner leads to an increase of the signal-to-noise ratio by a factor of the square root of two. MCD spectra are expressed as $\Delta\epsilon$ ($\epsilon_l - \epsilon_r$), which is the difference between the molar extinction coefficients for left and right circularly polarized light respectively, in units of M^{-1} cm^{-1}. Protein concentrations are based on the appropriate extinction coefficients and given below.

Strain in the frozen glass or magnet windows may cause depolarization of the light beam, which will result in a decrease in the intensity of the CD signal. Depolarization was assessed and corrected for by measurement of the decrease in the CD signal for a standard sample of D-tris ethylenediamine cobalt (III). The CD spectrum of the standard was measured without the magnet in position, and with the standard placed after the magnet without a sample. No residual strain

birefrigence was found in the magnet windows. Individual samples caused varying amounts of depolarization of the light beam due to strain in the frozen glass. This was corrected for in assessing the delta extinction coefficients. The depolarization was generally less than 5%, and never more than 10%.

Magnetization Plots

MCD magnetization plots were generated by monitoring the MCD intensity at a given frequency, at several fixed temperatures, as a function of magnetic field. Magnetization data is presented as percent magnetization versus $\beta B/2kT$. Where β is the Bohr magneton, B is the magnetic flux, k is the Boltzmann constant and T is the absolute temperature. Percent magnetization refers to signal intensity as a percentage of the intensity at complete magnetic saturation. The expressions for deriving the theoretical curves are given in chapter II.1. The experimental and theoretical curves were calculated and plotted on an OKI IF800 model 30 microcomputer using software developed by Michael K. Johnson and Deborah E. Bennett (appendix I).

3.1.2 EPR

EPR spectra were recorded on a Varian E-line X-band spectrometer. Temperatures between 7-100 K were obtained by use of an Air Products Helitrans low-temperature cryostat. The temperatures were controlled by monitoring the temperature with a gold/chromel thermocouple positioned 3 cm below the sample and a heater connected to a controller. A calibrated silicon diode (Lake Shore Cryogenics), in frozen aqueous solution, was placed in the sample compartment in lieu of the sample in order to access the temperature to within 0.25 K.

The magnetic field was calibrated with a solution of 2,2-diphenyl-1-picrylhydrazyl (DPPH) and a with a nuclear magnetic resonance probe, and was found to be accurate to within 0.25% of the scan range. The frequency measurements were accurate to $\pm$ 0.0025 GHz. Quantitation of spectra was as outlined in chapter II.2. Care was taken to ensure that neither the sample nor the standard was saturated. Several standard samples of metamyoglobin cyanide and cytochrome c were quantitated against CuEDTA. The precision of the instrument was found to be greater than 1%, and the accuracy greater than 3%. The quantitation of less concentrated protein samples, such as are found in this work, are within 10%, unless

otherwise stated.

3.1.3 UV-Visible and Room Temperature CD Spectroscopy

UV-Visible spectroscopy was performed using a Cary 219 spectrometer. The samples were placed in quartz 1 mm cuvettes, which could be fitted with rubber septa for use with anaerobic samples. Extinction coefficients for determining protein concentration, based on their UV-visible absorbances are given below.

CD spectra were run on the Jasco J500C interfaced to the OKI IF 800 model 30 microcomputer. All CD spectra have been corrected for background by digitally removing any contributions from the solvent or the cuvette on the computer. The sample cuvettes were as used for UV-visible spectroscopy.

3.2 Sample Preparation and Handling

In order to form an optical quality glass upon freezing, all MCD samples were made 50% v/v in ethylene glycol. After injection into the sample cell, the sample

was immediately frozen by rapid immersion into liquid helium. An EPR tube was filled simultaneously to the filling of the MCD cell to facilitate comparison of the results of the two spectroscopic techniques. The EPR samples were frozen, simultaneously to the MCD samples by rapid immersion in liquid nitrogen. EPR samples were stored in liquid nitrogen prior to use. In no instance did the addition of glassing agents have any effect on the UV-Visible, EPR, or room temperature CD spectra. Ethylene glycol, however, did affect the reducibility of certain iron-sulfur clusters in some proteins. (see Thermus thermophilus Fd below). All proteins were stored in liquid nitrogen, prior to use.

Anaerobic samples were handled either on a gas line, in which argon was passed over a BASF copper catalyst to remove oxygen, or in a Vacuum Atmospheres inert atmosphere box (<1 ppm oxygen) equipped with a HE-493 Dri-train, an A0316-C oxygen analyzer, an AM-2 moisture analyzer, and a pedatrol pressure control.

Proteins were in buffered solutions as per figure legends. Tris (hydroxymethyl) aminomethane hydrochloride, henceforth referred to as Tris or Tris-HCl, was obtained from Aldrich and adjusted to the appropriate pH with a concentrated solution of hydrochloric acid. Tris (hydroxymethyl)

methylaminopropane sulfonic acid, Taps, and Piperazine-N,N'-bis [2-ethane-sulfonic acid], Pipes, were purchased from Sigma, and adjusted to the proper pH by concentrated sodium hydroxide and sulfuric acid as needed. Phosphate buffers were prepared by mixing the appropriate amounts of the mono- and dibasic potassium phosphate solutions. Potassium ferricyanide was obtained from Matheson, Coleman and Bell. Sodium dithionite >90% purity was purchased from Kodak Chemicals. Unless otherwise specified, dithionite was added anaerobically to a degassed solution of the appropriate buffer and was prepared immediately prior to use. The dithionite was added in ten-fold excess over the protein concentration, unless otherwise stated. Dithionite was stored in an amber bottle, in the inert atmosphere box.

CuEDTA was made by addition of a ten-fold excess of EDTA (Mallinckrodt) to a solution of exactly 1 mM cupric sulfate (MCB). The standard solution was stored frozen in an EPR tube. Metmyoglobin cyanide (MetMbCN) was prepared by oxidizing a 1 mM solution of myoglobin (Sigma) with a ten-fold excess of ferricyanide. The ferricyanide was then removed by gel filtration using a Sephadex G-25 column. A hundred-fold excess of a buffered solution of potassium cyanide was then added, and, the solution was concentrated by amicon ultrafiltration. The final

concentration of the MetMbCN was determined by UV-Visible spectroscopy $\epsilon_{540}=11.3mM^{-1}cm^{-1}$ (1). MetMbCN was stored frozen in an EPR tube. Cytochrome c, from Sigma Chemicals, was prepared in the same manner as the MetMbCN, except for the addition of KCN. The concentration was determined using $\epsilon_{578}=11.2mM^{-1}cm^{-1}$ (2).

Unless otherwise stated, solutions were made-up in water which was first glass-distilled and then passed through an ion-exchange column. Water purity was established by conductivity measurements. All other chemicals not explicitly listed here were of the highest purity available.

3.2.1 Clostridium pasterianum

Bacterial grow-up

Clostridium pasterianum, was grown by a procedure, based on that described by Rabinowitz (3) with minor modifications. Solid calcium carbonate was placed on the bottom of two 50 ml serum vials. Approximately 10 ml of

pureed potato followed by 12-14 ml of 2% sucrose in tap water was added. The mixture was gently boiled for one-half hour under nitrogen to drive off any dissolved oxygen. The vials were then stoppered with crimped rubber septa and autoclaved for twenty minutes. When cool, two drops of 2 M K_2CO_3 and four drops of 2 M pyrogallol was added. Finally, the vials were incubated with lyophilized C. pasteurianum cultures (American Type Culture Collection #6013). The bacteria were allowed to grow for three days at 30 ^{o}C, on a shaker. As the bacteria grow, hydrogen gas is evolved. It was therefore necessary to release the pressure on the vials daily, by careful insertion of a sterile syringe needle into the septa.

The potato mixture was then spooned under nitrogen into four 50 ml serum vials which contained a layer of solid calcium carbonate at the bottom, 15 ml of tap water, and 15 ml of synthetic medium consisting of: 40 g sucrose (commercal table sugar), 4 ml 7.4% w/v $MgCl_2$-$6H_2O$, 1 ml 20% w/v NaCl, 0.2 ml 10% w/v Na_2MoO_4-$2H_2O$, 0.1 ml 100 ug/ml biotin, 0.1 ml 100 ug/ml p-aminobenzoic acid, 2.0 ml 7.1% Na_2SO_4 and 16 ml 20% NH_4Cl, all in 900 ml of tap water. The vials were degassed and autoclaved (15 minutes at 121 ^{o}C) prior to innoculation. These vials were then left on a shaker for thirty-six hours at 30 ^{o}C. Again, it was necessary to

relieve the pressure whenever the septa appeared to be "bulging".

Each of the four vials was subsequently used to innoculate a liter Erlenmeyer flask containing a layer of solid $CaCO_3$ and 250 ml of the above described synthetic medium, sterilized for fifteen minutes at 121 ^{o}C. 10 ml of a sterile solution of 5% KH_2PO_4 plus 9.2% K_2HPO_4-$3H_2O$ was added separately to the flask while the medium was still hot. 2 ml of 5% $FeCl_3$-$6H_2O$ was added just prior to innoculation. These flasks were allowed to grow for two days at 37^{o}C. A steady flow of nitrogen was passed through the medium during growth in order to maintain anaerobicity and to act as a source of convection. An absorption reading of 11-12 at 660 nm can be used to determine the onset of the late log phase.

Two flasks were used to innoculate a twenty liter carboy containing 15 l of the identical medium as the above-described flasks, except that the phosphate concentration was doubled. Due to the strength of the innoculant, the carboy was not autoclaved. The bacteria were grown for forty-eight hours at 37 ^{o}C. Nitrogen was vigorously bubbled through the growth medium.

Four liters were set aside to act as innoculant for other carboys. This innoculant can be stored in the refrigerator for periods as long as a month and still remain viable. The remaining bacteria were harvested by

flow-through centrifugation using a Sorvall RC-5B centrifuge equipped with a TZ-28 reorientating density gradient zonal rotor and a 6 K continuous flow system. The flow rate was approximately eight liters per hour. A large decrease in flow rate resulted in only a small increase in cell yield. The average yield was 100-125 g wet cell paste per thirty liters of medium. The cell paste was stored at -70 ^{o}C, for periods up to a year, pending protein isolation.

Protein isolation

All isolation procedures were carried out at 4 ^{o}C under aerobic conditions unless otherwise stated. Four to five hundred grams of wet cell paste were thawed overnight and then suspended in 0.05 M potassium phosphate buffer, pH 7.8, to a final volume of 900 ml. Aliquots of 30 ml each were sonicated for three minutes to rupture the cell membranes. The cells were then spun for one hour at 18,000 rev/min. using a Sorvall RC-5B centrifuge equipped with a GSA rotor. The supernate was placed on a DEAE-52 ion exchange column (4.5 x 20 cm) equilibrated with four liters of 0.05 M phosphate buffer, pH 7.8. The column was subsequently washed with 400 ml of deionized water. The rubredoxin (Rd) and the ferredoxin

(Fd) were coeluted using a linear salt gradient of 1.8 l each 0.7 M NaCl and 0.1 M NaCl in water. The brown and pink fractions were collected and concentrated using a 200 ml Amicon ultrafiltration stirred cell fitted with a YM5 membrane, to a final volume of 20 ml. The proteins were then diluted to 200 ml with 0.15 M Tris-HCl pH 7.4 and applied to a second DEAE-52 column (3 x 30 cm) equilibrated with the same Tris buffer. The proteins were eluted with a linear salt gradient of 1.5 l each 0.27 M and 0.07 M NaCl in the Tris buffer. The brown ferredoxin was eluted just after the pink rubredoxin. The rubredoxin was concentrated and desalted in an Amicon fitted with a YM5 membrane. Average yield was approximately 10 mg/500 g cell paste. The purity ratio A_{490}/A_{280} = 0.38, which compares quite favorably to the purity ratio for single crystal absorption of 0.41 (3).

The ferredoxin was made 60% saturated in ammonium sulfate and any precipitate formed was removed by centrifugation and discarded. The supernate was then made 100% saturated in ammonium sulfate and allowed to sit overnight at 5°C. The ferredoxin was collected as a precipitate after centrifugation, 10 minutes at 18,000 rev/min. The average Fd yield was 20mg/500g cell paste. The purity ratio A_{400}/A_{280}=0.73 compared with the single crystal ratio of 0.80 (3).

It was found that the Fd yield decreased with

increasing isolation time. The Rd was less affected. Pressurized Pharmacia columns were found to be superior to gravity feed columns in that they both decrease the time necessary for the isolation, and increased the resolution between the Fd and the Rd.

Reconstitution of C. pasteurianum Fd

Production of Apoprotein: Apoferredoxin was prepared as described in reference 3. The procedure was carried out aerobically. The Fd in 0.15 M Tris-HCl pH 7.4, ca. 1 mg/ml was made 8% w/v in trichloroacetic acid, with a 30% w/v solution. The protein was then left for one hour at 0 ^{o}C. The distinct smell of hydrogen sulfide was detected. The solution was then spun for ten minutes at 0 ^{o}C and 15,000 rev/min. The clear supernate was discarded. If any traces of brown color remained in the precipitate, the apoprotein was resuspended in Tris buffer, 0.15 M pH 8.0 and reprecipitated.

Reconstitution with iron and sulfide: Apoprotein was incubated for two hours under scrubbed argon in the presence of 8 M Urea and 20 ul of 2-mercaptoethanol. Then 0.078 ml of 0.1 M ferrous ammonium sulfate and 0.078 ml of 0.1 M sodium sulfide were added. The ferrous ammonium sulfate and the sodium sulfide were prepared in degassed

water immediately prior to use. The protein was diluted three-fold with degassed 0.1 M Tris pH 8.5 and incubated for thirty minutes at 37 ^{o}C. The Fd was then isolated by DEAE-52 ion chromatography column (0.8 x 8 cm). After the protein was applied, the column was washed with 10 ml of 0.15 M Tris-HCl pH 7.4 and then with 20 ml of 0.23 M NaCl in 5 mM Tris pH 7.4. The protein was finally eluted with 0.58 M NaCl in the Tris buffer. A black precipitate, ferrous sulfide, remained on the top of the column, and did not affect the Fd elution. The Fd was concentrated and desalted in an Amicon with a YM5 membrane.

Ferricyanide treated C. pasteurianum Fd

Oxidative damaged C. pasteurianum Fd was obtained by addition of a stoichiometric amount of ferricyanide to reconstituted protein. The Fd was incubated at room temperature with the ferricyanide until no further change in the absorption spectrum was observed. Further degradation of the Fd was obtained by slow addition of a twenty-fold excess of ferricyanide. The protein was then allowed to stand overnight a 0^{o}C. The excess ferricyanide was removed by Sephadex G-25 gel filtration (0.8 x 8.0

cm). All ferricyanide additions were performed aerobically.

3.2.2 Thermus thermophilus Ferredoxin

Thermus thermophilus Ferredoxin was provided by James A. Fee of Los Alamos National Laboratory. T. thermophilus was grown according to the procedure of Findling et al. (4). The Fd was isolated as described by Hille et al. (5). The purity index was $A_{400}/A_{290}=0.62$. Protein concentration was determined using $\epsilon_{400}= 28,140 M^{-1}cm^{-1}$.

Ferricyanide oxidized

The ferricyanide oxidized sample was generated by incubating the protein with a five-fold excess of ferricyanide at room temperature until no further change in the absorption spectrum was observed, approximately sixty minutes. Prior to MCD analysis, the ferricyanide was removed by Sephadex G-25 gel filtration chromatography. The protein was then concentrated in an Amicon YM10.

Partially reduced

T. thermophilus Fd, in which the [3Fe-xS] cluster is reduced, while the [4Fe-4S] cluster remains oxidized, is henceforth referred to as partially reduced T. thermophilus Fd. The protein was partially reduced by addition of excess sodium dithionite to Fd in 50% v/v ethylene glycol.

Fully reduced: Fully reduced T. thermophilus Fd refers to Fd in which both clusters are reduced. The fully reduced protein was obtained by addition of excess sodium dithionite prior to the addition of 50% v/v ethylene glycol.

3.2.3 Azotobacter vinelandii Fd I

Azotobacter vinelandii FdI was provided either as purified protein, by William V. Sweeney, Hunter College in New York, or as crude extract, by Brian Hales, Louisiana State University. Dr. Sweeney isolated the protein according to the procedure of Yoch et al. (6). The crude extract was a side-product of a nitrogenase preparation. After the removal of the nitrogenase enzymes (7), Fd I was eluted as crude extract with 0.4 M

NaCl in 0.025 M Tris pH 7.4 The extract was then diluted five-fold and loaded onto a second DEAE-52 column (0.8 x 8.0 cm), and equilibrated with 0.1 M NaCl in 0.005 M Tris-HCl pH 7.4. Subsequently, the column was washed with 50 ml of 0.2 M NaCl in 0.005 M Tris pH 7.4. The Fd I was eluted with 0.4 M NaCl. After concentration in an Amicon YM10 to a volume of 0.5 ml, the protein was placed on a Sephadex G-100 gel filtration column, equilibrated with 0.1 M Tris pH 8.0. The brown fraction, containing the Fd, was made 40% saturated in ammoniun sulfate at 0 ^{o}C. The solution was spun for 10 minutes at 15,000 rev/min. Any precipatate formed was discarded. Finally, the supernate was made 100% saturated in ammonium sulfate at 0 ^{o}C. The Fd I was collected as a precipitate after centrifugation at 15,000 rev/min. for ten minutes (8) Protein concentrations were calculated by absorption spectroscopy, ϵ_{400}=29,800 $M^{-1}cm^{-1}$. Purity ratios ranged from 0.5 for Dr. Sweeney's preparation to 0.4 for Fd isolated from the nitrogenase preparation. The lower purity for the latter may be due, in part, to the prolonged heat treatment associated with the nitrogenase isolation. No significant difference between the preparations was observed by EPR, UV-Visible, CD or MCD spectroscopy.

3.2.4 *E. coli* nitrate reductase

Nitrate reductase from *E. coli* was isolated according to the method of Adams and Mortenson and generously provided by same (9). As isolated, the enzyme contained 0.80±0.05 g-atom of molybdenum, 14.4±0.5 g-atom of acid labile sulfide, and 16.3 ± 1 g-atom of non-heme iron per 200,000 g of protein. The specific activities were in the range of 80-90umol of nitrate produced per min. per mg of protein. The molybdenum content was obtained by the dithiol method (10). The acid labile sulfur content was determined by the formation of methylene blue (11) and iron content was determined by complexation with o-phenanthroline (12). Specific activities were measured by anaerobic oxidation of methyl viologen (9). Protein concentrations were determined by the Lowery method using bovine serum albumin as a standard. All the above-mentioned analyses were performed by Drs. Adams and Mortenson prior to the shipment of the enzyme. The enzyme was sent frozen on dry ice by overnight mail.

References

1. Smith, D.W., and Williams, R.J.P., (1970) Struct. Bonding 7, 1-45

2. Margoliash, E., and Schejter, A. (1966) Adv. Protein Chem., 21, 113-286

3. Rabinowitz, J. (1971) in "Methods in Enzymology" Vol. XXIV (San Pietro, A., ed.), pp. 431-446, Academic Press, New York

4. Findling, K.L., Yoshida, T., and Fee, J.A., (1984) J. Biol. Chem. 259, 123

5. Hille, R., Yoshida, T., Tarr, G.E., Williams, C.H., Ludwig, M.L., Fee, J.A., Kent, T.A., Huynh, B.H., and Munck, E. (1983) J. Biol. Chem. 258, 13008-13013

6. Yoch, D.C., and Arnon, D.I., (1972) J. Biol. Chem. 247, 4514-4520

7. Burgess, B.K., Jacobs, D.B., and Stiefel, E.I., (1980) Biochim. Biophys. Acta 614, 196-209

8. Morgan, T.V., Stephens, P.J., Burgess, B.K., and Stout, C.D. (1984) Febs Lett. 167, 137-141

9. Adams, M.W.W., and Mortenson, L.E., (1982) J. Biol. Chem. 257, 1791-1799

10. Bulen, W.A., and LeComte, J.M., (1966) Proc. Natl. Acad. Sci. USA 56, 979-986

11. Chen, J.S., and Mortenson, L.E., (1977) Anal. Biochem. 79, 157-165

12. Lovenberg, W., Buchanan, B.B., and Rabinowitz, J.C., (1963) J. Biol. Chem. 238, 3899-3913

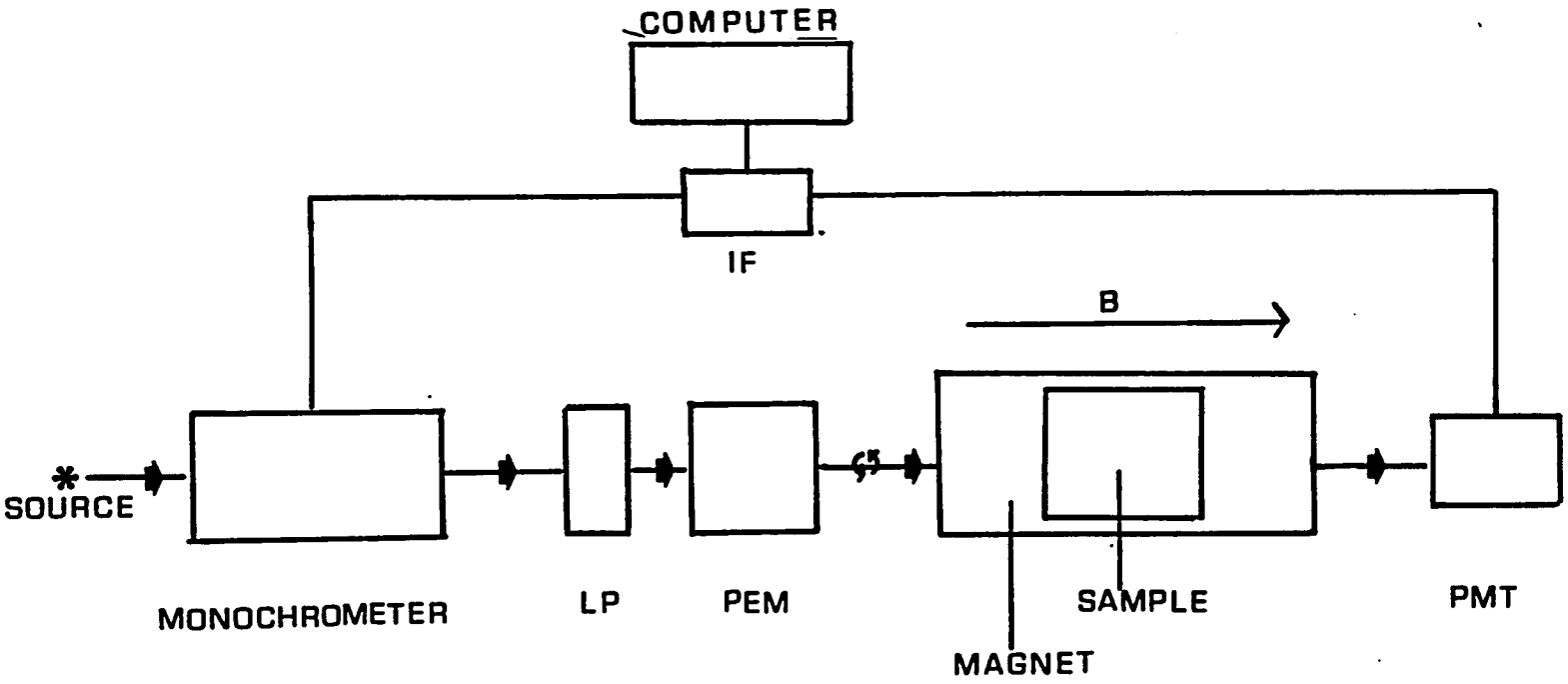

Figure III.1 Schematic of the MCD spectropolarimeter. The source,, monochrometer, linear polarizer (LP), photoelastic modulator (PEM), and photomultiplier tube (PMT) comprise the Jasco J500C circular dichrograph. The magnet is an Oxford SM3, split coil, 5 tesla, superconducting magnet. The interface (IF) is a Jasco IF 500, and the computer is an OKI IF 800, model 30.

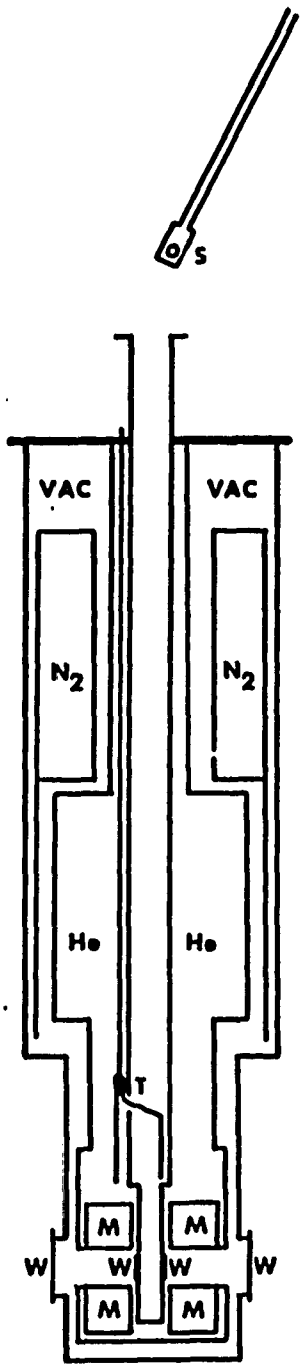

Figure III.2 Schematic of an Oxford SM3, split coil, 5 tesla, superconducting magnet. M = magnetic coil, W = spectracil windows, T = needle valve, and S = sample.

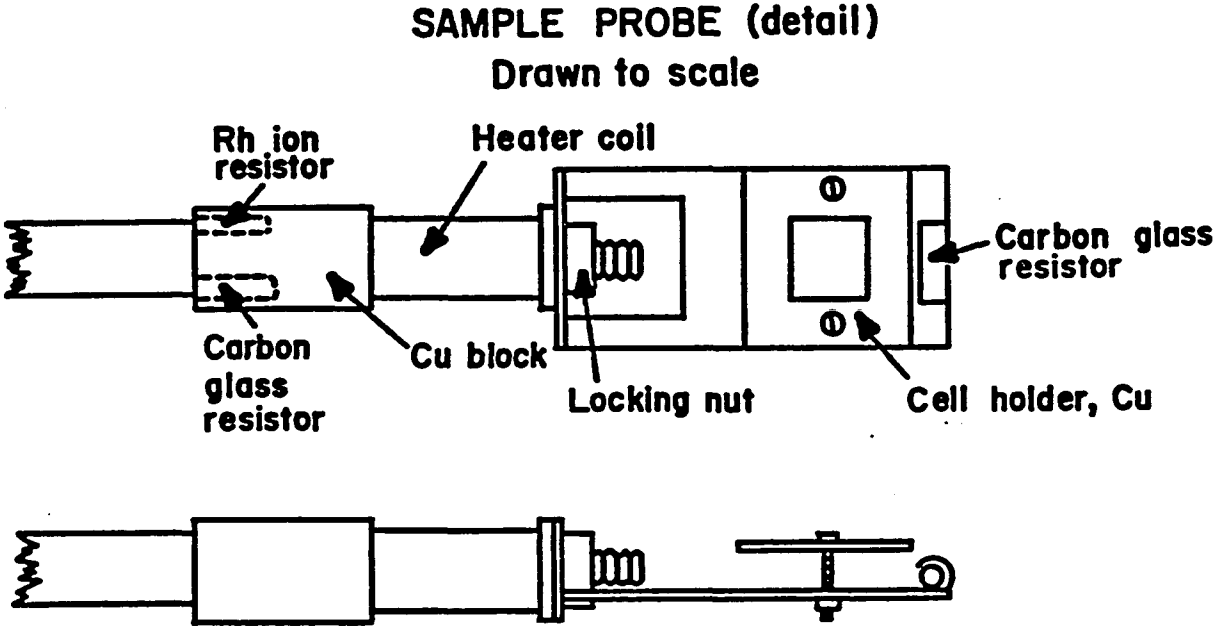

Figure III.3 Schematic of the magnet sample probe.

Chapter 4

Clostridial proteins

4.1 Clostridium pasteurianum Rubredoxin

4.1.1 Introduction

Rubredoxins (Rd) contain one or two monomeric iron centers. Although a general role has yet to be ascertained, Rds constitute one of the best characterized metalloproteins, and the simplest class of iron-sulfur proteins. This introduction summarizes the pertinent structural and electronic information which has been deduced by a wide range of spectroscopic techniques.

Clostridium pasteurianum (C. pasteurianum) Rd is typical of other single center Rds. It has a molecular weight of approximately 6000 Da, and a single iron atom per protein molecule. Several rubredoxins, including those from C. pasteurianum, Micrococcus aerogenes, Peptostreptococcus elsdenii, Micrococcus lactylyticus,

Desulfovibrio gigas, and Desulfovibrio desulfuricans have been sequenced. They are all characterized by the presence of four cysteine residues and a preponderance of acidic residues (1). Furthermore, no histidine or arginine residues have been found in any of these Rds. Three tyrosine residues are always present. Cysteines 6,9,39 and 42, which bind the iron atom to the protein, are universally conserved.

Two center Rds are generally much larger, up to three times the molecular weight. They contain two redox active sites, with one iron atom per site. These proteins also have a large degree of homology with the monomeric Rds.

As isolated C. pasteurianum Rd is bright red. Absorption maxima occur at 750, 490, 380, and 280nm with extinction coefficients of 340, 8,800, 10,700, and 21,100 M^{-1} cm^{-1} respectively (2). It can undergo a one electron reduction at -57 mV versus the standard hydrogen electrode at pH 7.0. Reduction with sodium dithionite results in a complete loss of color. Absorption maxima for the reduced Rd are found at 333, 311 and 275nm, with extinction coefficients of 6,100, 10,800, 24,800 M^{-1} cm^{-1} respectively.

The UV-visible absorption spectra have been assigned on the basis of to a predominantly axial distortion of a tetrahedral ligand field (3). In oxidized rubredoxin all d-d transitions are spin forbidden. These spin-forbidden

ligand field transitions are hidden under the more intense sulfur to iron charge transfer absorptions. The charge transfer mechanism is thought to involve the promotion of electrons from molecular orbitals localized mainly on the sulfur ligands to orbitals localized predominantely on the iron atoms. Two sulfur-to-iron charge transfer transitions have been assigned in the oxidized Rd, each corresponding to a parent tetrahedral $^6A_1$ to $^6T_2$ transition, under T_d symmetry. Both transitions are split due to the axial distortion of the excited state. The absorbances at 380 and 490nm have been assigned to $^6A_1$ to E transitions, while the absorbances at 347 and 565nm have been assigned to $^6A_1$ to $^6B_2$. This data is consistent with effective D_2 symmetry.

Ferrous Rd, d^6, has one allowed d-d transition, corresponding to the ^5E to ^5T transition of T_d parentage. This transition occurs outside of the UV-visible region. The sulfur to iron charge transfer transitions are more energetic for the ferrous Rd than for the ferric Rd, due to the increase in electric charge on the iron atom. Hence ferrous Rd is virtually colorless (3).

The circular dichroism spectra of both the ferric (4,5) and the ferrous (6) rubredoxin have been measured. As expected from the optical spectra, ferric Rd gives rise to a CD spectrum with a number of transitions in the visible and UV regions, whereas transitions from the

ferrous Rd are observed in the UV and near-IR. Eaton and Lovenberg have been able to identify the ^5E to ^5T ligand field transition in the reduced protein, in the near-IR CD. The CD spectra provide additional evidence for a distorted tetrahedral environment about the iron atom.

Magnetic susceptibility studies of the Rd in both oxidation states (7) were carried out using the Evans NMR technique (8). As both states are paramagnetic, the magnetic susceptibilities exhibit a Curie law inverse temperature dependence when $\beta B << 2kT$. The effective moments were found to be equal to 5.85 ± 0.20 BM and 5.05 ± 0.20 BM for the oxidized and reduced protein respectively. These values are in consistent with high spin ferric (S=5/2) and ferrous (S=2) ions.

C. pasteurianum Rd can be enriched with ^{57}Fe by reconstitution, thus enabling the use of Mössbauer spectroscopy. The Mössbauer further confirms the presence of high spin Fe(III) and high spin Fe(II) in the oxidized and reduced Rd. Approximate estimates of the axial and rhombic the zero field splitting parameters D, and E, respectively, were calculated from the Mossbauer data collected in the presence of a magnetic field (9). The spectrum of ferric Rd was simulated using a value of 1.4 cm^{-1} for D, with E/D equal to 0.25. This ratio implies a large rhombic distortion ($0 < E/D < 0.33$, zero being totally axial). The reduced protein was found to have a value of D equal to 7.63 cm^{-1} with E/D equal to

0.28. Again indicative of large rhombic distortion.

Resonance Raman (RR) spectra have been reported for C. pasteurianum Rd (10-12), D. gigas Rd (13) and the synthetic analog $Fe(S_2\text{-}o\text{-}xyl)_2^-$ (12). By invoking vibrational coupling, Czernuszewicz et al. have been able to assign all the vibrations as arising from a distorted tetrahedron. Raman spectra of crystalline samples were quite similar to solution spectra. As vibrational spectroscopy is very sensitive to conformational changes, it follows that the iron coordination does not significantly change upon crystallization (11). This is of great importance in interpreting the X-ray diffraction results (see below).

Definitive structural analysis can only be provided by X-ray diffraction. Unfortunately, X-ray diffraction has many inherent difficulties in regard to protein chemistry. First, the sample must be crystalline, not a trivial matter in most cases. Secondly, the crystal structure must be equivalent to the solution structure if the results are to have any physiological significance. Additionally, high molecular weights (minimally 6,000 Da) increase dramatically, the complexity of the data analysis. As a result, very few protein structures have been solved to a resolution of <1.2 Å. Finally, care must be taken to ensure that the crystal does not undergo degradation due to the X-ray radiation.

C. pasteurianum Rd does meet these criteria.

Crystals were grown by saturating the solution with 80% ammonium sulfate at pH 4 (14) mentioned above, no significant changes occur upon crystallization. By use of heavy atom derivation and anomalous scattering, the X-ray structure of C. pasteurianum Rd has been solved at 3 Å (15), 2.5 Å (16) 2 Å (17) and finally 1.2 Å (18) resolution. The limiting factor for high resolution x-ray data is the ability to collect enough data points before the crystal degrades. The advent of fast and simultaneous detectors was crucial in the solution of the 1.2 Å data. While the 2 Å solution correctly identified the distorted tetrahedral iron environment, one iron-sulfur bond was erroneously found to be substantially shorter than the other three. Upon further refinement, the bond lengths were found to be nearly equal, ranging from 2.24-2.33 Å. The bond angles varied from 104^{o}-114^{o} for the S-Fe-S angles. Five of the six angles differed by more than three times the standard deviation from the perfect tetrahedral value of 109.5^{o}. The latest refinement is generally accepted to be accurate. Unfortunately, much of the early work on C. pasteurianum Rd, such as the single crystal absorption, was based on the incorrect, early diffraction analysis, rendering them difficult to interpret. The cause of the original error is still unknown. The structural refinement of rubredoxin illustrates that protein structures based on X-ray diffraction data at resolutions

greater than 2 Å are not always infallible. Like all physical techniques used in the characterization of metalloproteins, X-ray diffraction is most powerful when used in conjunction with other techniques.

A second useful X-ray technique for the study of structural aspects of metalloproteins is extended X-ray absorption fine structure (EXAFS). In principle, EXAFS can provide information concerning the number, type, and distances of atoms in the immediate coordination sphere of an isolated metal center in a metalloprotein. While it has the major advantage of not being limited to samples in the crystalline state, it is limited in not being able to furnish angular information, and by the requirement for synchrontron radiation. Like x-ray diffraction, protein degradation during the course of the experiment is a major concern. This is even more severe for EXAFS due to the large flux.

EXAFS studies of Rd (19-20) indicated equivalence in the iron-sulfur bond distances, predating the 1.2 Å X-ray diffraction result by several years. The average distance for ferric Rd was found to be 2.30 ± 0.04 Å with a root-mean-square deviation from this average of 0.06 ± 0.04 Å.

The magnetic properties of Rd have been probed via EPR spectroscopy. The EPR spectra of P. elsdenii (3), P. oleovorans (21), C. acidi-urici (21), and C. pasteurianum (9) Rd are all characterized by a resonance at g~9

arising from the lowest doublet, and at g~4.3 arising from the middle doublet. Peisach et al. also reported additional high field resonances at g=1.22, 0.90 for the P. oleovorans also arising from the lowest doublet. Using the effective g-values of the lower and middle doublets, a value of E/D=0.28 was determined for the P. oleovorans. The zero-field splitting parameter was estimated to be 1.76 cm^{-1}, by studies of the inverse temperature dependence of the g=4.3 signal. The high field resonances have not been observed in C. pasteurianum Rd (9). Shultz, therefore, estimated the zero field splitting parameters by simulating EPR spectra using a procedure that allowed for contributions from g-strain to the linewidths, and found E/D=0.25 and D=1.4 cm^{-1}.

This work presents EPR and low temperature MCD data from both the ferric and the ferrous C. pasteurianum Rd. Although the MCD of D. gigas Rd and desulforedoxin in both oxidation states (22), and ferric C. pasteurianum Rd (23) has been previously published, no magnetization data has been reported. A detailed study was therefore undertaken to investigate the MCD magnetization behavior of these complex (S>1/2), but well-characterized ground states. These studies are important in establishing and testing a protocol for analyzing MCD magnetization data for chromophores with S>1/2 ground states. Moreover, oxidized Rd provides an excellent example for assessing

the influence of the polarization of the electronic transitions on the MCD magnetization plots for ground state doublets with large g-value anisotropy. The utility of variable temperature MCD spectroscopy in determining zero field splitting parameters was also investigated. The results show that MCD magnetization data provide a viable method for estimating the polarization of electronic transitions for samples which are randomly oriented in a frozen glass, and a means of determining ground state zero field splitting parameters.

4.1.2 Results

Oxidized Rd

EPR

EPR spectroscopy was undertaken in order to obtain accurate g-values for use in simulating MCD magnetization curves. EPR spectra of ferric C. pasteurianum Rd were recorded in the range of 8 to 70 K (fig. IV.1). The spectra consist of a resonance at g=9.4, observable to 15 K, from the lowest doublet, and a broader resonance at g = 4.7, 4.3, and 4.0 from the middle doublet. The spectra are identical to those previously reported, showing that the presence of ethylene glycol (added to form an optical glass upon freezing as required for MCD spectroscopy) does not alter the ground state properties.

MCD

The rubredoxins are very well suited for study by MCD, having the largest MCD extinction coefficients of any of the iron-sulfur proteins. The low temperature MCD spectra of ferric C. pasteurianum Rd at 1.55, 4.22, 7.2, 11.0, 20.0 K and 4.5 tesla, along with the corresponding room temperature UV-visible spectrum are given in figure IV.2. The MCD spectra resemble those of Rivoal et al., which were recorded at 0.83 tesla and at temperatures down to 16 K (23) except for an additional shoulder, to the low wavelength side of the negative MCD band at 400 nm, was observed in the earlier work. We have not observed this feature at any temperature or magnetic field, and in light of previous work (24), we conclude that it seems likely that it can be attributed to the glass sample cell used. Six temperature dependent MCD bands (C-terms) are resolved in the wavelength region 330-650 nm.

MCD magnetization data were collected at the peak maxima of each transition, at temperatures between 1.55 and 140 K. Magnetization plots at 400, 466, 501, and 555 nm are given in figure IV.3. Magnetization plots at 344 and 370 nm closely resemble those at 555 and 501 nm respectively (data not shown). The presence of low-lying zero-field components that become thermally populated with increasing temperature, is indicated by the

"nesting" of the magnetization data, which is apparent at all wavelengths investigated. As C. pasteurianum Rd contains only a single chromophore, the pronounced wavelength dependence of the magnetization plots is attributed to differences in the polarization of the electronic transitions. Figure IV.4 graphically shows the effect on the magnetization curves, of systematically varying the polarization ratio from +1 to -100 of a transition arising from a hypothetical ground state with $g_{\parallel} = 9.68$ and $g_{\perp} = 0.75$. These g-values are those anticipated for the lowest doublet of an S = 5/2 system with E/D = 1/3 (fig. IV.5). The data are plotted in terms of percentage magnetization (MCD intensity as a percentage of the maximum intensity), since it is generally not possible to evaluate the transition dipole moments and hence predict the absolute intensity of MCD transitions.

Assuming D ~ 1.4 cm^{-1}, then at 1.55 K only the lowest doublet will be significantly populated. It should therefore be possible to obtain estimates of the polarization ratios for transitions originating from the lowest doublet, by fitting the data at this temperature to equation II.6. The g-value for the high field was obtained directly from the EPR spectrum cited above. Although g has not been observed for the C. pasteurianum Rd, it is believed to be very similar to the P. oleovorans, and therefore a value of 1.07 was chosen.

The best fits of the theoretical simulations to the experimental data, using these parameters, are depicted by the solid lines in figure IV.3. The corresponding values of m_z/m_+ are given in the figure legend. Clearly, the transitions at 370, 400, 466, and 501 nm are all predominantly (>80%) x,y-polarized, since the absolute value of the polarization ratio does not exceed 0.3 in any instance. In contrast the transitions at 344 and 555 nm are predominantly z-polarized.

Since the transitions at 501 and 400 nm were found to be almost exclusively x,y-polarized, detailed studies of the temperature dependence of the MCD intensity at these wavelengths were carried out in order to determine the magnitude of the axial zero field splitting parameter, D. It is crucial to this analysis to investigate only those transitions which are of unique polarization in order to minimize the number of parameters in the theoretical expression. The ground state used to derive the Boltzmann coefficients is depicted in figure IV.5. Completely rhombic symmetry, as indicated by EPR, has been assumed. A magnetic field of 0.24 tesla was employed. At this field, the MCD intensity was completely linear as a function of magnetic field for temperatures down to 1.7 K. Furthermore, use of a very small magnetic field minimizes field induced mixing of the zero-field components. The experimental data was fit to equation II.14, with X=3.5 and Y=7.0,

using c_1, c_2, c_3, and D as parameters. At both wavelengths, optimal fits were obtained for D = 1.4 cm^{-1} (fig. IV.6). The theoretical curves were not however, particularly sensitive to the values of D. Satisfactory fits, based on the sun of the residual squares, and on the estimated experimental errors, were obtained for $1.0<D<2.0$ cm^{-1}.

Reduced C. pasteurianum Rd

No EPR signal in the range 10-70 K was observed in the reduced Rd. EPR spectra are seldom observed in non-Kramers' systems, due to the presence of zero-field splitting, which prevents resonance from occuring at the commonly employed frequencies.

The low temperature MCD was recorded at temperatures between 1.6 and 55 K and at 4.5 tesla (fig. IV.7). The MCD is observed only in the near-UV region, due to the complete absence of visible chromophores. The spectra resemble the room temperature MCD spectrum of Eaton and Lovenberg (3), except for the markedly improved resolution. A striking similarity to the MCD spectrum of reduced D. gigas Rd is also observed (22). D. gigas desulforedoxin gives rise to a qualitatively similar, although much broader, MCD spectrum (22).

MCD magnetization data was collected only at 330 nm (fig. IV.8). Absorbance by the polypeptide backbone, and dithionite in the near-UV decreases the signal-to-noise

ratio of the negative band at 310 nm, rendering magnetization data at this wavelength less reliable. As with the ferric Rd, the magnetization data exhibits pronouced nesting which is indicative of the presence of low-lying excited states, or zero field components. At the lowest temperature, and large magnetic fields, the data becomes almost linear in field, and shows little indication of saturation. The MCD intensity is virtually independent of temperature to approximately 10 K, and the intensity at 4.2 K is equal to the intensity at 1.7 K, for any given field. It was therefore concluded that the lowest energy level has M_S=0, and that D must be >0. More complete analysis of the magnetization data was not attempted since the theoretical expressions have not yet been deduced for non-Kramers' ground states.

4.1.3 Discussion

The low temperature MCD data for oxidized C. pasteurianum Rd is consistent with the single crystal absorption and room temperature MCD analysis of Eaton and Lovenberg (3). The visible spectrum in the region 330 to 650 nm was assigned to two allowed S $\longrightarrow$ Fe(III) charge transfer transitions, 650-430 and 430-330 nm, respectively. They are assigned to $^6A_1 \longrightarrow {}^6T_2$ transitions of tetrahedral parentage. The assignment of the 430-330 absorption was questioned by Rivoal and

coworkers (23), since they observed four transitions in this region, and only three are theoretically predicted as a result of spin-orbit coupling to the excited state. The present work resolves this apparent contradiction since one of the transitions observed by Rivoal et al. is shown to be an artifact of the experimental conditions.

The tetrahedral transitions are split by axial distortions of the excited state into $^6A_1 \longrightarrow {}^6B_2$ and $^6A_1 \longrightarrow {}^6E$. Due to symmetry considerations, the former are expected to be z-polarized, while the latter are expected to be x,y-polarized. Hence, the MCD maxima at 344 and 555 nm are assigned to the $^6B_2$ transition, and the maxima at 370, 400, 466, and 501 nm are assigned to the ^6E transition. This assignment concurs with that made on the basis of polarized single crystal absorption studies where polarization ratios were obtained relative to the crystallographic rather than the molecular axes.

It should be emphasized that D_{2d} symmetry is the effective optical symmetry of the chromophore, indicative of predominantly axial distortion of the excited states. However, the currently available EPR, RR, and X-ray crystallographic studies would indicate somewhat lower symmetry for the ground state.

In agreement with Mössbauer and EPR studies, the axial zero-field splitting parameter for ferric C. pasteurianum Rd was estimated at 1.4 ± 0.5 cm^{-1} via the

inverse temperature dependence of the low temperature MCD. For transitions of unique polarization, MCD spectroscopy offers an independent means of assessing the magnitude of the zero field splittings, and is not sensitive to relaxation effects. This method is particularly useful for investigating systems which are EPR silent and/or which cannot be studied by Mössbauer spectroscopy, e.g. non-Kramers' systems, and metalloproteins which do not contain iron.

In contrast to the oxidized spectrum, the MCD spectrum of reduced C. pasteurianum Rd is not well understood. Eaton and Lovenberg attribute both maxima to B or C-terms, since they correspond very closely to the absorbance maxima (3). The clear temperature dependence in the low temperature MCD spectra leaves little doubt that the maxima are indeed two C-terms of opposite sign. As the only spin allowed d-d transition occurs in the near-IR, these intense transitions are attributed to sulfur-to-iron charge transfer.

The magnetization data for reduced rubredoxin closely resembles that of the high spin (S=2) Fe II cytochrome in reduced cytochrome c oxidase (25). We therefore conclude that reduced Rd has an S=2 ground state, with a predominantly axial zero-field splitting, such that D>0. This is consistent with the magnetic susceptibility (7) and Mössbauer (9) studies. A graphical depiction of the ground state, in accordance

with the Mössbauer results is given in figure IV.9. Clearly the Zeeman components no longer exist as discrete doublets. Furthermore, significant mixing of the sublevels is expected even in the presence of small applied magnetic fields. The assumptions, therefore, implicit in the derivations of theoretical magnetization curves given in chapter II, are not valid in this instance. The theory necessary to simulate this data is not developed at this time. For the same reasons, it was not possible to derive a rigorous equation for determining the axial zero-field splitting parameter for ferrous Rd.

In summary, low temperature MCD has been shown to provide a method for determining the molecular polarization of electronic transitions for a randomly oriented paramagnetic chromophores with large ground state g-value anisotropy. At present the theoretical basis for interpreting such data is generally only available for Kramers' ground states. In conjunction with the form of the MCD spectrum, MCD magnetization data affords an opportunity for detailed assignment of optical transitions. Furthermore, zero-field splitting parameters can be evaluated from the temperature dependence of a discrete MCD transitions.

4.2 Clostridium pasteurianum Ferredoxin

4.2.1 Introduction

Clostridium pasteurianum ferredoxin (C. pasteurianum Fd) is a low molecular weight protein, approximately 6,000 Da, which contains eight iron and eight inorganic sulfur atoms. First isolated in 1962, it was one of the first known iron-sulfur proteins (26). The physiological function of C. pasteurianum Fd is currently unknown, but may be the transfer of electrons to the hydrogenase system (27). It has also been postulated that it may function as an iron storage protein (28).

When isolated with minimal oxygen exposure, C. pasteurianum Fd contains two [4Fe-4S] clusters, which cycle between the +1 and the +2 oxidation states. The midpoint potential is approximately -400 mV versus the normal hydrogen electrode (27). The oxidized protein is brown, with a broad absorption at 380-400 nm. Reduction is accompanied by a substantial loss of color (27).

X-ray crystallographic studies have been completed for the Micrococcus aerogenes Fd (29), P. aerogenes Fd

(30), A. vinelandii Fd (31), Chromatium high potential iron protein (32), and several synthetic analogs, e.g. $[(C_2H_5)_4N]_3[Fe_4S_4(S\text{-}p\text{-}C_6H_4Br)_4]$ (33), all of which are believed to contain at least one [4Fe-4S] cluster. X-ray crystallographic data indicates that the [4Fe-4S] cluster has a cubane-type structure, with four iron and four inorganic sulfur atoms at alternate corners of a cube, with cysteinyl sulfurs completing tetrahedral coordination about the iron atoms (29). The cube shows considerable distortion, and is therefore often described as "interpenetrating tetrahedra". One tetrahedron has iron atoms for vertices, while the other has sulfur atoms. The eight iron Fd from P. aerogenes, which closely resembles C. pasteurianum Fd, has an average iron-iron distance of 2.74 Å, and an average iron-sulfur distance of 2.22 Å, in the oxidized protein. Upon reduction, these values decrease to 2.69 Å and 2.17 Å for the iron-iron, and the iron-sulfur distances respectively (30). Both the P. aerogenes and the M. aerogenes Fds contain two identical [4Fe-4S] clusters, which are separated by 12 Å.

No significant difference between the oxidized ferredoxin-type and the reduced HiPIP $[4Fe\text{-}4S]^{2+}$ clusters was observed by X-ray diffraction, despite a midpoint

potential difference of almost 800 mV (32). The structural similarity between the [4Fe-4S] clusters led to the development of the three-state hypothesis (34). Simply stated, this theory maintains that the tetrameric clusters have three available oxidation states. Physiologically, only two of these states are accessible to any given protein, i.e. $[4Fe\text{-}4S]^{+2,\ +3}$ of the HiPIP or $[4Fe\text{-}4S]^{+1,\ +2}$ of the Fds. The potential difference arises not from the clusters themselves, which are identical, but from the polypeptide backbone. The polypeptide can either stabilize the +3 oxidation state of the HiPIP, or the +1 oxidation state of the reduced ferredoxin.

In addition to X-ray diffraction, structural information concerning tetrameric clusters has also been obtained from EXAFS studies (35). There is good correlation between the previously mentioned X-ray diffraction studies and the EXAFS data from C. pasteurianum Fd. EXAFS indicates an iron-iron distance of 2.727 Å and an iron-sulfur distance of 2.249 Å for oxidized Fd, and 2.744 Å and 2.262 Å for the iron-iron and iron-sulfur distances in the reduced protein, respectively. Additionally, EXAFS unambiguously demonstrates that there is no structural change in the

protein between the solution and the powder or frozen solution. Furthermore, no significant differences between the [4Fe-4S] clusters in reduced HiPIP, oxidized C. pasteurianum Fd, and $[Fe_4S_4(S\text{-benzyl})_4]^{2-}$, were found.

Mössbauer studies on oxidized C. pasteurianum Fd (36-38) clearly showed the presence of strong antiferromagnetic coupling, between the iron atoms, to yield a diamagnetic, S = 0 ground state. Although the cluster formally consists of two ferric and two ferrous ions, the electrons are actually delocalized to yield a valence intermediate between the +3 and the +2 oxidation states for all four iron atoms. The additional electron per cluster in the reduced C. pasteurianum Fd is shared between one pair of iron atoms. Thus the formal valences for the reduced cluster are a single Fe III and three Fe II, but in reality two iron atoms are high spin ferrous, and the other two are intermediate between ferric and ferrous. As with the oxidized protein, strong antiferromagnetic coupling is present, resulting in an S = 1/2 ground state.

Reduced C. pasteurianum Fd is paramagnetic, and therefore EPR is frequently employed to elucidate both the electronic nature of the individual clusters and the

interactions between the clusters (36, 39-41). The fully reduced Fd exhibits a complex, seven line EPR spectrum, centered at g=1.95. The complexity of this spectrum is attributed to weak magnetic interaction between the clusters. When a single equivalent of reductant is carefully added, the protein can be semi-reduced (36). The partially reduced C. pasteurianum Fd gives rise to an axial EPR signal, $g_{\perp}$ =1.92 and $g_{\parallel}$=2.05, which has a maximum intensity when the concentration of reductant is one electron per protein molecule.

As early as 1974 investigators observed a small, variable EPR signal at g=2.01, in aerobically isolated C. pasteurianum Fd (39). The signal is markedly enhanced by prolonged exposure to oxygen or inorganic oxidants such as sodium hexachloroiridate, 1,2-aminocyclohexane-tetraacetatemanganate (III), and potassium ferricyanide (42). Thomson et al. were the first to correctly identify this paramagnet as a trinuclear cluster via the low temperature MCD (43). This assignment was later confirmed by Resonance Raman spectroscopy (44). Maximum EPR intensity of the g=2.01 signal corresponds to 0.8 spins/mole (44). Reduction of a sample with a fully developed g = 2.01 signal shows no evidence of any $[4Fe\text{-}4S]^{1+}$ cluster remaining (43). Hence addition of a

large excess of ferricyanide results in the destruction of both [4Fe-4S] clusters and the creation of approximately one [3Fe-xS] cluster. The mechanism for this destruction/conversion remains unclear.

In previous low temperature MCD and EPR studies of C. pasteurianum Fd the samples were contaminated with small amounts, ~ 10%, of [3Fe-xS] clusters (45). The EPR and MCD experiments reported here were undertaken with two principal objectives: 1) To obtain the MCD spectra and MCD magnetization data of the pure 2[4Fe-4S] Fd by reconstituting the protein with iron and sulfide. Containing only tetrameric clusters, the spectroscopic properties of the reduced eight iron Fd would serve as a fingerprint for identifying [4Fe-4S] clusters in multicluster iron-sulfur enzymes; 2) To investigate the conditions required for, and the spectroscopic consequences of, the conversion of [4Fe-4S] clusters to [3Fe-xS] clusters.

4.2.2 Results

C. pasteurianum Fd as Isolated

Rabinowitz reports a purity ratio, A_{390}/A_{280} of 0.83 for a single crystal of oxidized C. pasteurianum Fd (46). Depending on the isolation time, purity ratios of 0.70-0.75 were obtained in this work. The purity ratio was found to decrease with increasing isolation time. The UV-visible absorption spectra of reduced and oxidized C. pasteurianum Fd is given in figure IV.9.

During the course of isolating the Fd, a hitherto unreported copper protein was isolated from C. pasteurianum. It was identified as a copper protein by EPR spectroscopy (fig. IV.10). The axial spectrum has $g_{\perp}$ = 2.04, $g_{\parallel}$ = 2.21, and $A_{\parallel}$ = 19 mT. The distinctive hyperfine splitting, characteristic of an I = 3/2 nucleus, is characteristic of a copper center. The EPR spectrum of a 1 mM solution of copper EDTA is given in the lower trace for comparison. The unknown protein is a type II copper protein, according to the nomenclature of Vanngard, by virtue of the large hyperfine coupling constant (47). No hyperfine coupling was observed in g since $A_{\perp}$ is expected to be an order of magnitude smaller than $A_{\parallel}$. The linewidth is therefore larger than the hyperfine splitting, and the splitting will not be observed. This hyperfine interaction will, however, contribute to the linewidth. Interestingly, the bacteria

was able to synthesize the copper protein even though no copper was added to the media. Presumably, the concentration of copper in the tap water must have been sufficient.

The oxidized, as isolated C. pasteurianum Fd exhibited an isotropic EPR signal with g = 2.01, of variable intensity, which has been attributed to a variable quantity of [3Fe-xS] clusters (fig.IV.11a). Quantitation of the g=2.01 signal accounted for an average of 0.08 spins/molecule, or roughly 4% of the total clusters present. Decreasing the isolation time or degassing the buffer solutions used in the isolation procedure lowered the concentration of [3Fe-xS] clusters.

Reduction of the as isolated sample by a ten-fold excess of dithionite yielded the EPR spectrum given in figure IV.12a. This broad and complex spectrum, centered at g = 1.95, arises from spin coupling of the two, S = 1/2, $[4Fe\text{-}4S]^{+1}$ clusters, which are believed to be 12 Å apart (29-30). The spin quantitations for three distinct protein preparations ranged from 1.0 to 1.3 spins/molecule.

Reconstituted C. pasteurianum Fd

After reconstitution with iron and sulfide, an EPR signal which was similar to the oxidized as isolated signal, but with greatly decreased signal intensity was observed (fig. IV.11b). Spin quantitation of this signal accounted for < 0.01 spin/molecule. The low temperature MCD of this sample was featureless and independent of temperature, indicative of the absence of any appreciable concentration of paramagnetic iron-sulfur clusters.

Figure IV.12b shows the EPR spectrum of reconstituted C. pasteurianum Fd, reduced with a ten-fold excess of dithionite. The spectrum is similar to the as-isolated, reduced spectrum, given in the upper trace. After reconstitution, the quantitation of this signal increased to 1.7 $\pm$ 0.15 spins/molecule.

The MCD spectra of the reduced, reconstituted protein, from 800 to 250 nm, at 1.55, 4.22, and 8.80 K, and 4.5 tesla, are given in figure IV.13. The spectra closely resemble the spectra of Johnson et al. (45), which were recorded in the range 800 to 350 nm. By minimizing the amount of dithionite added, it was possible to substantially increase the scan range into the near-UV. Absorption of the incident radiation by dithionite and the polypeptide backbone leads to a decrease in the signal-to-noise ratio below 330 nm. The

low temperature MCD spectra exhibit more than nine, well resolved, discrete temperature dependent transitions, in contrast to the featureless absorption spectrum given by the dashed line of figure IV.9. The corresponding magnetization data, collected at several prominent peaks in the MCD spectrum was found to be independent of wavelength. A representative plot, measured from the trough at 620 nm to the peak at 532 nm, is given in figure IV.14. The solid line in the figure is the theoretical curve corresponding to an isolated, isotropic, S = 1/2 ground state, with g = 1.95. The experimental data are well fit to the theoretical curve, and therefore the MCD spectrum was attributed to the EPR active $[4Fe\text{-}4S]^{+1}$ clusters.

C. pasteurianum Fd oxidatively damaged

The reconstituted protein was exposed to air for fifteen hours at 0 ^{o}C. The form of the EPR spectra, in both oxidation states, resembled the spectra cited above of the reconstituted protein. The spin concentration of the g = 2.01 signal increased to 0.02 spins/ molecule. The MCD spectra in both oxidation states were indistinguishable from the freshly reconstituted protein (data not shown).

Addition of a 1.5 fold stoichiometric excess of ferricyanide/protein for sixty minutes at room temperature resulted in a ten fold increase in the g = 2.01 EPR signal, to 0.2 spins/molecule. The MCD spectrum of this sample was dominated by contributions from the ferricyanide (data not shown).

The Fd was then reduced with a large excess of dithionite. It was necessary to employ a larger excess of reductant due to the presence of excess ferricyanide in the sample. The EPR spectrum of this sample resembled the spectra depicted in figure IV.12, and accounted for 1.1 spins/molecule. The MCD spectra of dithionite reduced, ferricyanide treated C. pasteurianum Fd from 800-350 nm, at 1.65, 4.22, 8.2, and 13.0 K, and 4.5 tesla, are given in figure IV.15. Ferricyanide is diamagnetic in the reduced state, and therefore, will not contribute significantly to the low temperature MCD spectra. Magnetization data were collected at the prominent peaks at 750 and 400 nm, at temperatures between 1.66 and 8.2 K, and magnetic fields between 0 and 4.5 tesla (fig. IV.16). The magnetization data exhibits strong wavelength dependence. The data at 750 are fit by a theoretical curve arising from an axial ground state with $g_{\parallel}$ = 8.0, and $g_{\perp}$ = 0.0. At 400 nm, the data can be

reproduced by assuming that 50% of the MCD intensity originates from an axial, $g_{\parallel} = 8.0$, $g_{\perp} = 0.0$ ground state, and 50% from an isotropic $g = 1.95$ ground state. Since the EPR spectrum only exhibits the $g = 1.95$ signal, it follows that the axial species is EPR silent.

4.2.3 Discussion

The presence of only a small EPR signal at $g = 2.01$, and the absence of a temperature dependent MCD spectrum, arising from the oxidized reconstituted C. pasteurianum Fd, clearly demonstrates the virtual absence of [3Fe-xS] clusters after reconstitution. The MCD spectra given in figure IV.13 are therefore the first spectra of reduced C. pasteurianum Fd containing only [4Fe-4S] clusters. A comparison of the MCD spectra of reduced C. pasteurianum Fd and reduced Desulfovibrio africanus Fd I (48) at 1.55 K and approximately 4.5 tesla is given in figure IV.17. The reduced D. africanus Fds both give rise to simple rhombic EPR spectra, $g = 2.06, 1.94, 1.89$ (48), indicative of isolated $[4Fe\text{-}4S]^{+1}$ clusters, whereas the reduced C. pasteurianum Fd exhibits a complex EPR spectrum due to spin-spin interaction involving the two [4Fe-4S] clusters. The magnitude of the spin coupling in

reduced C. pasteurianum Fd must be << 1 cm^{-1} in order not to abolish the EPR spectrum. In contrast, the magnitude of the Zeeman splittings, in the low temperature MCD experiment, with magnetic fields of 4.5 tesla, are greater than 4 cm^{-1}. Weak, intercluster coupling of this magnitude is therefore insignificant in the MCD.

In order to quantify chromophores via the intensity of the MCD spectrum, it is necessary to compare the spectra of analogous chromophores, of known concentration, under near identical conditions. The MCD extinction coefficients, of C. pasteurianum Fd, and D. africanus Fd I and II, are very similar per [4Fe-4S] cluster. At 1.55 K, and 4.5 tesla for C. pasteurianum Fd and 4.9 tesla for D. africanus Fd I and II, the following extinction coefficients per [4Fe-4S] cluster were observed:

Wavelength (nm)	C. pasteurianum Fd	D. africanus Fd I	D. africanus Fd II
740	26	33	37
620	-29	-28	-25
530	52	48	47
360	47	50	48

These extinction coefficients provide a standard for the quantitation of [4Fe-4S] clusters in more complex, mulicomponent metalloproteins (see chapter VI).

The magnetization data from the reduced, reconstituted C. pasteurianum Fd, are well fit by theoretical data corresponding to an isolated, isotropic, S = 1/2 ground state, with $g = 1.95$. According to the previous discussions on magnetization data (chapters II.1 and IV.1), the form of the magnetization curve from this type of ground state is independent of the polarization of the electronic transitions. In the absence of any additional paramagnetic chromophores, magnetization plots arising from such states are independent of wavelength. This was indeed, observed for C. pasteurianum Fd, after reconstitution.

Recently, certain tetrameric clusters have been shown to exhibit ground states with $S > 3/2$ (49). These states are characterized by the presence of a weak signal at approximately $g = 5.5$ and a corresponding decrease in the quantitation of the $g = 1.95$ EPR signal. Although no MCD magnetization data is currently available for these systems, the theory predicts that such curves would approach saturation at a much steeper rate than an S = 1/2 system. Furthermore, nesting may be observed if the excited Zeeman components are thermally accessible over

the range of the experiment. We found no evidence for the presence of any S > 1/2 ground states in reduced, reconstituted C. pasteurianum Fd.

In agreement with Thomson et al. (43), a significant change was observed in the EPR and MCD spectra of C. pasteurianum Fd upon addition of strong oxidants. A summary of the EPR quantitations for the various Fd samples investigated is given below. Clearly, if C. pasteurianum Fd is to be used as a standard for quantifying EPR spectra, it must be reconstituted first.

Sample	oxidized spins/molecule	reduced spins/molecule
as isolated	0.08	1.25
reconstituted	<0.01	1.70
air exposed 15 hours	0.02	-----
1.5 excess of ferricyanide	0.20	1.10

Unlike reduced, reconstituted Fd, magnetization data arising from reduced, ferricyanide treated sample exhibited clear wavelength dependence. This dependence is attributed to the presence of two chromophores, with distinctly different ground states, although variations in the electronic polarizations may also be contributing

(see chapters IV.1 and V). Theoretical magnetization curves were utilized to determine the contributions of each individual chromophore to the total intensity of a particular transition. At 750 nm, virtually 100% of the MCD intensity has been attributed to an axial chromophore with g = 8.0, 0.0, 0.0, which has been shown to correspond to the ground state of a reduced [3Fe-xS] cluster (43). While the $[4Fe\text{-}4S]^{+1}$ clusters would also be expected to contribute at this wavelength, the extinction coefficient for the [3Fe-xS] cluster is an order of magnitude larger, and therefore overwhelms any contributions from the $[4Fe\text{-}4S]^{+1}$ clusters. At 400 nm, the magnetization data is consistent with equal contributions from both types of clusters.

In conclusion it was found that $[4Fe\text{-}4S]^{+1}$ clusters gave rise to both qualitatively and quantitatively similar low temperature MCD spectra, regardless of the number of such clusters present in the system. MCD, therefore provides an invaluable method for identifying, and quantifying these clusters. Secondly, in the absence of contaminating [3Fe-xS] clusters, magnetization plots of reduced C. pasteurianum Fd are well fit by equation II. 7, with $g_{isotropic}$ = 1.95. Thirdly, MCD magnetization curves provide an effective method for selectively monitoring the transitions of an individual chromophore

in a complex, multicomponent protein. Finally, ferricyanide can drastically alter $[4Fe\text{-}4S]^{+1,+2}$ clusters, but does not generate a Chromatium- type HiPIP $[4Fe\text{-}4S]^{+3}$ cluster.

References

1. Yasunobu, K., and Tanaka, M., (1973) in "Iron-Sulfur Proteins" Vol. II (Lovenberg, W. ed.), pp 27-123, Academic Press, New York

2. Lovenberg, W. (1971) Methods Enzymology 24, 477-480

3. Eaton, W., and Lovenberg, W., (1973) in "Iron-Sulfur Proteins" Vol. II, (Lovenberg, W. ed.), pp 131-162, Academic Press, New York

4. Atherton, N.M., Garbett, K., Gillard, R.D., Mason, R., Mayhew, S.J., Peel, J.L., and Stangroom, J.E., (1966) Nature 212, 590-593

5. Lovenberg, W., and Williams, W., (1969) Biochem. 8, 141-148

6. Eaton, W.A., and Lovenberg, W., (1970) J. Am. Chem. Soc. 92, 7195-7198

7. Phillips, W.D., Weiher, J.F., and McDonald, C.C., (1970) Nature 227, 574-576

8. Evans, D.F., (1959) J. Chem. Soc. 20903-20905

9. Schulz, C., (1979) PhD dissertation, University of Illinois at Urbana-Champaign

10. Long, T.V., and Loehr, T.M., (1970) J. Am. Chem. Soc. 92, 6384-6386

11. Long, T.V., Loehr, T.M., Allkins, J.R., and Lovenberg, W. (1971) J. Am. Chem. Soc. 93, 1809-1811

12. Yachandra, V.K., Hare, J., Moura, I., and Spiro, T.G., (1983) J. Am. Chem. Soc. 105, 6455-6461

13. Czernuszewicz, R.S., LeGall, J., Moura, I, and Spiro, T.G., (1986) J. Inorg. Chem. 25, 696-700

14. Watenpaugh, K.D., Sieker, L.C., and Jensen, L.H., (1980) J. Mol. Biol. 138, 615-633

15. Herriott, J.R., Sieker, L.C., Jensen, L.H., and Lovenberg, W., (1970) J. Mol. Biol. 50, 391-406

16. Watenpaugh, K.D., Sieker, L.C., Herriott, S.R., and Jensen, L.H., (1972) Cold Spring Harbor Symp. Quant. Biol. 36, 359-367

17. Jensen, L.H. (1973) in "Iron-Sulfur Proteins" Vol. II, (Lovenberg, W. ed.), pp 164-193, Academic Press, New York

18. Watenpaugh, K.D., Sieker, L.C., and Jensen, L.H., (1979) J. Mol. Biol. 131, 509-522

19. Schulman, G., Eisenberger, P., Blumberg, W.E., and Stombaugh, N.A., (1975) Proc. Nat. Acad. Sci. USA 72, 4003-4007

20. Sayers, D.E., Stern, E.A., and Herriott, J.R., (1976) J. Chem. Phys., 64, 427-428

21. Peisach, J., Blumberg, W.E., Lode, E.T., and Coon, M.J.. (1971) Ann. N.Y. Acad. Sci. 222, 539-561

22. Johnson, M.K., Robinson, A.E., Thomson, A.J., (1982) in "Iron-Sulfur Proteins" (Spiro, T.G., ed.) pp. 367-406, Wiley and Sons, New York

23. Rivoal, J.C., Briat, B., Cammack, R. Hall, D.O., Rao, K.K., Douglas, I.N., and Thomson, A.J., (1977) Biochim. Biophys. Acta 493, 122-131

24. Thomson, A.J., Brittain, T., Greenwood, C., and Springall, J.P., (1977) Biochem. J., 165, 327-336

25. Thomson, A.J., and Johnson, M.K., (1980) Biochem. J. 191, 411-420

26. Mortenson, L.E., Valentine, R.C., and Carnahan, J.E., (1962), Biochem. Biophys. Res. Comm., 7, 448-

27. Mortenson, L.E. and Nakos, G. (1973) in "Iron-Sulfur Proteins" Vol. I, (Lovenberg, W., ed.), pp.37-64, Academic Press, New York

28. Thauer, R.K., and Schonheit, P. (1982) in "Iron-Sulfur Proteins" (Spiro, T.G., ed.), pp. 125-141, Academic Press, New York

29. Sieker, L.C., Adman, E.T., and Jensen, L.H. (1972) Nature 235, 40-42

30. Adman, E.T., Sieker, L.C., and Jensen, L.H. (1976) J. Biol. Chem. 251, 3801-3806

31. Ghosh, D., Furey, W., Robbins, A.H. and Stout, C.D., (1982) J. Mol. Biol. 158, 73-109

32. Carter, C.W., Kraut, J., Freer, S.T., Alden, R.A., Sieker, L.C., Adman, E.T., and Jensen, L.H., (1972) Proc. Nat. Acad. Sci. USA 69, 3526-3529

33. Stephan, D.W., Papaefthymiou, G.C., Frankel, R.B., and Holm, R.H., (1983) Inorg. Chem. 22, 1550-1557

34. Carter, C.W., Freer, S.T., Xuong, N.H., Alden, R.A., and Kraut, J. (1971) Cold Spring Harbor Symp. Quant. Biol. 36, 381-385

35. Teo, B., Shulman, R.G., Brown, G.C., and Meixner, A.E., (1979) J. Am. Chem. Soc. 101, 5624-5631

36. Gersonde, K., Schlaak, H.E., Breitenbach, M., Parak, F., eicher, H., Zgorzalla, W., Kalvius, M.G., and Mayer, A., (1974) Eur. J. Biochem. 43, 307-317

37. Thompson, C.L., Johnson, C.E., Dickson, D.P.E., Cammack, R., Hall, D.O., Weser, U.K., and Rao, K.K., (1974) Biochem. J. 139, 97-103

38. Cammack, R., Dickson, D.P.E., and Johnson, C.E., (1977) in "Iron-Sulfur Proteins" Vol. III (Lovenberg, W., ed.) pp.283-330, Academic Press, New York

39. Sweeney, W.V., Bearden, A.J., and Rabinowitz, J.C. (1974) Biochem. Biophys. Res. Comm. 59, 188-194

40. Mathews, R., Charlton, S., Sands, R.H., and Palmer, G., (1974) J. Biol. Chem. 249, 4326-4328

41. Gayda, J.P., Bertrand, P., More, C. LeGall, J., and Cammack, R.C., (1981) Biochem. Biophys. Res. Comm. 99, 1265-1270

42. Harmer, M.A., and Sykes, A.G., (1981) Biochem. Biophys. Res. Comm. 101, 83-87

43. Thomson, A.J., Robinson, A.E., Johnson, M.K., Cammack, R., Rao, K.K., and Hall, D.O., (1981) Biochim. Biophys. Acta 637, 423-432

44. Johnson, M.K., Spiro, T.G., and Mortenson, L.E., (1982) J. Biol. Chem. 257, 2447-2452

45. Johnson, M.K., Thomson, A.J., Robinson, A.E., Rao, K.K., and Hall, D.O., (1981), Biochim. Biophys. Acta 667, 433-451

46. Rabinowitz, J. (1971) Methods Enzymol. 24, 431-446

47. Vanngard, T., (1972) Copper Proteins in "Biological Applications of EPR" (Swartz, H.M., ed.), pp. 411-447, John Wiley, New York

48. Hatchikian, E.C., Cammack, R., Patil, D.S., Robinson, A.E., Richards, A.J.M., George, S., and Thomson, A.J., (1984) Biochim. Biophys. Acta 784, 40-47

49. Lindahl, P.A., Day, E.P., Kent, T.A., Orme-Johnson, W.H., and Munck, E., (1985) J. Biol. Chem. 260, 11160-11173

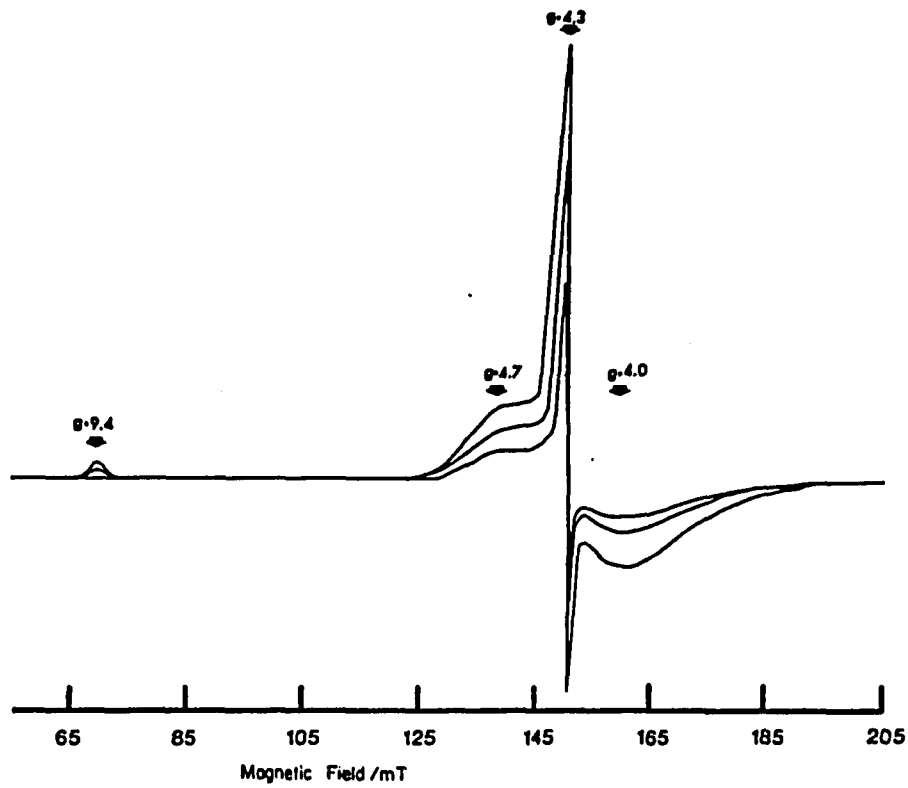

Figure IV.1 EPR spectra of oxidized C. pasteurianum Rd. Protein concentration: 0.034 mM in 0.15 M Tris-HCl, pH 7.4, containing 50% v/v ethylene glycol. Conditions of measurement were: temperatures, 10, 13, 19.5 K; microwave frequency, 8.990 GHz, modulation amplitude, 0.63 mT, microwave power, 1 mW, gain, 1,000.

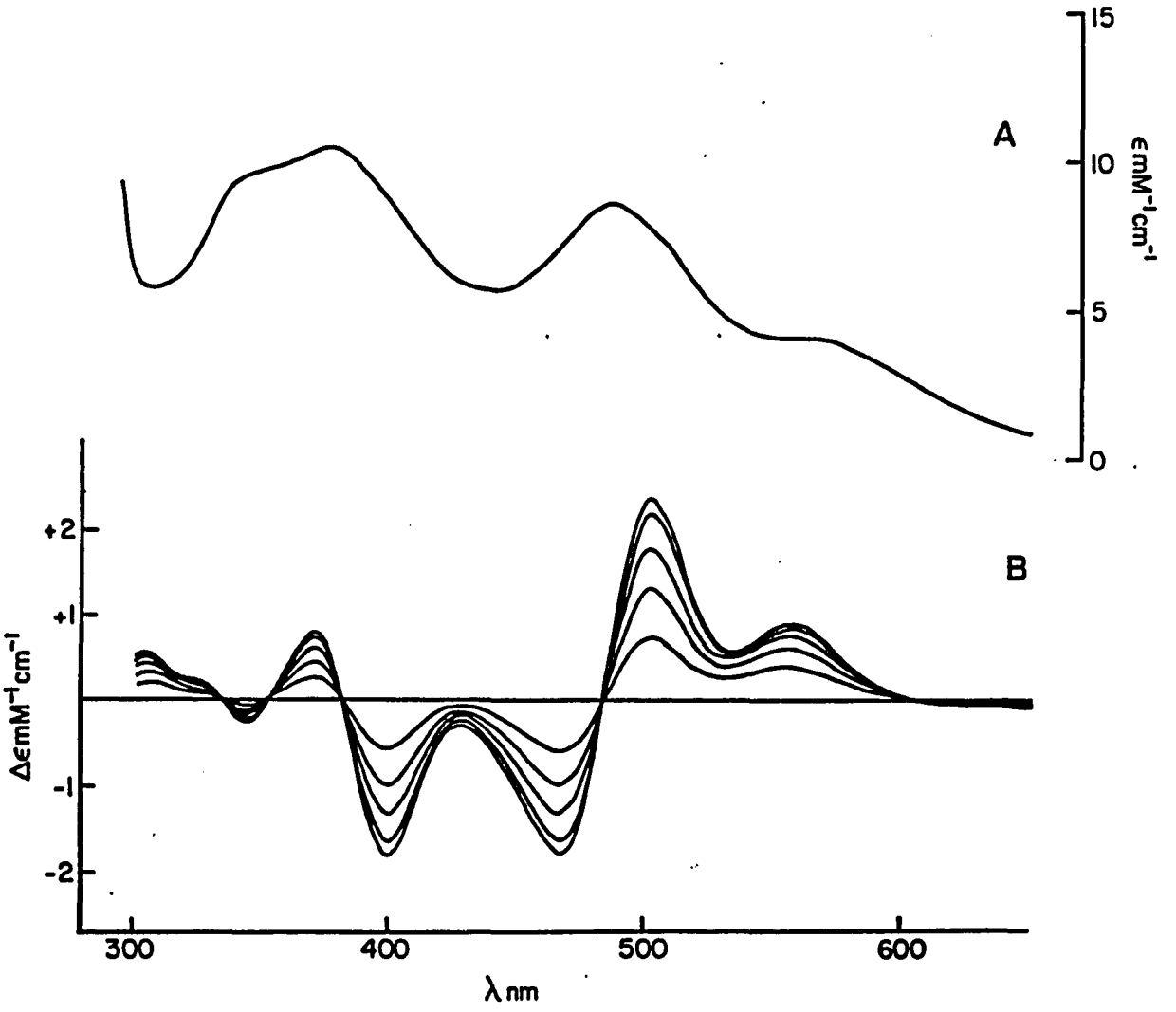

Figure IV.2 Low temperature MCD and room temperature UV-visible absorption spectra of oxidized C. pasteurianum Rd. The protein concentration was as per figure IV.1. (a) room temperature UV-visible absorption (b) MCD recorded at 1.55, 4.22, 7.2, 11.0, and 20 K, a magnetic field of 4.5 tesla, and with a pathlength of 0.169 cm.

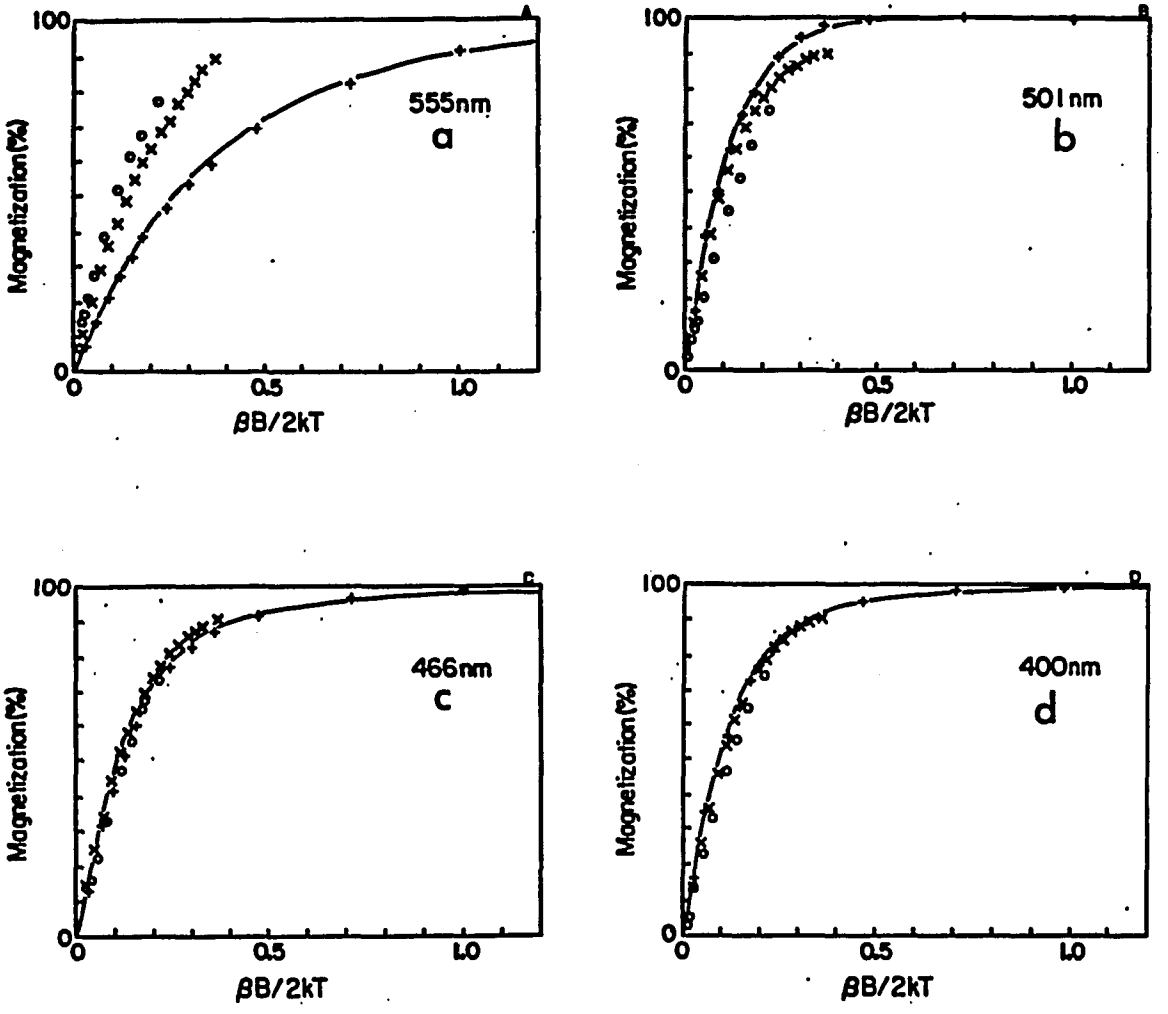

Figure IV.3 MCD magnetization data for oxidized C. pasteurianum Rd. Sample was as per figure IV.1. Temperatures 1.55 K (+), 4.22 K (x), at magnetic fields between 0 and 4.5 tesla, (o) temperatures between 7.2 anad 140 K and 4.5 tesla. Solid lines indicate theoretical fits to experimental data at 1.55 K with $g_{\parallel}$ = 9.4, and $g_{\perp}$ = 1.07. (a) wavelength, 555 nm; m_z/m_+, -100 (b) wavelength, 501 nm; m_z/m_+, +0.1 (c) wavelength, 466 nm; m_z/m_+, -0.3 (d) wavelength, 400 nm, m_z/m_+, -0.1

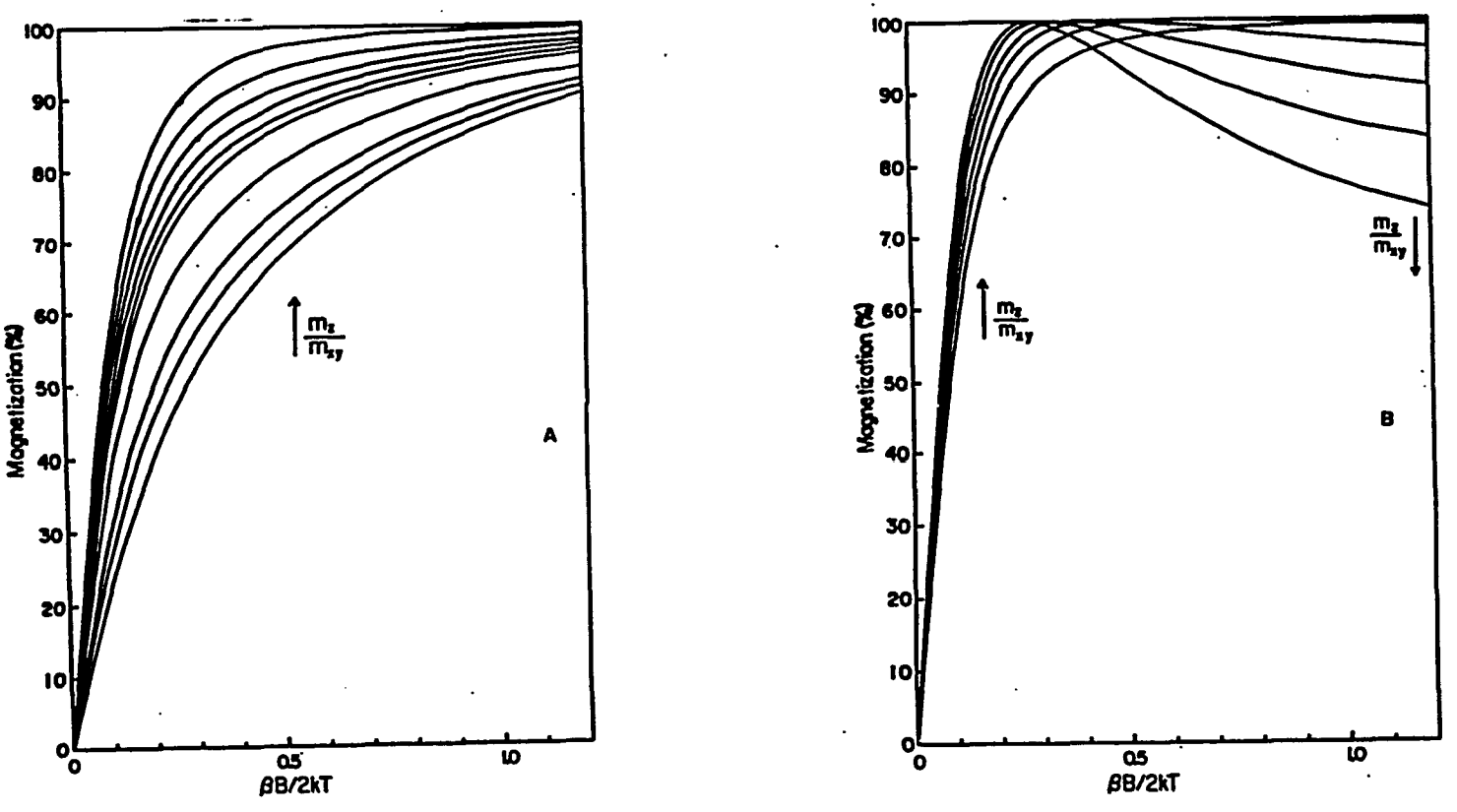

Figure IV.4 **Theoretical MCD magnetization data.** The theoretical data was calculated using equation II.6, with $g_{\parallel} = 9.68$, and $g_{\perp} = 0.75$. (a) $m_z/m_+ = 0.0, -0.2, -0.4, -0.6, -0.8, -1.0, -2.0, -5.0, -10.0, -100$ (b) $m_z/m_+ = 0.0, 0.2, 0.4, 0.6, 0.8$, and 1.0

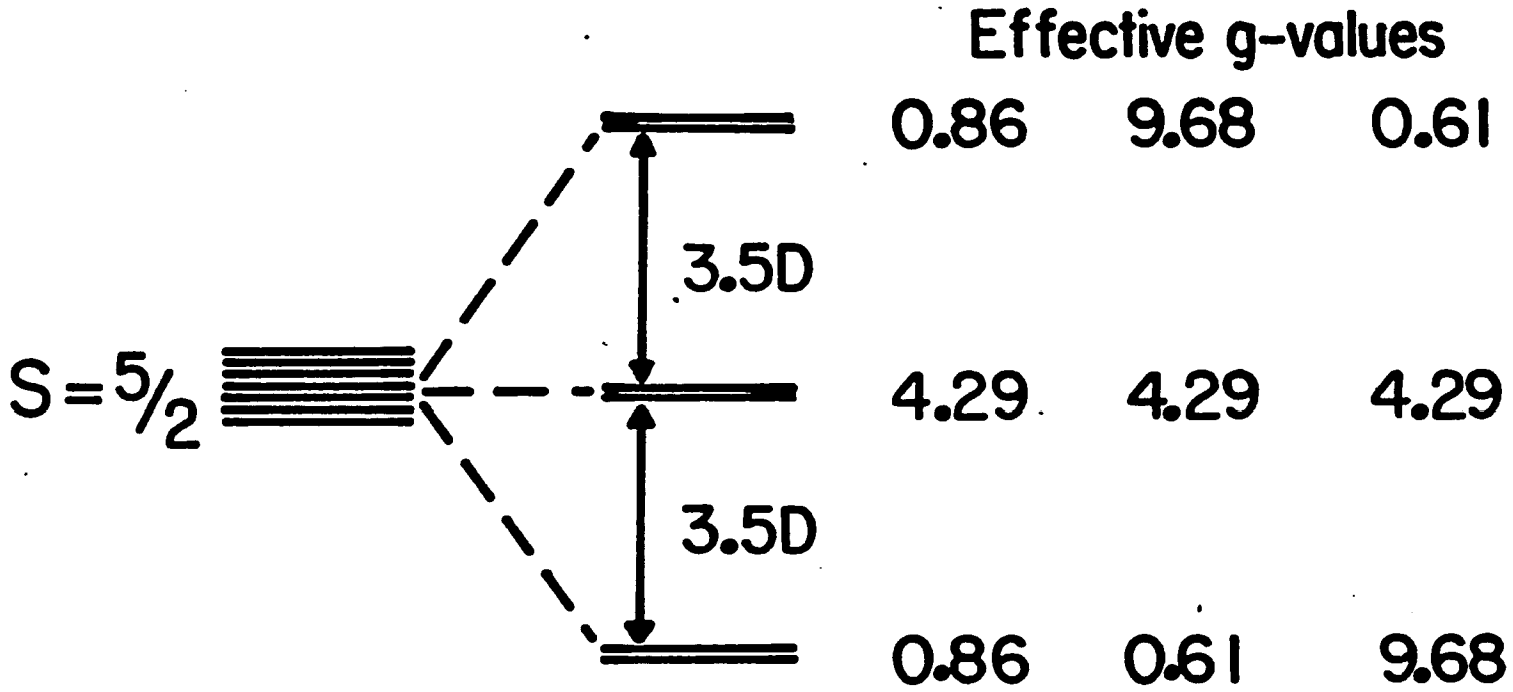

Figure IV.5 Zero field splitting of an S = 5/2 state with completely rhombic symmetry, E/D = 1/3.

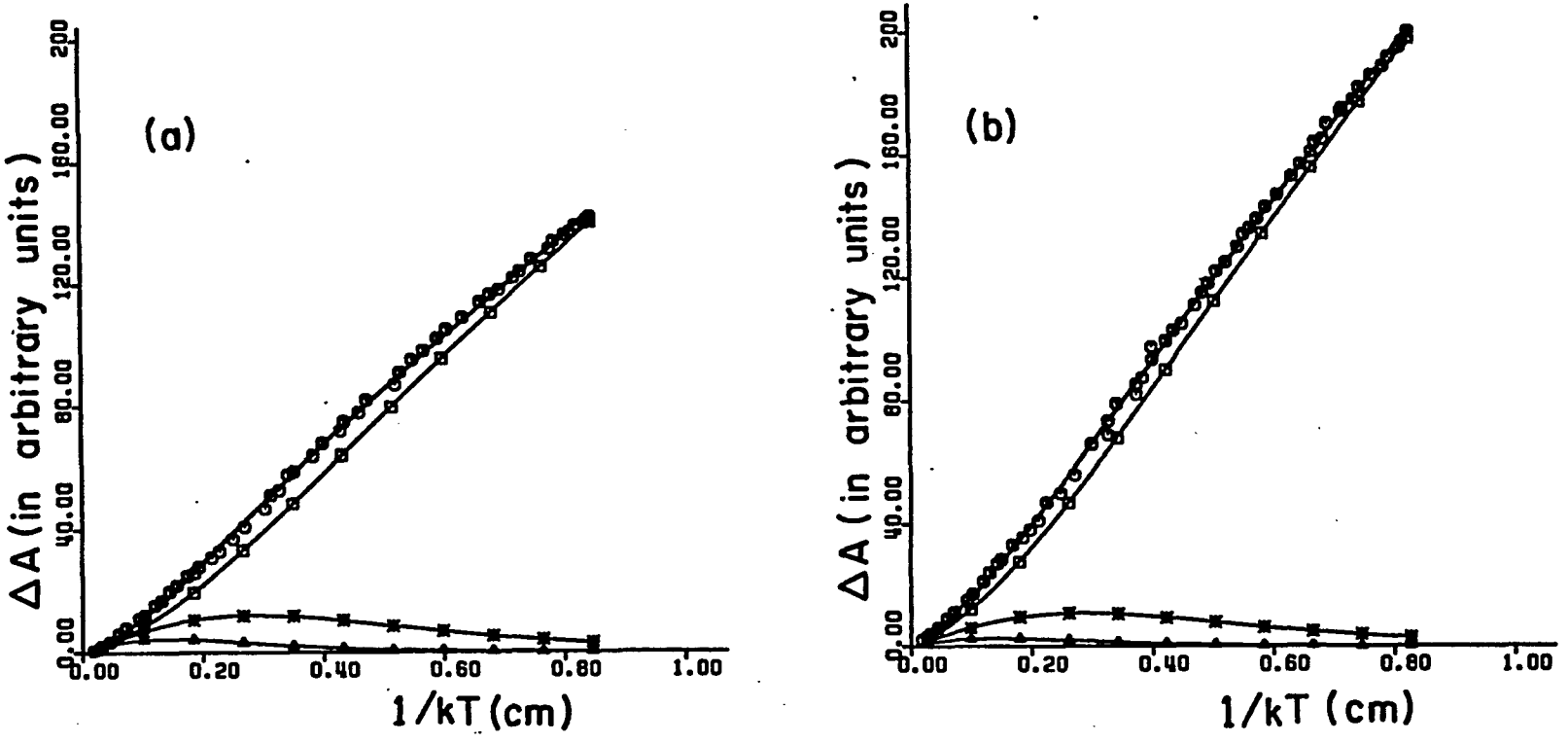

Figure IV.6 MCD temperature dependence of oxidized C. pasteurianum Rd. The magnetic field was 0.24 tesla. Circles represent the experimental data, and the solid line represents the computer generated "best-fit". □, *, and ▲, indicate the individual contributions from the lowest, middle, and upper doublets respectively. All individual contributions are plotted as positive regardless of the sign of the C-term. (a) wavelength, 400 nm; D = 1.4 cm^{-1}, c_1 = 711, c_2 = 950, c_3 = -939 (b) wavelength, 501 nm; D = 1.4 cm^{-1}, c_1 = 1029, c_2 = 839, c_3 = -528 (c values are in arbitrary units, and indicate only the relative contributions of the C-terms).

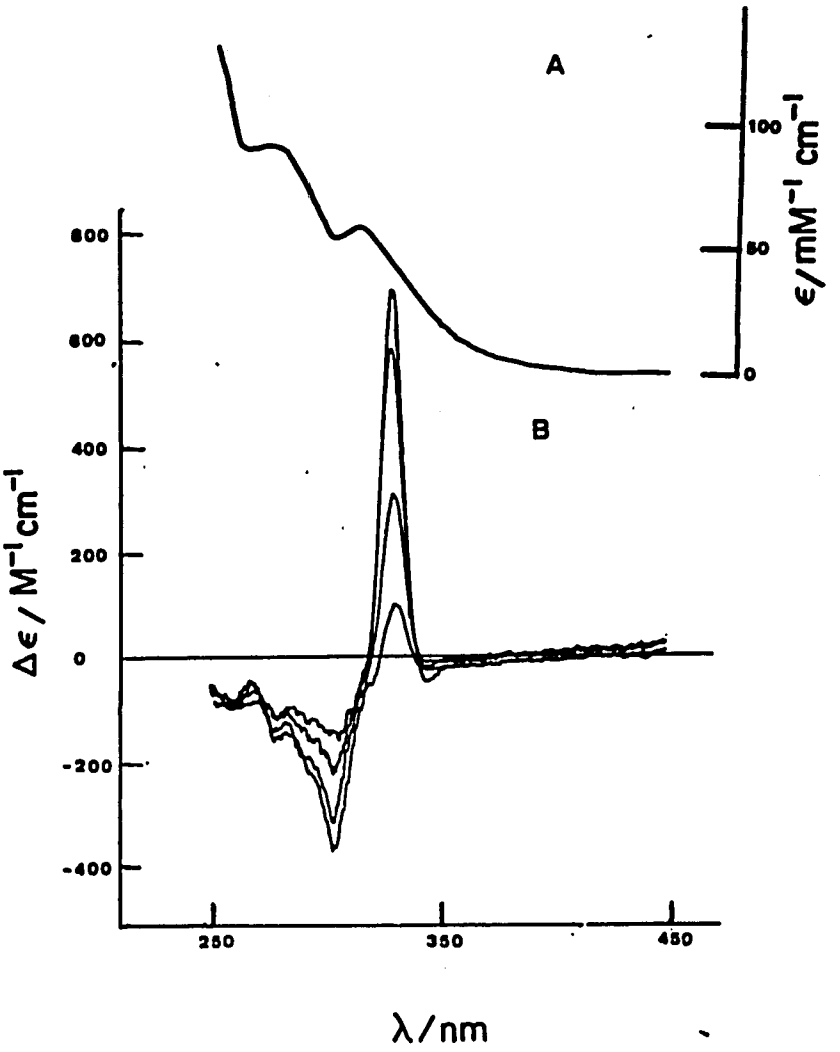

Figure IV.7 Low temperature MCD and room temperature UV-visible absorption spectra of reduced C. pasteurianum Rd. Protein concentration was 0.108 mM in 0.15 M Tris-HCl buffer, pH 7.4, containing 50% v/v ethylene glycol. The protein was reduced by addition of a ten-fold stoichiometric excess of dithionite. (a) room temperature UV-visible absorption spectrum (b) MCD recorded at temperatures of 1.62, 8.50, 30.0 and 55.0 K, a magnetic field of 4.5 tesla, and with a pathlength of 0.1628 cm.

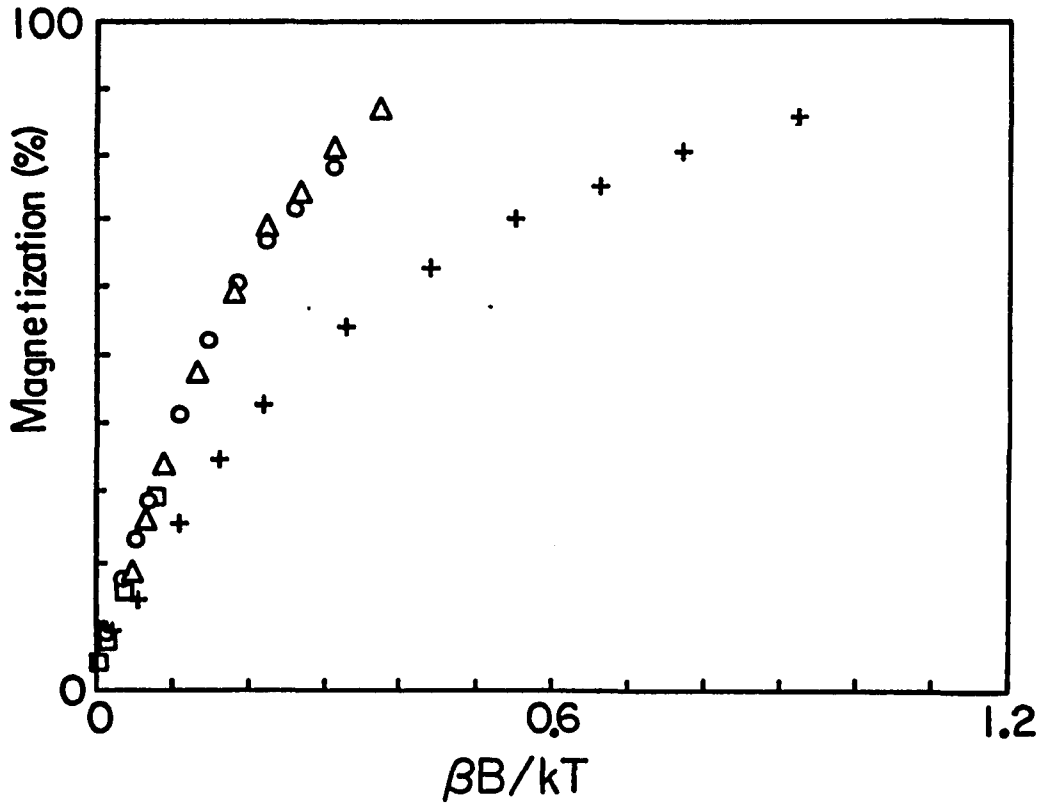

Figure IV.8 MCD magnetization data for reduced C. pasteurianum Rd. The sample was as per figure IV.7. Temperatures were: 1.67 K (+), 4.22 K (△), 4.80 K (o), and 19.5 K (□). Magnetic fields were between 0 and 4.5 tesla, and the wavelength was 330 nm.

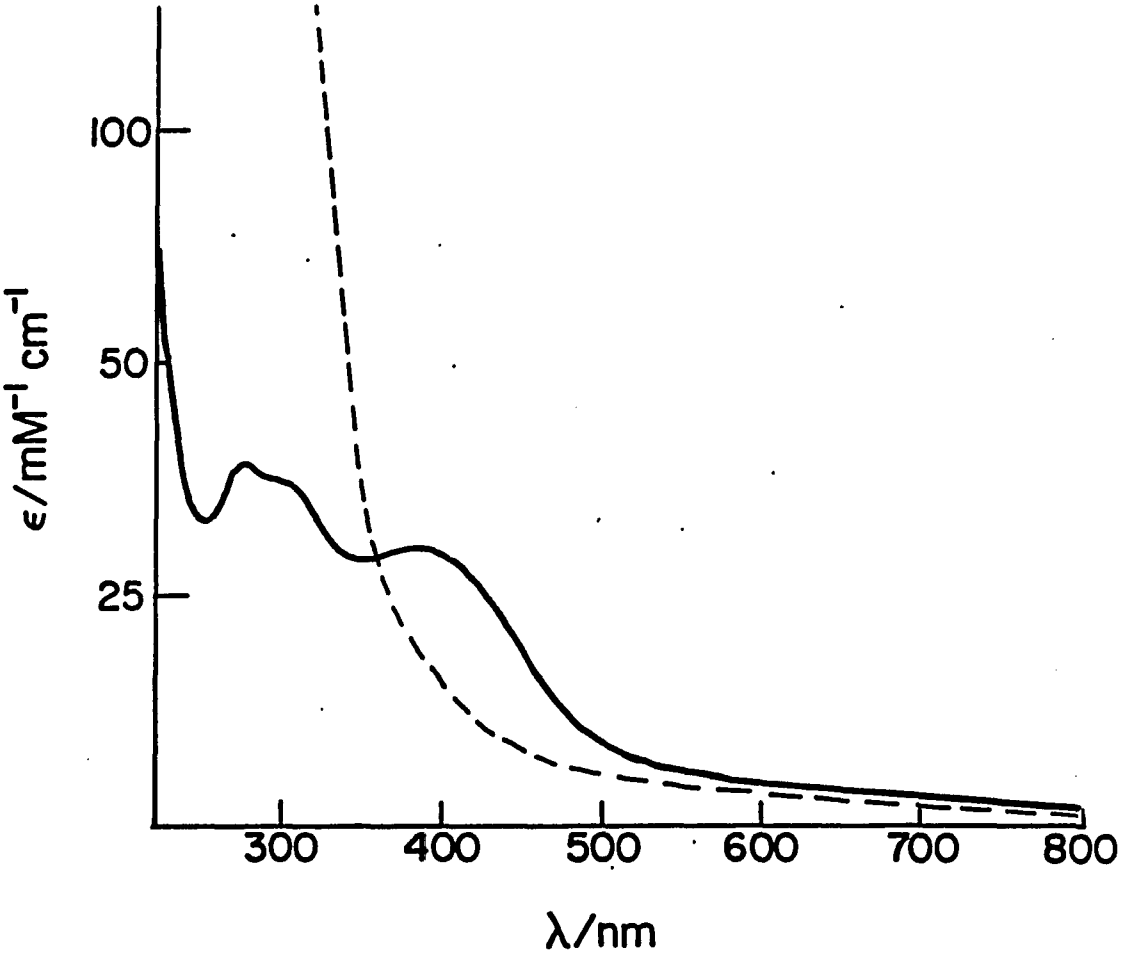

Figure IV.9: **Room temperature UV-visible spectra of oxidized and dithionite-reduced** C. pasteurianum **Fd.** Protein concentration was 0.197 mM in 0.15 M Tris-HCl buffer, pH 7.4. Solid line is as isolated spectrum, dashed line is spectrum of Fd reduced with a ten fold excess of dithionite.

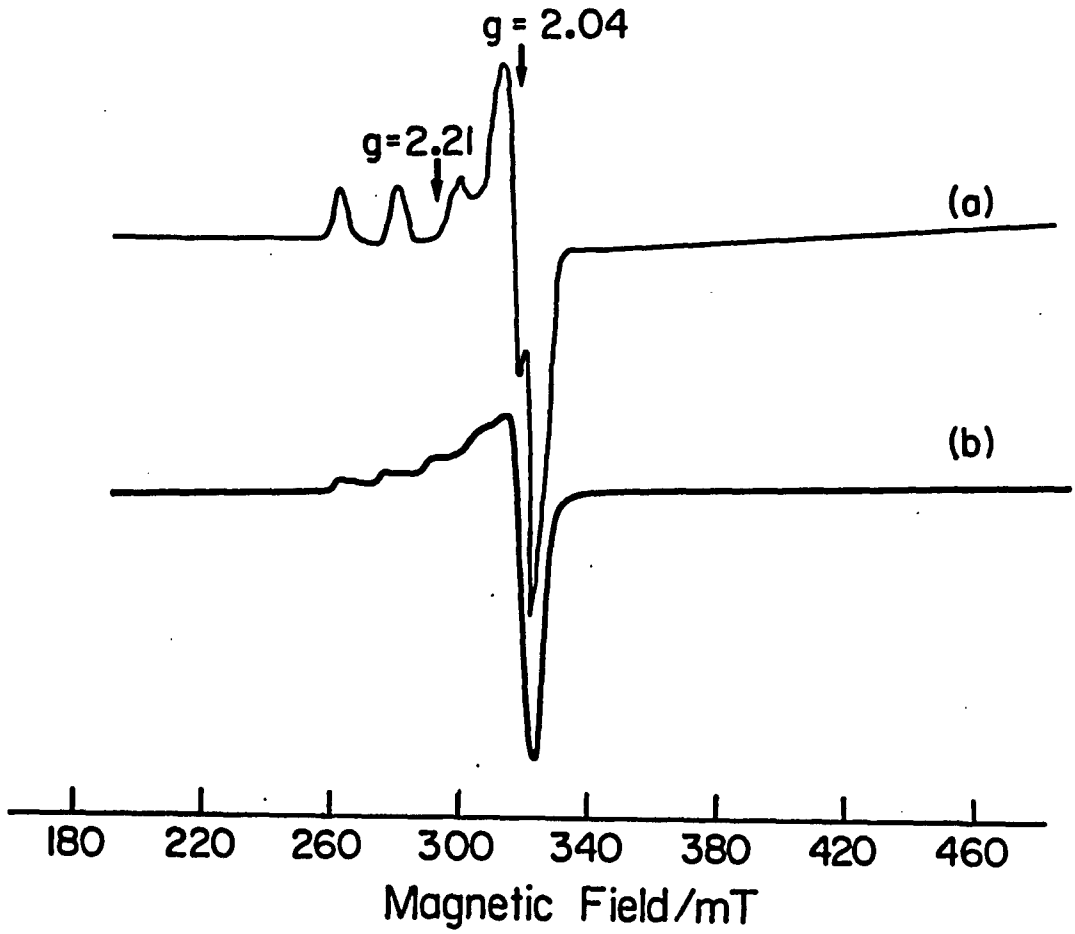

Figure IV.10: EPR spectra of C. pasteurianum copper protein and copper EDTA. Conditions of measurement were: temperature, 20 K; microwave power, 2 mW; modulation amplitude, 0.63 mT; microwave frequency, 8.985 GHz (a) C. pasteurianum copper protein, concentration unknown, in 0.15 M Tris-HCl buffer, pH 7.4, gain 6300 (b) Cu-EDTA, 1.0039 mM in deionized water.

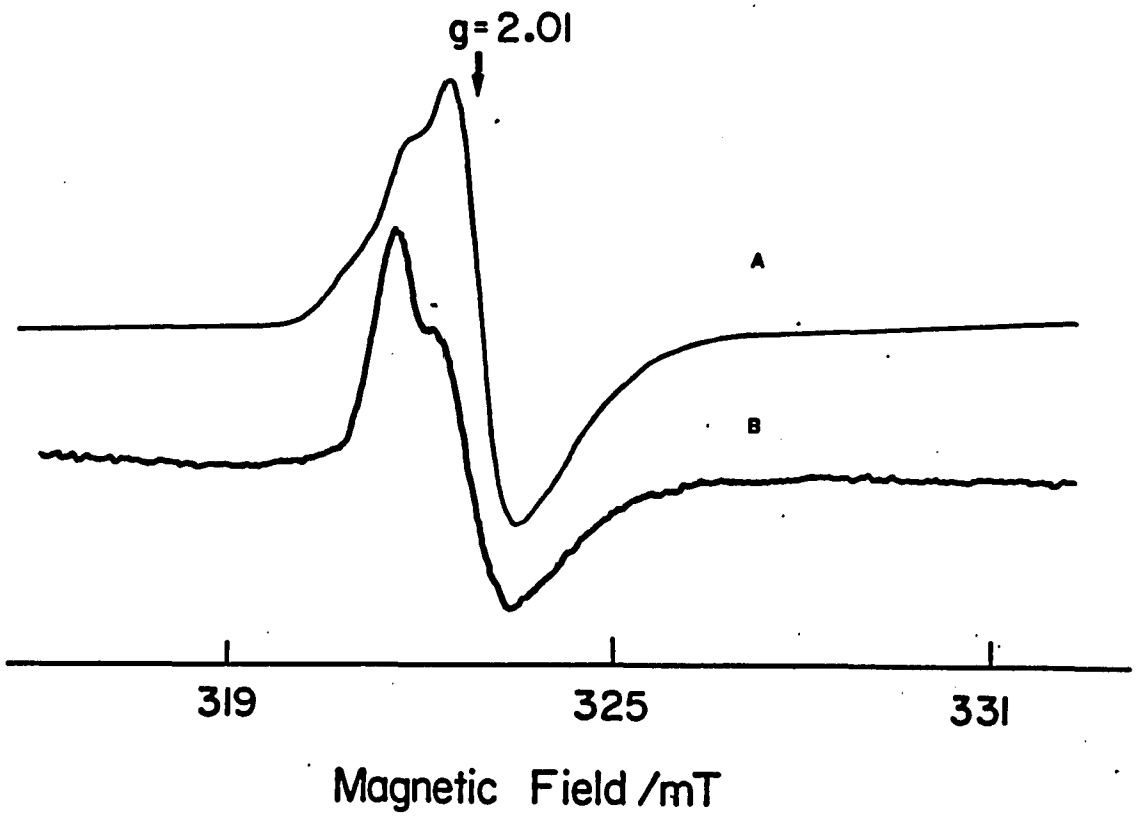

Figure IV.11: **EPR spectra of oxidized** C. pasteurianum **Fd.** Conditions of measurement were: temperature, 11.5 K; microwave power, 1 mW; modulation amplitude, 0.63 mT; microwave frequency, 8.987 GHz; (a) C. pasteurianum Fd as isolated. Protein was as per figure IV.9; gain, 800. (b) Reconstituted C. pasteurianum Fd. Protein concentration was 0.120 mM in 0.15 M Tris-HCl buffer, pH 7.4; gain, 6300.

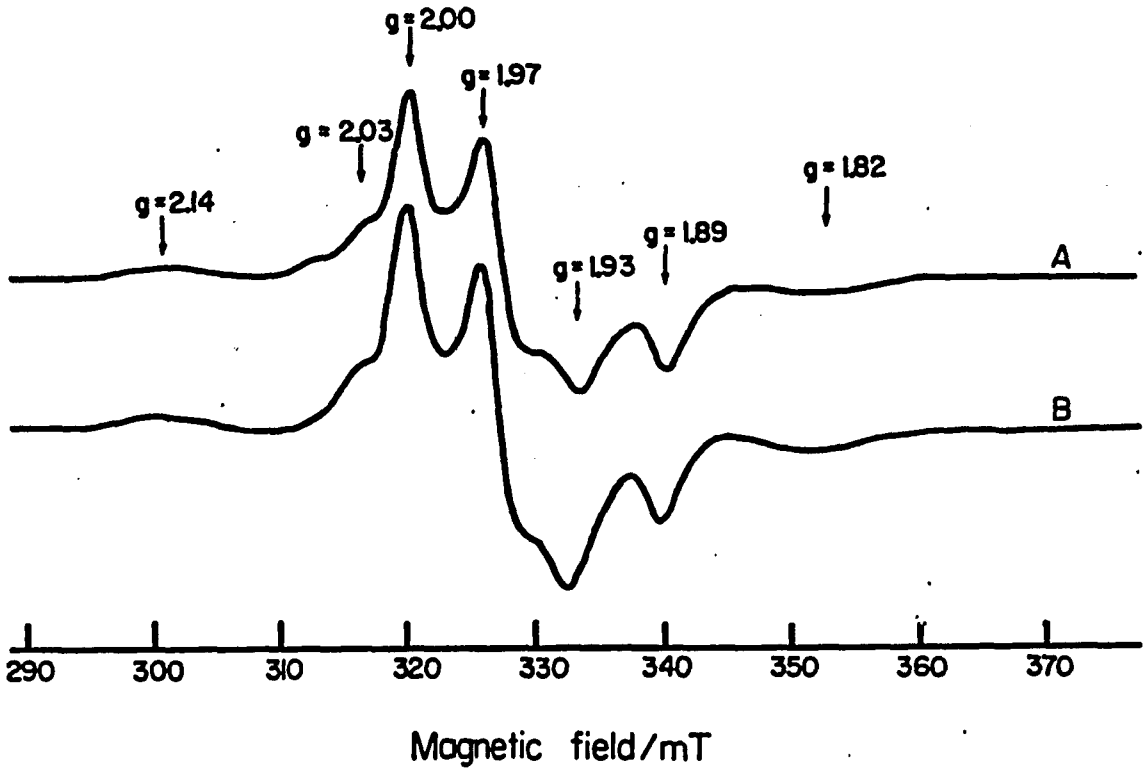

Figure IV.12: EPR spectra of dithionite-reduced C. pasteurianum Fd. Conditions of measurement were: Temperature 11.5 K; microwave power, 1 mW; modulation amplitude, 0.63 mT; microwave frequency, 8.989 GHz; (a) protein was as per figure IV.9; gain 400 (b) protein was as per figure IV.11b, with a ten fold excess of dithionite.

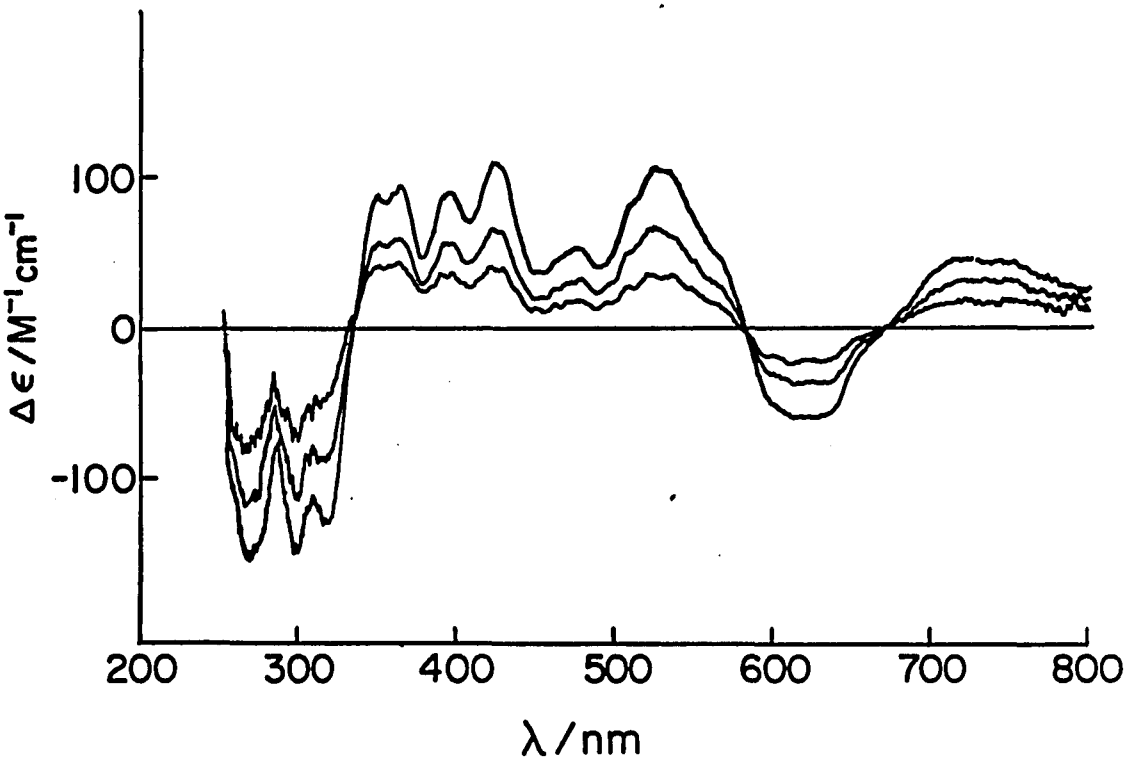

Figure IV.13: MCD spectra of reconstituted, dithionite reduced C. pasteurianum Fd. Protein was as per figure IV.12b. Conditions of measurement were: temperatures, 1.55, 4.22, and 8.80 K; magnetic field 4.5 tesla; pathlength, 0.1592 cm.

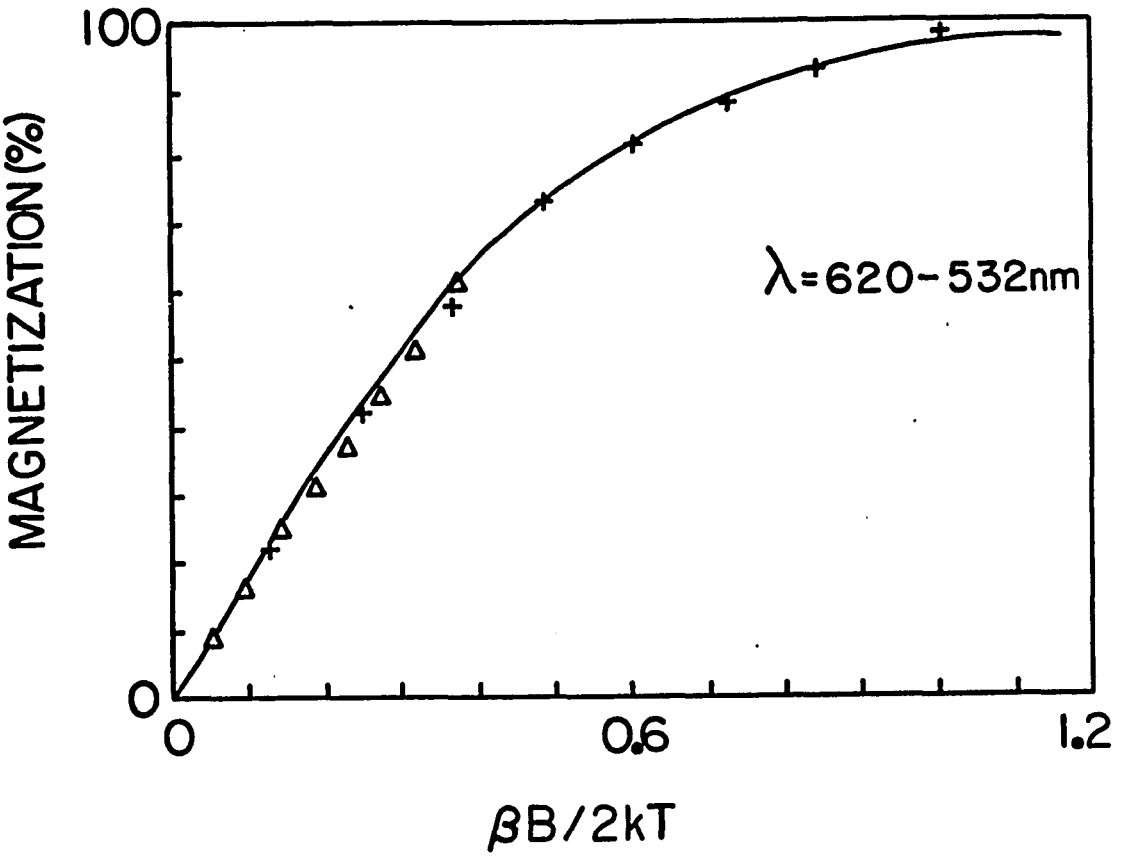

Figure IV.14: **Magnetization plot for dithionite reduced, reconstituted** C. pasteurianum **Fd.** The conditions of measurement were as per figure IV.13. Wavelength was fron the trough at 620 nm to the peak at 532 nm. Temperatures were: (+) 1.55 K, (△) 4.22 K. Magnetic fields were between 0 and 4.5 tesla. The solid line is the theoretical curve for $g_{isotropic} = 1.95$.

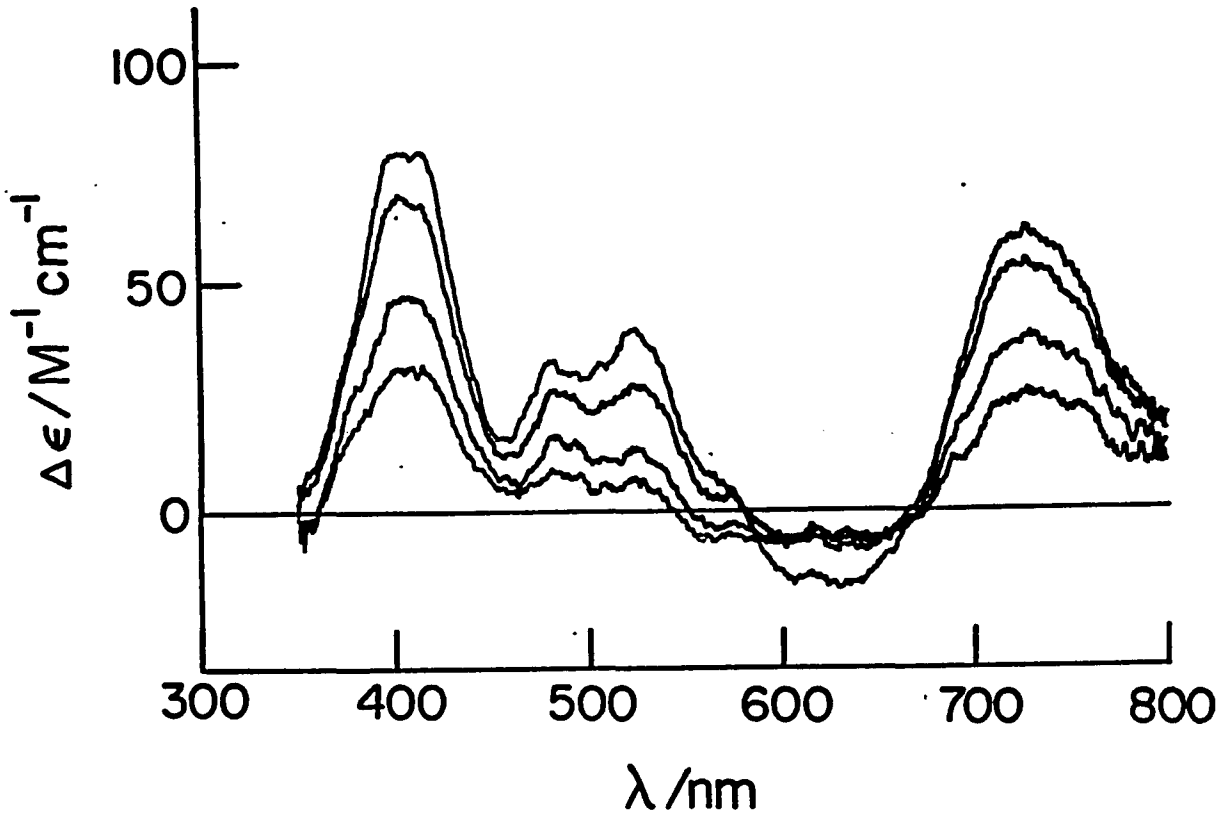

Figure IV.15: MCD spectra of dithionite reduced, ferricyanide treated C. pasteurianum Fd. Protein was 0.110 mM in 0.15 M Tris-HCl buffer, pH 7.4, 1.5 fold excess potassium ferricyanide, 20 fold excess dithionte. Conditions of measurement were: temperatures 1.65, 4.22, 8.2 and 13.0 K; magnetic field 4.5 tesla; pathlength, 0.1587 cm.

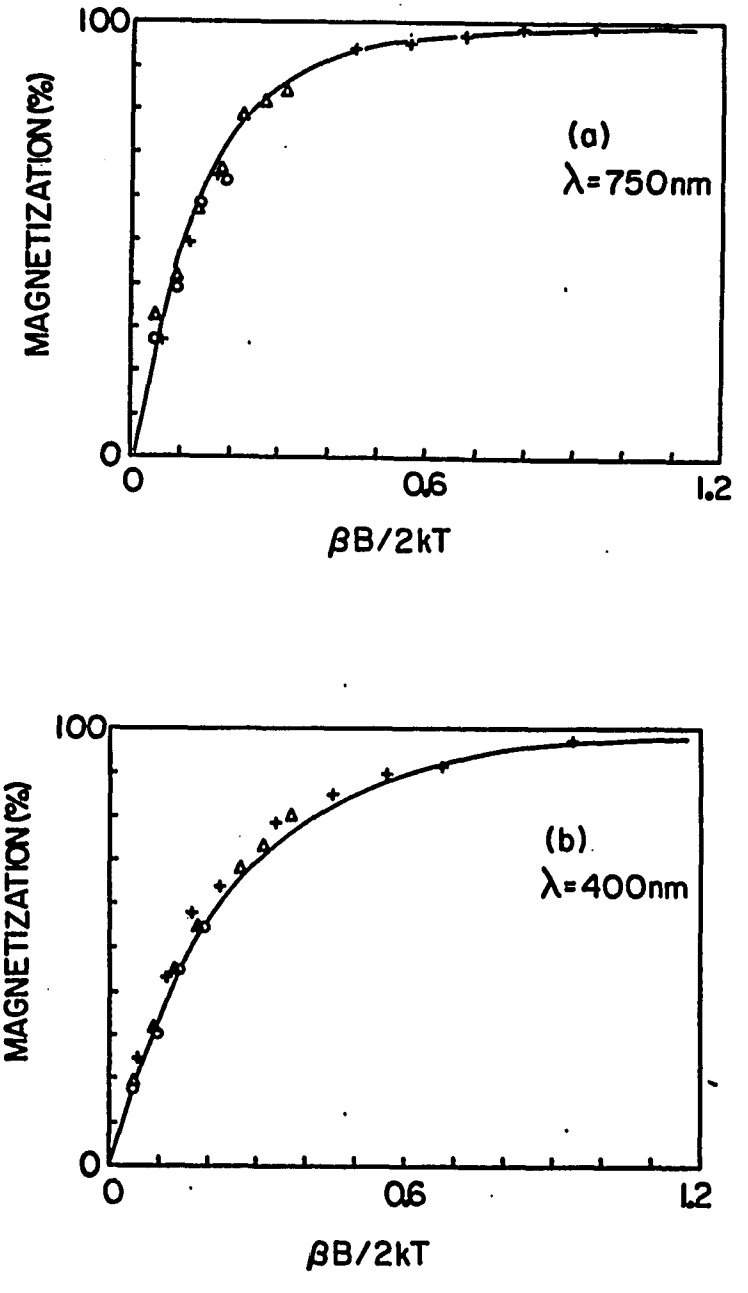

Figure IV.16: **Magnetization plots of dithionite-reduced, ferricyanide treated** <u>C. pasteurianum</u> **Fd.** Conditions of measurement as per figure IV.15. Temperatures: (+) 1.66 K, (△) 4.22 K, (o) 8.2 K. Magnetic fields were between 0 and 4.5 tesla. (a) wavelength, 750 nm; solid line corresponds to the theoretical curve for $g_{\parallel} = 8.0$, $g_{\perp} = 0.0$ (b) wavelength, 400 nm; solid line corresponds to the composite theoretical curve for 50% $g_{\parallel} = 8.0$, $g_{\perp} = 0.0$, and 50% $g_{isotropic} = 1.95$.

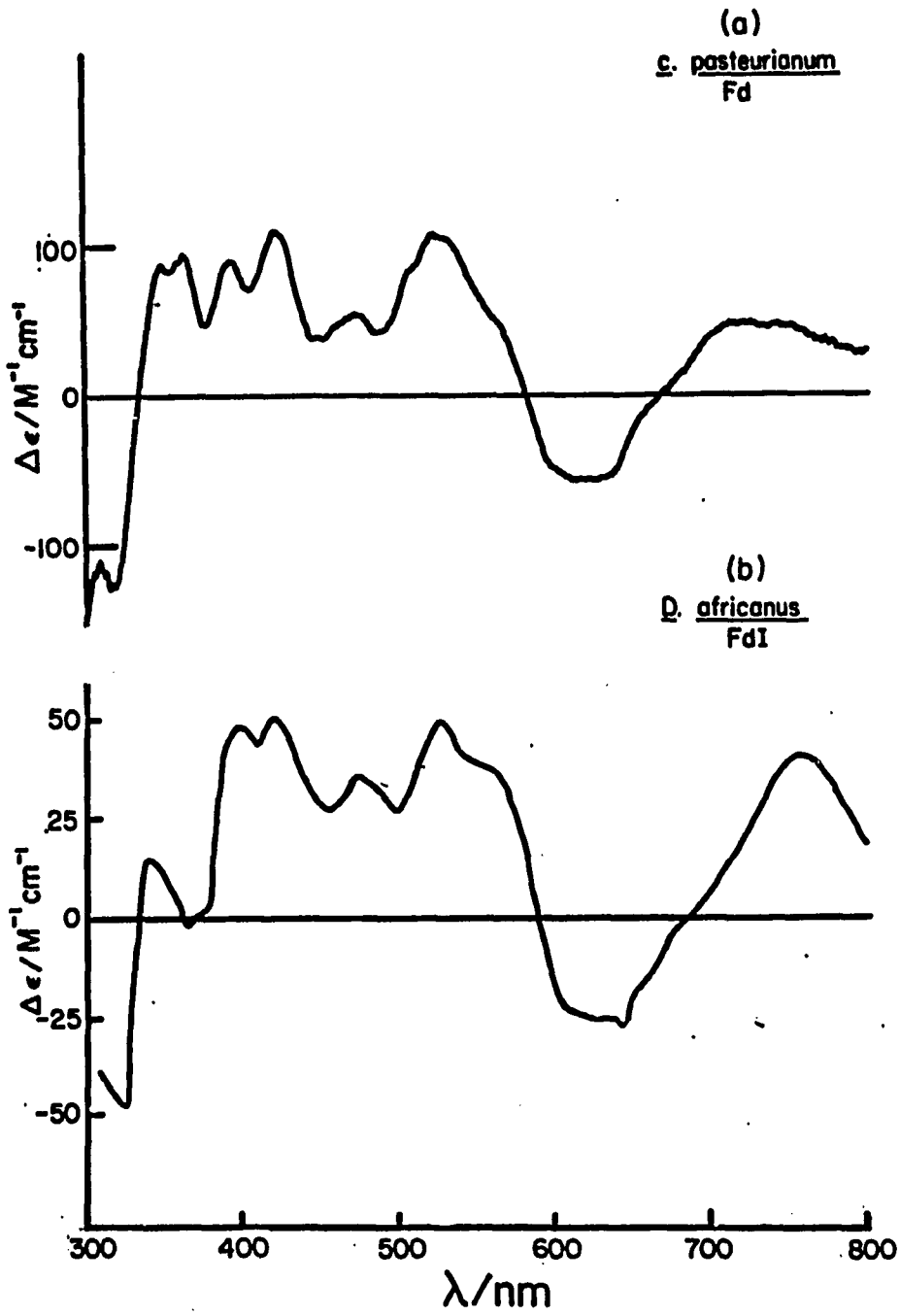

Figure IV.17: Comparison of MCD spectra of dithionite-reduced C. pasteurianum Fd and D. africanus Fd I. Temperature was 1.55 K. (a) C. pasteurianum Fd as per figure IV.13. magnetic field 4.5 tesla (b) D. africanus Fd I, reproduced from reference 48. magnetic field 4.9 tesla

Chapter 5

The Seven Iron Ferredoxins
T. thermophilus Fd and A. vinelandii Fd I

5.1 Introduction

A. vinelandii Fd I, and to a lesser extent, T. thermophilus Fd, are among the best characterized seven iron ferredoxins. A. vinelandii Fd I (often referred to as A. vinelandii iron-sulfur protein III in the older literature), has a molecular weight of approximately 14,500 Da, contains six to seven g-atoms of iron, and six to seven g-atoms of acid labile sulfide, per molecule of protein (1). The physiological function of A. vinelandii Fd I is thought to be the transfer of electrons to the

nitrogenase system (2), although the data is not conclusive. T. thermophilus Fd has a molecular weight of approximately 10,000 Da. It also contains six to seven g-atoms of iron, and six to seven g-atoms of acid labile sulfide per molecule of protein (3). Both proteins have analogous iron-sulfur cluster compositions, i.e. one [3Fe-xS] cluster and one cubane [4Fe-4S] cluster. The midpoint potentials of the [3Fe-xS] clusters are -250 mV (4) and -420 mV (5,6) , and the midpoint potentials of the $[4Fe\text{-}4S]^{1+,2+}$ clusters are -530 (4) and < -600 mV (7,8) for the T. thermophilus and the A. vinelandii ferredoxins respectively.

The structure of the [3Fe-xS] cluster remains controversial despite X-ray crystallographic data for A. vinelandii Fd I at 3.0 Å (9), 2.5 Å (1), and 2.0 Å (10,11). According to the latest X-ray diffraction study, the [3Fe-xS] cluster in A. vinelandii Fd I has the composition $[3Fe\text{-}3S](S\gamma)_5(oxo)$. The oxo moiety is believed to be solvent oxygen, donated from either water or hydroxyl ion, but not from glutamate (10). the [3Fe-3S] cluster adopts a nearly planar configuration, with approximate tetrahedral coordination about each of the iron atoms (fig. I.2c). The iron-iron distances are large, averaging almost 4.1 Å. X-ray diffraction studies of two other proteins which contain [3Fe-xS] clusters, D.

gigas Fd II (12) and inactive aconitase (13) have recently been completed. The resolution of the D. gigas Fd II study was not sufficient to resolve the iron atoms. X-ray crystallographic studies on aconitase, however, indicate an iron-iron distance of 2.7 Å. It has therefore been suggested that the trimeric cluster in A. vinelandii Fd I and aconitase are structurally inequivalent (13). No X-ray diffraction data is currently available for T. thermophilus Fd.

EXAFS data for D. gigas Fd II (14) and inactive aconitase (15) indicate iron-iron distances of 2.71 Å for both proteins. This shorter distance is similar to the iron-iron distance found in [2Fe-2S] and [4Fe-4S] clusters. Based on iron and acid labile sulfide analysis, together with the EXAFS data, Bienert et al. proposed a [3Fe-4S] stoichiometry. They further suggested a cubic structure very similar to the [4Fe-4S] cluster with one iron atom removed (fig. I.2d) (15). Very recently, EXAFS analysis for A. vinelandii Fd I, oxidized with a twenty-fold excess of ferricyanide, has been completed (16). Addition of a large excess of ferricyanide to A. vinelandii Fd I is thought to completely degrade the [4Fe-4S] cluster while leaving the [3Fe-xS] cluster intact. Contrary to the X-ray diffraction results, the EXAFS data indicates a [3Fe-4S]

core stoichiometry, with iron-iron distances of 2.7 Å and iron-sulfur distances of 2.3 Å. Furthermore, the Fourier transform of the A. vinelandii Fd I EXAFS data is virtually superimposable on the aconitase transform.

A cluster stoichiometry of [3Fe-4S] has also been proposed by Johnson et al based on resonace raman data from a wide variety of [3Fe-xS] cluster containing proteins, including A. vinelandii Fd I, T. thermophilus Fd, D. gigas Fd II, ferricyanide treated C. pasteurianum Fd, and inactive aconitase, all in the oxidized state (17,18). Polarization studies and normal mode calculations could be rationalized in terms of several proposed [3Fe-4S] structures, but not in terms of a [3Fe-3S] cluster. Furthermore, the resonance raman spectra of all the proteins studied, were remarkably similar. Since resonance raman is extremely sensitive to small structural perturbations, this data argues against any structural inhomogeneity in this class of clusters.

The Mössbauer spectra are also very similar for all [3Fe-xS] clusters studied thus far (19-23). The Mössbauer data from T. thermophilus Fd and A. vinelandii Fd I (20,23) indicate that the iron atoms in the oxidized [3Fe-xS] cluster are present as high spin ferric ions, and that the ground state of this cluster is S = 1/2. The Mössbauer data for the reduced proteins indicate that two

of the iron atoms are equivalent in the reduced cluster. While formally the reduced [3Fe-xS] cluster contains two ferric and one ferrous ions, the valances are more accurately described by one ferric ion, and two ions which are intermediate between ferric and ferrous. The Mössbauer studies also indicate that the reduced [3Fe-xS] clusters are paramagnetic, with a ground state of integer spin, such that $S > 1$, and a negative axial zero field splitting parameter, $D < 0$. Although Mössbauer does not provide direct structural information, it does present strong evidence for homogeneity within this class of clusters.

The EPR spectra arising from the oxidized [3Fe-xS] clusters of T. thermophilus Fd and A. vinelandii Fd bear strong resemblance to each other and to other well characterized, oxidized [3Fe-xS] clusters (4, 20, 24-29) (also see chapters IV.2 and VI). The EPR spectra of these clusters are characterized by a sharp resonance at $g = 2.02$ and a broader high field resonance. Relative to other paramagnetic iron-sulfur clusters, oxidized [3Fe-xS] clusters exhibit fast spin relaxation, and are therefore, only observed in the EPR at temperatures below 30 K.

The presence of a [4Fe-4S] cluster, structurally, electronically, and magnetically analogous to the

[4Fe-4S] clusters in C. pasteurianum Fd (chapter IV.2) has been confirmed by Mössbauer spectroscopy for both A. vinelandii Fd I and T. thermophilus Fd (20, 23), by X-ray crystallography for the A. vinelandii Fd I (10), and by EPR spectroscopy for T. thermophilus Fd (27). The tetrameric cluster in T. thermophilus Fd is reducible with dithionite to yield a complex EPR signal, with $g_{average}$ = 1.94. This signal has been attributed to the S = 1/2, $[4Fe\text{-}4S]^{1+}$ cluster, interacting via weak spin-spin interaction, with the S = 2, reduced [3Fe-xS] cluster (27). Since a similar signal is not observed upon dithionite reduction of A. vinelandii Fd I, at neutral pH, the midpoint potential of the [4Fe-4S] cluster, in this protein, is therefore lower than -530 mV (7,8). A $g_{average}$ = 1.94 EPR signal has been reported A. vinelandii Fd I samples, reduced with dithionite at pH 9.0 (7). Unfortunately, this treatment also results in the partial destruction of the constituent iron-sulfur clusters.

The [4Fe-4S] cluster of A. vinelandii Fd I was found to have bond distances and bond angles which closely resemble those from other [4Fe-4S] clusters (10, chapter IV.2). The average iron-iron distance was 2.84 Å, and the average iron-sulfur distance was 2.28 Å, for the oxidized protein. The [3Fe-xS] cluster was found to be 11 Å from

the [4Fe-4S] cluster (10).

The tetrameric clusters of the seven-iron ferredoxins differ in their reactions with strong oxidizing agents, such as ferricyanide. Ferricyanide incubation of samples of A. vinelandii Fd I results in a novel three electron oxidation of the [4Fe-4S] cluster, leading to the formation of an EPR active radical species, probably a cysteinyldisulfide radical (8). As previously cited, prolonged incubation with a large excess of ferricyanide results in the selective destruction of the [4Fe-4S] cluster (16). By contrast, T. thermophilus Fd is reported to be very resistant to oxidative degradation (4, 30). Proton NMR studies of samples of dithionite reduced T. thermophilus Fd, treated with excess solid ferricyanide, have been interpreted in terms of conversion of the [4Fe-4S] cluster to a [3Fe-xS] cluster (30).

This research was undertaken in order to compare the spectroscopic and electronic properties of the oxidized and reduced iron-sulfur clusters in A. vinelandii Fd I and T. thermophilus Fd. Low temperature MCD, EPR, and room temperature UV-visible spectroscopy was employed. Detailed magnetization data was collected in order to better characterize the ground state physics of the [3Fe-xS] clusters. Additionally, the effect of pH on the

reduced [3Fe-xS] clusters was investigated. The question as to the physiological origin of the [3Fe-xS] in A. vinelandii Fd I was addressed by monitoring the EPR spectrum of an anaerobically isolated sample. Finally, the effect of ferricyanide of [4Fe-4S] clusters from a broad range of iron-sulfur proteins was examined.

5.2 Results

The room temperature absorption spectra for the samples of T. thermophilus Fd and A. vinelandii Fd I used in the EPR and MCD investigations, are given in figure V.1. Depending on the conditions of reduction by dithionite, two stable reduced states were obtainable for T. thermophilus Fd. Anaerobic addition of dithionite (up to a 100-fold excess), at room temperature, to samples containing 50% v/v ethylene glycol resulted in a stable, partially-reduced sample, with $A_{reduced}/A_{oxidized}$, at 400 nm, equal to 0.84. In contrast, addition of dithionite (>

4-fold excess), at room temperature, prior to the addition of 50% v/v ethylene glycol resulted in a stable fully reduced sample, with $A_{reduced}/A_{oxidized}$, at 400 nm, equal to 0.67. These absorption changes are consistent with those attributed to the partially-reduced (reduced [3Fe-xS], $[4Fe\text{-}4S]^{2+}$) and fully reduced (reduced [3Fe-xS], $[4Fe\text{-}4S]^{1+}$) Fd by Hille *et al.* in a combined optical/EPR reductive titration (20). This method of producing a stable partially-reduced state offers a considerable simplification compared to reduction by NADPH in the presence of a catalytic amount of $Fd{:}NADPH^{+}$ reductase (20). In contrast, dithionite reduction of *A. vinelandii* Fd I, at pH 7.8, in the presence or absence of ethylene glycol, invariably produced the partially-reduced (reduced [3Fe-xS], $[4Fe\text{-}4S]^{2+}$) sample, with $A_{reduced}/A_{oxidized}$ equal to 0.84 at 400 nm, irrespective of the excess of dithionite. This is consistent with a redox potential of < -800 mV for the [4Fe-4S] cluster in *A. vinelandii* Fd I (7, 8).

T. thermophilus Fd and *A. vinelandii* Fd I as isolated

EPR spectra of *T. thermophilus* Fd and *A. vinelandii* Fd I as isolated at 12 K, are shown in figure V.2. Both spectra exhibit a sharp peak at $g = 2.02$ and a relatively

broad feature to higher field, characteristic of oxidized [3Fe-xS] clusters (31). The form of the EPR spectra were invariant as a function of pH over the range 6.3 to 8.5. The signal from T. thermophilus Fd exhibits greater anisotropy and faster spin relaxation. At 12 K, the EPR signals begin to saturate at microwave powers greater than 2 mW and 10 mW for A. vinelandii Fd I and T.thermophilus Fd respectively (fig. V.3). Relative to other types of iron-sulfur clusters, both proteins exhibit rapid relaxation, being observed only at temperatures below 30 K.

Quantitation of the EPR signals in figure V.2 accounts for 0.7 $\pm$ 0.1 spin/molecule for A. vinelandii Fd I, and 1.0 $\pm$ 0.1 spin/molecule for T. thermophilus Fd. Anaerobically isolated A. vinelandii Fd I exhibited an identical EPR signal to that of the aerobically isolated protein, except for a slightly higher spin quantitation. This argues against the [3Fe-xS] cluster being an artifact of aerobic, oxidative damage.

The low temperature MCD of as isolated A. vinelandii and T. thermophilus ferredoxins, at temperatures between 1.55 and 16.5 K, and at a magnetic field of 4.5 tesla, are given in figure V.4. The MCD spectrum of A. vinelandii Fd I is identical to that reported previously by Morgan et al. (8). There were no changes observed in

the MCD spectra of either of the oxidized proteins in the pH range 6.3 to 8.5. Although assignment of these complex low temperature MCD spectra has yet to be acheived, the spectra are useful fingerprints of cluster type. Figure V.5 illustrates the striking similarity of the MCD spectra of several oxidized proteins, believed to contain [3Fe-xS] clusters. Below 500 nm, all oxidized [3Fe-xS] clusters characterized to date, have a similar pattern of MCD transitions that are attributable to sulfur to Fe(III) charge transfer bands.

All of the MCD transitions given in figure V.4 display pronounced temperature dependence, indicative of a paramagnetic, spin degenerate, ground state. In order to elucidate the nature of the ground state, magnetization data was collected at wavelengths corresponding to each of the major bands in the spectrum. The magnetization plots were indistinguishable, within experimental error, at all wavelengths investigated. A representative plot is given in figure V.6. All of the experimental points lie on the same curve, irrespective of the temperature of measurement, indicative of a ground state which is an isolated Kramers' doublet. No excited states are thermally accessible over the range of the experiment (1.55 to 100 K). The experimental data are well fit by

theoretical curves constructed for $g_{isotropic}$ equal 2.01. It was therefore concluded that all the transitions, which are resolved in the low temperature MCD spectra, originate from a paramagnet with an S = 1/2 ground state. This is the same paramagnet which is also responsible for the g = 2.01 EPR signal. The intensities of the MCD signals of A. vinelandii Fd I and T. thermophilus Fd, after normalization for differences in concentration, pathlength, and depolarization of the light beam, correlate well with the observed EPR spin quantitations.

Partially-reduced T. thermophilus Fd and A. vinelandii Fd I

Anaerobic incubation of A. vinelandii Fd I and T. thermophilus Fd with a 10-fold excess of dithionite, at room temperature, and pH 7.8 in the presence of 50% v/v ethylene glycol, results in the near complete loss of the g = 2.01 EPR signal (< 2% of the original intensity), in both cases. No additional EPR signals were observed for the partially reduced A. vinelandii Fd I. In contrast, an extremely broad and weak signal appears at the extreme low field region of the X-band EPR spectrum of partially-reduced T. thermophilus Fd (fig. V.7). This EPR spectrum is identical to that reported previously, and is attributed to a $\Delta M_S = 4$ transition between the $M_S = \pm 2$

components of the S = 2 ground state of the reduced [3Fe-xS] cluster (28).

The low temperature MCD spectra for the partially reduced T. thermophilus Fd and A. vinelandii Fd I, at pH 7.8, temperatures between 1.57 and 24.5 K, and a magnetic field of 4.5 tesla, are given in figure V.8. As is the case for the as isolated proteins, the $[4Fe\text{-}4S]^{2+}$ clusters are diamagnetic and thus do not contribute to the temperature dependence of the MCD spectra. The MCD spectra are therefore attributed to the paramagnetic, reduced [3Fe-xS] clusters. The form of the MCD spectra are remarkedly similar to that of other reduced [3Fe-xS] clusters. The MCD spectra of several reduced proteins, containing [3Fe-xS] clusters, at 4.22 K and 4.5 tesla, are given in figure V.9. Under the conditions stated, the low temperature MCD spectra for T. thermophilus Fd, D. gigas Fd II (32), A. vinelandii Fd I, D. gigas hydrogenase (33), and inactive aconitase (34) originate from reduced [3Fe-xS] clusters, for E. coli nitrate reductase (35) the spectrum originates from a reduced [3Fe-xS] cluster, and three or four $[4Fe\text{-}4S]^{1+}$ clusters, and for butanol extracted succinate dehydrogenase (36) and fumarate reductase complex (37) the spectra originates from a reduced [3Fe-xS] cluster, a $[2Fe\text{-}2S]^{1+}$ cluster, a $[4Fe\text{-}4S]^{1+}$ cluster, and an undetermined

quantity of cyctochrome. The intensities of the low temperature MCD spectra of T. thermophilus Fd and A. vinelandii Fd I, together with the absence of any EPR signals attributable to $[4Fe\text{-}4S]^{1+}$ clusters, are consistent with reduction of the [3Fe-xS] clusters occuring without any cluster conversion to yield [4Fe-4S] clusters. The observed difference in the [3Fe-xS] cluster content of the seven iron ferredoxins, as indicated by the EPR quantitations of the as isolated samples, is mirrored by the MCD intensities of the reduced [3Fe-xS] clusters.

In order to elucidate the electronic ground state properties of the reduced [3Fe-xS] clusters, MCD magnetization data were recorded for the partially-reduced seven iron ferredoxins at the peak maxima of each of the major bands. Magnetization data for partially-reduced T. thermophilus Fd recorded at 705 nm, 420 nm, and 377 nm, are given in figure V.10. The corresponding data for partially-reduced A. vinelandii Fd I recorded at 690 nm, 440 nm, and 380 nm are given in figure V.11. The nesting of the magnetization data, that is observed at all wavelengths for both samples, is indicative of a ground state with $S > 1/2$, with significant zero field splitting such that low lying energy levels can become thermally populated over the

temperature range of the experiment (1.6 to 100 K). The pronounced differences, in the MCD magnetization data between the two ferredoxins, are indicative of substantial differences in the ground state zero field splitting of the two reduced [3Fe-xS] clusters.

Preliminary analysis of the magnetization data has been undertaken by fitting only the lowest temperature data to theoretical expressions derived for an S = 1/2 doublet and ignoring field-induced mixing of zero field components (see chapters II.1 and IV.1). The magnetization data for partially-reduced T. thermophilus Fd does not exhibit wavelength dependence, indicating that all the transitions are of similar polarization. Moreover the lowest temperature data (1.57 K) are well fit by theoretical data for a ground state doublet with effective g-values of $g_{\parallel}$ = 8.0 and $g_{\perp}$ = 0.0. These are the predicted effective g-values for a $M_S = \pm 2$ doublet originating from a S = 2 ground state with purely axial zero field splitting (38). The magnetization data for the reduced [3Fe-xS] cluster in T. thermophilus Fd can be understood in terms of a S = 2 ground state with axial zero field splitting such that a $M_S = \pm 2$ doublet is lowest in energy, D < 0, without significant population in the $M_S = \pm 1$ doublet at 1.57 K. Such an energy level scheme is depicted in figure II.4. Since $g_{\perp}$ = 0.0, all

temperature dependent MCD transitions from the ground state are x,y-polarized, and the resultant MCD magnetization data is invariant of wavelength, in the absence of additional paramagnets.

In contrast, the magnetization data for partially-reduced A. vinelandii Fd I at the lowest temperature 1.60 K, exhibits distinct wavelength dependence. The magnetization behavior at 690 and 380 nm is unique among metal centers investigated by MCD spectroscopy, thus far, in that the data at the lowest temperature rises to a maximum, and then decreases with increasing magnetic field. In the absence of multiple chromophores, the wavelength dependence observed can only arise as a result of differences in the polarization of electronic transitions from a ground state with large g-value anisotropy (see chapter IV.1). In an S = 2 system, z-polarized transitions from the $\tilde{M}_S = \pm 2$ doublet are possible if $g_\perp \neq 0$. This situation arises if the zero field splitting is predominately rhombic, $E \neq 0$. The effect of a rhombic zero field splitting is to remove the degeneracy of the lowest two non-Kramers' doublets (fig. II.4). Full analysis of the magnetization data shown in figure V.11, taking into account field induced mixing, has yet to be attempted. It presents a complex theoretical problem since the field induced mixing must

be averaged over all angles, and will require inclusion of numerous parameters, including effective g-values, relative extinction coefficients, polarization ratios, and fractional populations for all of the doublets which comprise the ground state manifold. Therefore the analysis has been confined to fitting the lowest temperature data using equation II.6. Satisfactory fits to the experimental data of figure V.11 was obtained at all wavelengths using the effective g-values, $g_{\parallel} = 6.5$ and $g_{\perp} = 0.6$, if the polarization ratio m_z/m_+ for transitions from the lowest doublet is allowed to vary such that the bands at 690 and 380 nm are predominantly x,y-polarized, and the band at 440 nm is predominantly z-polarized. This fit is not unique, and is shown purely for illustrative purposes to demonstrate how such magnetization data could arise.

In order to determine the magnitude of the axial zero field splitting parameter, D, for the reduced [3Fe-xS] clusters of the partially-reduced T. thermophilus Fd and A. vinelandii Fd I, detailed studies of the temperature dependence of the MCD signals over the temperature range 4.2 to 100 K were preformed. Data for the T. thermophilus Fd were collected at 705 and 420 nm, and for the A. vinelandii Fd at 690 nm. The later wavelength was chosen, due to the requirement for unique

polarization electronic transition. Magnetization data at this wavelength indicate predominantly x,y-polarization. At 4.22 K, the MCD intensity at these wavelengths was found to linear as a function of magnetic field for fields up to and including those used in this investigation, i.e. 0.6 tesla and 0.5 tesla for the T. thermophilus and A. vinelandii Fds respectively. The analysis of the data closely follows that of Browett et al (39) and assumes the zero field splitting is axial with $D < 0$, such that the $M_S = \pm 2$ and ± 1 are both doublets. The magnetization data indicate that this is a good assumption for the T. thermophilus Fd. The experimental data were fit to equations II.11 and II.15, using non-linear regression with c_1, c_2, and D for parameters. Since the upper level is a singlet, c_3 was set to zero. The diamagnetic contributions were assumed to be negligible compared to the paramagnetic contributions in the range of temperatures employed. The best fits to the data were obtained for $D = 2.1\ cm^{-1}$ and $2.3\ cm^{-1}$ for T. thermophilus Fd at 705 and 420 nm respectively, and $D = 2.0\ cm^{-1}$ for A. vinelandii Fd I at 690 nm. Figure V.12 shows the experimental data, the computer generated best fit curve, and the computed contributions from each of the ground state doublets. The experimental data points along with the computor

generated points, which comprise figure V.12, are given in Appendix 2. In order to estimate the uncertainty in the value of D thus obtained, the experimental data were fit, allowing only c_1 and c_2 to vary, for a wide range of fixed values of D (0.5 to 10 cm^{-1}). Satisfactory fits, given the uncertainty in the experimental data points, for the partially-reduced T. thermophilus Fd were obtained for values of D in the range 1.2 to 3.2 cm^{-1}, at both wavelengths investigated. Values of D in the range of 1.0 to 4.0 cm^{-1} afforded satisfactory fits to the data for partially-reduced A. vinelandii Fd I.

The low temperature MCD spectrum of partially-reduced T. thermophilus Fd was independent of pH over the range investigated, 6.3-8.5. The low temperature MCD spectrum of partially reduced A. vinelandii Fd I, on the other hand, displays pronounced pH dependence. Figure V.13 shows the low temperature MCD spectra of partially-reduced A. vinelandii Fd I at pH 6.3, temperatures between 1.60 and 9.60 K, and a magnetic field of 4.5 tesla. These spectra are distinctly different from those recorded at pH 7.8 and 8.3. The low and high pH spectra are reversibly interconvertible. EPR spectra recorded for samples at pH 6.3 indicate that approximately 30% of the [3Fe-xS] clusters remain oxidized, even after the protein was incubated for three

hours, at room temperature with a fifty-fold excess of dithionite. This is presumably a consequence of the lower reduction potential of dithionite at the lower pH, although a decrease in the midpoint potential of the [3Fe-xS] cluster cannot be ruled out. No signals arising from $[4Fe\text{-}4S]^{1+}$ clusters were observed in the EPR spectrum. It was therefore concluded that the protein was predominantly, partially-reduced at pH 6.3. Computer subtraction of 30% of the oxidized MCD spectrum of A. vinelandii Fd I from the low pH MCD spectrum under identical conditions, produces only minor changes in the partially-reduced low pH MCD spectrum. In no instance was it possible to obtain the spectrum of the high pH, partially-reduced A. vinelandii Fd I, by differencing the contributions of the oxidized [3Fe-xS] cluster from the MCD spectrum of the partially-reduced protein at low pH. Since the $[4Fe\text{-}4S]^{2+}$ cluster does not contribute significantly to the low temperature MCD spectrum of the partially-reduced protein (see above), it was concluded that the reduced [3Fe-xS] cluster in A. vinelandii Fd I can exist in two distinct forms, dependent on the pH of the buffer. Figure V.14 gives a comparison of the MCD spectra of the low and high pH forms of the partially-reduced A. vinelandii Fd I at 4.22 K and a magnetic field of 4.5 tesla.

In order to elucidate the nature of the ground state of the low pH form of the reduced [3Fe-xS] cluster in A. vinelandii Fd I, magnetization data were collected at 385, 439, and 483 nm (fig. V.15). The data magnetize much more rapidly than would be expected for an isolated S = 1/2 ground state. Furthermore, the data exhibit pronounced nesting that is wavelength dependent. Due to the contributions from the oxidized [3Fe-xS] cluster, it was not possible to analyze the magnetization data in detail. The data, however, are consistent with a ground state with S = 1 or 2.

An identical pH effect has been reported for the reduced [3Fe-xS] cluster in A. chroococcum Fd (40). This sample was reported to be devoid of any significant EPR signals. The similarity in the properties of these two ferredoxins is not surprising in light of the fact that their EPR, MCD, and CD spectra are indistinguishable. They differ in that A. chroococcum Fd is reported a form a partially-reduced eight iron Fd (i.e. containing one $[4Fe\text{-}4S]^{1+}$ and one $[4Fe\text{-}4S]^{2+}$ cluster) upon reduction with dithionite at pH > 8.8 (40), whereas A. vinelandii Fd I is reported to form a fully reduced eight iron Fd (i.e. containing two $[4Fe\text{-}4S]^{1+}$ clusters) upon reduction with dithionite at pH > 8 (7). Clearly, both of these proteins undergo [3Fe-xS] to [4Fe-4S] cluster conversion

upon reduction at alkaline pH.

Fully-reduced T. thermophilus Fd and A. vinelandii Fd I

As previously stated, reduction of both iron-sulfur clusters in T. thermophilus Fd was effected by anaerobic addition of an excess of dithionite prior to the addition of 50% v/v ethylene glycol. Figure V.16 shows the EPR spectrum arising from fully-reduced T. thermophilus Fd. In addition to the aforementioned broad low field resonance, attributed to the reduced [3Fe-xS] clusters, a complex signal centered at $g = 1.94$ is observed. The $g = 1.94$ signal is identical to that reported previously (4, 20, 28) and is attributed to the $S = 1/2$, $[4Fe\text{-}4S]^{1+}$ cluster, which is interacting via weak spin-spin interaction with the $S = 2$, reduced [3Fe-xS] cluster (28). Quantitation of the $g = 1.94$ signal, given in figure V.16 accounted for between 0.6 and 0.7 spins/molecule.

A comparison between the low temperature MCD spectra of the fully- and the partially-reduced T. thermophilus Fd 1.57 and 4.5 tesla is given in figure V.17. Comparison of the two spectra indicate that the reduced [3Fe-xS] cluster dominates the MCD spectra in both redox states. The intensity of the low temperature MCD spectrum arising from the $[4Fe\text{-}4S]^{1+}$ cluster is an order of magnitude

weaker than that arising from the reduced [3Fe-xS] cluster. The contribution from the $[4Fe\text{-}4S]^{1+}$ to the MCD spectrum of the fully-reduced T. thermophilus was obtained by taking the difference between the partially- and the fully-reduced spectra under identical conditions (lower trace of fig. V.18). The resultant spectrum resembles the spectra of C. pasteurianum Fd and D. gigas Fd I given in figure IV.17. Furthermore, after normalization for the EPR spin quantitation, the extinction coefficients of the MCD spectrum are consistent with those given in chapter IV.2.

Attempts to fully-reduce A. vinelandii Fd I, in the pH range 6.3 to 8.5 were unsuccessful. Stephans et al have recently reported production of the fully-reduced A. vinelandii Fd I, and the subsequent conversion of the reduced [3Fe-xS] cluster to form a $[4Fe\text{-}4S]^{1+}$ cluster, albeit in low yields, by reduction of the protein with dithionite at alkaline pH. These conditions also result in the destruction of the a large fraction of the iron-sulfur clusters.

Ferricyanide treated T. thermophilus Fd and A. vinelandii Fd I

The effect of ferricyanide on the UV-visible, CD, MCD, and EPR spectral properties of A. vinelandii Fd I,

have been extensively studied by Stephens *et al*. (8, 16, 42). These experiments were, therefore, not repeated in this work. *T. thermophilus* Fd was found to be extremely resistant to ferricyanide oxidation, consistent with previous spectroscopic studies (4, 30). Neither the EPR nor the MCD exhibited any change after incubation of a five-fold excess of ferricyanide for two hours, at room temperature.

5.3 Discussion

The foregoing results enable a critical comparison of the electronic and magnetic properties of the iron-sulfur clusters in the seven iron Fds from *A. vinelandii* and *T. thermophilus*. Low temperature MCD studies confirm the presence of approximately one [3Fe-xS] cluster in both proteins. No conversion of [3Fe-xs] clusters to form [4Fe-4S] clusters was observed in the pH range 6.3 to 8.5, under reducing conditions (cf. Aconitase (19)). Reduction and subsequent

identification of the additional center as a [4Fe-4S] cluster was possible only for T. thermophilus Fd. The presence of a $[4Fe\text{-}4S]^{2+}$ cluster in A. vinelandii Fd I is, however, well established via Mössbauer(23) and X-ray crystallography (9, 10). Our results are consistent with a midpoint potential below -600 mV for the tetrameric cluster in A. vinelandii Fd I, in agreement with previously reported studies (7, 8).

The low temperature MCD and EPR results reported here attest to a close similarity in the electronic and magnetic properties of the oxidized [3Fe-xS] clusters in these ferredoxins, and in other proteins (see chapters IV.2 and VI). It seems probable that the large difference in the midpoint potentials of the clusters, (~200 mV), is a consequence of variations in the polypeptide environment, rather than major differences in the [3Fe-xS] clusters themselves. Perhaps the most significant difference in the spectroscopic properties of the oxidized [3Fe-xS] clusters is found in the anisotropy and spin relaxation of their EPR signals. While the factors affecting these properties are not well understood at this time, a correlation between small g-value anisotropy and slow spin relaxation has been observed. This correlation is best rationalized in terms of differences in the energy of a low lying excited

state, that can mix with the ground state, contributing to the anisotropy and enhanceing the spin-lattice relaxation.

No heterogeneity within the class of oxidized [3Fe-xS] clusters was observed by either the EPR and MCD spectroscopy. The anomalous structure, as determined by X-ray crystallography , reported for A. vinelandii Fd I can only be rationalized in terms of different structures for the crystalline protein and the protein in a solution or frozen glass. Resonance Raman data, does not, however, support this hypothesis (17). Since the available spectroscopic and analytical data for a wide range of [3Fe-xS] clusters are consistent with a [3Fe-4S] core structure with iron-iron distances of 2.7 Å, the possibility of an error in the analysis of the X-ray crystallographic data for A. vinelandii Fd I must be considered.

Low temperature MCD studies, including detailed investigations of the temperature and magnetic field dependence, proved to be of great utility in elucidating the electronic and magnetic properties of the reduced [3Fe-xS] clusters in these ferredoxins. The MCD magnetization data are consistent with an $S = 2$ ground state, with $D < 0$, such that the $M_S = \pm 2$ sublevels are lowest in energy. The observed differences in the

magnetization data can be rationalized in terms of the nature of the ground state zero field splitting, with the reduced [3Fe-xS] cluster in A. vinelandii Fd I having a significant rhombic component compared to the predominantly axial zero field splitting for the equivalent center in T. thermophilus Fd. The nature and the magnitude of the structural perturbations that are responsible for the difference in the ground state zero field splitting are presently unknown. The magnitude of the axial zero field splitting parameters were found to be compariable for the two reduced [3Fe-xS] clusters, i.e. $D = 2.2 \pm 1.0\ cm^{-1}$ for T. thermophilus Fd and $D = 2.5 \pm 1.5\ cm^{-1}$ for A. vinelandii Fd I.

The interpretation of the MCD magnetization data for the reduced [3Fe-xS] clusters in these two ferredoxins provides an explanation for the absence of a $\Delta M_S = 4$ X-band EPR transition for partially-reduced A. vinelandii Fd I, in terms of the zero field splitting of the S = 2 ground state. EPR resonance will not be possible for a non-Kramers' ground state with significant rhombic zero field splitting such that the splitting of the lowest doublet ($M_S = \pm 2$ in this case) is greater than the microwave energy (approximately 0.3 cm^{-1} for X-band). Therefore, although observation of a low field EPR signal for a reduced iron-sulfur protein is indicative of a

reduced [3Fe-xS] cluster, the absence of this signal does not necessarily preclude the presence of this type of center.

MCD studies do indicate distinct low and high pH forms of the reduced [3Fe-xS] cluster in A. vinelandii Fd I, analogous to that reported for the reduced [3Fe-xS] cluster in A. chroococcum Fd. No such pH dependence was observed for the analogous cluster in T. thermophilus Fd or D. gigas Fd II (41). The structural changes accompanying the interconversion of the two forms are currently unknown. The ease and reversibility of the interconversion make a major structural reorganization unlikely. The change is thought to possibly arise from a protonation-deprotonation equilibrium, involving either a cysteinyl sulfur or a cluster sulfide ion (41). This cluster heterogeneity was only observed for the reduced [3Fe-xS] cluster, and therefore does not account for the inconsistency in the structural data that has been reported for the oxidized cluster.

The question of the origin of the [3Fe-xS] cluster in these seven iron ferredoxins was addressed. Many [3Fe-xS] clusters are artifacts of aerobic isolation, resulting from the degradation of a [4Fe-4S] cluster. This certainly the case for the [3Fe-xS] cluster in aconitase (43) and C. pasteurianum Fd (chapter IV.2).

Recent investigations of E. coli fumarate reductase (38), beef heart succinate dehydrogenase (36), and E. coli nitrate reductase (chapter VI) indicate that some [3Fe-xS] clusters are intrinsic components of functional enzymes. Fumarate reductase has been observed in vivo (39). The present study provides two pieces of evidence which suggest that the [3Fe-xS] clusters are a native component of A. vinelandii Fd I and T. thermophilus Fd. First, a full complement of oxidized [3Fe-xS] clusters were present in anaerobically isolated A. vinelandii Fd I. Second, no significant conversion of [4Fe-4S] clusters accompanied the dithionite reduction of either Fd at pH 6.3 to 8.5, nor was there any appreciable conversion of [4Fe-4S] clusters to [3Fe-xS] clusters upon incubation of these ferredoxins with a large excess of ferricyanide (see chapter IV.2). Perhaps the best arguement in favor of these [3Fe-xS] clusters being isolation artifacts, comes from the reported reconstitution of A. vinelandii Fd I as an eight iron, 2[4Fe-4S], Fd (42). The spectroscopic data reported in reference 42 do not, however, support the claim that reconstituted A. vinelandii Fd I contains two tetrameric clusters. Both the spin quantitation and the form of the EPR spectrum of the reduced sample, as well as the corresponding UV-visible spectrum, indicate the presence of no more

than one $[4Fe\text{-}4S]^{1+}$ cluster. It is uncertain at this time whether the [3Fe-xS] cluster in A. vinelandii can be reconstituted from apoprotein as a [4Fe-4S] cluster.

Finally the effect of ferricyanide on several low potential $[4Fe\text{-}4S]^{2+,\ 1+}$ clusters from a variety of proteins was investigated. The [4Fe-4S] cluster in A. vinelandii Fd I is readily degraded by oxidizing agents such as ferricyanide. This degradation product has been characterized as a cysteinyl radical (17). T. thermophilus Fd was unaffected by addition of ferricyanide in the pH range 6.3 to 8.5. The MCD and EPR spectra of the ferricyanide treated sample was indistinguishable from the as isolated protein. No evidence for [4Fe-4S] to [3Fe-xS] cluster conversion was observed in T. thermophilus. Addition of ferricyanide to C. pasteurianum Fd caused degradation of [4Fe-4S] clusters to form [3Fe-xS] clusters (chapter IV.2). A large excess of ferricyanide (> 10 fold excess) caused complete destruction of the clusters to yield apoprotein. Finally, the iron-sulfur clusters of E. coli nitrate reductase were not significantly affected by addition of ferricyanide (chapter VI). In the four systems studied, which contained tetrameric centers, neither a MCD spectrum, nor an EPR spectrum resembling the spectrum of oxidized Chromatium HiPIP was observed.

It was therefore concluded that the redox potential is not the sole factor in mediating the oxidation state of the tetrameric clusters.

In summary, the following conclusions were reached as a result of these investigations on the ferredoxins from A. vinelandii Fd I and T. thermophilus Fd: 1) no significant electronic or magnetic heterogeneity exists within the class of oxidized [3Fe-xS] clusters. The MCD and EPR spectra are consistent with a uniform cluster structure, with minor differences arising as a result of differences in the protein environment. 2) The magnetic and electronic properties of reduced [3Fe-xS] clusters are very similar. The [3Fe-xS] cluster in A. vinelandii Fd I is anomolous in that it exhibits a pH dependent low temperature MCD spectrum. 3) Reduced [3Fe-xS] clusters which give rise to a low field EPR resonance, corresponding to a $M_S = 4$ transition exhibit predominantly axial zero field splitting. 4) $[4Fe\text{-}4S]^{2+}$ clusters display heterogeneity in terms of their oxidative lability. Although several reactions have been observed, including conversion of [4Fe-4S] clusters to [3Fe-xS] clusters or to a radical (17), in no instance was a ferredoxin-type, low potential [4Fe-4S] superoxidized to the $[4Fe\text{-}4S]^{+3}$ state by the addition of ferricyanide.

References

1. Stout, C.D., Ghosh, D., Pattabhi, V., and Robbins, A.H., (1980) J. Biol. Chem. 255, 1797-1800

2. Scherings, G., Haaker, H., and Veeger, C., (1977) Eur. J. Biochem. 77, 621-630

3. Sato, S., Nakazawa, K., Hon-Nami, K., Oshima, T., (1981) Biochim. Biophys. Acta 668, 277-289

4. Ohnishi, T., Blum, H., Sato, S., Nakazawa, K., Hon-Nami, K., and Oshima, T., (1980) J. Biol. Chem. 255, 345-348

5. Yoch, D.C., and Arnon, D.I., (1972) J. Biol. Chem. 247, 4514-4520

6. Sweeney, W.V., Rabinowitz, J.C., and Yoch, D.C., (1975) J. Biol. Chem. 250, 7842-7847

7. Stephens, P.J., Morgan, T.V., Stout, C.D., and Burgess, B.K., (1986) in "Frontiers of Bioinorganic Chemistry" (Xavier, A.V. ed.), pp. 637-646, VCH publishers, Weinheim

8. Morgan, T.V., Stephens, P.J., Devlin, G., Stout, C.D., and Burgess, B.K., (1984) Proc. Nat. Acad. Sci. USA 81, 1931-1935

9. Ghosh, D., Furey, W., O'Donnell, S., and Stout, C.D., (1981) J. Biol. Chem. 256,129-130

10. Ghosh, D., O'Donnell, S., Furey, W., Robbins, A.H., and Stout, C.D., (1982) J. Mol. Biol. 158, 73-109

11. Howard, J.B., Lorsbach, T.W., Ghosh, D., Melis, K., and Stout, C.D., (1983) J. Biol. Chem. 258, 508-522

12. Sieker, L.C., Adman, E.T., Jensen, L.H., and LeGall, J., (1984) J. Mol. Biol. 179, 151-155

13. Robbins, A.H., and Stout, C.D., (1985) J. Biol. Chem. 260, 2328-2333

14. Antonio, M.R., Averill, B.A., Moura, I., Moura, J.J.G., Orme-Johnson, W., Teo, B.K., and Xavier, A.V., (1982) J. Biol. Chem. 257, 6646-6649

15. Beinert, H., Emptage, M.H., Dreyer, J., Scott, R.A., Halin, J.E., Hodgson, K.O., and Thomson, A.J., (1983) Proc. Nat. Acad. Sci. USA 80, 393-396

16. Stephens, P.J., Morgan, T.V., Devlin, F., Penner-Hahn, J.E., Hodgson, K.O., Scott, R.A., Stout, C.D., and Burgess, B.K., (1985) Proc. Nat. Acad. Sci. USA 82, 5661-5665

17. Johnson, M.K., Czernuszewicz, R.S., Spiro, T.G., Fee, J.A., and Sweeney, W.V., (1983) J. Am. Chem. Soc. 105, 6671-6678

18. Johnson, M.K., Czernuszewicz, R.S., Spiro, T.G., Ramsey, R.R., and Singer, T.P., (1983) J. Biol. Chem. 258, 12771-12774

19. Kent, T.A., Dreyer, J.C., Kennedy, M.C., Huynh, B.H., Emptage, M.H., Beinert, H., and Munck, E., (1982) Biochem. 79, 1096-1100

20. Hille, R., Yoshida, T., Tarr, G.E., Williams, C.H., Ludwig, M.L., and Fee, J.A., (1983) J. Biol. Chem. 258, 13008-130013

21. Moura, J.J.G., Moura, I., Kent, T.A., Lipscomb, J.D., Huynh, B.H., LeGall, J., Xavier, A.V., and Munck, E., (1982) J. Biol. Chem. 257, 6259-6267

22. Kent, T.A., Emptage, M.H., Merkle, H., Kennedy, M.C., Beinert, H., and Munck, E., (1985) J. Biol. Chem. 260, 6871-6881

23. Emptage, M.H., Kent, T.A., Huynh, B.H., Rawlings, J., Orme-Johnson, W.H., and Munck, E., (1980) J. Biol. Chem. 255, 1793-1796

24. Cammack, R., Rao, K.K., Hall, D.O., Moura, J.J.G., Xavier, A.V., Bruschi, M., LeGall, J., Deville, A., and Gayda, J.P., (1977) Biochim. Biophys. Acta 490, 311-321

25. Gayda, J.P., Bertrand, P., Guigliarelli, B., and Meyer, J., (1983) J. Chem. Phys. 79, 5732-5733

26. Moura, J.J.G., LeGall, J., and Xavier, A.V., (1984) Eur. J. Biochem. 141, 319-322

27. Bertrand, P., Guigliarelli, B., Meyer, J., and Gayda, J.P., (1984) Biochimie 66, 77-79

28. Hagen, R.H., Dunham, W.R., Johnson, M.K., and Fee, J.A., (1985) Biochim. Biophys. Acta 828, 369-374

29. Guigliarelli, B., Bertrand, P., More, C., Papavassiliou, P., Hatchikian, E.C., and Gayda, J.P., (1985) Biochim. Biophys. Acta 810, 319-324

30. Nagayama, K., Imai, T., Ohmori, D., and Oshima, T., (1984) Febs Lett. 169, 79-84

31. Beinert, H., and Thomson, A.J. (1983) Arch. Biochem. Biophys. 222, 333-361

32. George, S.J., Richards, A.J.M., Thomson, A.J., and Yates, M.G. (1984) Biochem. J. 224, 247-251

33. Johnson, M.K., Zambrano, I.C., Czechowski, M.H., Peck, H.D. Jr., DerVartanian, D.V., and LeGall, J., (1986) in "Frontiers of Bioinorganic Chemistry", (Xavier, A.V., ed.), pp. 36-44, VCH publishers, Weinheim

34. Johnson, M.K., Thomson, A.J., Richards, A.J.M., Peterson, J., Robinson, A.E., Ramsay, R.R., and Singer, T.P. (1984) J. Biol. Chem. 259, 2274-2282

35. Johnson, M.K., Bennett, D.E., Morningstar, J.E., Adams, M.W.W., and Mortenson, L.E., (1985) J. Biol. Chem. 260, 5456-5463

36. Johnson, M.K., Morningstar, J.E., Bennett, D.E., Ackrell, B.A.C., and Kearney, E.B., (1985) J. Biol. Chem. 260, 7368-7378

37. Morningstar, J.E., Johnson, M.K., Cecchini, G., Ackrell, B.A.C., and Kearney, E.B., (1985) J. Biol. Chem. 260, 13631-13638

38. Johnson, M.K., Morningstar, J.E., Cecchini, G., and Ackrell, B.A.C., (1985) Biochem. Biophys. Res. Commun. 131, 653-658

39. Browett, W.R., Fucaloro, A.F., Morgan, T.V., and Stephens, P.J., (1983) J. Am. Chem. Soc. 105, 1868-1872

40. George, S.J., Richards, A.J.M., Thomson, A.J., and Yates, M.G., (1984) Biochem. J. 224, 247-251

41. Morgan, T.V., Stephens, P.J., Devlin, F., Burgess, B.K., and Stout, C.D., (1985) Febs Lett. 183, 206-210

42. Kent, T.A., Dreyer, J.L., Kennedy, M.C., Huynh, B.H., Emptage, M.H., Beinert, H., and Munck, E., (1982) Proc. Nat. Acad. Sci. USA 79, 1096-1100

43. Thomson, A.J., Robinson, A.E., Johnson, M.K., Moura, J.J.G., Moura, I., Xavier, A.V., and LeGall, J., (1981) Biochim. Biophys. Acta 670, 93-100

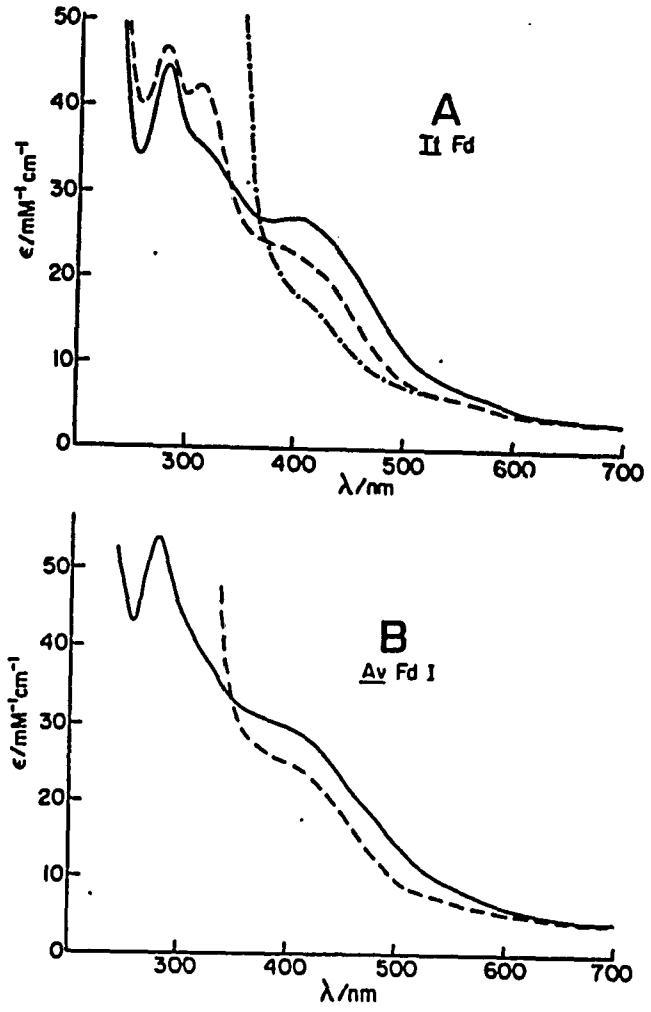

Figure V.1: **Room temperature UV-visible absorption spectra of** T. thermophilus **Fd and** A. vinelandii **Fd I. (a)** T. thermophilus Fd as isolated (——), partially reduced (---), and fully reduced (-·-) in 100 mM potassium phosphate buffer, pH 7.8, with 50% v/v ethylene glycol. Partial reduction and complete reduction affected as per text. Sample concentrations were 0.306 mM for as isolated and partially reduced, 0.215 mM for fully reduced. (b) A. vinelandii Fd I as isolated (——) and partially-reduced (---) in 100 mM Tris-HCl buffer, with 50% v/v ethylene glycol. Reduction affected as per text. Sample concentration was 0.181 mM.

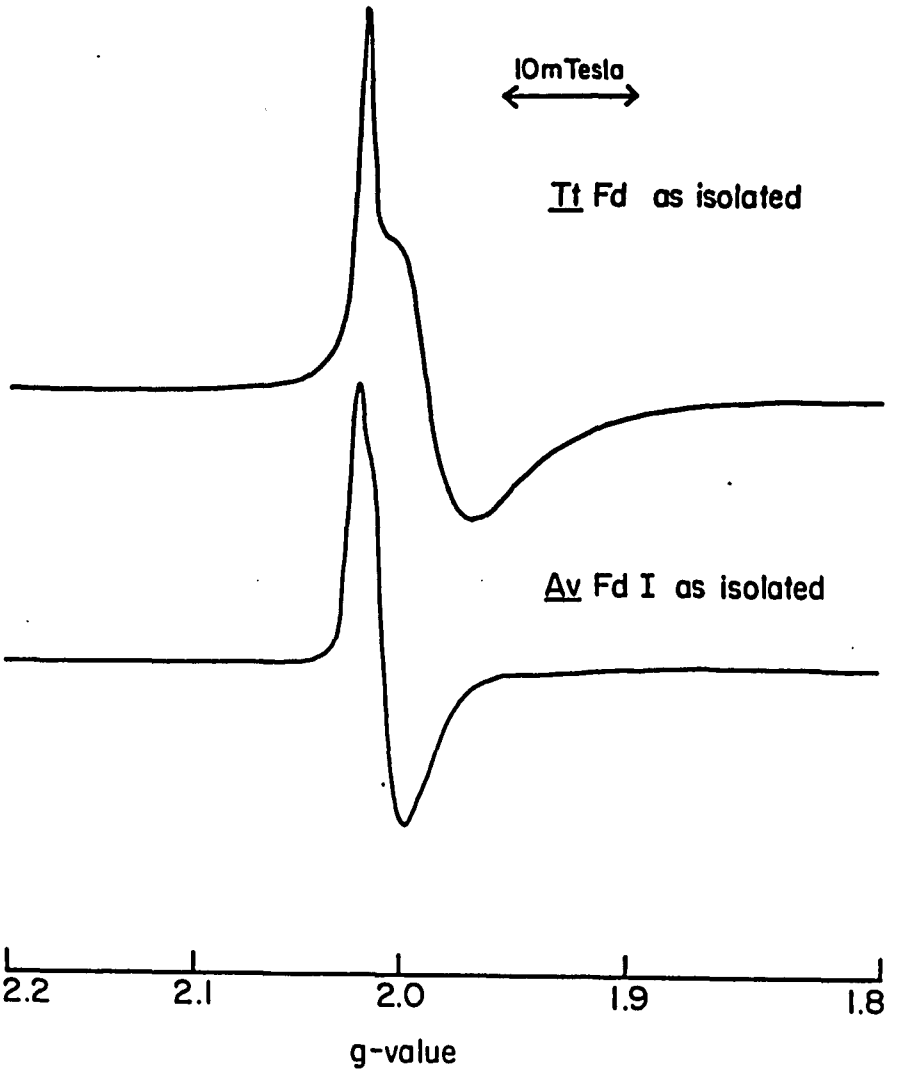

Figure V.2: X-band EPR spectra of T. thermophilus Fd and A. vinelandii Fd I, as isolated. Samples were identical to those used in figure V.1. Temperature 11 K, microwave power 1 mW, modulation amplitude 0.63 mT, microwave frequency 9.017 GHz.

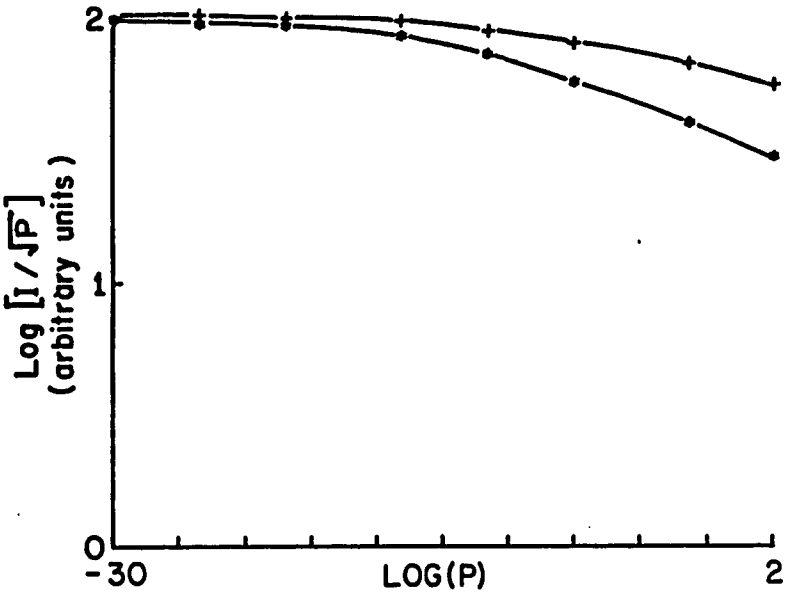

Figure V.3: EPR power saturation studies of T. thermophilus Fd and A. vinelandii Fd I as isolated. Samples were identical to those used in figure V.1. Temperature 12 K, modulation amplitude 0.63 mT, microwave frequency 9.017 GHz, + and * correspond to T. thermophilus Fd and A. vinelandii Fd I respectively.

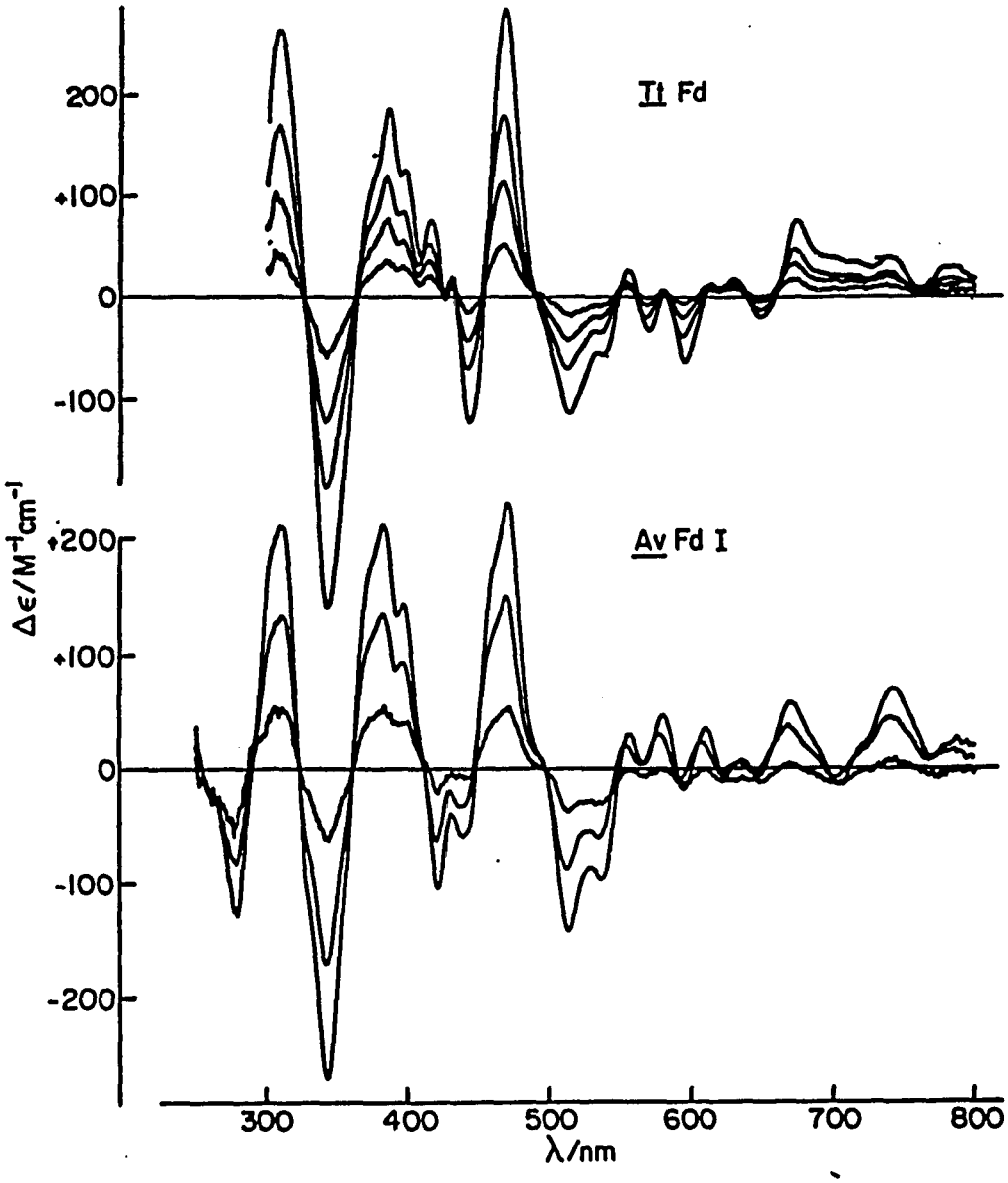

Figure V.4: Low temperature MCD spectra of T. thermophilus Fd and A. vinelandii Fd I, as isolated. Samples were identical to those used in figure V.1. (a) As isolated T. thermophilus Fd, temperatures 1.55 K, 4.22 K, 9.0 K, and 16.5 K, pathlength 0.163 cm, magnetic field 4.5 tesla. (b) As isolated A. vinelandii Fd I, temperatures 1.55 K, 4.22 K, 14.7 K, pathlength 0.156 cm, magnetic field 4.5 tesla.

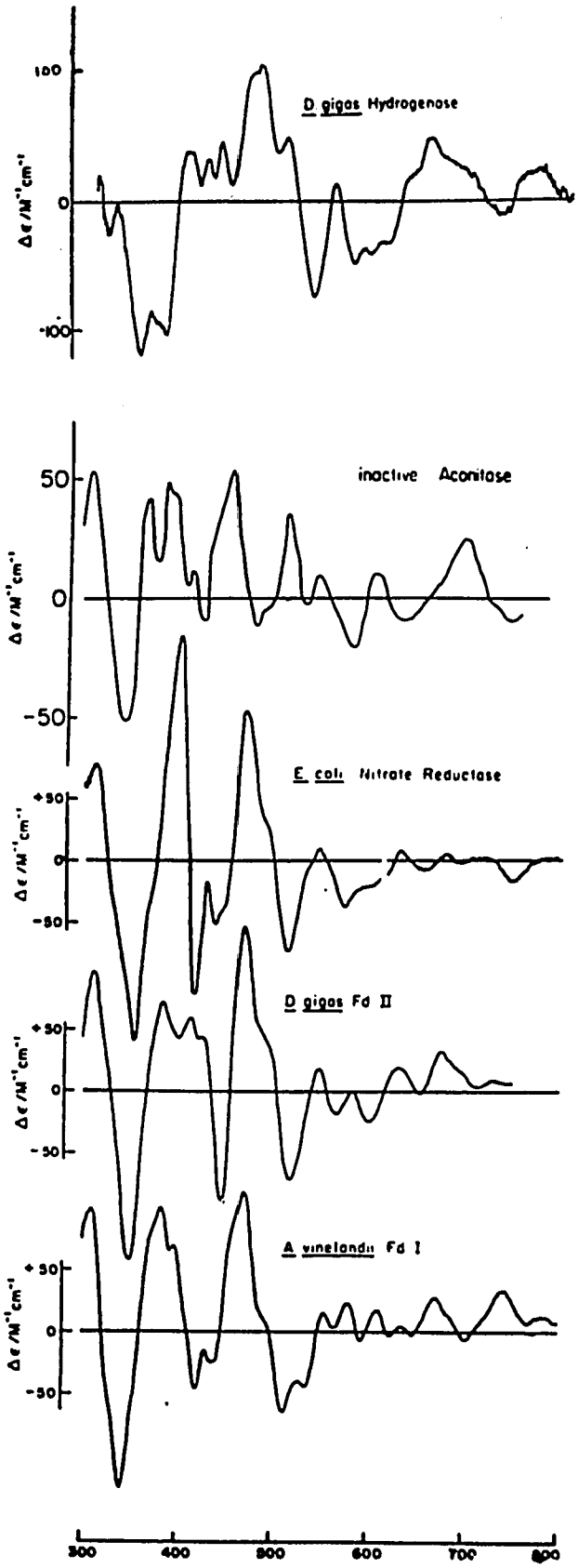
D gigas Hydrogenase
inactive Aconitase
E coli Nitrate Reductase
D gigas Fd II
A vinelandii Fd I
Δε/M⁻¹cm⁻¹
300
400
500
600
700
800

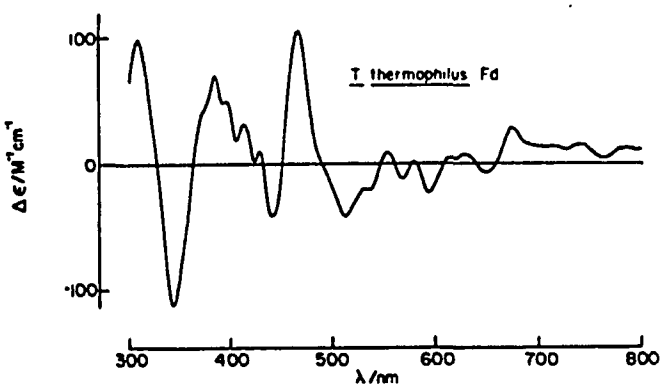

Figure V.5: **Comparison of MCD spectra of several proteins containing oxidized [3Fe-xS] clusters.** All spectra were recorded at 4.22 K and 4.5 tesla. D. gigas hydrogenase reproduced from reference 33. Inactive aconitase reproduced from reference 34. E. coli nitrate reductase reproduced from reference 35. D. gigas Fd II reproduced from reference 43. A. vinelandii Fd I as per figure V.4. T. thermophilus Fd as per figure V.4.

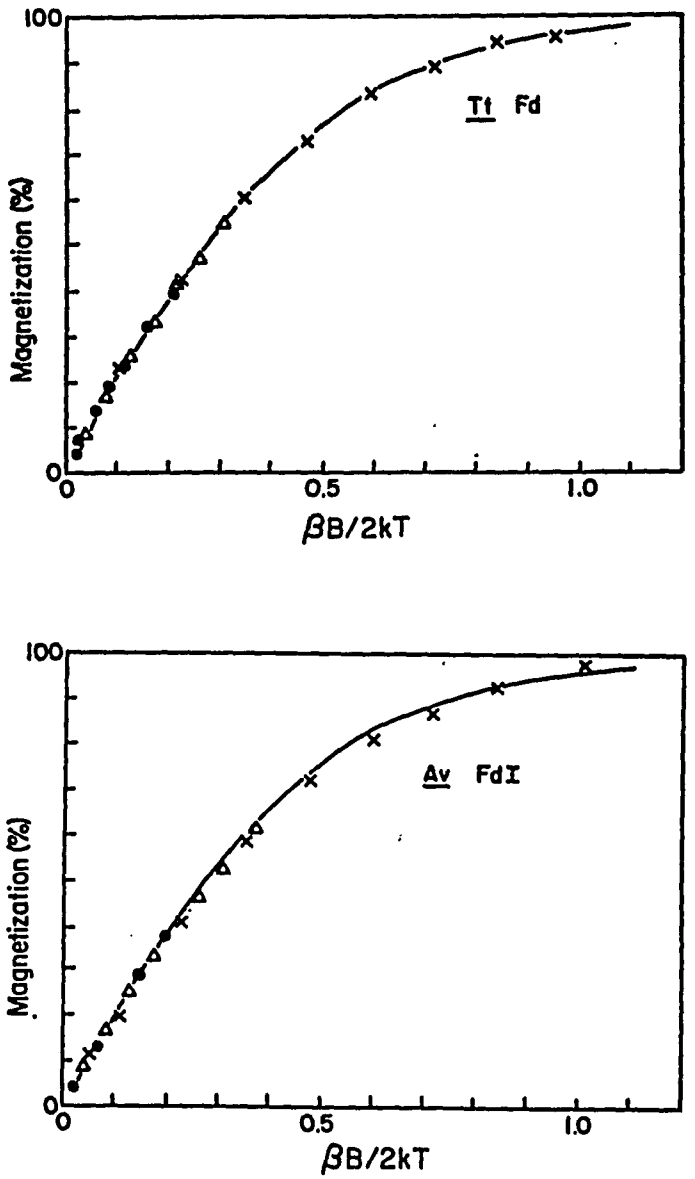

Figure V.6: MCD magnetization plots for T. thermophilus Fd and A. vinelandii Fd I, as isolated. Condition of measurement were as per figure V.4, except for magnetic field. (a) as isolated T. thermophilus Fd, wavelength 343 nm. (b) as isolated A. vinelandii Fd I, wavelength 343 nm. Temperatures 1.55 K (x), 4.22 K (△), 9-100 K (●); magnetic fields between 0 and 4.5 tesla for temperatures between 1.55 and 4.22 K and 4.5 tesla for temperatures above 4.22 K. Solid lines are theoretical magnetization plots for $g_{isotropic} = 2.01$.

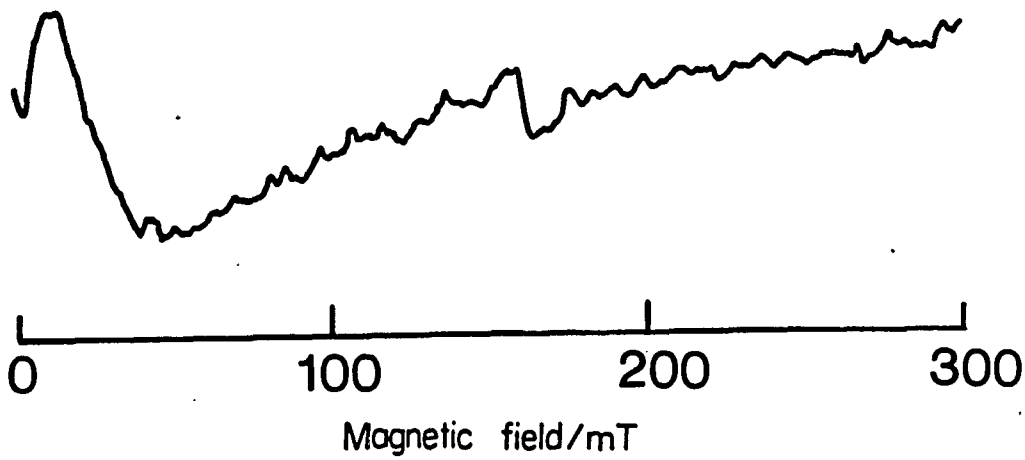

Figure V.7: X-band EPR spectrum of partially-reduced T. thermophilus Fd. Protein was as per. figure V.1. Temperature 11 K, microwave power 10 mW, modulation amplitude 0.63 mT, microwave frequency 9.565 GHz.

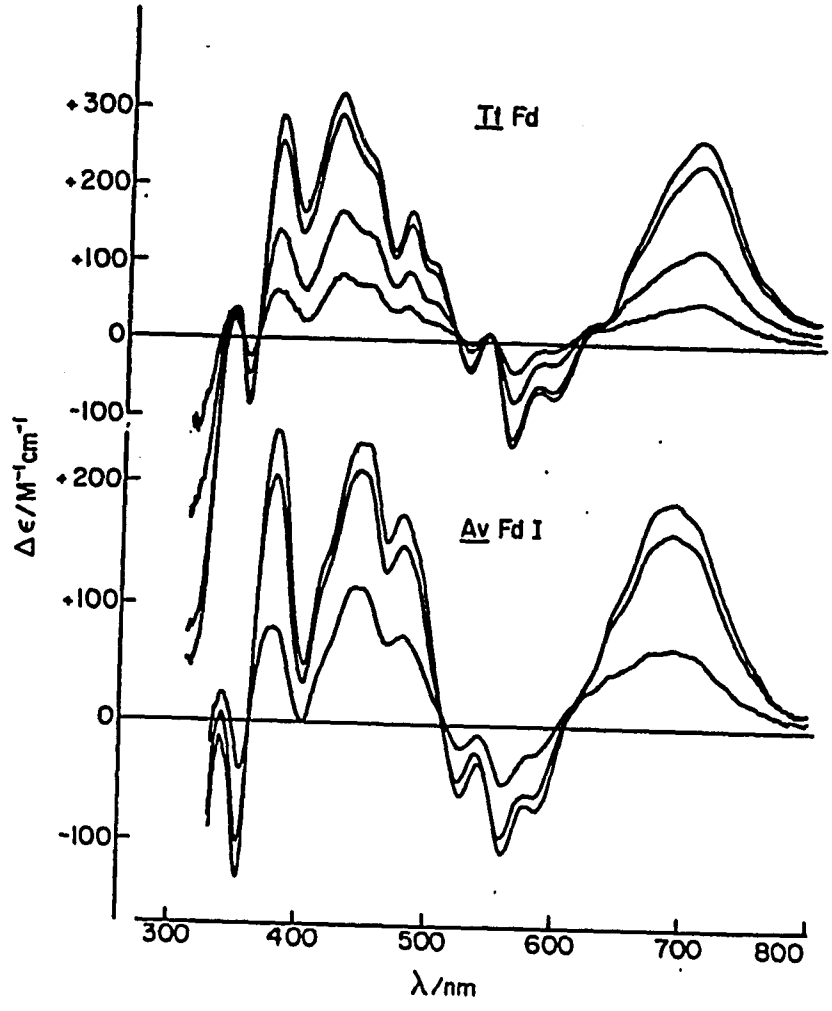

Figure V.8: Low temperature MCD spectra of partially-reduced T. thermophilus Fd and A. vinelandii Fd I. Samples were as per figure V.1. (a) partially-reduced T. thermophilus Fd, temperatures 1.57 K, 4.22 K, 10.9 K, and 24.5 K, pathlength 0.158 cm, magnetic field 4.5 tesla. (b) partially-reduced A. vinelandii Fd I, temperatures 1.60 K, 4.22 K, and 15.3 K, pathlength 0.164 cm, magnetic field 4.5 tesla.

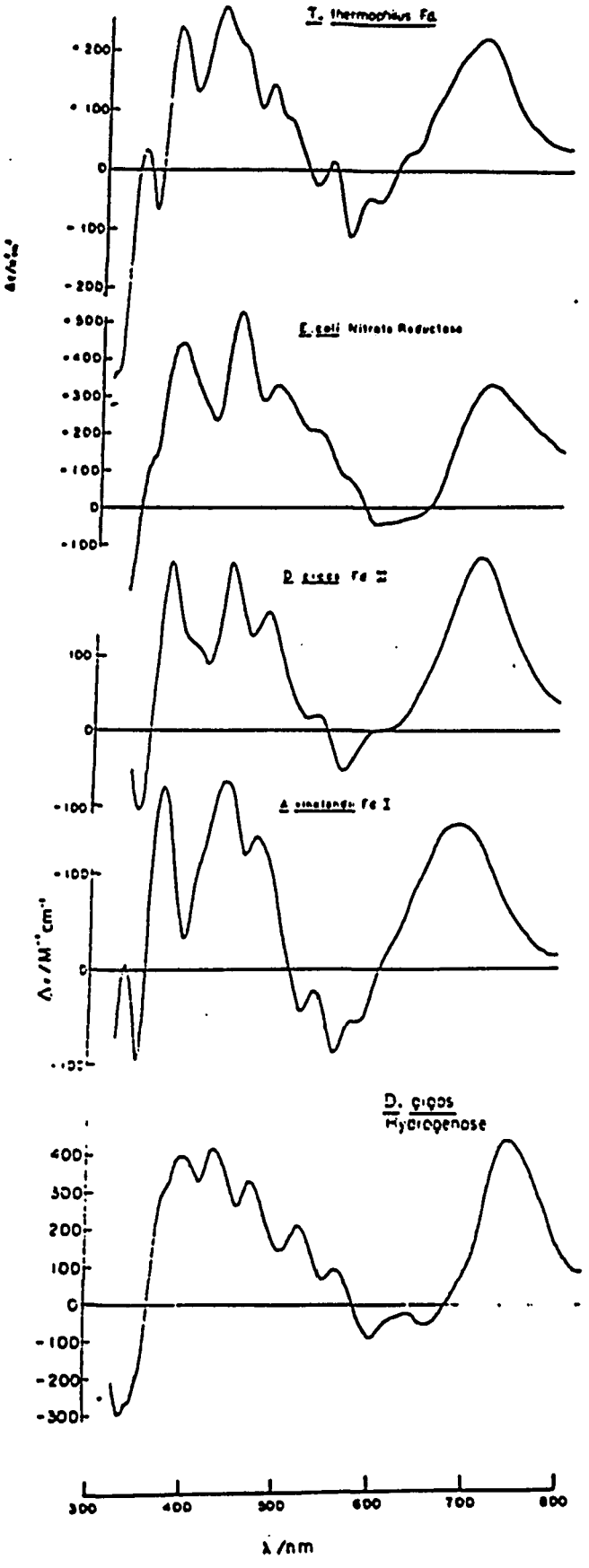
T. thermophilus Fd
E. coli Nitrate Reductase
D. gigas Fd II
A. vinelandii Fd I
D. gigas
Hydrogenase
Δε/M⁻¹cm⁻¹
λ/nm
300
400
500
600
700
800

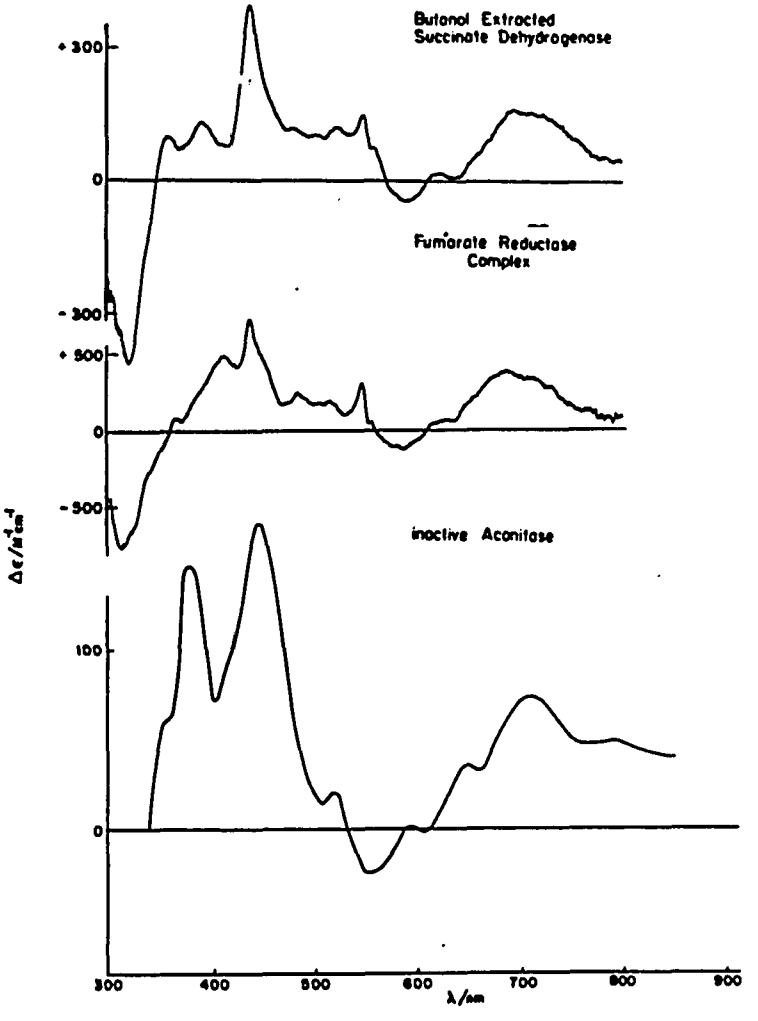

Figure V.9: Comparison of several proteins containing reduced [3Fe-xS] clusters. All spectra were recorded at 4.22 K and 4.5 tesla. T. thermophilus Fd as per figure V.8. E. coli nitrate reductase reproduced from reference 35. D. gigas Fd II reproduced from reference 32. A. vinelandii Fd I as per figure V.8. D. gigas hydrogenase reproduced from reference 33. Butanol extracted succinate dehydrogenase reproduced from reference 36. Fumarate reductase complex reproduced from reference 37. Inactive aconitase reproduced from reference 34.

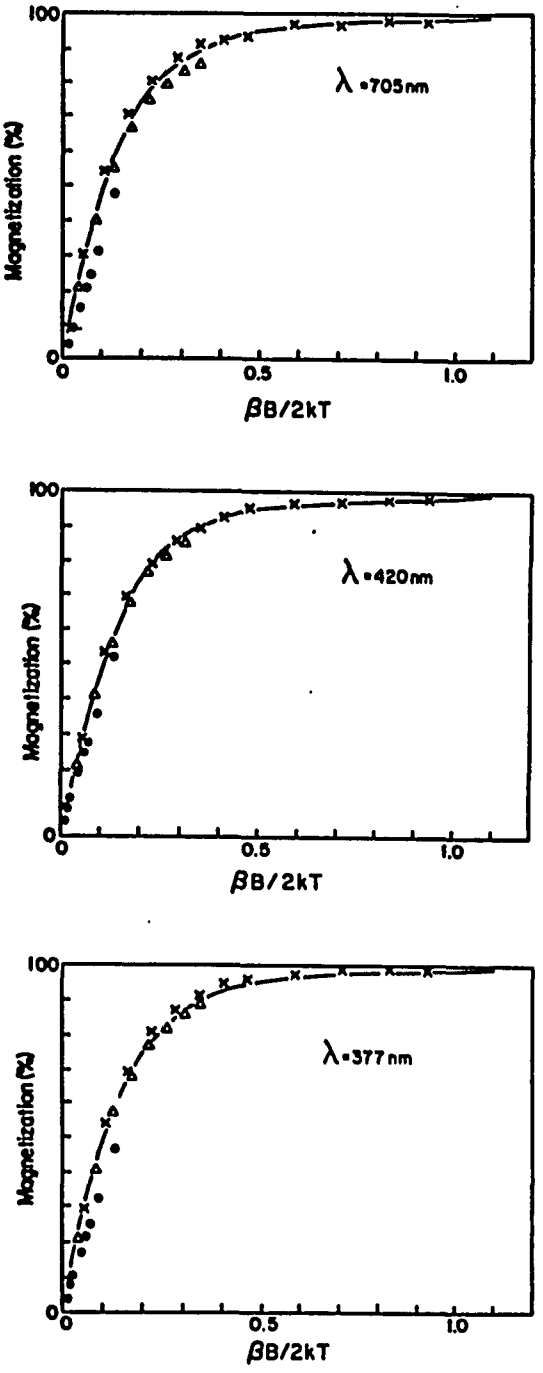

Figure V.10: MCD magnetization plots for partially-reduced T. thermophilus Fd. Conditions of measurement were as per figure V.8, except for temperatures and magnetic fields. Wavelengths 705 nm, 420 nm, and 377 nm; temperatures 1.57 K (x), 4.22 K (△), 9-100 K (●); magnetic fields between 0 and 4.5 tesla for 1.57 and 4.22 K data, and 4.5 tesla for 9-100 K data. Solid lines are the theoretical magnetization curves for $g_{||} = 8.0$ and $g_{\perp} = 0.0$.

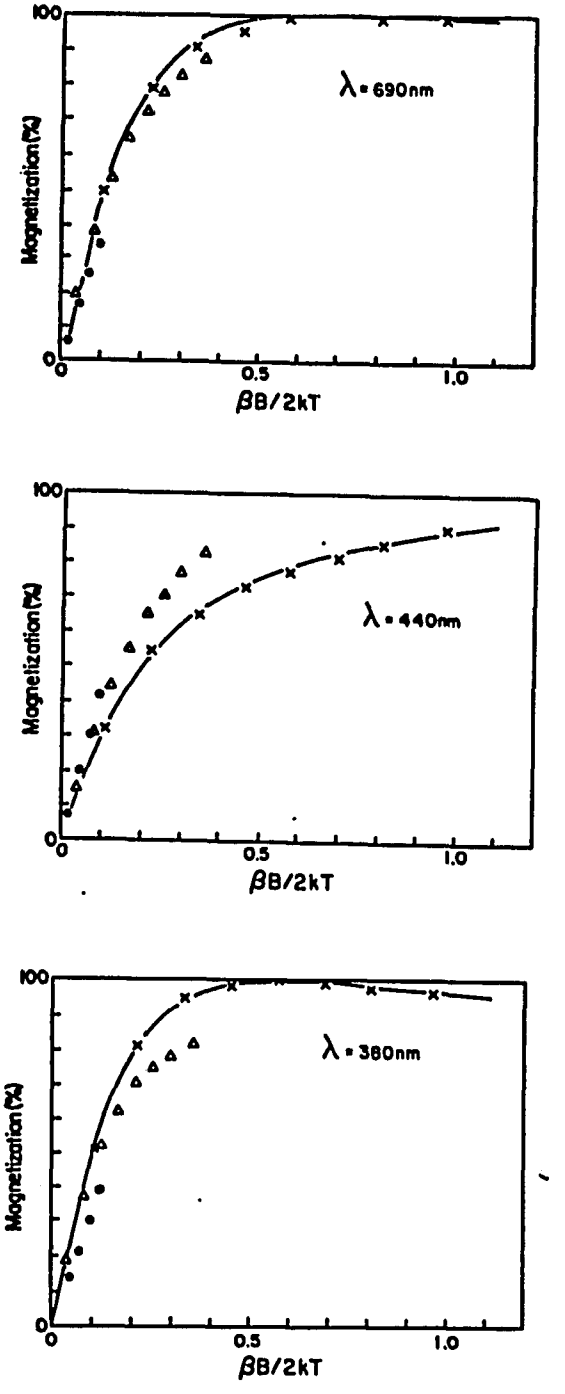

Figure V.11: MCD magnetization plots for partially-reduced A. vinelandii Fd I. Conditions of measurement were the same as those used in figure V.8 except for temperatures and magnetic fields. Wavelenghs 690 nm, 440 nm, and 380 nm; temperatures 1.60 K (x), 4.22 K (△), 10-100 K (●); magnetic fields were between 0 and 4.5 tesla for 1.60 and 4.22 K data, and 4.5 teslat for 10-100 K data. Solid lines are theoretical magnetization curves for $g_{\parallel}$ = 6.5 and $g_{\perp}$ = 0.6 with m_z/m_+ = 0.35 (690 nm), -1.4 (440) nm, and 0.5 (380 nm).

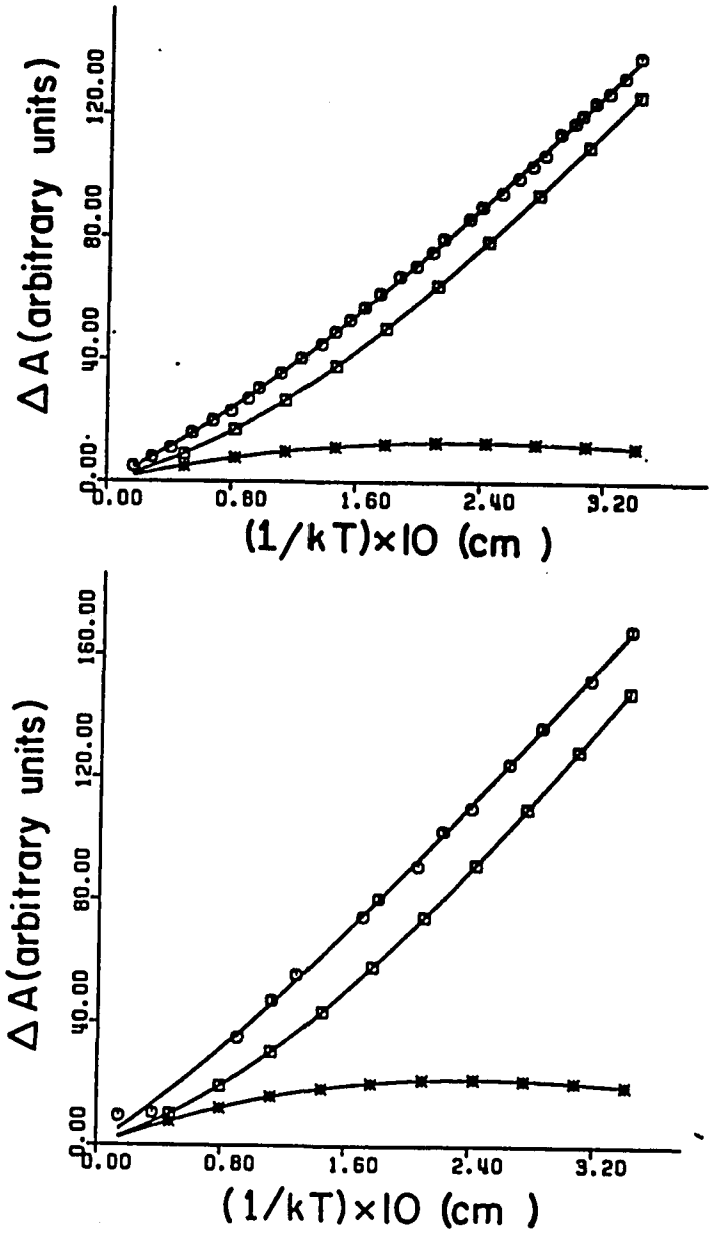

Figure V.12: MCD temperature dependence of partially-reduced T. thermophilus Fd and A. vinelandii Fd I. Circles are experimental data, solid lines are the best fit to the data, and the contributions to the total intensity from the $M_S = \pm 1$ and ± 2 are given by * and □ respectively.

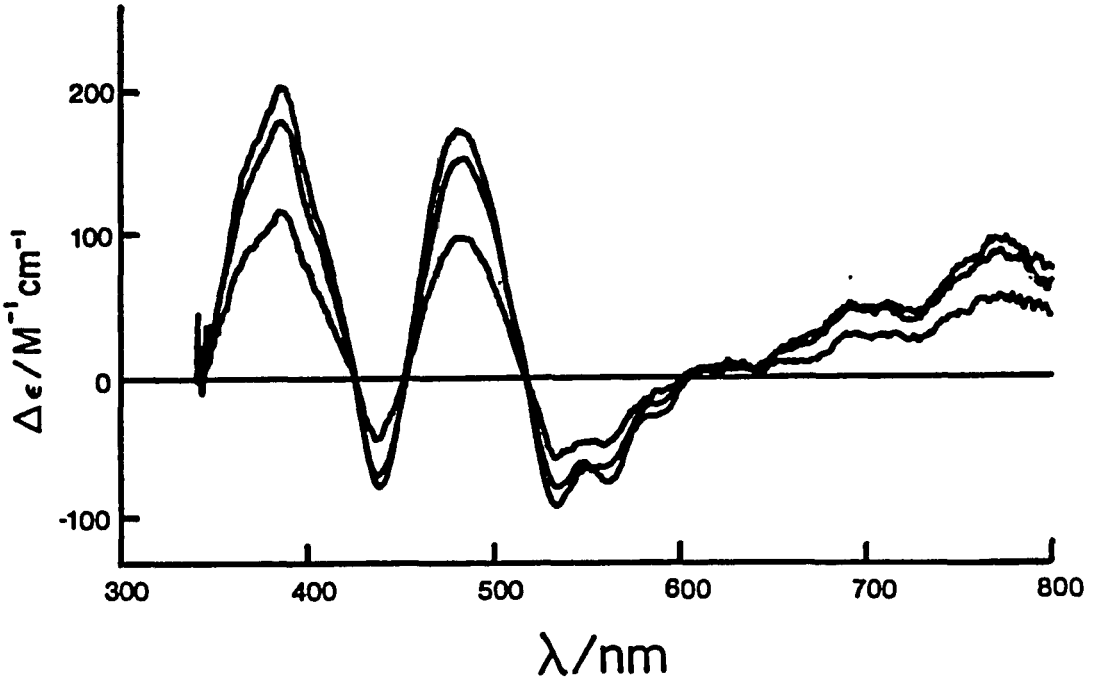

Figure V.13: Low temperature MCD spectra of partially-reduced A. vinelandii Fd I at pH 6.4. Protein was 0.080 mM in 100 mM pipes buffer, pH 6.4 with 50% v/v ethylene glycol. Conditions of measurement were: temperatures 1.60 K, 4.22 K, and 9.6 K, magnetic field 4.5 tesla, pathlength 0.1646 cm.

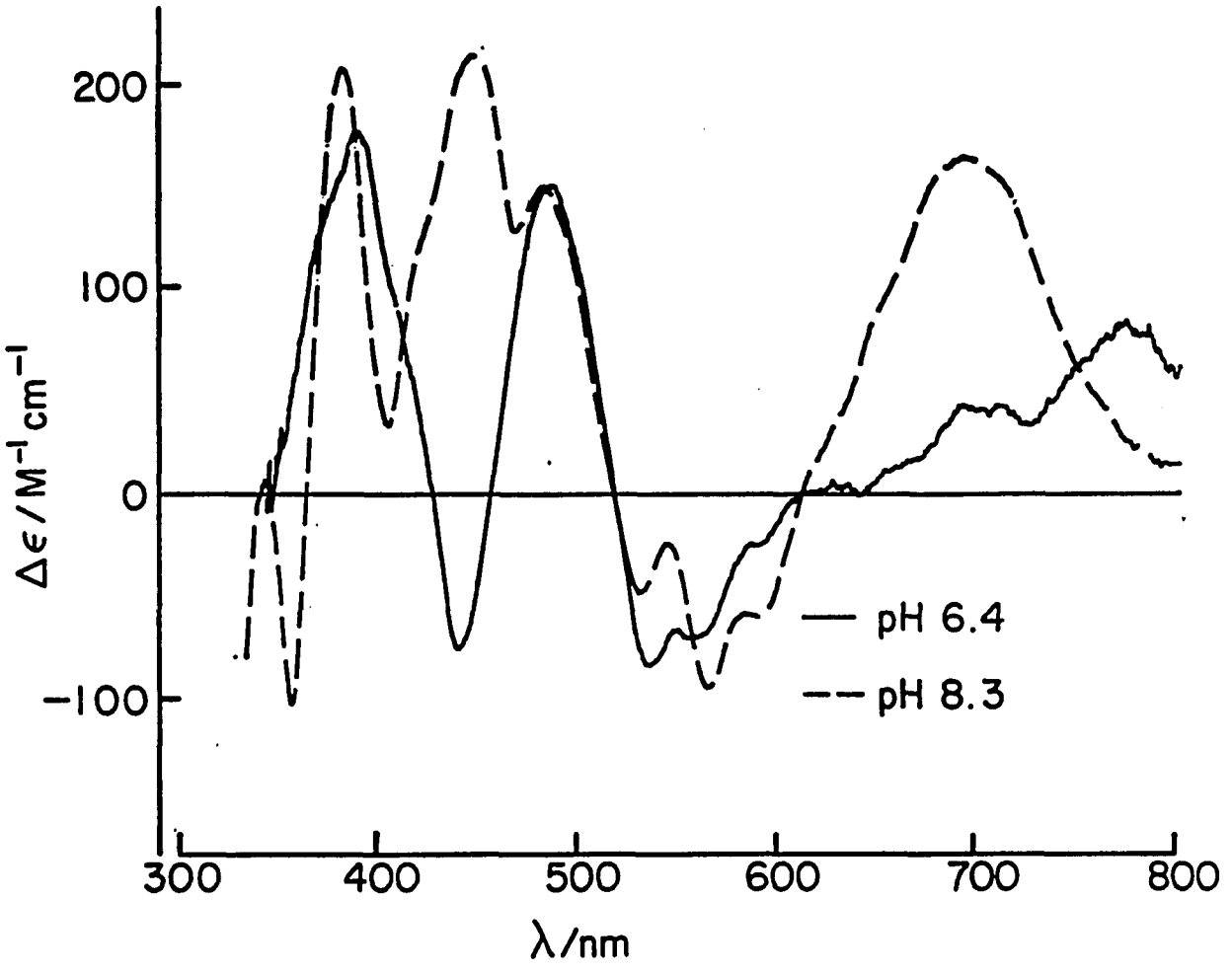

Figure V.14: Comparison of the low and high pH MCD spectra of partially-reduced A. vinelandii Fd I. Broken line, 0.101 mM Fd in 100 mM taps, pH 8.3, with 50% v/v ethylene glycol, pathlength 0.170 cm. Solid line, as per figure V.13. Both spectra were recorded at 4.22 K and a magnetic field of 4.5 tesla.

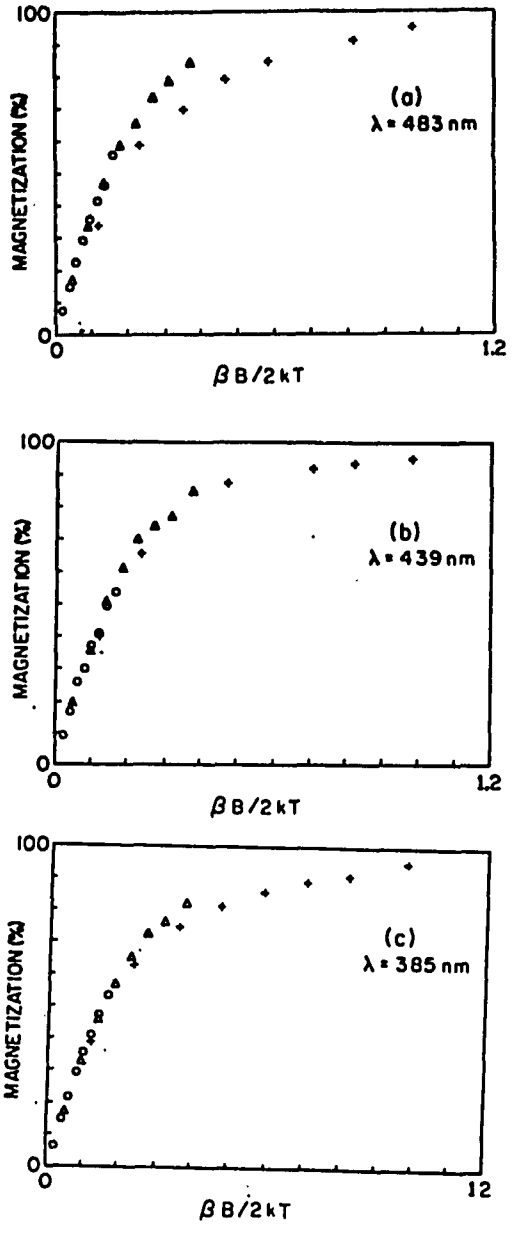

Figure V.15: Magnetization data for low pH partially-reduced A. vinelandii Fd I. Conditions of measurement were as per figure V.13 except for magnetic fields. Temperatures: 1.60 K (+), 4.22 K (Δ), and 9.6 K (o), magnetic fields were between 0 and 4.5 tesla

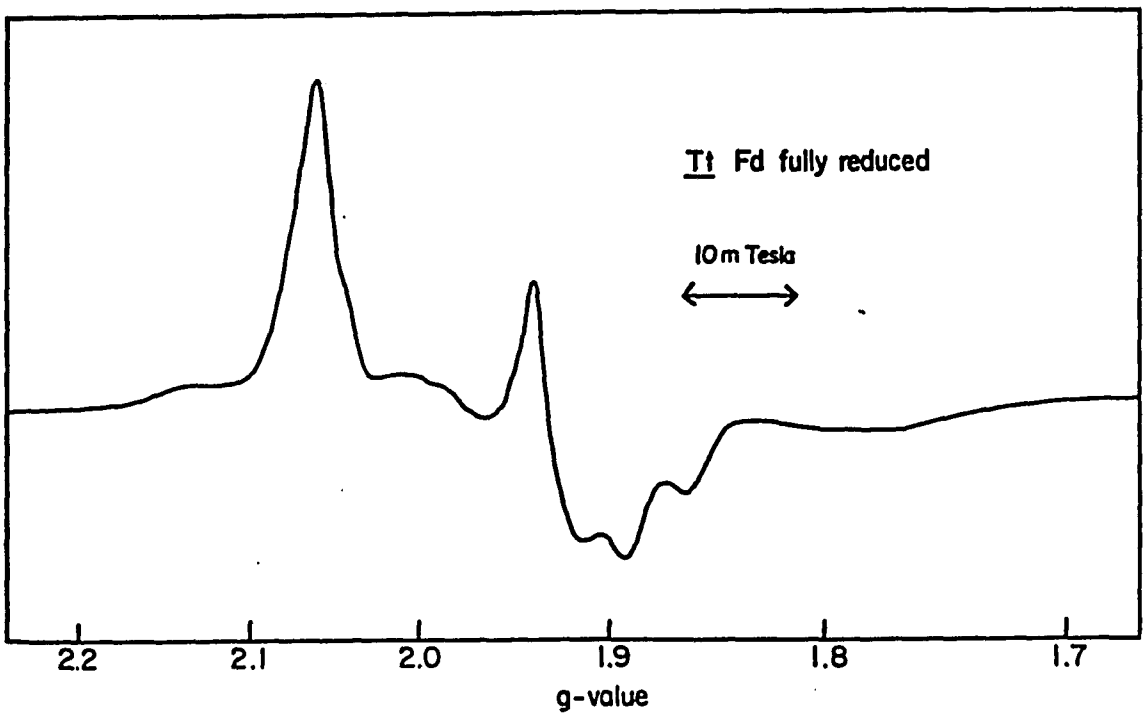

Figure V.16: X-band EPR spectrum of fully-reduced T. thermophilus Fd. Sample was as per figure V.1. Temperature 10 K, microwave power 1 mW, modulation amplitude 0.63 mT, microwave frequency 9.02 GHz.

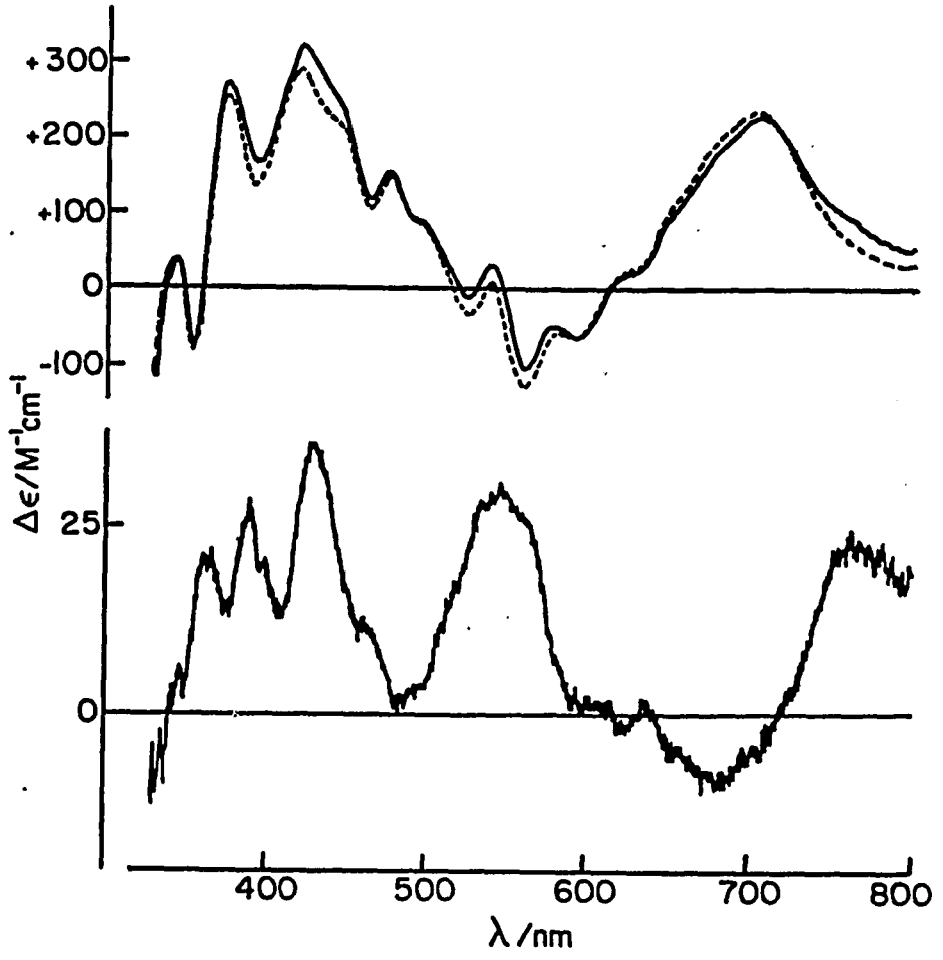

Figure V.17: Comparison of low temperature MCD spectra of fully- and partially-reduced T. thermophilus Fd. Upper panel: comparison bo the MCD spectra of fully-reduced (solid line) and partially-reduced (broken line) T. thermophilus Fd at 1.57 K and 4.5 tesla. Samples were as per figure V.1. Lower panel: difference spectrum, fully-reduced minus partially-reduced at 1.57 K and 4.5 tesla.

Chapter 6

E. coli Nitrate reductase

6.1 Introduction

Nitrate reductase catylizes the biological reduction of nitrate to nitrite. This reduction is an integral part of two vital metabolic processes: the nitrogen cycle and anaerobic respiration (1). Nitrate reductase which is associated with the former are termed "assimilatory" due to their role in assimilating nitrogen into the cell. They are generally associated with eukaryotic organisms, including green algae (*e.g.* *Chlorella vulgaris*), fungi (*e.g.* *Neurospora crassa*), and higher plants (*e.g.* spinach). The prosthetic groups associated with assimilatory nitrate reductase are molybdenum, heme, and flavin (2).

Dissimilatory nitrate reduction refers to the utilization of nitrate, in the absence of oxygen, as the terminal electron acceptor in the electron transport

chain. Nitrate respiration is thought to be directly analogous to aerobic respiration, both in terms of electron transport and in the coupling to oxidative phosphorylation *via* the proton pump (3). Dissimilatory nitrate reduction does not lead to the incorporation of nitrogen into the cell. These enzymes are generally isolated from prokaryotic organisms, most commonly *E. coli*, *Klebsiella aerogenes* and *Pseudomonas aeruginosa*. Dissimilatory nitrate reductase does contain molybdenum, and often heme, but not flavin. Non-heme iron is often found in these enzymes (4).

E. coli will synthesize nitrate reductase when grown anaerobically in the presence of nitrate. The enzyme is released from the membrane either by detergent (5), or by heat treatment (6). The detergent extracted enzyme is commonly referred to as nitrate reductase I, and molecular weights 200-350 kDa have been reported (5,7). Nitrate reductase I is believed to have three subunits: α, β, and γ, with approximate molecular weights of 155, 63, and 19 kDa respectively. Subunit γ contains the natural electron donor, cytochrome *b*. Subunits α and β are located at the cytoplasmic side (8), while γ is located on the periplasmic surface (9). Nitrate reductase II refers to the enzyme isolated by heat treatment and is believed to be equivalent to Nitrate reductase I without subunit γ (6). A diverse range of molecular weights, and metal and sulfide contents have been reported for nitrate

reductase II. Currently the molecular weight is thought to be approximately 200 kDa/monomer (6). The enzyme is often isolated as a oligomer, and hence molecular weights as high as 1,000 kDa have been reported (10). The isolated enzymes have been reported to contain 0.2-0.85 g atoms of molybdenum, 4.5-20 g atoms of non-heme iron, and 8-20 g atoms of acid-labile sulfide (5-10), per monomer.

The molybdenum is present as a molybdenum cofactor, abbreviated Mo-co. Mo-co is found in both types of nitrate reductase, as well as in several hydroxylases, e.g. xanthine oxidase, sulfite oxidase, and aldehyde oxidase (11). The cofactor is characterized by its ability to restore activity to nit-1 mutant of Neurospora crassa nitrate reductase, which is deficient in molybdenum. Among the dissimilatory nitrate reductases, reconstitution studies have been reported only for the enzyme from P. denitrificans (12). These studies must be viewed with caution, however, as Ramadoss et al. have been able to restore activity to demolydo C. vulgaris by addition of inorganic molybdenum salts, albeit only 30% of the maximal activity was restored (13). Characterization of fluorescent derivatives have shown the cofactor to consist of a Mo-pterin moiety (14, 15). Among the dissimilatory enzymes, nitrate reductase from P. denitrificans yielded a pterin derivative upon oxidation (12).

EXAFS studies indicate inequivalence among the

Mo-centers in molybdoenzymes. Currently, EXAFS data has been published for two hydroxylases (16), sulfite oxidase and xanthine dehydrogenase, and two nitrate reductases (17), one assimilatory, C. vulgaris and one dissimilatory, E. coli. The molybdenum center from C. vulgaris nitrate reductase was found to closely resemble the center from sulfite oxidase. In the oxidized state, both are thought to have two terminal oxygens and two or three sulfur atoms at 1.7 Å and 2.4 Å from the molybdenum atom respectively. Upon reduction, a single oxygen atom and several sulfur atoms are found at 1.68 Å and 2.38 Å respectively. Xanthine dehydrogenase has one terminal oxygen at 1.70 Å, one sulfur atom at 2.15 Å, and two sulfur atoms at 2.47 Å when oxidized, and one terminal oxygen at 1.68 Å, and three sulfur atoms at 2.38 Å when reduced. E. coli nitrate reductase, oxidized with nitrate, has one terminal oxygen at 1.66 Å, and two sulfur atoms at 2.42 Å. No terminal oxygens were observed in the reduced enzyme. Two or three sulfur atoms were found at 2.36 Å. The various Mo-centers, as ascertained from the EXAFS data, are given in figure VI.1.

The potentials of the Mo(IV)/Mo(V) and the Mo(V)/Mo(VI) couples in dissimilatory nitrate reductase, +180 and +220 mV versus NHE at pH 7 respectively, are anomolously high for a molybdoenzyme (18). These potentials for nitrate reductase lie almost 500 mV above the corresponding potentials of sulphite oxidase. All

potentials were measured by monitoring the Mo(V) EPR signal during potentiometric titrations. As the nitrate/nitrite couple has a potential of +421 mV, while the sulphite/sulphate couple has a potential of -454 mV (19), it is not surprising that nitrate reductase Mo-center has a higher potential. However, the means by which nature is able to modulate the potential of the Mo-center is still poorly understood.

The molybdenum center from a wide variety of enzymes has been investigated by EPR spectroscopy (9,20-30). Of the three common oxidation states, only Mo (V) is EPR active. Vincent and Bray have identified five different Mo (V) signals in E. coli nitrate reductase, which they have designated as: high pH, low pH, nitrate complex, nitrite complex, and non-functional (29). The low pH signal, g=1.9989, 1.9855, 1.9628, is split by a single exchangable proton, $A(^1H)$=1.11, 0.84, and 0.81 mT. The low pH species can reversibly interconvert to the high pH species, g=1.9870, 1.9805, 1.9612, with an apparent pKa of 8.26. No exchangable proton was originally observed in the high pH spectrum. It was therefore postulated that the dissociation of this exchangeable proton was responsible for the pH dependence. Later work has shown that the high pH species also has an exchangable proton, but with a much smaller coupling constant, $A(^1H)_{av}$=0.3 mT (30). It is now thought that the proton which is detectable by EPR is probably not the proton which

controls the interconversion. Additionally, George et al. have demonstrated that the apparent pKa for this process is dependent on the concentration of anions e.g. chloride, flouride, nitrate, or nitrite, present in the solution. Substanial changes in the low pH spectrum are observed when nitrate or nitrite is added to the enzyme. This change is thought to arise from the binding of substrate at the molybdenum center. Less pronounced changes have been observed with other anions (30). No changes were observed in the high pH spectrum. It was therefore concluded that it is the low pH species which is catalytically active. Similar signals have been reported for K. aerogenes (23), M. denitrificans (24), and spinach (20) nitrate reductase.

Most of the research in this area has concentrated on the Mo-center, because it is thought to be the active site. Several pieces of evidence support this. First, molybdenum is necessary for enzymatic activity. Secondly, EXAFS studies of E. coli nitrate reductase show a pronounced difference at the molybdenum center in the presence of nitrate. Finally, EPR studies indicate that the substrate produced marked changes in the Mo(V) signal.

Nitrate reductase does however, contain other prosthetic groups. In dissimilatory nitrate reductase these groups are iron-sulfur centers. In order to fully understand the mechanism for this reduction, it is

imperative to characterize the nature and function of the iron-sulfur centers.

Many of the above-cited EPR studies have noted the presence of additional features in the EPR spectra at low temperatures (<30 K), which have been attributed to the iron centers (9, 22-25, 28, 29). Vincent and Bray observed an iron-sulfur EPR signal at g=2.01 in oxidized E. coli nitrate reductase and two distinct signals attributed to iron-sulfur centers, which could be differentiated by power saturation, in the dithionite reduced enzyme (29). Similar EPR signals have recently been reported for the dissimilatory nitrate reductase from P. aeruginosa (25).

In light of the paucity of information concerning the iron-sulfur centers, MCD, EPR, and core extrusion studies were undertaken to identify the nature and number of the iron-sulfur clusters in E. coli nitrate reductase. Additionally, EPR studies of whole cells were undertaken in order to investigate these centers in vivo. Furthermore, preliminary studies into the effect of cyanide and ferricyanide on the iron-sulfur centers were undertaken, as the former was found to reversibly inhibit the enzyme, while the later has been shown to enhance activity to up to 250% of the original activity (31). The results demonstrate the utility of low temperature MCD in conjunction with EPR, for investigating the metal centers in complex multicomponent

metalloenzymes.

6.2 Results

Samples of E. coli nitrate reductase used in this work were found to contain 0.80±0.05 g atoms of molybdenum, 14.4±0.5 g atoms of acid labile sulfide, and 16.3±1.6 g atoms of non-heme iron, per mole of enzyme. A molecular weight of 200,000 Da has been assumed throughout. The enzyme exhibited specific activities in the range of 80-90 umol of nitrite produced per min per mg.

Extrusion Studies

The iron-sulfur clusters were extruded according to the method of Gillum et al. (32). The protein was unfolded in a solution of 80% hexamethylphosphoramide. The type and quantity of iron-sulfur centers extruded were assesed by means of the absorption spectra recorded between 10 and 90 minutes after the addition of thiophenol. C. pasteurianum Fd was used as a reference. The results are consistent with the presence of approximately four [4Fe-4S] clusters as the sole extrusion product. All assays, iron, molybdenum, and

sulfide determinations, and extrusion studies were performed by Drs. Adams and Mortenson, Exxon Corporate Research Laboratory, Annandale, New Jersey.

EPR and MCD studies

As isolated nitrate reductase-EPR spectra for E. coli nitrate reductase in the range of 10-40 K are given in figure VI.2. At temperatures of 40 K and above, the EPR spectrum is identical to that of the high pH molybdenum signal observed by Vincent and Bray (29), g=1.987, 1.980, 1.961. The spectrum is not a simple rhombic spectrum due to a near isotropic coupling with an exchangeable proton, $A(^1H)_{av}$~0.34 mT (30). The spectrum is further complicated by the presence of a small amount of the low pH species. The appearance of the high pH Mo(V) spectrum was unexpected, as the pH was well below the reported pKa of 8.26 (29). However, this result can now be rationalized since recent experiments have shown the pKa to be dependent on the chloride concentration of the buffer (30). Quantitation of the signal at 40 K revealed that it accounts for only fifteen percent of the total molybdenum present. The remaining molybdenum was presumed to be present as either Mo(IV) or Mo(VI), both of which are EPR silent. Repeated freeze/thawing or prolonged storage at 77 K resulted in the loss of the Mo(V) signal.

Below 30K, a relatively broad signal, centered at g=2.01 is observed. The paramagnet responsible for this

signal exhibits very rapid spin relaxation properties as power saturation is barely evident even at 10 K and a microwave power of 100 mW. Quantitation of three distinct enzyme preparations yielded values of 0.32 - 0.44 spins/molecule. The most accurate quantitations of this species are obtained at high powers and low temperatures in order to saturate the signal intensity arising from the Mo(V) species. The spectral characteristics are consistent with an oxidized iron-sulfur cluster. Two types of iron sulfur clusters are known to give rise to EPR signal, g>2, when oxidized. These are the HiPIP type [4Fe-4S] cluster and the [3Fe-xS] cluster. The spectrum and relaxation properties most closely resemble those of oxidized [3Fe-xS] clusters in bacterial Fds, e.g. A. vinelandii Fd I and T. thermophilus Fd (fig. VI.3). EPR signals from the oxidized [3Fe-xS] clusters in these proteins do, however, account for between 0.7 and 1.0 spin/molecule (chapter V). Spanning at least five hundred gauss, the nitrate reductase EPR spectrum is much broader than that of the oxidized [3Fe-xS] spectrum from A. vinelandii Fd I, but similar to that from T. thermophilus Fd.

The MCD spectra of the as isolated enzyme at 1.51, 4.22, and 11.6 K, and 4.9 tesla are given in figure VI.4. The numerous well resolved features observed in the MCD spectra contrast markedly to the featureless room temperature absorption spectrum (data not shown). The

absorption spectrum was analogous to that reported previously (5), consisting of a pronounced shoulder at 410 nm, and a slight shoulder at 320 nm. The low temperature MCD spectra exhibit more than a dozen distinct temperature dependent transitions (C-terms), revealing the complexity of the electronic transitions which comprise the absorption envelope. Due to their temperature dependence, all electronic transitions, observed in the MCD, must be arising from paramagnetic chromophore(s).

The temperature and magnetic field dependence of all transitions are similar, except in the region 390-420 nm. A representative MCD magnetization plot, at 470 nm is shown in figure VI.5. The experimental points are well fit by theoretical data for an isotropic, S=1/2, Kramers' doublet, with g=2.01. The theoretical curve is depicted by the solid line in the figure. The MCD spectrum can therefore be attributed to the EPR-active oxidized iron-sulfur center and/or Mo(V). As both centers have average g-values close to 2, it is difficult to distinguish between the two possibilities on the basis of magnetization data alone. To determine the origin of the transitions, MCD experiments were conducted on enzyme samples which had greatly diminished Mo(V) EPR signals as a result of repeated freeze/thawing. The low temperature MCD spectra were almost identical to those of the pristine enzyme. The MCD spectra are therefore

associated predominantly with the oxidized iron-sulfur center. Any chromophoric transitions arising from the Mo(V) center must lie underneath the iron-sulfur transitions.

Of the three type of iron-sulfur clusters, which are known to be paramagnetic in the oxidized state, i.e. HiPIP [4Fe-4S] clusters, [3Fe-xS] clusters, and the EPR silent P-clusters in nitrogenase, the low temperature MCD of the as isolated E. coli nitrate reductase bears the closest resemblance to the oxidized [3Fe-xS] clusters of the bacterial Fds (fig. VI.6). The intensity of the sharp biphasic feature centered at 410 nm, in the MCD spectrum of E. coli nitrate reductase was variable for several enzyme preparations (fig. VI.7). This signal is similar to the MCD spectra of low spin ferric hemes (33), and has therefore been attributed to trace quantities of the natural electron donor, cytochrome b. Since the intensity was variable, it is likely that cytochrome b is present as an impurity and not as an integral part of the heat extracted enzyme. The intensity of the signal, arising from the cyctochrome b, is consistent with a concentration of cyctochrome which is approximately 1% of the molybdenum concentration. The form and intensity of the MCD spectra in all other regions is comparable to the spectra of other [3Fe-xS] clusters.

In order to ascertain if the [3Fe-xS] cluster is present in in vivo, EPR spectra of whole cells grown

anaerobically in the presence of nitrate were recorded. No signals, which could be attributed to either iron or molybdenum, were observed in the high activity, whole cells, which were handled anaerobically or in air, or in cells which were treated with ferricyanide. EPR signals assigned to an oxidized iron-sulfur cluster and to Mo(V) were observed in oriented membrane multilayers, prepared from E. coli grown anaerobically in the presence of nitrate (9). The g=2.01 signal was also observed in membrane vesicles of K. aerogenes, also grown anaerobically in the presence of nitrate (23). It is likely that the concentration of the metal centers in nitrate reductase, in whole cells, was below the detection limits of the EPR spectrometer. The possibility that the [3Fe-xS] cluster was generated upon preparation of the oriented membranes or the membrane vesicles cannot be discounted.

Reduced nitrate reductase-The various types of EPR signals which can be observed upon reduction of E. coli nitrate reductase are shown in figure VI.8. Reduction results in the loss of the Mo(V) EPR signal, and the broad signal centered around g=2.01. In their place, new signals are observed at temperatures below 30 K. The form and intensity of these new signals were found to be dependent on the reduction protocol, but not on the nature or the pH of the buffer.

Samples which were incubated for a few minutes at room temperature in the presence to a twenty-fold stoichiometric excess of sodium dithionite resulted in a spectrum similar to that reported by Vincent and Bray (29) (fig. VI.8a). The spectrum is a composite of two overlapping signals, a rhombic species, with g=2.041, 1.945, and 1.921, and a near-axial species, with g=2.003, 1.888, and 1.870. The two species can be distinguished by their power saturation characteristics, as the rhombic species saturates faster (fig. VI.9). Quantitation of the complete spectrum yields 0.6±0.1 spins/molecule.

Photoreduction in the presence of EDTA/proflavin results in the less resolved spectrum, centered around g=1.94, which is shown in figure VI.8b. This spectrum quantifies to 1.2±0.1 spins per molecule. The increased spin quantitation and the decreased resolution are indicative of the generation of an additional paramagnet, with a lower midpoint potential. Spin-spin interaction between the paramagnets is probably responsible for the broadening of the spectrum. In some instances, dithionite reduced enzyme also gave rise to this type of spectrum, with a similar spin quantitation. The precise conditions necessary to elicit this spectrum from the dithionite reduced sample are not entirely clear, although increased incubation time and a larger excess of dithionite do appear to favor the spectrum with the higher spin quantitation.

Reduction by dithionite in the presence of methyl viologen, results in the broad, near-isotropic signal centered at g=1.95 (fig. VI.8c). The sharp biphasic signal at g=2.004 is due to the presence of reduced methyl viologen radical. Spin quantitation of the g=1.95 signal for several distinct enzyme samples, gave values between 2.9-3.5 spins/molecule. The large degree of uncertainty in the spin concentration is primarily due to the difficulty in estimating the contribution of the methyl viologen radical to the total signal intensity. Integrations were generally performed at 15 K and 10 mW microwave power, in order to partially saturate the radical signal.

The features of the EPR spectra of the reduced enzyme most resemble that of reduced [4Fe-4S] clusters, i.e. g_{av}=1.95 and observable only below 40 K as a result of rapid spin relaxation. The progressive broadening which accompanies the successive reduction reflects weak magnetic interactions between the clusters, as discussed above. This phenomenon has been observed in the eight iron Fd from C. pasteurianum (chapter IV.2).

Nitrate reductase samples which gave rise to the EPR signal in figure VI.8c were investigated by MCD spectroscopy. Figure VI.10 shows the MCD spectra in the range of 800-330 nm, at 1.49, 4.22, and 14.0 K, and at a magnetic field strength of 4.5 tesla. It was not possible to obtain the MCD spectra in the near-UV do to

absorbance of the incident radiation, in this region by dithionite and the polypeptide backbone. Again, the low temperature MCD data reveals the complexity of the electronic transitions which comprise the absorption spectrum. Reduced methyl viologen, at the concentrations used does not give a significant MCD spectrum. All the observed transitions are therefore attributed to the reduced iron-sulfur clusters.

In order to ascertain the nature of the iron-sulfur clusters responsible for the various MCD transitions, detailed magnetization data at several wavelengths were collected. Figure VI.11 shows magnetization plots at 385, 450, and 740 nm. These plots show definite wavelength dependence. In light of the previous results presented in this work, two phenomena can be responsible for this dependence: the presence of overlapping spectra arising from two or more paramagnetic chromophores and/or differences in the polarization of electronic transitions arising from a ground state exhibiting large g-value anistropy. It is likely that both phenomena are present in this system.

From the above results of the investigations of the oxidized enzyme, it is clear that a [3Fe-xS] cluster is present. By analogy with other well characterized [3Fe-xS] clusters, this center is expected to be paramagnetic, but EPR silent (see chapters IV.2 and V). Furthermore, these centers exhibit intense low

temperature MCD signals in the reduced state. MCD magnetization plots of reduced [3Fe-xS] clusters are very distinctive. To a first approximation, magnetization plots of [3Fe-xS] clusters, below 2 K, can be simulated by a theoretical curve with $g_{||}$=8.00, and $g_{\perp}$=0.0, provided the zero field splitting is predominantly axial (see chapter II.1). This theoretical curve is given by the solid line in figure VI.11.

The paramagnet giving rise to the g=1.95 EPR signal would also be expected to contribute to the MCD spectrum. MCD magnetization data from $[4Fe-4S]^{1+}$ clusters is virtually independent of polarization effects since transitions arise from an S=1/2 ground state with little g-value anisotropy. Theoretical magnetization for an S=1/2 ground state, with $g_{isotropic}$=1.95 is given by the dashed line in figure VI.11.

Experimental magnetization data for the reduced nitrate reductase at 385 and 740 nm are intermediate between the two theoretical curves. In each case, the experimental data at 1.49 K can be fit by the summation of 75% of the intensity of the g=8.0, 0.0, 0.0 curve, and 25% of the intensity from the g=1.95 curve. At 450 nm, the magnetization data is markedly different. Experiments on the reduced [3Fe-xS] cluster of A. vinelandii (chapter V) have demonstrated that the presence of a large ground state rhombic distortion, and significant contribution from z-polarized transitions at

this wavelength, can elicit this type of magnetization data from a [3Fe-xS] cluster. The amount of z-polarization can not be accurately assesed due to the presence of additional paramagnetic chromophores.

The magnetization data is therefore consistent with the presence of both reduced [3Fe-xS] and [4Fe-4S] clusters in E. coli nitrate reductase. Figure VI.12 presents a comparison of the low-temperature MCD spectra of well characterized Fds containing similar clusters. Under the conditions stated, the low temperature MCD spectra for D. gigas Fd II and A. vinelandii Fd I originate from a reduced [3Fe-xS] cluster, and the spectrum for C. pasteurianum Fd originates from two [4Fe-4S] clusters. Based on the results of chapters IV-V, and additional work in this lab (34), ϵ values per reduced [3Fe-xS] cluster are between 200 and 300 M^{-1} cm^{-1} for the dominant bands at approximately 380, 450, and 720 nm, a magnetic field of 4.5 T, and a temperature of 4.22 K. Notably, the MCD extinction coefficients for reduced [3Fe-xS] clusters are four to six times those associated with a reduced [4Fe-4S] cluster (see chapter IV.2). Therefore, the magnetization data and the MCD spectra, both in form and intensity, for the fully reduced enzyme are consistent with the presence of a single [3Fe-xS] cluster and three or four [4Fe-4S] clusters.

Low-temperature MCD spectra have been reported for several reduced [2Fe-2S] clusters (34-36). The form of

these spectra is quite different from those of reduced [3Fe-xS] and [4Fe-4S] clusters. There is no evidence for any [2Fe-2S] clusters in this enzyme.

Ferricyanide treated-In order to investigate the effect of ferricyanide on E. coli nitrate reductase, EPR spectra of enzyme treated for eight hours with 0.5 mM ferricyanide at room temperature were obtained. In this state the enzyme exhibited 250% of the original activity. Below 10 K, the spectrum resembles the as isolated spectrum, except for the absence of any Mo(V) signals (fig. VI.13b). Neither the form nor the intensity of the [3Fe-xS] appears to be affected by the ferricyanide. Above 30 K an unidentified signal is observed with g=2.023, 1.999 (fig. VI.13a). This signal persists above 140 K, and is assumed to arise from a radical species.

Dithionite reduction, of the ferricyanide treated enzyme results in an EPR spectrum very similar to figure VI.8a (data not shown). In light of the numerous EPR spectra which can be generated upon reduction it cannot be definitively concluded that the [4Fe-4S] clusters have not been altered.

The results do suggest that, unlike C. pasteurianum Fd (see chapter IV.2), there is no appreciable conversion of [4Fe-4S] clusters to [3Fe-xS] clusters by oxidative degradation. It should be noted, however, that these

results are preliminary; the analysis having been conducted on only one enzyme preparation. These experiments need to be repeated before the results can be conclusive.

Cyanide treated-Adams and Mortenson have demonstrated that cyanide results in a complete loss of enzymatic activity (31). Addition of 20 mM cyanide to the as isolated enzyme resulted in the complete absence of any signals below 15 K. At higher temperatures, an EPR signal indistinguishable from the high temperature, ferricyanide signal (fig. VI.13a) was observed. The paramagnet responsible for this signal is not been characterized at this time.

Figure VI.14 shows the MCD spectra for the cyanide treated enzyme. The spectra is devoid of features except in the region 375-500 nm. Magnetization data at 450 nm is indicative of low spin ferric heme. Therefore, the transitions observed in these spectra are attributed to cytochrome b. The complete lack of any appreciable MCD or EPR iron-sulfur signal is the result of complete destruction of the [3Fe-xS] cluster. The loss of this cluster may be the cause of the inhibition. If so, then reactivation by ferricyanide (31) must result in reconstitution of the [3Fe-xS] cluster. This seems unlikely. MCD and EPR experiments on reactivated, cyanide treated enzyme would definitively answer this

question. Lack of sufficient enzyme prevented the implementation of this experiment.

Dithionite reduction of the cyanide inactivated enzyme gave rise to an EPR spectrum very similar to the dithionite reduced sample. Cyanide, therefore, appears not to have dramatically effected the [4Fe-4S] clusters.

6.3 Discussion

The combination of low-temperature MCD, quantitative EPR, and core extrusion studies indicate the presence of approximately one [3Fe-xS] and three or four [4Fe-4S] clusters, in addition to molybdenum, in samples of *E. coli* nitrate reductase isolated by heat treatment.

EPR of *E. coli* nitrate reductase as isolated indicate that 15% on the molybdenum is present as Mo(V). This value is intermediate between the 25% reported by Vincent and Bray (29) and the 9% reported by DerVartanian and Forget (27). The previously mentioned lability of the molybdenum may be responsible for this discrepancy. The facile conversion to both lower and higher oxidation states is an alternative explanation. The disappearance of the Mo(V) signal after prolonged exposure to

ferricyanide suggests oxidation to the +6 state. Similarly, the disappearance of this signal after prolonged exposure to cyanide is probably due to reduction to the +4 state.

While ferricyanide activation and cyanide inhibition induce redox changes in the Mo-center, these changes alone cannot be responsible for the changes in the observed enzymatic activity. Other oxidants such as nitrate, dichloroindophenol, methylene blue, and oxygen did not enhance the activity (31). Likewise, the enzyme was not inhibited even after prolonged exposure to strong reductants such as dithionite (31). While competitive binding to the molybdenum is the likely cause of substrate inhibition, the mechanism for enchanced activity with ferricyanide is presently unclear. The spectroscopic studies reported in this work indicate that it is not as result of oxidation or changes at the iron-sulfur clusters.

The MCD and EPR unambiguously show the presence of a [3Fe-xS] cluster, in both the oxidized and the reduced enzyme (this is in contrast to aconitase, which has been shown to undergo a [3Fe-xS] to [4Fe-4S] conversion upon reduction (37)). The MCD and EPR differ, however, in terms of the number of [3Fe-xS] clusters which are present in the as isolated enzyme. While the MCD data are consistent with the majority of the enzyme molecules containing a [3Fe-xS] cluster, the spin quantitiation of

the EPR signal associated with the oxidized center accounts for less than half a spin per molecule.

Quantitation of a chromophore *via* the intensity of the MCD spectrum requires comparison with spectra of an analogous chromophore, of known concentration, under identical conditions. In view of the distinct similarity of the low-temperature MCD spectra of as-isolated *D. gigas* Fd II and *A. vinelandii* Fd I with that of nitrate reductase, in regions not associated with cytochrome, approximate quantitation based on the MCD intensity is appropriate. For both the oxidized and the reduced [3Fe-xS] cluster, the MCD intensity is consistent with one [3Fe-xS] cluster per molecule. Therefore, the EPR quantitation is thought to be low. The most likely cause of the low spin quantitation is, that due to the breadth of the EPR signal, significant intensity at the extreme high and low field regions of the spectrum are loss in the baseline. Spin quantitations, at temperatures lower than those presently attainable with the existing instrumentation, are necessary to test this hypothesis.

The low temperature MCD and EPR studies also suggest that the [3Fe-xS] cluster is an integral part of the active enzyme. All samples used in this work, except for the cyanide treated samples, displayed normal catalytic activity. *E. coli* nitrate reductase is therefore the first example of an active enzyme which contains a [3Fe-xS] center. While Godfrey *et al.* found the amount

of [3Fe-xS] cluster to be preparation dependent in P. aeruginosa nitrate reductase (25), we found the variation in both the MCD and the EPR signal intensity attributable to this center to be well within the experimental limits. The absence of any appreciable increase in the g=2.01 signal upon prolonged exposure to ferricyanide, would suggest that the [3Fe-xS] cluster is probably not the result of oxidative degradation. Finally, although the results of the studies on whole cells were inconclusive, the previously cited membranes studies (9, 23) suggest that the [3Fe-xS] cluster is present in vivo.

Core extrusion indicates four [4Fe-4S] clusters, while the EPR of the reduced enzyme indicates three or four [4Fe-4S] clusters of varying potentials. It is perhaps significant that the core extrusion studies did not indicate the presence of a [3Fe-xS] cluster. Core extrusion results must be viewed with caution, as [3Fe-xS] clusters have yet to be extruded intact. In aconitase, the well-characterized [3Fe-xS] cluster extrudes as a [2Fe-2S] cluster (40). It was therefore concluded that either the [3Fe-xS] cluster extrudes as a [4Fe-4S] cluster, or that it simply fall apart, under the conditions used. Given the uncertainty in both the metal analysis, the molecular weight, and the experimental techniques, the data is consistent with the presence of one [3Fe-xS] and three or four [4Fe-4S] clusters in E.

coli nitrate reductase.

Perhaps most importantly, this work has dramatically demonstrated the utility of a combination of low temperature EPR and MCD spectroscopies (including MCD magnetization data) for characterizing iron-sulfur clusters in a complex, multicomponent enzyme. Clearly, MCD spectroscopy will play an increasingly important role in deconvoluting the optical transitions from discrete centers and characterizing the metal centers in complex metalloenzymes.

References

1. Jones, R.W., Lamont A., and Garland, P.B. (1980) Biochem. J. 190, 79-94

2. Hewitt, E.J., and Notton, B.A. (1980) in "Molybdenum and Molybdenum and Molybdenum Containing Enzymes" (Coughlan, M. ed.), pp. 275-325, Pergamon Press, Oxford

3. Smith, L. (1968) in "Biological Oxidations" (Singer, T. ed.), pp. 55-122, Interscience, New York

4. Gutteridge, S., Bray, R.C., Notton, B.A., Fido, R.J., and Hewitt, E.J. (1983) Biochem. J 213, 137-142

5. Forget, P. (1974) Eur. J. Biochem. 42, 325-332

6. Mac Gregor, C.H. (1978) in "Methods in Enzymology" (Fleischer,S. and Packer, L. eds.) 347-355, Academic Press, New York

7. Clegg, R.A. (1976) Biochem. J. 153, 533-541

8. Graham, A. and Boxer, D.H. (1980) Febs Lett. 113, 15-20

9. Blum, H. and Poole, R.K. (1982) Biochem. Biophys. Res. Commun. 107, 903-909

10. Taniquichi, S., and Itagaki, E. (1960) Biochim. Biophys. Acta 44, 263-279

11. Nason, A., Antoine, A.D., Ketchem, P.A., Frazier, W.A., and Lee, D.K. (1970) Proc. Nat. Acad. Sci. USA 65, 137-144

12. Ishizuka, M., Toraya, T., and Fukui, S. (1984) Biochim. Biophys. Acta 788, 133-143

13. Ramadoss, C.S., Shen, T.C., and Vennesland, B. (1981) J. Biol. Chem. 256, 11532-11537

14. Johnson, J.C. Hainline, B.E., and Rajagopalan, K.V. (1980) J. Biol. Chem. 255, 1783-1786

15. Rajagopan, K.V. (1985) Biochem. Soc. Trans. 13, 401-403

16. Cramer, S.P., Wahl, R., and Rajagopalan, K.V. (1981) J. Am. Chem. Soc. 103, 7721-7727

17. Cramer, S.P. Solomonson, L.P., Adams, M.W.W., and Mortenson, L.E. (1984) J. Am. Chem. Soc. 106, 1467-1471

18. Vincent, S.P. (1979) Biochem. J. 177, 757-759

19. Barber, M.J., Bray, R.C., Cammack, R., and Coughlan, M.P. (1977) Biochem. J. 163, 279-287

20. Gutteridge, S. Bray, R.C., Notton, B.A., Fido, R.J. and Hewitt, E.J. (1983) Biochem. J. 213, 137-142

21. Solomonson, L.P., Barber, M.J., Howard, W.D., Johnson, J.L., and Rajagopalan, K.V. (1984) J. Biol. Chem. 259, 849-853

22. Van't Riet, J., Van Ee, J.H., Wever, R., Van Gelder, B.F. and Planta, R.J. (1975) Biochim. Biophys. Acta 405, 306-317

23. Bosma, H.J., Wever, R., and Van't Riet, J. (1978) Febs Lett. 90, 107-111

24. Forget, P., and Dervartanian, D.V. (1972) Biochim. Biophys. Acta 256, 600-606

25. Godfrey, C., Greenwood, C., Thomson, A.J., Bray, R.C., and George, G.N. (1984) Biochem. J. 224, 601-608

26. Bray, R.C., George, G.N., Gutteridge, S., Norlander, L., Stell, J.G.P., and Stubley, C. (1982) Biochem. J. 203, 263-267

27. Dervartanian, D.V., and Forget, P. (1975) Biochim. Biophys. Acta 379, 74-80

28. Bray, R.C., Vincent, S.P., Lowe, D.J., Clegg, R.A., and Garland, P.B. (1976) Biochem. J. 155, 201-203

29. Vincent, S.P., and Bray, R.C. (1978) Biochem. J. 1971, 639-647

30. George, G.N., Bray, R.C., Morpeth, F.F., and Boxer, D.H. (1985) Biochem. J. 227, 925-931

31. Johnson, M.K., Bennett, D.E., Morningstar, J.E., Adams, M.W.W., and Mortenson, L.E. (1985) J. Biol. Chem. 260, 5456-5463

32. Adams, M.W.W., and Mortenson, L.E. (1982) J. Biol. Chem. 257, 1791-1799

33. Gillum, W.O., Mortenson, L.E., Chen, J.S., and Holm, R.H. (1977) J. Am. Chem. Soc. 99, 584-595

34. Vickery, L., Nozawa, T., and Saver, K. (1976) J. Am. Chem. Soc. 98, 351-357

35. Johnson, M.K., Morningstar, J.E., Bennett, D.E., Ackrell, B.A.C., and Kearney, E.B. (1985) J. Biol. Chem. 260, 7368-7378

36. Johnson, M.K., Robinson, A.E., and Thomson, A.J. (1982) in "Iron-Sulfur Proteins" (Spiro, T.G. ed.) Vol.4, pp. 367-406, John Wiley and Sons, New York

37. Thomson, A.J., Cammack, R., Hall, D.O., Rao, K.K., Briat, B., Rivoal, J.C., and Badoz, J. (1977) Biochim. Biophys. Acta 493, 132-141

38. Kennedy, M.C., Emptage, M.H., Dreyer, J.L., and Beinert, H. (1983) J. Biol. Chem. 258, 11098-11105

39. Kurtz, D.M., Holm, R.H., Ruzicka, F.J., Beinert, H., Coles, C.J., and Singer, T.P. (1979) J. Biol. Chem. 254, 4967-4969

40. Thomson, A.J., Robinson, A.E., Johnson, M.K., Moura, J.J.G., Moura, I., Xavier, A.V., and LeGall, J. (1981) Biochim. Biophys. Acta 670, 93-100

41. George, S.J., Richards, A.J.M., Thomson, A.J., and Yates, M.G. (1984) Biochem. J. 224, 247-251

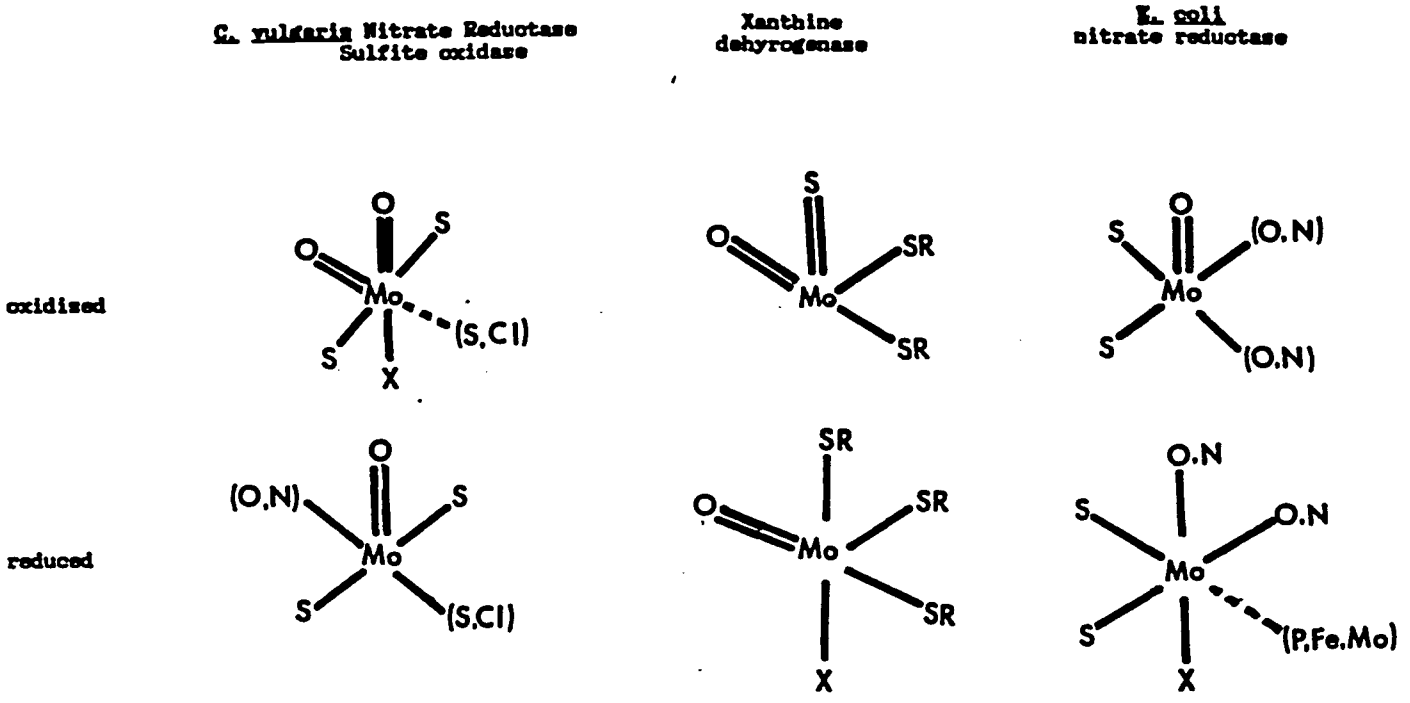

Figure VI.1: Structure of the molybdenum center for sulfite oxidase, xanthine dehydrogenase, and nitrate reductase from C. vulgaris and E. coli. The hydroxylase structures were taken from reference 16, and the nitrate reductase structures were taken from reference 17.

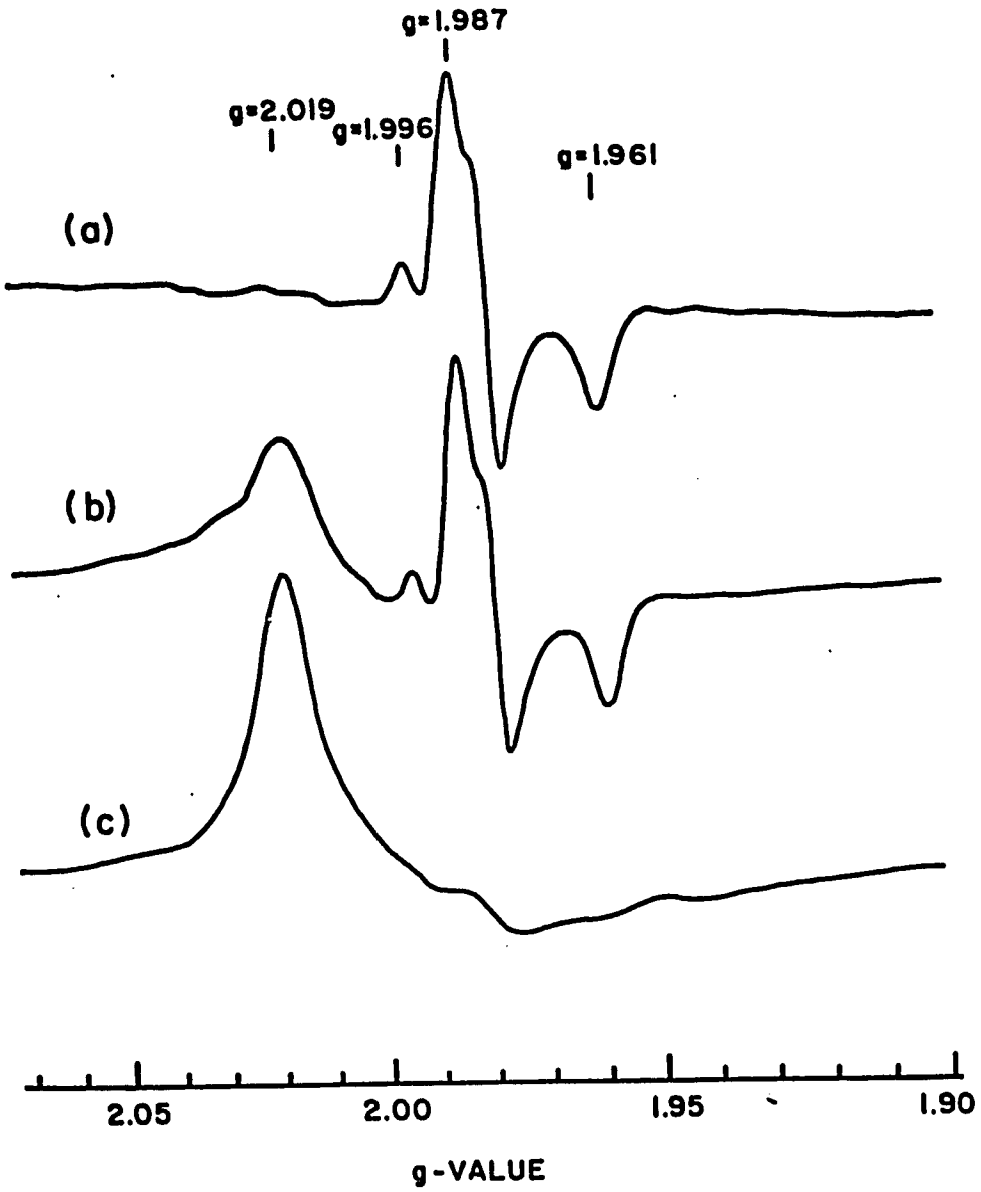

Figure VI.2: EPR spectra for as-isolated E. coli nitrate reductase. Enzyme concentration was 12.5 mg/ml, 50 mM Tris/HCl buffer, pH 8.0, 50% v/v ethylene glycol. The microwave frequency was 9.020 GHz and the modulation amplitude was 0.63 mT. (a) temperature, 40 K; microwave power, 1 mW; gain, 2500 (b) temperature, 20 K; microwave power, 1 mW; gain, 2000 (c) temperature, 10 K; microwave power, 10 mW; gain, 500.

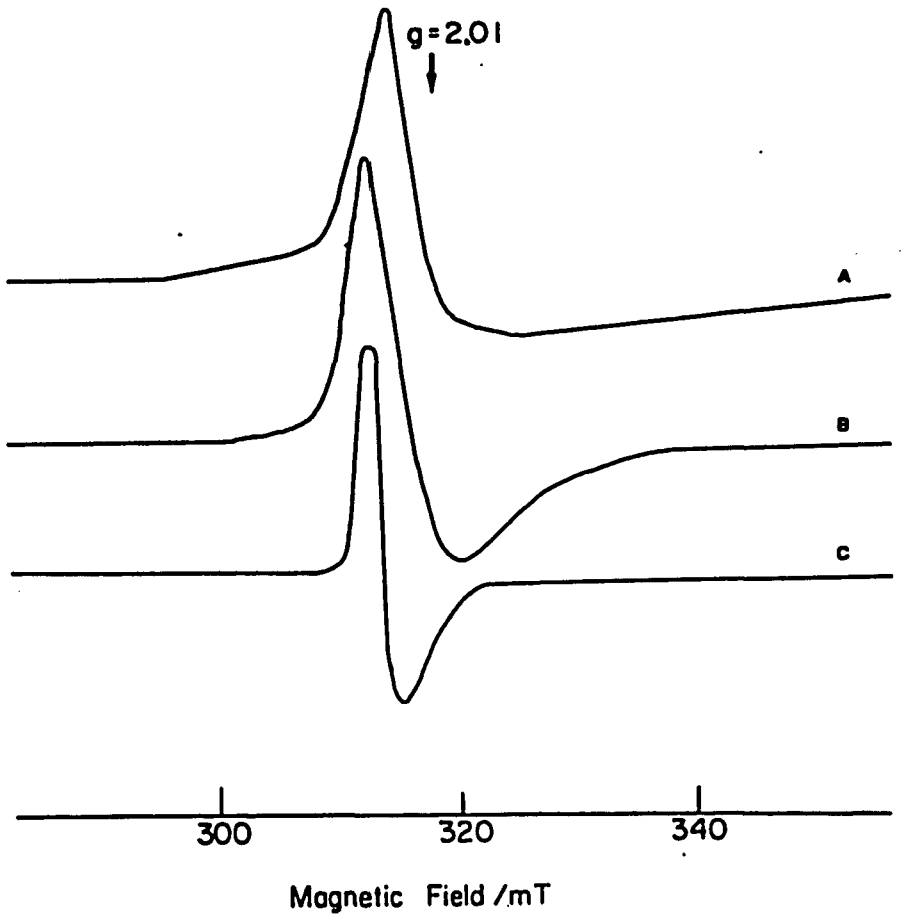

Figure VI.3: Comparison of EPR spectra for oxidized [3Fe-xS] clusters. Temperature, 10 K; microwave power, 10 mW; microwave frequency, 9.020 GHz; modulation amplitude, 0.63 mT (a) E. coli nitrate reductase, enzyme concentration as per figure VI.2. The Mo(V) signal has been manually subtracted. gain, 500 (b) T. thermophilus Fd, enzyme concentration was 0.316 mM, in 100 mM potassium phosphate buffer, pH 7.7, 50% v/v ethylene glycol. gain, 100 (c) A. vinelandii Fd I, protein concentration was 0.211 mM, in 1.0 M Tris/HCl buffer, pH 8.5, 50% v/v ethylene glycol. gain, 630 Note: under the conditions used A. vinelandii Fd I is highly power saturated. Therefore, the intensity of spectrum (c) is not directly comparable to spectra (a) and (b).

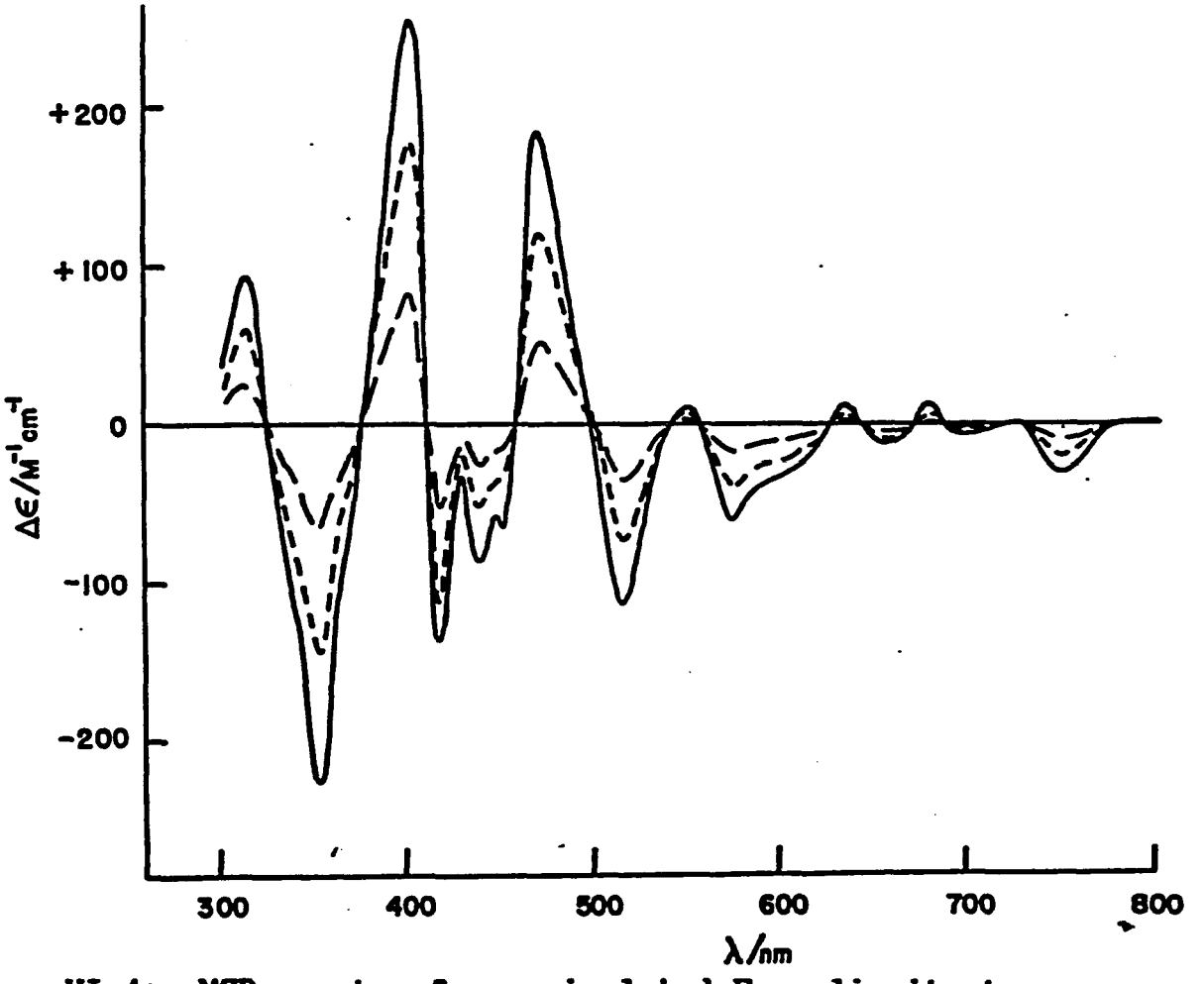

Figure VI.4: MCD spectra for as-isolated *E. coli* nitrate reductase. The enzyme concentration was as per figure VI.2. The conditions of measurement were: magnetic field, 4.9 T; pathlength, 0.170 cm; temperatures, 1.51 K (——), 4.22 K (---), and 11.6 K (— —).

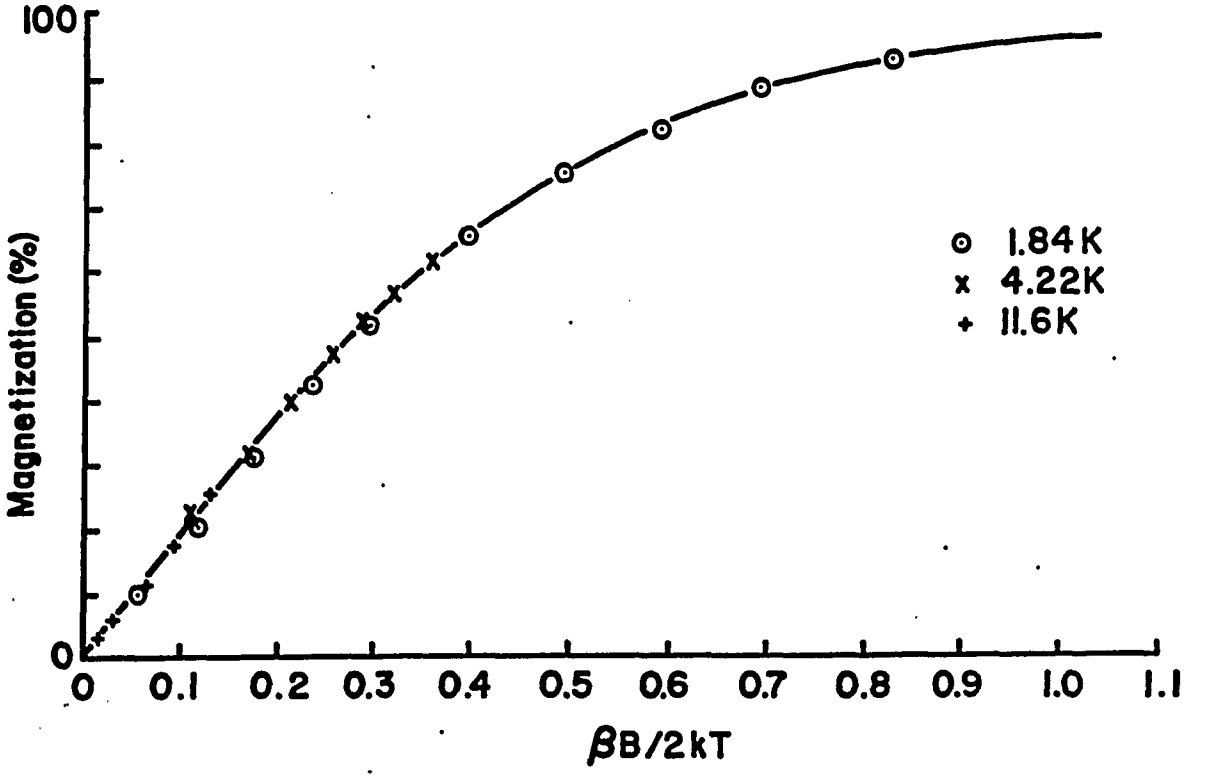

Figure VI.5: MCD magnetization plot for as-isolated E. coli nitrate reductase. The conditions of measurement were as for figure VI.4; wavelength, 470 nm. Temperatures correspond to 1.84 K (O), 4.22 K (X), and 11.6 K (+); magnetic fields were between 0 and 4.5 T. The solid line is the theoretical magnetization curve for $g_{isotropic}=2.01$.

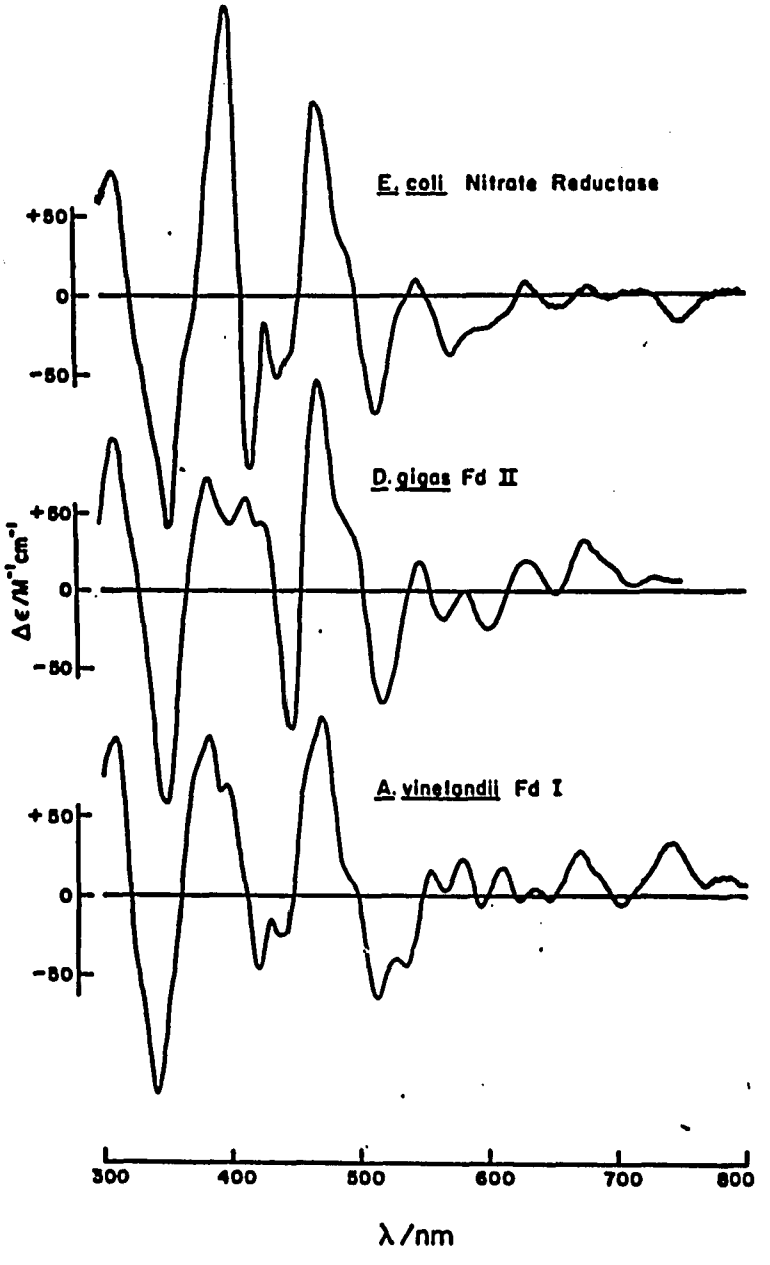

Figure VI.6: Comparison of MCD spectra for as-isolated samples of *E. coli* nitrate reductase, *A. vinelandii* Fd I, and *D. gigas* Fd II. The conditions of measurement were: temperature, 4.22 K; magnetic field, 4.9 T. *D. gigas* Fd II spectrum was taken from reference 40.

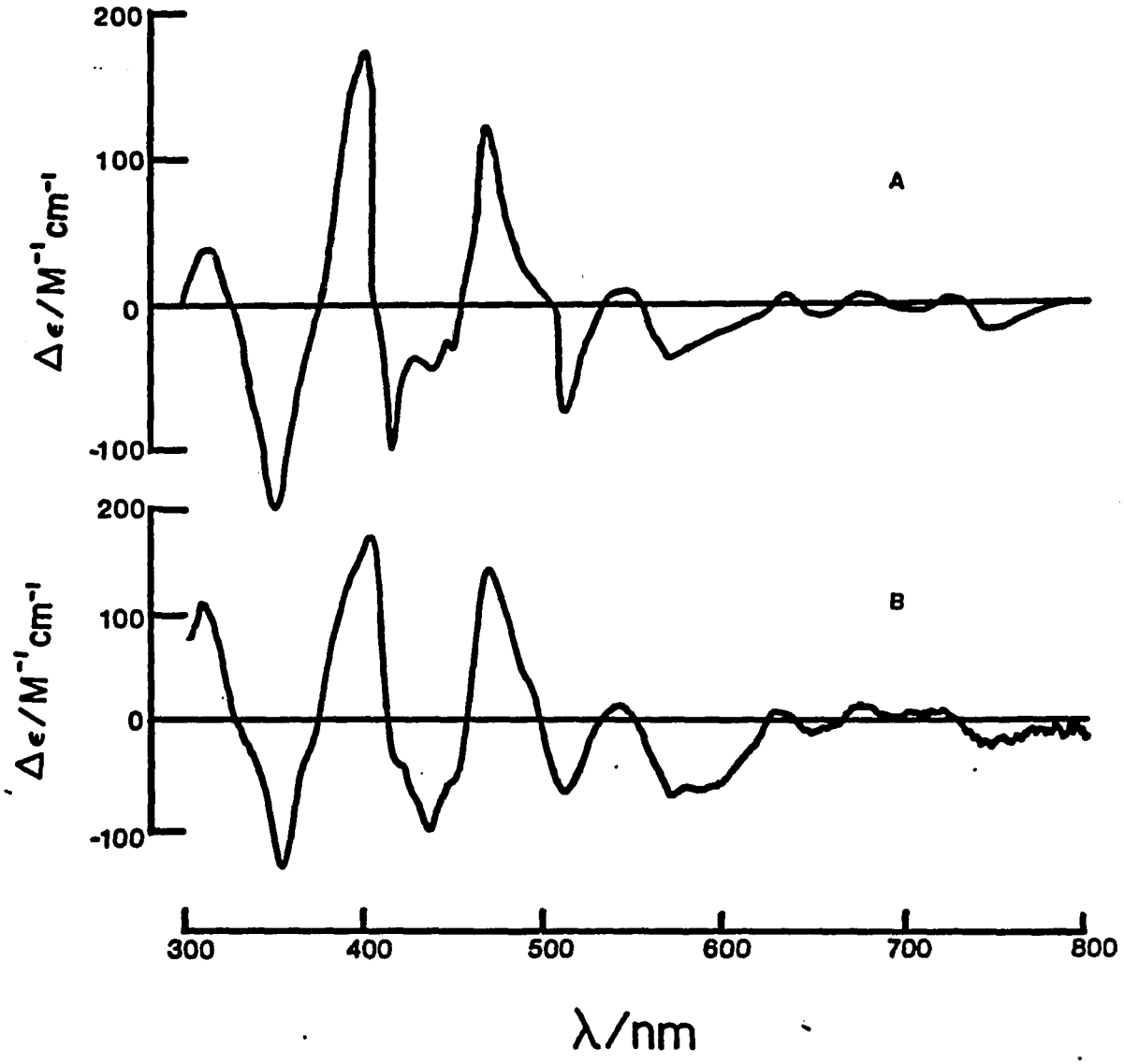

Figure VI.7: Comparison of MCD spectra of two distinct preparations of as-isolated E. coli nitrate reductase. Enzyme concentrations as per figure VI.2. The conditions of measurement were: temperature, 4.22 K; magnetic field, 4.9 T. (a) maximal heme content of four preparations of E. coli nitrate reductase studied. (b) minimal heme content of four preparations of E. coli nitrate reductase studied.

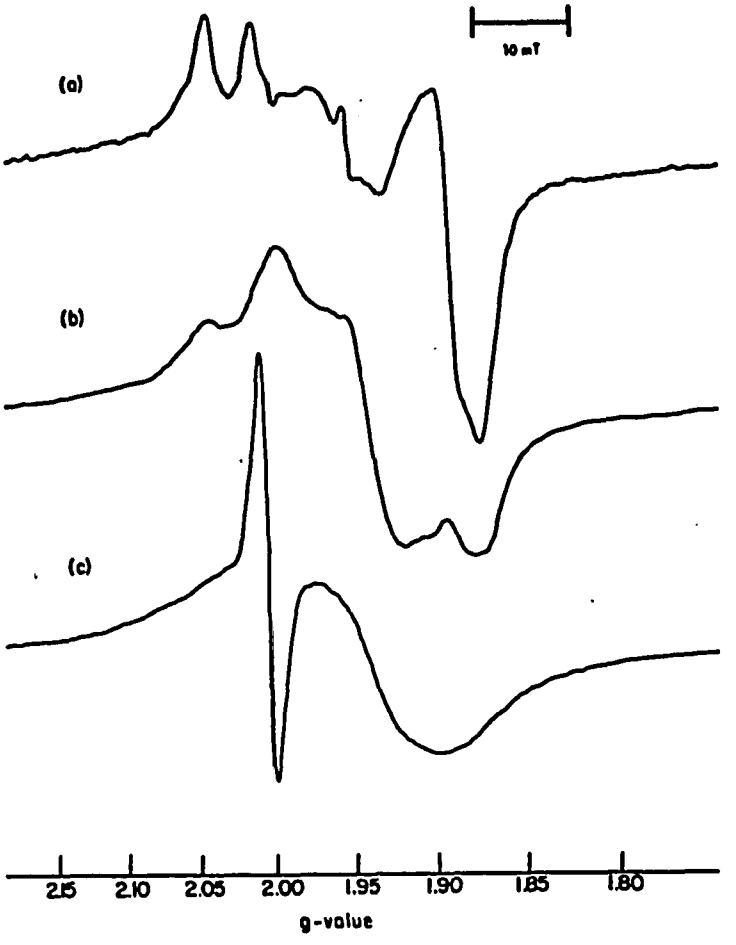

Figure VI.8: EPR spectra for reduced E. coli nitrate reductase. modulation amplitude 0.63 mT (a) reduced with a twenty-fold excess of sodium dithionite and incubated for two minutes at room temperature, prior to freezing. Enzyme concentration was 19.5 mg/ml, 50 mM Tris/HCl, pH 8.0. Temperature, 20 K; microwave power, 2 mW; gain, 6300; microwave frequency, 9.020 GHz. (b) sample contained 50 mM EDTA and 40 uM proflavin and was reduced by irradiation for fifteen minutes at room temperature, prior to freezing. Enzyme concentration was 16.5 mg/ml, 100 mM phosphate, pH 7.0. Temperature, 10 K; microwave power, 2 mW; gain, 5000; microwave frequency, 8.985 GHz. (c) sample was reduced with a twenty-fold excess of sodium dithionite in the presence of 0.1 mM methyl viologen and incubated for five minutes at room temperature, prior to freezing. Enzyme concentration was 16.5 mg/ml, 100 mM Tris/HCl, pH 8.0. Temperature, 20 K; microwave power, 0.5 mW; gain, 3200; microwave frequency, 8.990 GHz.

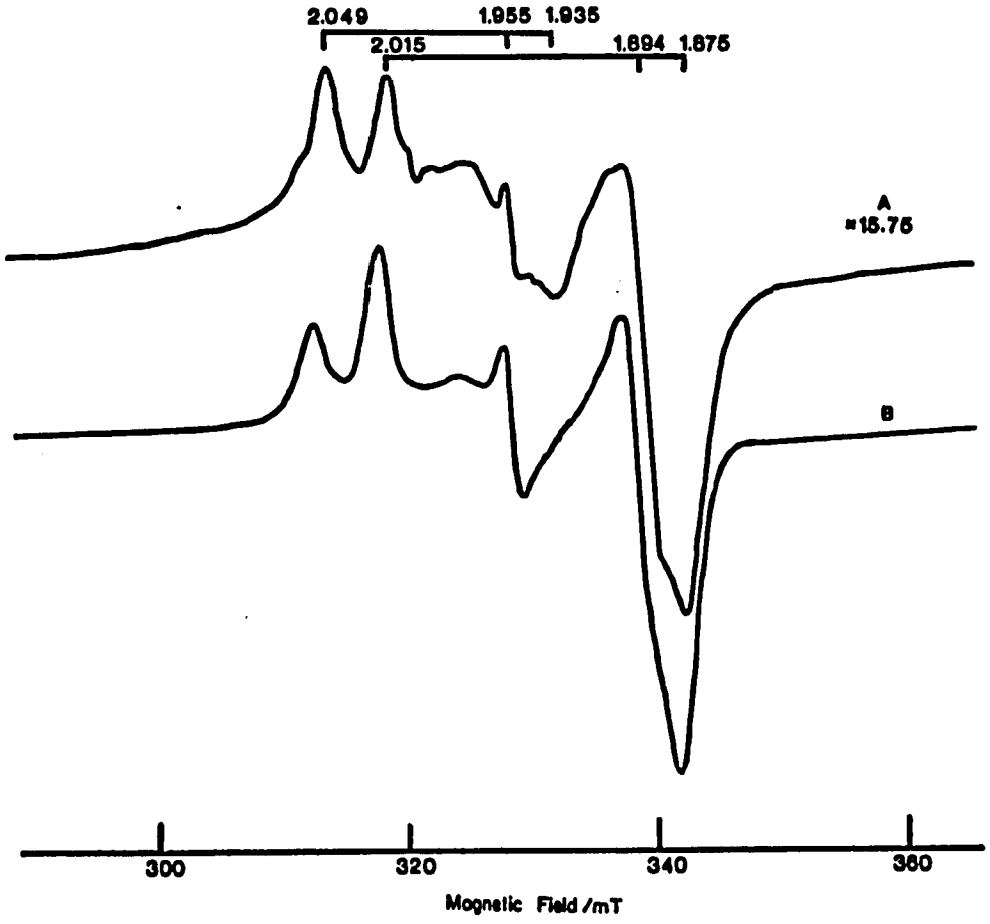

Figure VI.9: Power dependence of the EPR spectra of dithionite reduced E. coli nitrate reductase. Conditions were as per figure VI.8a. Microwave powers were (a) 2 mW and (b) 100 mW.

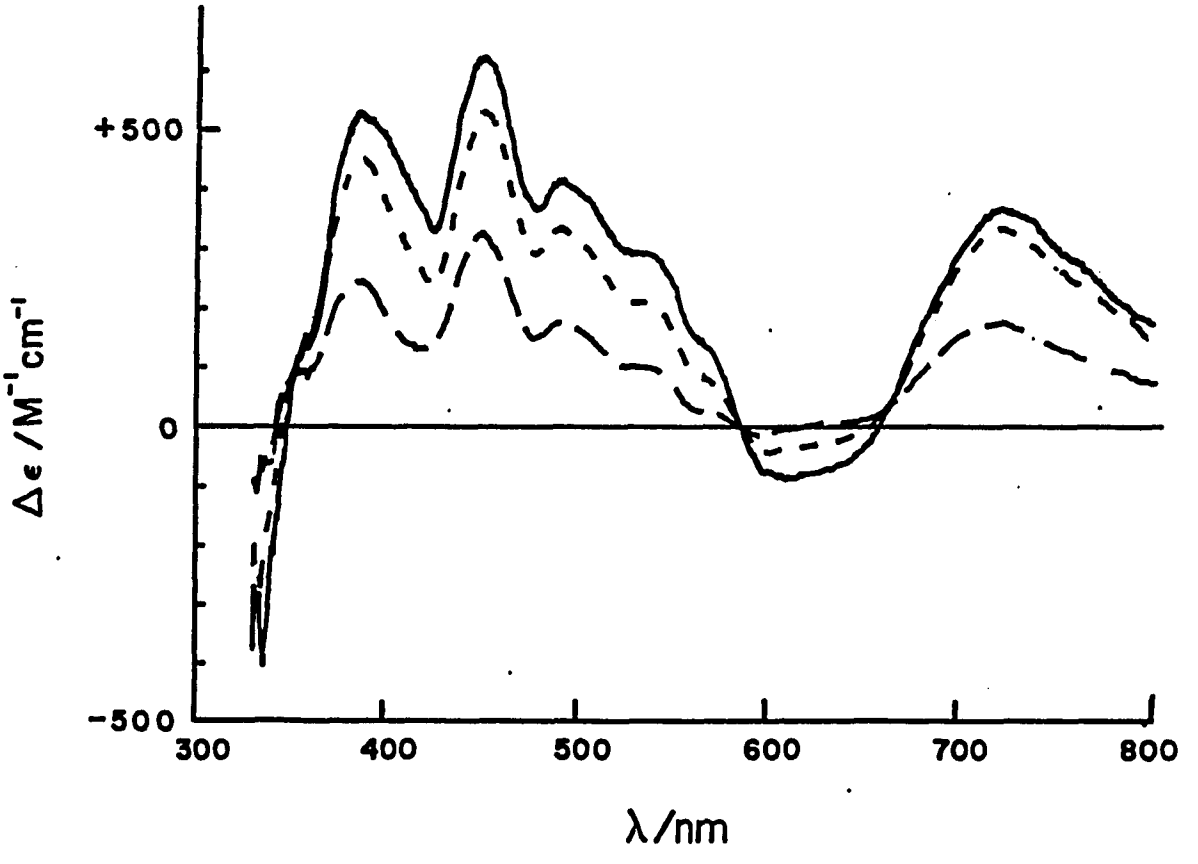

Figure VI.10: MCD spectra of reduced E. coli nitrate reductase Enzyme was as per figure VI. 8c, made 50 % v/v ethylene glycol. Temperatures were: 1.5 K (——), 4.22 K (---), and 14 K (— —). The magnetic field was 4.5 tesla.

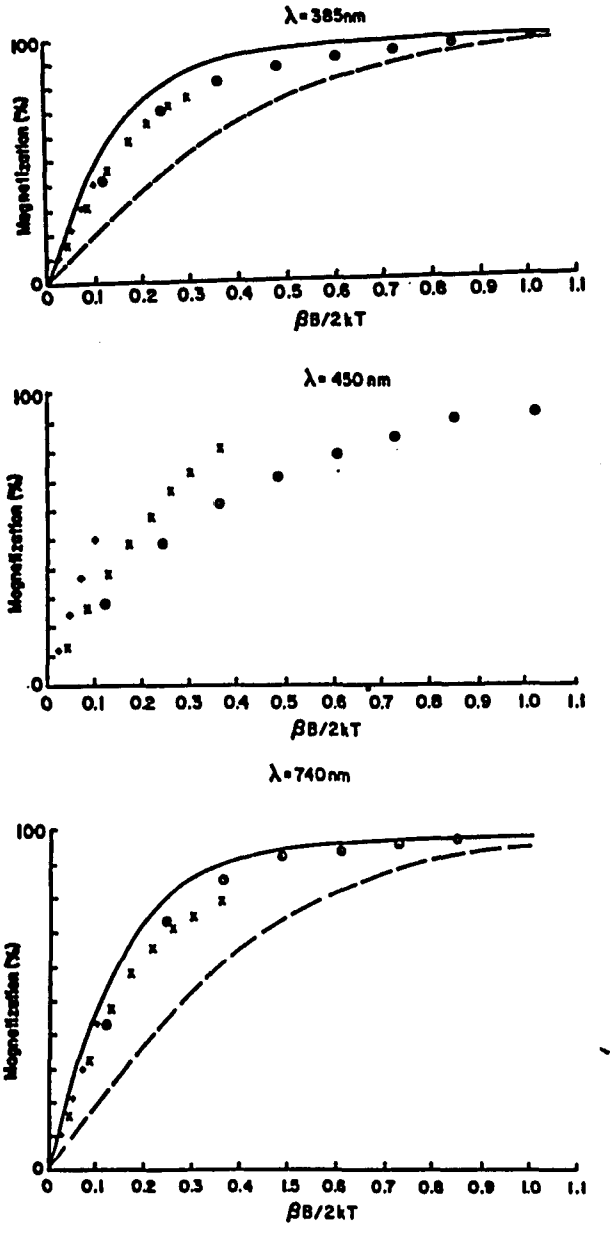

Figure VI.11: MCD magnetization plots for reduced E. coli nitrate reductase. The conditions of measurement were as per figure VII.10. Wavelengths were 385 nm (a), 450 nm (b), and 740 nm (c). Temperatures were: 1.49 K (O), 4.22 K (X), and 14.9 K (+). Magnetic fields were between 0 and 4.5 T. The solid line is the theoretical magnetization curve for g_z = 8.0 and g_x = 0.0, and the broken line is the theoretical magnetization curve for $g_{isotropic}$ = 1.95.

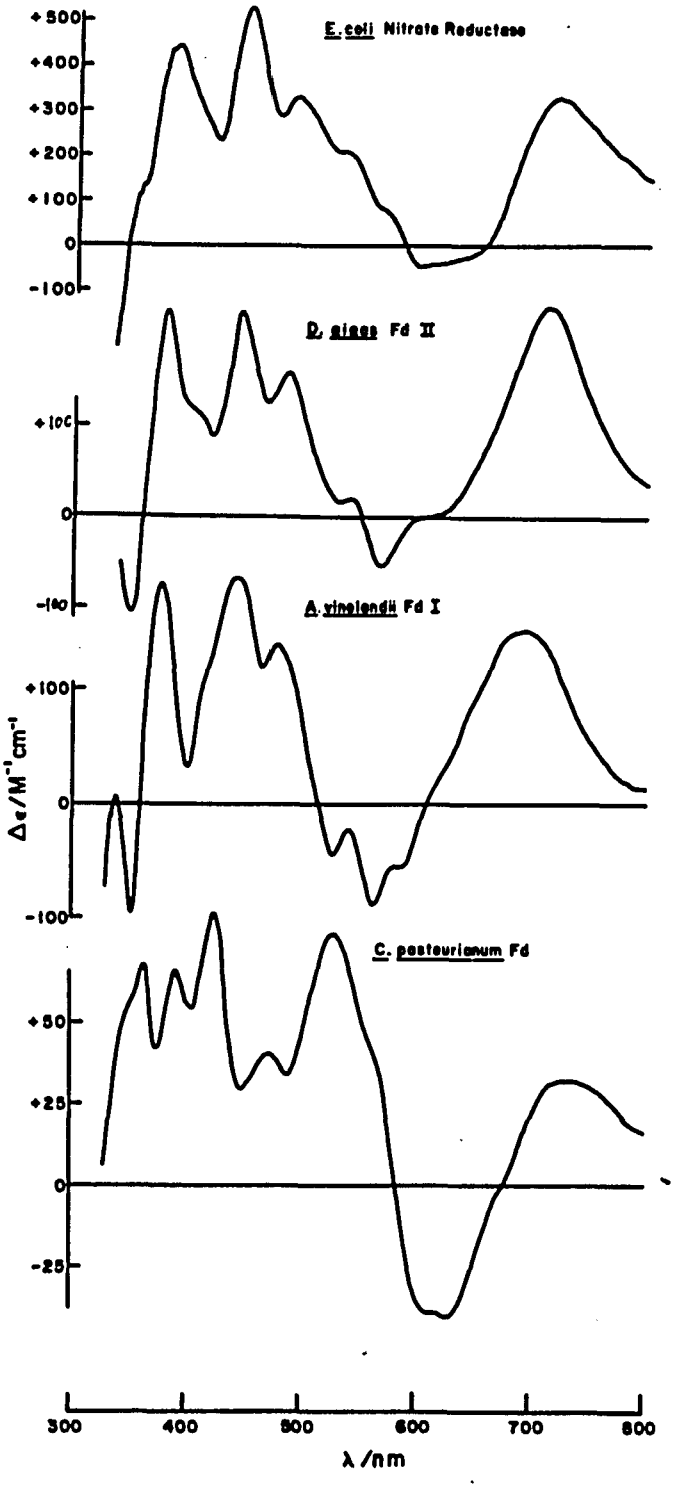

Figure VI.12: Comparison of MCD spectra for reduced samples of E. coli nitrate reductase, D. gigas Fd II, A. vinelandii Fd I, and C. pasteurianum Fd. All samples were reduced with sodium dithionite. The nitrate reductase sample was 0.1 mM in methyl viologen. The conditions of measurement were: temperature - 4.22 K, magnetic field - 4.5 T (5 T for the D. gigas Fd II). The D. gigas Fd II spectrum was taken from reference 41.

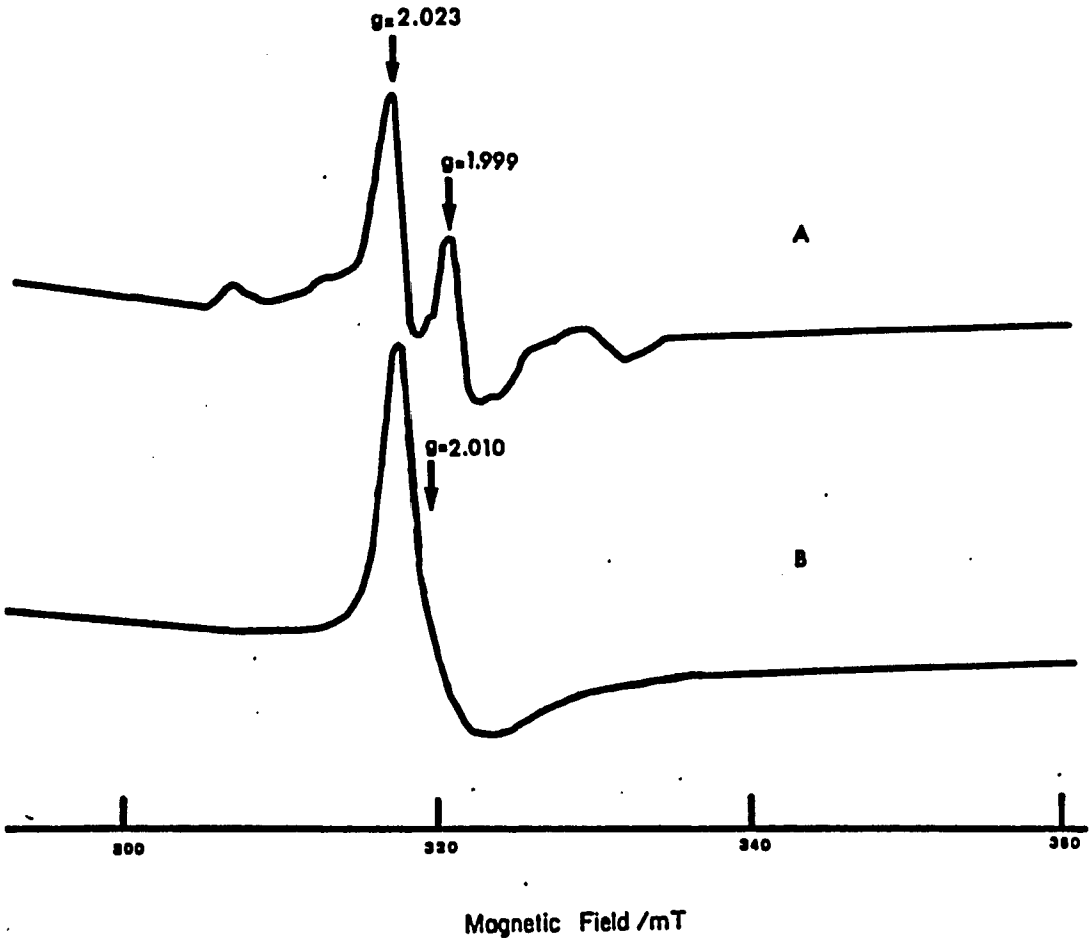

Figure VI.13: EPR spectra of ferricyanide treated E. coli nitrate reductase. Enzyme concentration was 19.5 mg/ml in 100 mM potassium phosphate buffer, pH 7.2, incubated with 0.5 mM ferricyanide for eight hours at room temperature, prior to freezing. microwave frequency, 8.990 GHz; modulation amplitude 0.63 mT. (a) temperature, 65 K; microwave power, 0.5 mW; gain, 25,000; (b) temperature, 10 K; microwave power, 2 mW; gain, 3,200.

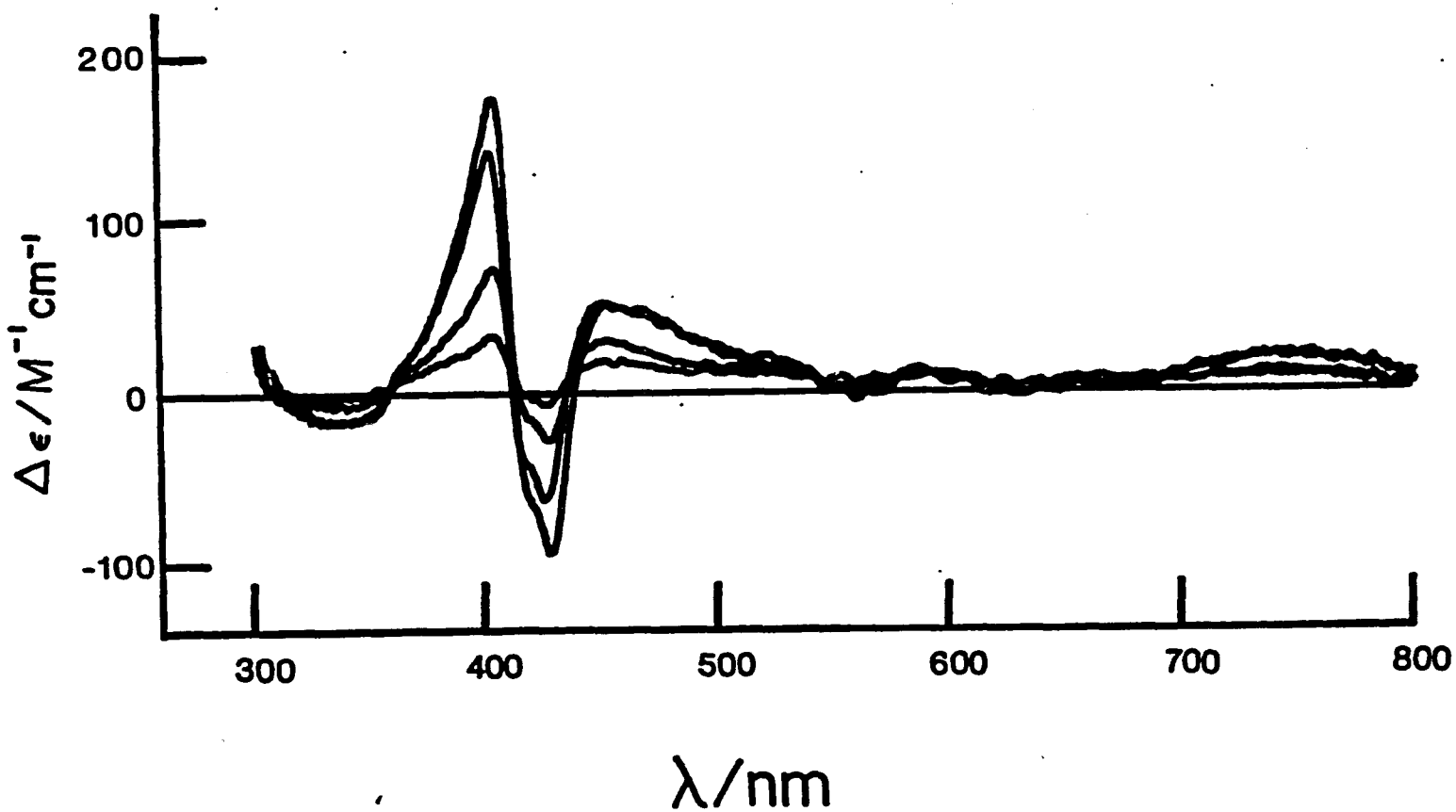

Figure VI.14: MCD spectra of cyanide inactivated E. coli nitrate reductase. Enzyme concentration was 13.9 mg/ml in 100 mM potassium phosphate buffer, pH 7.2, 50% v/v ethylene glycol and incubated for ten minutes at room temperature with 20 mM cyanide, prior to freezing. Conditions for measurement were: temperatures, 1.59 K, 4.22 K, 12.5 K, and 30 K; magnetic field, 4.5 tesla.

Appendix A

Computer Programs

(a) program for plotting and simulation of MCD magnetization data
(b) program for editing MCD magnetization data
(c) program for quantitating EPR spectra

A

```
LIST
1 REM       This program begins by assigning values to constants using READ
2 REM       statements.  Then other information is input interactively,
3 REM       beginning with a title, external file name, if any, number of
4 REM       temperatures, etc.
10 DEFDBL V,R
20 DEFINT J,N,P,Q,M,L
30 DIM V(25),R(25),F1(25),F2(25),A1(25),A2(25),I1(30),I2(30),I(30),W(30),F(25),A
(25),IN(30),X(25),T(25),Z(25),S$(25),AA(20,25),Y(20,25),B(20,25),XX(20,25),ZZ(20
,25)
40 N=6
50 NW=30
60 FOR U=1 TO N : READ V(U),R(U) : NEXT U
70 DATA 0.0337652415,0.0858622458
80 DATA 0.169395328,0.180380762
90 DATA 0.380690398,0.233956993
100 DATA 0.619309604,0.233956993
110 DATA 0.830604672,0.180380762
120 DATA 0.966234744,0.0858622459
130 FOR M=1 TO NW : READ W(M) : NEXT M
140 DATA 0.0,0.03,0.06,0.09,0.12,0.15,0.20,0.25,0.30,0.35,0.40,0.50,0.6,0.7,0.8,
0.9,1.0,1.1,1.2,1.3,1.4,1.5,1.6,1.7,1.8,1.9,2.0,2.1,2.2,10.0
150 PRINT "PROGRAM FOR PLOTTING AND SIMULATING MCD MAGNETIZATION DATA"
160 INPUT "Enter Title";R$
161 INPUT "DO YOU WANT TO INPUT EXPERIMENTAL DATA FROM EXISTING DATA FILE";Y$
162 IF Y$="y" OR  Y$="Y" GOTO 2200
170 INPUT "How many temperatures";E
180 FOR J=1 TO E
190 PRINT "Temperature (J) number";J:INPUT T(J)
200 INPUT "How many fields at this temperature";Y(J)
210 INPUT "What color do you want the points to be?: Color is : Black 0,Blue 1,R
ed 2,Magenta 3,Green 4,Cyan 5,Yellow 6,White 7";Z(J)
220 INPUT "What [illegible] you want to use (+,*,$,O)";S$(J)
230 CLS:PRINT "Temperature:";T(J)
240 FOR I=1 TO Y(J)
250 PRINT "Field #";J
260 INPUT "What are the field (in millivolts off multimeter) and intensity (mm)"
;AA(I,J),Y(I,J)
270 R(I,J)=.0558*AA(I,J)
280 XX(I,J)=(.4669*R(I,J))/(2*.695*T(J))
290 NEXT I
300 NEXT J
310 GOSUB 400
320 INPUT "Estimate magnetization limit (mm)";ML
330 FOR J=1 TO E
340 FOR I=1 TO Y(J)
350 ZZ(I,J)=(Y(I,J)-ML)*100
360 NEXT I
370 NEXT J
380 GOSUB 600
381 INPUT "DO YOU WANT TO SAVE THIS EXPERIMENTAL DATA";I
382 IF Y$="y" OR  Y$="Y" THEN GOTO 2000
390 END
400 CLS
410 PRINT R$
420 FOR J=1 TO E
430 PRINT "Temperature = ";T(J);"K"
440 PRINT "Field (gmps)" TAB(20) "Reduced Field" TAB(40) "Intensity"
450 FOR I=1 TO Y(J)
460 PRINT AA(I,J) TAB(20) XX(I,J) TAB(40) Y(I,J)
470 NEXT I
```

```
500 IF YS="N" OR YS="n" GOTO 590
510 LPRINT RS
520 FOR J=1 TO E
530 LPRINT "Temperature = "T(J)"K"
540 LPRINT "Field (mW)" TAB(20) "BetaB/2kT" TAB(40) "Intensity"
550 FOR I=1 TO X(J)
560 LPRINT AA(I,J) TAB(20) XX(I,J) TAB(40) Y(I,J)
570 NEXT I
580 NEXT J
590 RETURN
600 CLS
610 SCALE(-50,550),(932,-97)
620 LINE (0,0)-(540,300),PSET,7,B
630 FOR I=0 TO 540 STEP 45
640 LINE (I,0)-(I,5),PSET,7
650 NEXT I
660 FOR I=0 TO 300 STEP 30
670 LINE (0,I)-(5,I),PSET,7
680 NEXT I
690 SYMBOL (0,-10),"0"
700 SYMBOL (525,-10),"1.2"
710 SYMBOL (200,-10),"BetaB/2kT"
720 SYMBOL (-30,100),"MAGNETIZATION (%)",1,1,7,1,PSET
730 SYMBOL (-30,2),"0%"
740 SYMBOL (-35,303),"100%"
750 FOR J=1 TO E
760 T$=S$(J)
770 FOR I=1 TO X(J)
780 SYMBOL (XX(I,J)*(540/1.2)-8,ZZ(I,J)*3+7),T$,1,1,Z(J),0,PSET
790 NEXT I
800 NEXT J
810 LOCATE 0,24:PRINT "Do you want to overlap simulated data";
820 Y$=INKEY$:IF Y$="" THEN 820
830 CLS 24,1
840 IF Y$="n" OR Y$="N" GOTO 860
850 GOSUB 1170
860 LOCATE 0,24:PRINT "Do you want a hard copy?";
870 A$=INKEY$:IF A$="" THEN 870
880 CLS 24,1
890 IF A$="N" OR A$="n" GOTO 920
900 LOCATE 0,1:PRINT R$ "  Limit = " ML "mm"
910 COPY
920 LOCATE 0,24:PRINT "Do you want to change estimated magnetization limit";
930 G$=INKEY$:IF G$="" THEN 930
940 CLS 24,1
950 IF G$="N" OR G$="n" GOTO 1100
960 FOR J=1 TO E
970 T$=S$(J)
990 FOR I=1 TO X(J)
990 SYMBOL(XX(I,J)*(540/1.2)-3,ZZ(I,J)*3+7),T$,1,1,Z(I),0,XOR
1000 NEXT I
1010 NEXT J
1020 LOCATE 0,1:INPUT "New value of magnetization limit (mm) ";ML
1030 CLS 1,1
1040 FOR J=1 TO E
1050 FOR I=1 TO X(I)
1060 ZZ(I,J)=(Y(I,J)/ML)*100
1070 NEXT I
1080 NEXT J
1090 GOTO 750
1100 LOCATE 0,24:PRINT "Do you want to erase screen before printing";
1110 F$=INKEY$:IF F$="" THEN 1110
1120 CLS 24,1
1130 IF F$="N" OR F$="n" GOTO 1160
```

```
1160 RETURN
1170 LOCATE 0,24:PRINT "Is theoretical data on file?";
1171 Y$=INKEY$:IF Y$="" THEN 1171
1172 CLS 24,1
1173 IF Y$="N" OR Y$="n" GOTO 1178
1174 GOTO 4000
1175 LOCATE 0,24:PRINT "Do you have an axial system with BPER=0";
1180 C$=INKEY$:IF C$="" THEN 1180
1190 CLS 24,1
1200 IF C$="Y" OR C$="y" GOTO 1230
1210 LOCATE 0,1:INPUT "Values for MZ/M+,BPAR,BPER";M,BPAR,BPER
1220 CLS 1,1
1230 S=BPAR/BPER
1240 FOR L=1 TO NW
1250 G=BPER*W(L)
1260 FOR J=1 TO N
1270 X=SQR(V(J)^2*(S^2-1)+1)
1280 C=(V(J)^2-1)/X
1290 B=V(J)^2*S/X
1300 F1(J)=C*(EXP(G*X)-EXP(-G*X))/(EXP(G*X)+EXP(-G*X))
1310 F2(J)=B*(EXP(G*X)-EXP(-G*X))/(EXP(G*X)+EXP(-G*X))
1320 NEXT J
1330 I1(L)=0
1340 FOR P=1 TO N
1350 A1(P)=F1(P)*R(P)
1360 I1(L)=A1(P)+I1(L)
1370 NEXT P
1380 I2(L)=0
1390 FOR Q=1 TO N
1400 A2(Q)=F2(Q)*R(Q)
1410 I2(L)=A2(Q)+I2(L)
1420 NEXT Q
1430 I(L)=SQR(2!)*M*I1(L)+I2(L)
1440 NEXT L
1450 CO=0
1460 FOR J=1 TO NW
1470 FOR P=1 TO NW
1480 IF I(J)<I(P) GOTO 1520
1490 CO=CO+1
1500 IF CO=NW THEN GOTO 1540
1510 NEXT P
1520 CO=0
1530 NEXT J
1540 SL=I(J)
1550 FOR L=1 TO NW
1560 IN(L)=(I(L)/SL)*100!
1570 NEXT L
1580 FOR H=1 TO NW-11
1590 PSET(W(H)*540/1.2,IN(H)*3)
1600 NEXT H
1601 LOCATE 0,24:PRINT "Do y"    " to save this theoretical data?"
1602 Y$=INKEY$:IF Y$="" THEN 1602
1603 CLS 24,1
1604 IF Y$="y" OR Y$="Y" GOTO 5000
1610 LOCATE 0,24:PRINT "Hard copy of tabulated simulated data?"
1620 D$=INKEY$:IF D$="" THEN 1620
1630 CLS 24,1
1640 IF D$="N" OR D$="n" GOTO 3120
1650 LPRINT "SIMULATED MCD MAGNETIZATION DATA"
1660 LPRINT "MZ/M+ = "M
1670 LPRINT "BPAR = "BPAR "BPER = "BPER
1680 LPRINT "BetaB/2kT" TAB(40)"MCD Intensity"TAB(60) MAGNETIZATION"
1690 FOR I=1 TO NW
1700 LPRINT W(I) TAB(40) I(I) TAB(60) IN(I)
```

```
1730 LOCATE 0,1:INPUT "GPAR = ";GPAR
1740 CLS 1,1
1750 FOR L=1 TO NW
1760 FOR J=1 TO N
1770 C = V(J)*GPAR*W(L)
1780 F(J)=V(J)*(EXP(C)-EXP(-C))/(EXP(C)+EXP(-C))
1790 NEXT J
1800 I(L)=0
1810 FOR P=1 TO N
1820 A(P)=F(P)=R(P)
1830 I(L)=A(P)+I(L)
1840 NEXT P
1850 NEXT L
1860 CO=0
1870 FOR J=1 TO NW
1880 FOR P=1 TO NW
1890 IF I(J)<I(P) GOTO 1930
1900 CO=CO+1
1910 IF CO=NW THEN GOTO 1950
1920 NEXT P
1930 CO=0
1940 NEXT J
1950 BL=I(J)
1960 FOR L=1 TO NW
1970 IN(L)=(I(L)/BL)*100!
1980 NEXT L
1990 FOR N=1 TO NW-11
2000 PSET(W(N)*540/1.2,IN(N)*3)
2010 NEXT N
2011 LOCATE 0,24:PRINT "Do you want to save this theoretical data?";
2012 YS=INKEYS:IF YS="" THEN 2012
2013 CLS 24,1
2014 IF YS="Y" OR YS="y" GOTO 8000
2020 LOCATE 0,24:PRINT "Hard copy of tabulated simulated data?";
2030 ES=INKEYS:IF ES="" THEN 2030
2040 CLS 24,1
2050 IF ES="N" OR ES="n" GOTO 2120
2060 LPRINT "SIMULATED MCD MAGNETIZATION DATA"
2070 LPRINT "GPAR = "GPAR "GPER = 0 "
2080 LPRINT "BetaB/2kT" TAB(40) "MCD Intensity" TAB(60) "Magnetization%"
2090 FOR I=1 TO NW
2100 LPRINT W(I) TAB(40) I(I) TAB(60) IN(I)
2110 NEXT I
2120 LOCATE 0,24:PRINT "Do you want to superimpose more simulated data";
2130 FS=INKEYS:IF FS="" THEN 2130
2140 CLS 24,1
2150 IF FS="Y" OR FS="y" GOTO 1470
2160 RETURN
2200 REM SUBROUTINE FOR READING EXPERIMENTAL DATA FILE
2210 INPUT "FILENAME";F$
2220 OPEN F$ FOR INPUT AS#1
2230 INPUT#1,E
2240 FOR J=1 TO E
2250 INPUT #1,T(J),X(J),Z(J),S$(J)
2260 FOR I=1 TO X(J)
2270 INPUT #1,AA(I,J),Y(I,J)
2280 NEXT I
2290 NEXT J
2295 CLOSE #1
2300 FOR J=1 TO E
2310 FOR I=1 TO X(J)
2320 R(I,J)=.05564*AA(I,J)
2330 XX(I,J)=(.4669*R(I,J))/(2*.695*T(J))
2340 NEXT I
```

```
3000 REM SUBROUTINE FOR CREATING EXPERIMENTAL DATAFILE
3005 PRINT "IF YOU WISH TO SAVE FILE TO DRIVE B TYPE 2: BEFORE YOUR FILENAME"
3010 INPUT "DESIGNATE A FILENAME";FS
3020 OPEN FS FOR OUTPUT AS#1
3030 PRINT#1,E
3040 FOR J=1 TO E
3050 PRINT #1,T(J),",";X(J),",";Z(J)",";SS(J)
3060 FOR I=1 TO X(J)
3070 PRINT #1,AA(I,J),",";Y(I,J)
3080 NEXT I
3090 NEXT J
3100 CLOSE #1
3101 GOTO 390
4000 REM SUBROUTINE FOR READING THEORETICAL DATAFILE
4010 LOCATE 0,1:INPUT "FILENAME";DFN$
4020 CLS 1,1
4030 OPEN DFN$ FOR INPUT AS#1
4035 INPUT #1,GPAR
4040 LOCATE 0,24:PRINT "Is the file for an axial system with GPER=0";
4050 Y$=INKEY$:IF Y$="" THEN 4050
4060 CLS 24,1
4070 IF Y$="y" OR Y$="Y" GOTO 4080
4080 INPUT #1,GPER
4090 FOR J=1 TO NW
4100 INPUT #1,W(J),I(J),IN(J)
4110 NEXT J
4120 CLOSE #1
4125 REM   Go to 1000 (display routine) if axial system with GPER=0
4128 REM   Else goto 1500 (a similar display routine)
4130 IF Y$="Y" OR Y$="y" GOTO 1000
4190 GOTO 1500
5000 REM SUBROUTINE FOR CREATING THEORETICAL DATAFILE
5010 LOCATE 0,1:INPUT "DESIGNATE A FILENAME";DFN$
5020 CLS 1,1
5030 OPEN DFN$ FOR OUTPUT AS#1
5040 PRINT #1,M,",";GPAR,",";GPER
5050 FOR I=1 TO NW
5060 PRINT #1,W(I),",";I(I),",";IN(I)
5070 NEXT I
5080 CLOSE #1
5090 GOTO 1610
6000 REM SUBROUTINE FOR CREATING THEORETICAL DATAFILE
6010 LOCATE 0,1:INPUT "DESIGNATE A FILENAME";DFN$
6020 CLS 1,1
6030 OPEN DFN$ FOR OUTPUT AS#1
6040 PRINT #1,GPAR
6050 FOR I=1 TO NW
6060 PRINT #1,W(I),",";I(I),",";IN(I)
6070 NEXT I
6080 CLOSE #1
6090 GOTO 2020
Ok
```

B

```
1000 REM PROGRAM FOR EDITING MCD DATAFILES
1010 DIM T(25),Z(25),S$(25),AA(20,25),Y(20,25),X(25)
1020 INPUT "WHAT FILE DO YOU WISH TO EDIT";F$
1030 OPEN F$ FOR INPUT AS #1
1040 INPUT #1,E
1050 FOR J=1 TO E
1060 INPUT #1,T(J),X(J),Z(J),S$(J)
1070 FOR I=1 TO X(J)
1080 INPUT #1,AA(I,J),Y(I,J)
1090 NEXT I
1100 NEXT J
1110 CLOSE #1
1120 CLS
1130 PRINT "TEMPERATURE NUMBER" TAB(20) "TEMPERATURE"
1140 FOR J=1 TO E
1150 PRINT J;T(J)
1160 NEXT J
1170 INPUT "DO YOU WISH TO CHANGE ANY OF THESE TEMPERATURES";Y$
1180 IF Y$="Y" OR  Y$="y" THEN GOTO 1470
1190 FOR J=1 TO E
1200 CLS
1210 PRINT "THE TEMPERATURE IS"T(J)"K"
1220 PRINT "FIELD NUMBER","FIELD" ,"INTENSITY"
1230 FOR I=1 TO X(J)
1240 PRINT I,AA(I,J),Y(I,J)
1250 NEXT I
1260 INPUT "DO YOU WANT TO CHANGE ANY OF THESE VALUES";Y$
1270 IF Y$="n" OR Y$="N" THEN GOTO 1320
1280 INPUT "WHAT FIELD NUMBER DO YOU WISH TO CHANGE";I
1290 INPUT "NEW FIELD (IN MILLIVOLTS),INTENSITY (mm)";AA(I,J),Y(I,J)
1300 INPUT "DO YOU WISH TO CHANGE ANOTHER VALUE";Y$
1310 IF Y$="y" OR Y$="Y" THEN GOTO 1280
1320 NEXT J
1330 REM SAVING THE NEW FILE
1340 INPUT "DO YOU WISH TO SAVE THIS DATA";Y$
1350 IF Y$="N" OR Y$="n" THEN GOTO 1460
1360 INPUT "WHAT FILENAME DO YOU WISH TO USE";F$
1370 OPEN F$ FOR OUTPUT AS #1
1380 PRINT #1,E
1390 FOR J=1 TO E
1400 PRINT #1,T(J),",";X(J),",";Z(J),",";S$(J)
1410 FOR I=1 TO X(J)
1420 PRINT #1,AA(I,J),",";Y(I,J)
1430 NEXT I
1440 NEXT J
1450 CLOSE #1
1460 END
1470 REM SUBROUTINE FOR CHANGING TEMPERATURES
1480 INPUT "WHICH TEMPERATURE NUMBER DO YOU WANT TO CHANGE";J
1490 INPUT "TYPE IN NEW VALUE";T(J)
1500 INPUT "DO YOU WANT TO CHANGE ANOTHER VALUE";Y$
1510 IF Y$="Y" OR Y$="y" THEN GOTO 1470
1520 GOTO 1190
```

C

```
10 REM PROGRAM FOR QUANTITATION OF EPR SPECTRA
11 CLS
20 DEFINT I-N : COLOR 7,2,0 : CONSOLE 0,25,0
30 DIM R(200),S(200),AR(200),AS(200)
35 REM INPUT VARIABLES FOR REFERENCE SPECTRUM,NR=INTERVALS, HR=HEIGHT OF INTERVA
L, GZR,GYR,GXR ARE G-VALUES FOR THE REFERENCE,XR=GAIN OF REFERENCE,YR=REFERENCE
CONCENTRATION
36 K=0
40 INPUT "Are you using complete EPR spectrum as reference(Y/N)";N$
50 IF N$="N" OR N$="n" GOTO 520
60 IF K=0 THEN GOTO 61 ELSE GOTO 150
61 INPUT "Number of intervals for reference spectrum (NR)";NR
70 INPUT "Width of intervals for reference spectrum (gauss)";HR
80 INPUT "G-values for reference spectrum (gz,gy,gx)";GZR,GYR,GXR
90 INPUT "Gain for reference spectrum";XR
91 INPUT "WHAT IS THE REFERENCE";R$
92 INPUT "WHAT POWER IS THE REFERENCE IN mW";PR$
100 INPUT "Concentration of reference sample (mM)";YR
101 INPUT "are these correct";Y$
102 IF Y$="N" OR  Y$="n" GOTO  61
110 PRINT "List intensity values for reference 1 to NR"
120 FOR I=1 TO NR
121 PRINT I
130 INPUT R(I)
140 NEXT I
144 REM LOOP FOR REINPUTING INTENSITIES OF REFERENCE IN CASE OF INPUT ERROR
145 INPUT "Is this correct";Y$
146 IF Y$="Y"OR Y$="y" GOTO 150 ELSE GOTO 120
150 AR=0
160 FOR I=1 TO NR
170 AR(I)=R(I)*(NR-(2*I)+1)
180 AR=AR+AR(I)
190 NEXT I
199 REM COMPUTING AVERAGE G-VALUES
200 GPR=(2/3)*SQR((GXR^2+GYR^2+GZR^2)/3)+(GXR+GYR+GZR)/9
201 INPUT "ARE YOU USING THE COMPLETE SAMPLE SPECTRUM";Z$
202 IF Z$="N" OR Z$="n" GOTO 2000
209 REM INPUT VALUES FOR SAMPLE SPECTRUM,NS=SAMPLE INTERVALS,HS=INTERVAL HEIGHT,
GZS,GYS,GXS=G-VALUES FOR SAMPLE, XS=SAMPLE GAIN,CS=CONCENTRATION OF SAMPLE
210 IF K=0 THEN GOTO 211 ELSE GOTO 290
211 INPUT "Number of intervals for sample spectrum (NS)";NS
220 INPUT "Width of intervals for sample spectrum (gauss)";HS
230 INPUT "G-values for sample spectrum (gz,gy,gx)";GZS,GYS,GXS
240 INPUT "Gain for sample spectrum";XS
244 INPUT "Sample concentration (mM)";CS
245 INPUT "WHAT POWER WAS THE SAMPLE RUN AT IN mW";PS$
246 INPUT "WHAT TEMPERATURE WAS THE SAMPLE RUN IN KELVIN";TS$
247 INPUT "WHAT DATE WAS THE SAMPLE RUN";D$
250 PRINT "List intensity values for sample 1 to NS"
260 FOR I=1 TO NS
261 PRINT I
270 INPUT S(I)
280 NEXT I
284 REM LOOP FOR REINPUTING INTENSITIES OF SAMPLE IN CASE OF INPUT ERROR
285 INPUT "IS this correct";Y$
286 IF Y$="Y"OR Y$="y" GOTO 290 ELSE GOTO 260
287 IF Z$="N" OR Z$="n" GOTO 2100
290 AS =0
300 FOR I=1 TO NS
310 AS(I)=S(I)*(NS-(2*I)+1)
```

```
340 GPS=(2/3)*SQR((GXS^2+GYS^2+GZS^2)/3)+(GXS+GYS+GZS)/9
344 REM LOOP IN CASE ONLY ABSORPTION BAND IS BEING USED
345 IF N$="N" OR N$="n" GOTO 355
350 YS=(HS^2*AS*BPR*XR*YR)/(BPS*XS*HR^2*AR)
353 REM JUMP TO SKIP CALCULATION FOR ABS.BAND ONLY
354 GOTO 360
355 YS=(YR*.5*AS*HS^2*BPR*XR)/(BPS*AR*HR*XS)
360 INPUT "Enter Title and Comments";C$
362 PC=YS/CS
365 REM PRINT VALUES IN CASE WHERE ENTIRE SPECTRUM WAS USED
370 LPRINT,"Title and Comments : ";C$
371 LPRINT ,"REFERENCE=";R$ TAB(50) "SAMPLE TEMPERATURE=";TS$"K"
372 LPRINT, D$
380 LPRINT,"gp(av) or T ref = ";GPR TAB(50) "gp(av) sample = ";GPS
381 LPRINT,"G-VALUES REF=";GZR","GYR","GXR TAB(50) "G-VALUES SAMPLE=";GZS","GYS"
," GXS
390 LPRINT,"NR = ";NR TAB(50) "NS = ";NS
400 LPRINT,"HR = ";HR"gauss" TAB(50) "HS = ";HS"gauss"
410 LPRINT,"Gain (ref) = ";XR TAB(50) "Gain (sample) = ";XS
420 LPRINT,"AR = ";AR TAB(50) "AS = ";AS
430 LPRINT,"Spin conc (ref) = ";YR"mM" TAB(50) "Spin conc(sam)=";YS"mM"
433 LPRINT, TAB(50) "Sample conc.=";CS"mM"
434 LPRINT ,"REFERENCE POWER=";PR$"mW" TAB(50)"SAMPLE POWER=";PS$"mW"
435 LPRINT  TAB(50)"SPIN CONCENTRATION PER MOLECULE";PC
440 LPRINT,"REFERENCE" TAB(40) "Interval #" TAB(60) "Intensity(cm)"
450 FOR I=1 TO NR
460 LPRINT TAB(40) I TAB(60) R(I)
470 NEXT I
480 LPRINT,"SAMPLE" TAB(40) "Interval #" TAB(60) "Intensity(cm)"
490 FOR I=1 TO NS
500 LPRINT TAB(40) I TAB(60) S(I)
510 NEXT I
511 INPUT "Check data---- Have you made any mistakes";Y$
512 IF Y$="y" OR Y$="Y" THEN GOTO 670
515 INPUT"DO YOU WANT TO QUANTIFY ANOTHER SAMPLE USING SAME REF";Y$
516 IF Y$="y" OR Y$="Y" THEN GOTO 517 ELSE GOTO 790
517 K=0
518 GOTO 201
519 REM INPUT VALUES FOR CASE WHEN ONLY ABSORPTION BAND IS USED
520 IF K=0 THEN GOTO 521 ELSE GOTO 620
521 INPUT "Number of intervals for reference absorption peak (NR)";NR
530 INPUT "Width of intervals for reference absorption peak (HR)";HR
540 INPUT "G-values for reference(gz>gy>gx)";GZR,GYR,GXR
550 INPUT "Gain for reference spectrum";XR
560 INPUT "Concentration of reference (mM)";YR
570 INPUT "Magnetic field at maximum of absorption peak (gauss)";BR
571 INPUT "what reference are you using";R$
572 INPUT "WHAT POWER WAS THE REFERENCE RUN AT";PR$
573 INPUT "ARE THESE VALUES CORRECT";Y$
574 IF Y$="N" OR Y$="n" GOTO 521
590 PRINT "List intensity values for absorption peak 1 to NR"
591 FOR I=1 TO NR
592 PRINT I
593 INPUT R(I)
594 NEXT I
615 INPUT"ARE THESE THE CORRECT";P$
616 IF P$="Y" OR P$="y" GOTO 620 ELSE GOTO 590
620 AR=0
630 FOR I=1 TO NR
640 AR=AR+R(I)
650 NEXT I
659 REM COMPUTE AVERAGE G-VALUE
660 GPR=(GXR^2+GYR^2)/(GZR+BR+2+SQR((1-(GYR^2/GZR^2))*(1-(GXR^2/GZR^2))))
665 GOTO 201
```

```
690 INPUT "How many sample intensities do you want to change";K
700 FOR J=1 TO K
710 INPUT "List #";N
711 INPUT "INPUT NEW INTENSITY";S
712 I=N
713 S(I)=S
720 NEXT J
721 GOTO 287
730 INPUT "Do you want to change any reference intensities";N$
740 IF N$="N" OR N$="n" GOTO 515
750 INPUT "How many reference intensities do you want to change";K
760 FOR J=1 TO K
770 INPUT "List #";I
771 INPUT "NEW INTENSITY";S
772 S(I)=S
780 NEXT J
781 INPUT "Are you using complete EPR spectrum as reference";Y$
782 IF Y$="N" OR Y$="n" GOTO 620
783 GOTO 150
790 END
2000 REM COMPUTE SAMPLE INTENSITY IF ONLY ABSORPTION BAND IS USED
2010 INPUT "NUMBER OF INTERVALS FOR SAMPLE SPECTRUM";NS
2020 INPUT "WIDTH OF INTERVALS FOR SAMPLE SPECTRUM (IN GAUSS)";HS
2030 INPUT "G-VALUES FOR SAMPLE SPECTRUM (Gz>GY>GX)";GZS,GYS,GXS
2040 INPUT "GAIN FOR SAMPLE SPECTRUM";XS
2050 INPUT "CONCENTRATION OF SAMPLE (mM)";CS
2060 INPUT "MAGNETIC FIELD AT MAXIMUM ABSORPTION (GAUSS)";BS
2070 INPUT "POWER OF SAMPLE SPECTRUM (mW)";PS$
2080 INPUT "TEMPERATURE OF SAMPLE (K)";TS$
2090 INPUT "DATE EPR WAS RAN";D$
2091 INPUT "ARE THESE VALUES CORRECT";Y$
2092 IF Y$="n" OR Y$"N" GOTO 360
2100 PRINT "LIST INTENSITY VALUES FOR ABSORPTION PEAK 1 TO NS"
2110 FOR I=1 TO NS
2120 PRINT I
2130 INPUT S(I)
2140 NEXT I
2150 INPUT "ARE THESE CORRECT";P$
2160 IF P$="N" OR P$="n" GOTO 2110
2170 AS=0
2180 FOR I=1 TO NS
2190 AS=AS+S(I)
2200 NEXT I
2210 REM COMPUTE AVERAGE G-VALUE FOR SAMPLE WHEN ONLY PARTIAL SPECTRUM USED
2220 GPS=(GXS^2+GYS^2)/(GZS+BS+2+SQR((1-(GXS^2/GZS^2))+(1-(GYS^2/GZS^2))))
2230 IF N$="Y"OR N$="y" GOTO 2300
2240 YS=(YR+AS+HS+GPR+XR)/(GPS+AR+HR+XS)
2250 GOTO 362
2300 YS=(YR+AS+HS+GPR+XR)/(GPS+.5+AR+HR^2+XS)
2310 GOTO 360
Ok
```

Appendix B

Experimental and best fit data points for temperature dependence of low temperature MCD

(a) Oxidized *C. pasteurianum* Rd 500 nm
(b) Oxidized *C. pasteurianum* Rd 465 nm
(c) Oxidized *C. pasteurianum* Rd 400 nm
(d) partially-reduced *T. thermophilus* Fd 705 nm
(e) partially-reduced *A. vinelandii* Fd I 690 nm

A

Y PTS	X PTS	FIT Y PTS	FIT X PTS
2.0000 E0	0.8269 E0	1.9765 E0	0.8140 E0
1.9700 E0	0.8175 E0	1.9425 E0	0.8002 E0
1.9500 E0	0.8129 E0	1.9085 E0	0.7865 E0
1.9200 E0	0.7949 E0	1.8745 E0	0.7727 E0
1.8900 E0	0.7863 E0	1.8384 E0	0.7582 E0
1.8600 E0	0.7674 E0	1.8043 E0	0.7444 E0
1.8200 E0	0.7475 E0	1.7701 E0	0.7307 E0
1.7800 E0	0.7378 E0	1.7359 E0	0.7169 E0
1.7500 E0	0.7194 E0	1.6997 E0	0.7023 E0
1.7400 E0	0.7158 E0	1.6654 E0	0.6886 E0
1.7000 E0	0.6934 E0	1.6311 E0	0.6748 E0
1.6500 E0	0.6852 E0	1.5967 E0	0.6611 E0
1.6400 E0	0.6724 E0	1.5602 E0	0.6465 E0
1.6100 E0	0.6661 E0	1.5257 E0	0.6328 E0
1.5700 E0	0.6481 E0	1.4911 E0	0.6190 E0
1.5300 E0	0.6339 E0	1.4565 E0	0.6053 E0
1.4700 E0	0.6087 E0	1.4197 E0	0.5907 E0
1.4300 E0	0.5887 E0	1.3849 E0	0.5770 E0
1.3900 E0	0.5755 E0	1.3501 E0	0.5632 E0
1.3600 E0	0.5643 E0	1.3151 E0	0.5495 E0
1.3400 E0	0.5534 E0	1.2779 E0	0.5349 E0
1.3000 E0	0.5430 E0	1.2428 E0	0.5211 E0
1.2500 E0	0.5232 E0	1.2075 E0	0.5074 E0
1.2200 E0	0.5066 E0	1.1721 E0	0.4936 E0
1.1800 E0	0.4944 E0	1.1345 E0	0.4781 E0
1.1500 E0	0.4845 E0	1.0989 E0	0.4653 E0
1.1100 E0	0.4718 E0	1.0631 E0	0.4516 E0
1.0500 E0	0.4486 E0	1.0273 E0	0.4378 E0
1.0300 E0	0.4360 E0	0.9892 E0	0.4233 E0
0.9850 E0	0.4232 E0	0.9530 E0	0.4095 E0
0.9750 E0	0.3997 E0	0.9168 E0	0.3958 E0
0.9350 E0	0.3997 E0	0.8804 E0	0.3820 E0
0.8750 E0	0.3837 E0	0.8439 E0	0.3682 E0
0.8550 E0	0.3737 E0	0.8051 E0	3.5369 E-1
0.8200 E0	0.3737 E0	0.7684 E0	3.3983 E-1
0.7900 E0	3.4112 E-1	0.7316 E0	3.2618 E-1
0.7350 E0	3.2701 E-1	0.6948 E0	3.1243 E-1
0.6900 E0	3.2701 E-1	0.6558 E0	2.9787 E-1
0.6600 E0	2.8976 E-1	0.6189 E0	2.8412 E-1
0.5600 E0	2.7148 E-1	0.5821 E0	2.7036 E-1
0.5000 E0	2.4808 E-1	0.5454 E0	2.5661 E-1
0.4700 E0	2.2482 E-1	0.5067 E0	2.4205 E-1
0.4100 E0	2.1160 E-1	0.4704 E0	2.2830 E-1
0.3800 E0	1.9846 E-1	0.4344 E0	2.1455 E-1
3.5500 E1	1.8566 E-1	0.3987 E0	2.0079 E-1
3.3000 E1	1.6928 E-1	3.6157 E1	1.8623 E-1
2.8500 E1	1.5146 E-1	3.2707 E1	1.7248 E-1
2.7000 E1	1.4388 E-1	2.9329 E1	1.5873 E-1
2.4000 E1	1.3080 E-1	2.6036 E1	1.4498 E-1
2.1000 E1	1.1990 E-1	2.2657 E1	1.3042 E-1
1.7000 E1	1.0277 E-1	1.9581 E1	1.1666 E-1
1.5000 E1	0.9404 E-1	1.6692 E1	1.0291 E-1
1.1000 E1	0.7194 E-1	1.3825 E1	0.8916 E-1
0.9000 E1	0.5995 E-1	1.1024 E1	0.7460 E-1
0.6000 E1	0.4496 E-1	0.8554 E1	0.6085 E-1
0.4000 E1	3.1974 E-2	0.6269 E1	0.4709 E-1
3.0000 E0	2.5925 E-2	0.4181 E1	3.3342 E-2
2.0000 E0	1.7986 E-2	2.1970 E0	1.8781 E-2

B

Y PTS	X PTS	FIT Y PTS	FIT X PTS
1.3800 E0	0.9529 E0	1.3803 E0	0.9351 E0
1.3700 E0	0.9404 E0	1.3520 E0	0.9155 E0
1.3500 E0	0.9223 E0	1.3238 E0	0.8959 E0
1.3100 E0	0.8937 E0	1.2956 E0	0.8762 E0
1.2800 E0	0.8720 E0	1.2674 E0	0.8566 E0
1.2400 E0	0.8365 E0	1.2393 E0	0.8370 E0
1.1900 E0	0.7894 E0	1.2125 E0	0.8189 E0
1.1500 E0	0.7736 E0	1.1844 E0	0.7986 E0
1.1100 E0	0.7379 E0	1.1563 E0	0.7790 E0
1.0800 E0	0.7129 E0	1.1282 E0	0.7594 E0
1.0400 E0	0.6819 E0	1.1002 E0	0.7397 E0
0.9900 E0	0.6339 E0	1.0722 E0	0.7201 E0
0.9150 E0	0.5846 E0	1.0454 E0	0.7014 E0
0.8650 E0	0.5710 E0	1.0174 E0	0.6818 E0
0.8100 E0	0.5309 E0	0.9893 E0	0.6621 E0
0.8000 E0	0.5102 E0	0.9612 E0	0.6425 E0
0.7700 E0	0.4962 E0	0.9331 E0	0.6229 E0
0.7300 E0	0.4718 E0	0.9049 E0	0.6032 E0
0.6900 E0	0.4455 E0	0.8779 E0	0.5845 E0
0.6350 E0	0.4232 E0	0.8495 E0	0.5649 E0
0.6100 E0	0.3997 E0	0.8210 E0	0.5453 E0
0.5900 E0	0.3837 E0	0.7923 E0	0.5256 E0
0.5550 E0	3.6061 E-1	0.7634 E0	0.5060 E0
0.5400 E0	3.5971 E-1	0.7343 E0	0.4864 E0
0.5200 E0	0.3786 E0	0.7063 E0	0.4677 E0
0.5100 E0	3.4112 E-1	0.6766 E0	0.4480 E0
0.4750 E0	3.5703 E-1	0.6465 E0	0.4284 E0
0.4600 E0	3.1279 E-1	0.6161 E0	0.4088 E0
0.4300 E0	3.0282 E-1	0.5852 E0	0.3881 E0
3.6500 E1	2.7148 E-1	0.5539 E0	0.3685 E0
3.4000 E1	2.4808 E-1	0.5236 E0	3.5081 E-1
3.0000 E1	2.2839 E-1	0.4913 E0	3.9117 E-1
2.8000 E1	2.1475 E-1	0.4584 E0	3.1154 E-1
2.6000 E1	1.9710 E-1	0.4251 E0	2.8191 E-1
2.4000 E1	1.8932 E-1	0.3913 E0	2.7227 E-1
2.3000 E1	1.7441 E-1	3.5714 E1	2.5264 E-1
2.0000 E1	1.5555 E-1	3.2435 E1	2.3394 E-1
1.8500 E1	1.4388 E-1	2.8982 E1	2.1431 E-1
1.6000 E1	1.3080 E-1	2.5537 E1	1.8468 E-1
1.4000 E1	1.1990 E-1	2.2129 E1	1.7504 E-1
1.1000 E1	1.0277 E-1	1.8790 E1	1.5541 E-1
1.0000 E1	0.9404 E-1	1.5556 E1	1.3578 E-1
0.7000 E1	0.7194 E-1	1.2615 E1	1.1708 E-1
0.5000 E1	0.5995 E-1	0.9719 E1	0.9745 E-1
3.0000 E0	0.4496 E-1	0.7069 E1	0.7781 E-1
2.0000 E0	3.1974 E-2	0.4719 E1	0.5818 E-1
0.5000 E0	2.5925 E-2	2.7191 E0	0.3855 E-1
0.5000 E0	1.7886 E-2	1.1202 E0	1.8916 E-2

C

Y PTS	X PTS	FIT Y PTS	FIT X PTS
1.4200 E0	0.8464 E0	1.4084 E0	0.8915 E0
1.4100 E0	0.8414 E0	1.3808 E0	0.8149 E0
1.4000 E0	0.8365 E0	1.3546 E0	0.7892 E0
1.3900 E0	0.8222 E0	1.3270 E0	0.7826 E0
1.3700 E0	0.8129 E0	1.2984 E0	0.7660 E0
1.3600 E0	0.8038 E0	1.2792 E0	0.7503 E0
1.3400 E0	0.7863 E0	1.2457 E0	0.7337 E0
1.3150 E0	0.7778 E0	1.2194 E0	0.7180 E0
1.2800 E0	0.7484 E0	1.1918 E0	0.7014 E0
1.2400 E0	0.7304 E0	1.1642 E0	0.6848 E0
1.2200 E0	0.7194 E0	1.1379 E0	0.6681 E0
1.1800 E0	0.6951 E0	1.1102 E0	0.6525 E0
1.1650 E0	0.6787 E0	1.0839 E0	0.6368 E0
1.1400 E0	0.6631 E0	1.0561 E0	0.6202 E0
1.0800 E0	0.6339 E0	1.0282 E0	0.6036 E0
1.0500 E0	0.6071 E0	1.0017 E0	0.5879 E0
1.0200 E0	0.5921 E0	0.9737 E0	0.5719 E0
0.9800 E0	0.5687 E0	0.9470 E0	0.5556 E0
0.9500 E0	0.5492 E0	0.9188 E0	0.5390 E0
0.9100 E0	0.5290 E0	0.8904 E0	0.5225 E0
0.8700 E0	0.5219 E0	0.8639 E0	0.5067 E0
0.8200 E0	0.4733 E0	0.8347 E0	0.4902 E0
0.7800 E0	0.4612 E0	0.8073 E0	0.4744 E0
0.7500 E0	0.4360 E0	0.7782 E0	0.4578 E0
0.7200 E0	0.4295 E0	0.7490 E0	0.4413 E0
0.6800 E0	0.3997 E0	0.7209 E0	0.4255 E0
0.6400 E0	0.3837 E0	0.6911 E0	0.4090 E0
0.5800 E0	3.5084 E-1	0.6611 E0	0.3924 E0
0.5800 E0	3.4112 E-1	0.6322 E0	0.3767 E0
0.5300 E0	3.2701 E-1	0.6015 E0	3.6008 E-1
0.5150 E0	3.1279 E-1	0.5721 E0	3.4434 E-1
0.4700 E0	3.0292 E-1	0.5408 E0	3.2778 E-1
0.4100 E0	2.6894 E-1	0.5092 E0	3.1121 E-1
0.3700 E0	2.5023 E-1	0.4789 E0	2.9547 E-1
3.3000 E1	2.2839 E-1	0.4466 E0	2.7890 E-1
3.1000 E1	2.1475 E-1	0.4161 E0	2.6316 E-1
2.8000 E1	1.9444 E-1	0.3836 E0	2.4659 E-1
2.6000 E1	1.8566 E-1	3.5110 E1	2.3002 E-1
2.5000 E1	1.7441 E-1	3.2025 E1	2.1428 E-1
2.2000 E1	1.5555 E-1	2.8797 E1	1.9771 E-1
2.0000 E1	1.4388 E-1	2.5763 E1	1.8197 E-1
1.7000 E1	1.3080 E-1	2.2622 E1	1.6540 E-1
1.5500 E1	1.1990 E-1	1.9557 E1	1.4883 E-1
1.2000 E1	1.0277 E-1	1.6738 E1	1.3309 E-1
1.1000 E1	0.9404 E-1	1.3894 E1	1.1652 E-1
0.8000 E1	0.7194 E-1	1.1336 E1	1.0078 E-1
0.6000 E1	0.5995 E-1	0.8823 E1	0.8421 E-1
3.5000 E0	0.4496 E-1	0.6526 E1	0.6764 E-1
2.0000 E0	3.1974 E-2	0.4570 E1	0.5190 E-1
1.0000 E0	2.5925 E-2	2.7793 E0	3.5936 E-2
0.5000 E0	1.7986 E-2	1.2905 E0	1.8768 E-2

D

Y PTS	X PTS	FIT Y PTS	FIT X PTS
1.3850 E0	9.4112 E-1	1.3226 E0	9.3142 E-1
1.3200 E0	9.3123 E-1	1.2762 E0	9.2139 E-1
1.2700 E0	9.2117 E-1	1.2297 E0	9.1136 E-1
1.2400 E0	9.1239 E-1	1.1817 E0	9.0101 E-1
1.2000 E0	9.0419 E-1	1.1353 E0	2.8088 E-1
1.1750 E0	2.9926 E-1	1.0888 E0	2.8095 E-1
1.1400 E0	2.8986 E-1	1.0424 E0	2.7093 E-1
1.0700 E0	2.8015 E-1	0.9846 E0	2.6058 E-1
1.0350 E0	2.7215 E-1	0.9484 E0	2.5055 E-1
0.9850 E0	2.6314 E-1	0.9023 E0	2.4052 E-1
0.9450 E0	2.5243 E-1	0.8566 E0	2.3049 E-1
0.9000 E0	2.3977 E-1	0.8096 E0	2.2014 E-1
0.8600 E0	2.9144 E-1	0.7644 E0	2.1011 E-1
0.7950 E0	2.1475 E-1	0.7186 E0	2.0009 E-1
0.7500 E0	2.0814 E-1	0.6752 E0	1.9006 E-1
0.7050 E0	1.9767 E-1	0.6300 E0	1.7971 E-1
0.6700 E0	1.8703 E-1	0.5867 E0	1.6968 E-1
0.6150 E0	1.7479 E-1	0.5441 E0	1.5965 E-1
0.5700 E0	1.6502 E-1	0.5022 E0	1.4962 E-1
0.5300 E0	1.5609 E-1	0.4598 E0	1.3927 E-1
0.4900 E0	1.4658 E-1	0.4186 E0	1.2925 E-1
0.4500 E0	1.3768 E-1	0.3803 E0	1.1922 E-1
0.4050 E0	1.2491 E-1	9.4196 E1	1.0919 E-1
9.5500 E1	1.1167 E-1	9.0347 E1	0.9884 E-1
9.0500 E1	0.9782 E-1	2.6730 E1	0.8881 E-1
2.7000 E1	0.8093 E-1	2.9226 E1	0.7878 E-1
2.9000 E1	0.8006 E-1	1.9841 E1	0.6876 E-1
2.0000 E1	0.6855 E-1	1.6474 E1	0.5840 E-1
1.6000 E1	0.5507 E-1	1.3338 E1	0.4838 E-1
1.1000 E1	0.4155 E-1	1.0929 E1	0.3835 E-1
0.8000 E1	2.9514 E-2	0.7448 E1	2.8321 E-2
0.5000 E1	1.7647 E-2	0.4608 E1	1.7970 E-2

E

Y PTS	X PTS	FIT Y PTS	FIT X PTS
1.6800 E0	9.4112 E-1	1.5469 E0	9.1825 E-1
1.5200 E0	9.1554 E-1	1.4164 E0	2.9505 E-1
1.3650 E0	2.8436 E-1	1.2857 E0	2.7152 E-1
1.2450 E0	2.6959 E-1	1.1581 E0	2.4832 E-1
1.1000 E0	2.3841 E-1	1.0305 E0	2.2480 E-1
1.0250 E0	2.2136 E-1	0.9070 E0	2.0160 E-1
0.9100 E0	2.0555 E-1	0.7846 E0	1.7807 E-1
0.8050 E0	1.8099 E-1	0.6671 E0	1.5487 E-1
0.7450 E0	1.7129 E-1	0.5595 E0	1.3167 E-1
0.5550 E0	1.2847 E-1	0.4427 E0	1.0815 E-1
0.4700 E0	1.1241 E-1	9.3809 E1	0.8495 E-1
9.5000 E1	0.8048 E-1	2.3718 E1	0.6142 E-1
1.0500 E1	9.5971 E-2	1.4905 E1	0.3822 E-1
0.8500 E1	1.4988 E-2	0.5921 E1	1.4698 E-2

Vita

Deborah Ellen Bennett was born in New York City on September 18, 1959 to Julius and Loretta Dix. She attended the Westlake School for Girls, graduating in 1977, magna cume laude and a four year member of the California High School Honor Society.

Deborah attended Duke University in Durham, North Carolina from 1976-1980, completing her high school cirriculum in her freshman year. As part of her studies, she conducted research under the direction of Dr. C. W. Anderson, entitled "Optically Transparent Electrodes for Use in Spectroelectrochemistry". She received her Bachelor of Science degree in Chemistry in 1980, graduating cume laude, and a member of the Dean's list.

In 1981 Deborah entered Louisiana State University, Baton Rouge Louisiana.

DOCTORAL EXAMINATION AND DISSERTATION REPORT

Candidate: Deborah E. Bennett

Major Field: Chemistry

Title of Dissertation: Spectroscopic Studies of Bacterial Iron-Sulfur Proteins

Approved:

Michael K Johnson
Major Professor and Chairman

Dean of the Graduate School

EXAMINING COMMITTEE:

Brian J. Hales

Robert J. Gale

Nicholas H. Fisch

W.N. Rolnick

Thomas C. Hall

Date of Examination: July 11, 1986